The University of Nottingham

UNITED KINGDOM · CHINA · MALAYSIA

EVALUATION OF DREADD RECEPTOR PHARMACOLOGY IN RECOMBINANT CELLS AND ASTROCTYES

Jessica Carpenter

September 2019

Thesis submitted for the degree of Doctor of Philosophy

School of Life Sciences

University of Nottingham

CONTENTS

ABSTRACT i

ACKNOWLEDGMENTS iv

ABBREVIATIONS v

Chapter 1 8

1.1 G Protein-Coupled Receptors 9

1.1.1 General Overview 9

1.1.2 Classification of GPCRs 9

1.1.2.1 Class A GPCRs 11

1.1.2.2 Class B GPCR 11

1.1.2.3 Class C GPCRs 11

1.1.3 Structural Characteristics of class A GPCRs 12

1.1.4 Activation Mechanisms of GPCRs 15

1.1.4.1 G-protein dependent signalling 18

1.1.4.1.1 Gαq signalling 22

1.1.4.1.2 Gαs signalling 22

1.1.4.1.3 Gαi/o signalling 23

1.1.4.1.4 Gα12/13 signalling 24

1.1.4.1.5 Gβγ subunit signalling 24

1.1.5 Termination of G protein signalling by β- arrestins 26

1.2 Receptor Pharmacology 28

1.2.1 Ligand Affinity 28

1.2.2 Ligand Efficacy 29

1.2.3 Receptor occupancy and its relation to affinity and efficacy 30

1.3 Muscarinic Acetylcholine Receptors 31

1.3.1 General Overview 31

1.3.2 Localisation of mAChRs in the Brain 32

1.3.3 Therapeutic potential in the CNS 33

1.3.3.1 Alzheimer's Disease 33

1.3.3.2 Schizophrenia 35

1.3.3.3 Parkinson's Disease 37

1.4 Allosteric Modulation of GPCRs 37

1.4.1 General Overview 37

1.4.2 Allosteric Binding Models 38

1.4.2.1 Monod-Wyman-Changeux Model 39

1.4.2.2 Allosteric Ternary Complex Model 40

1.4.2.3 Allosteric Two State Model 41

1.4.3 M1 mAChR Allosteric Modulators 42

1.4.3.1 BQCA is a promising M1 mAChR allosteric modulator 42

1.4.4 Bitopic Ligands 44

1.4.5 Advantages of using allosteric modulators 45

1.5 Astrocytes 47

1.5.1 General Overview 47

1.5.2 The Tripartite Synapse Allows Bidirectional Communicaiton between Neurone and Astrocyte 48

1.5.3 Spatiotemporal Dynamics of Calcium Signalling Within Astrocytes 49

1.5.4 Reactive Gliosis Is a Morphological Process That Allows Astrocytes to Protect the CNS 51

1.6 Chemogenetic DREADDs 53

1.6.1 General Overview 53

1.6.2 Advantages of Using DREADDs for Selective Receptor Activation 54

1.7 Aims of This Thesis 55

Chapter 2 56

2.1 Materials 57

2.2.1 Laboratory Reagents 57

2.1.2.1 Molecular biology reagents 57

2.1.2.2 Fluorescent dyes and indicators 57

2.1.3 Tissue Culture Reagents 57

2.1.4 Pharmacological Compounds 58

2.1.4.1 Fluorescent Ligands 59

2.2 Methods 59

2.2.1 PCR Protocol 59

2.2.2 Mutagenesis to Create the M1-DREADD Construct 60

2.2.3 PCR Amplification of M1-WT and M1- DREADD Constructs 61

2.2.4 PCR Fragment Subcloning into pJET1.2 Vector 62

2.2.5 Restriction Digest 63

2.2.6 Visualisation and Isolation of DNA Using Agarose Gel Electrophoresis 64

2.2.7 Gel Extraction of DNA 65

2.2.8 Ligation into pcDNA(+)neo Vector 65

2.2.9 Transformation of Component Cells with DNA Constructs 66

2.2.10 MiniPrep 67

2.2.11 MaxiPrep 68

2.2.12 DNA Sequencing 70

2.2.13 Cell Culture 70

2.2.13.1 Recombinant Cells 70

2.2.13.2 Astrocytes 71

2.2.14 Transfection 72

2.2.14.1 Stable Transfection in Recombinant Cells 72

2.2.14.2 Lipofectamine LTX Transfection of Astrocytes 73

2.2.14.3 Electroporation Transfection of Astrocytes Using Nucleofector™ Technology 74

2.3 Assays 75

2.3.1 Calcium Mobilisation Assay 75

2.3.2 SNAP-tagged Receptor Internalisation 76

2.3.3 Fluorescent Ligand Binding Assays 77

2.3.3.1 Fluorescent Ligand Binding Assays 77

2.3.3.2 Fluorescent Ligand Competition Assay 78

2.3.4 Nano Luciferase Complementation Assay 78

2.3.5 Astrocyte Stellation Assay 79

2.4 Data analysis 80

2.4.1 Calcium Mobilisation Assay 80

2.4.2 Receptor Internalisation 80

2.4.3 NanoBiT Complementation Assay 81

2.4.4 Time Course of Stimulation 81

2.4.5 Fluorescent Binding Studies 82

2.4.6 Astrocyte Stellation 84

2.4.7 Single Cell Calcium Response 84

2.5 Statistical analysis 85

2.5.1 Concentration Response Curves 85

2.5.2 Stellation Analysis 85

2.5.3 Single Cell Calcium Analysis 85

Chapter 3 86

3.1 Introduction 87

3.2 Results 90

3.2.1 Design of desired SNAP-tagged pcDNA3.1(+)neo vectors 90

3.2.2 Site Directed Mutagenesis to form the hM1-DREADD Receptor 93

3.2.3 Introducing Restriction Sites to Flank the hM1 Constructs to Allow Ligation within the SNAP-tagged pcDNA3.1(+)neo Vectors 93

3.2.4 Ligation into Desired Vectors to Achieve Recombinant Plasmids 94

3.2.5 Restriction Digests Verfies the hM1 Constructs are Present within the LgBiT SNAP-tagged pcDNA3.1(+)neo Vector 96

3.2.5 DNA Sequencing 97

3.2.5.1 The Interface between the 5HT3 Signal Sequence and SNAP-tag within the Vector 97

3.2.5.2 The Interface between the SNAP-tag and the Human M1 Receptor Sequence 98

3.2.5.3 Identification of the Two DREADD Point Mutations within the Human M1 Construct 98

3.2.5.4 In Frame Fusion of the M1 Receptor with the C-Terminal LgBiT Tag 100

3.2.6 Development of Stably Transfected SNAP- M1 and SNAP M1-DREADD Cell Lines, and Verificantion of Recetor Expression by SNAP-Labelling 100

3.3 Discussion 104

Chapter 4 105

4.1 Introduction 106

4.1.1 Allosteric Modulation Used to Improve Spatiotemporal Control of Receptor Signalling 106

4.1.2 Probe and Species Dependency of Allosteric Modulation 108

4.1.3 New Insights into DREADD Receptor Pharmacology – Can DREADDs be Used to Study mAChR Allosteric Modulation? 109

4.1.4 The Use of Fluorescent Indicators to Measure M1-WT and M1-DREADD Receptor Calcium Signalling 111

4.1.5 NanoBit complementation of mini G protein and β-arrestin2 to investigate intracellular signalling pathways 113

4.1.6 Novel Fluorescent Ligands to Investigate Ligand Binding at M1-DREADD Receptor 115

4.2 Results 118

4.2.1 Initial Characterisation of the SNAP- tagged Muscarinic M1 Wild Type and DREADD Receptors in the Calcium Mobilisation Assay 118

4.2.2 Characterisation of Orthosteric Ligand and Allosteric Modulator Effects on SNAP hM1-DREADD Induced Calcium Signalling 123

4.2.3 The Allosteric Effects of BQCA and VU0357017 on ACh and CNO Calcium Responses Mediated by the M1-DREADD Receptor 127

4.2.4 Allosteric Modulation of DREADD Receptor Agonists by BQCA 131

4.2.5 Evaluating Probe Dependence of BQCA in the CHO SNAP M1-DREADD System 137

Using Mini G protein and β-arrestin2 luciferase complementation assays to explore allosteric modulation of the M1-WT and M1-DREADD receptors 142

4.2.6 Mini Gq and β-ARR2 Protein Recruitment by M1-WT, and the Effect of BQCA 142

4.2.7 Mini Gq and β-ARR2 Protein Recruitment by M1-DREADD, and the Effect of BQCA 157

The Influence of BQCA on Ligand Binding at the M1-DREADD Receptor, Measured by Fluorescence Imaging 170

4.2.8 Determining the Functional Properties of Fluorescent Ligand III 172

4.2.9 Determination of III K_D Using Saturation Analysis 175

4.2.10 Establishing the Equilibrium Time Point for Whole Cell Competition Assays Using Fluorescent Ligand III 176

4.2.11 Determination of Clozapine Derivative and BQCA Affinities at the M1-DREADD Receptor, and the Effect of BQCA on Orthosteric Ligand Binding 180

4.3 Discussion 183

4.3.1 Assessment of Novel Functional and Binding Assays to Explore M1-WT and M1-DREADD Pharmacology 183

4.3.2 Agonist Pharmacology in the M1-WT NanoBiT Assay 186

4.3.3 Agonist Pharmacolgoy at the M1-DREADD and the Effect of Clozapine Derivatives 187

4.3.4 VU0357017 May Act as a Bitopic Ligand with Affinity for the M1 mACh Receptor 188

4.3.5 BQCA is an M1 Allosteric Modulator that Retains its Effects in the DREADD Receptor System 189

4.3.6 Proposed Allosteric Mechanism for BQCA 190

4.4 Conclusions 192

Chapter 5 193

5.1 Introduction 194

5.1.1 Utilising the M1q-DREADD to investigate calcium signalling in astrocytes 194

5.1.2 Limitations in Identifying Astrocytes 196

5.1.3 Utilising M3-DREADD Chimera to investigate Gαs activation of cAMP-dependent astrocyte stellation 197

5.1.4 DREADD transfection of astrocytes 200

5.2 Results 201

5.2.1 Validation of Astrocytes for Pharmacological Investigation 201

5.2.2 Effect of Allosteric Modulation on Astrocyte Muscarinic Calcium Responses 208

5.2.3 Induction of Stellation in Astrocytes 212

5.2.4 Lipofectamine and Nucleofection Methods were able to Produce GFP-expressing Astrocytes, However were Unsuccessful in Producing Viable DREADD-Expressing Cells 216

5.3 Discussion 220

5.3.1 Assessment of Single Cell Calcium Mobilisation and Stellation to Investigate Muscarinic Pharmacology in Astrocytes 220

5.3.2 Agonist Functional Responses in Non-Transfected Astrocytes 221

5.3.3 DREADD Receptors Could Allow the Investigation of the Cross-Talk between Calcium and cAMP Signalling 223

5.3.4 Reconciling the Difficulties of *In Vitro* Transfection Methodologies 225

5.4 Conclusion 227

Chapter 6 228

6.1 Improved Understanding of Orthosteric and Allosteric Ligands Acting at M1-DREADD Receptors 229

6.2 Novel Assay Systems for Exploring M1-DREADD Ligand Binding and Signalling Kinetics 230

6.3 The Role of the Muscarinic Receptor System in Astrocyte Calcium Signalling and Stellation 233

6.4 Future Perspective in Methodologies to Explore Spatiotemporal Signalling in Astrocytes 234

6.5 Overall Conclusion 236

References 238

ABSTRACT

The M1 muscarinic acetylcholine receptor (mAChR) is a G protein-coupled receptor (GPCR), linked to cellular signalling pathways via increased intracellular calcium concentrations. The M1 mAChR has been implemented in a number of physiological and pathological signalling mechanisms in the central nervous system (CNS). In addition, a significant role of Gαq-signalling has emerged in astrocytes as continuing roles for these CNS cells are discovered. As such, the M1 receptor continues to be investigated for CNS disorders, such as Alzheimer's disease; however, there are challenges associated with evaluating the specific role of individual mAChR subtypes, and also selective pharmacological targeting of these receptors due to the conserved nature of the orthosteric acetylcholine binding sites. Many cholinergic drugs therefore have negative non-selective side effects that limit their clinical efficacy. As an alternative, muscarinic receptor allosteric modulators may offer more spatiotemporal control of CNS pathways, and the possibility of increased subtype selectivity, to modulate M1 signalling. In parallel, DREADDs (designer receptors exclusively activated by designer drugs) provide an experimental method to study subtype selective signalling of muscarinic GPCRs, because they can be selectively activated by clozapine-N-oxide (CNO) – an otherwise biologically inert compound. This thesis first explored the use of the M1-DREADD receptor as an approach to examine allosteric modulation of signalling in recombinant systems, developing novel luciferase complementation assays to monitor effector recruitment and fluorescent ligand binding approaches, in comparison to more routine calcium mobilisation assays. Single cell calcium analysis and a morphological assay of stellation assessed the role of muscarinic signalling in primary astrocyte cells, with an intention to develop the M1-DREADD system for pharmacological control of calcium signalling in these cells.

Recombinant CHO and HEK293 cell lines were developed that expressed SNAP-tagged M1 wild type (WT) or M1-DREADD receptors for evaluation of calcium signalling and receptor internalisation, and the recruitment of either a mini Gq protein

or β-arrestin2 measured using luciferase complementation. In calcium assays, the M1-DREADD receptor demonstrated the expected orthosteric ligand pharmacology, highlighting the high potency of CNO metabolites, such as clozapine, that might be expected to be present during *in vivo* experiments. The representative M1 allosteric modulator benzyl quinolone carboxylic acid (BQCA) acted as a positive allosteric modulator (PAM) of the M1-DREADD receptor signalling in the presence of CNO, and other clozapine derivatives, consistent with the preservation of its allosteric binding site in this DREADD. Luciferase complementation assays detected the real time recruitment of mini Gq proteins or β-arrestin2 to the M1-DREADD and M1-WT receptors, together with the modulation of orthosteric agonist responses by BQCA. Finally, novel fluorescent pirenzepine-based tracers were identified with high affinity for the M1 DREADD receptor and these established a competition binding assay, from which the affinities of CNO and derivatives could be established. BQCA increased the affinity of these ligands in the binding assay, but also itself competed directly for the fluorescent tracer.

Finally, the role of muscarinic receptor signalling in astrocytes was investigated, in terms of calcium signalling and their role in forming a stellate morphology through modulation of Gαs cAMP-led pathways. Clozapine, and its derivatives, did not produce any off-target effects at the non-transfected astrocytes highlighting their use for selective activation of the muscarinic DREADD receptors within this cell type. However, it was shown that endogenous expression of muscarinic receptors in these primary cells could be a limitation when evaluating allosteric modulation. The M1-selective modulator BQCA did not act as a PAM when evaluating astrocytic calcium signalling, induced by acetylcholine and carbachol, perhaps due to the increased expression of M3 mAChRs, compared to M1 mAChRs, reported in these cells. It was not possible to recombinantly express the DREADDs sufficiently within primary astrocytes to study their signalling. In the future, the lack of muscarinic activation of endogenous Gαs signalling pathways in astrocytes indicates that a chimeric M3-DREADD coupled to Gαs might be a potentially selective tool to explore cAMP-dependent effects on the astrocytic cytoskeleton.

These data provide further insight into the signalling of the M1-DREADD receptor in response to orthosteric and allosteric ligands, and demonstrate the applicability of mini Gq and β-arrestin2 luciferase complementation to monitor the kinetics of these responses. The identification of a fluorescence ligands for these receptors opens the way to new homogeneous binding assays to study their pharmacology in more depth. Providing their cellular expression is improved, the use of Gq- and Gs-coupled DREADDs remain useful future options to provide novel understanding of the function and intracellular signalling pathways of astrocytes.

ACKNOWLEDGMENTS

Firstly, I would like thank both Dr. Nick Holliday and Dr. Tom Bellamy who have patiently supervised me over the last four years. Without your level headed, understanding and overall "you-can-do-it" attitudes I can't image I would have reached this stage. Thank you to my lab partners; Laura Humphrys, Desi Nesheva, Nikki Dijon, Zoe Smith and Rawan Hareeri. The girl power is strong! Thank you to BBSRC for funding this research through the DTP programme.

Matt…this was all your fault! But thank you for all our road trips in Delilah, for the many hours we had with Manolo, for renovating our first house together, for making it through your mouse allergy and my testing Year 2. Thank you for dealing with my tears, tantrums and, at times, total apathy. I can't wait to start our adventure together as Dr. & Dr. and Mr & Mrs.

I would like to thank both my parents Frances and David, my brother Michael, my sister-in-law Sujjada and little Douglas. You've put up with me for this long, so I *know* the best is yet to come. Thank you for your unwavering encouragement and genuine interest in my PhD project. You were only ever a phone call away. Thank you also for the emergency trips to the cheese shop to boost my spirits. Finally, an extra special thank you to Douglas for being so damn adorable!

Thank you Matt Heatley for helping me keep everything in perspective and being the epitome of chill. Thank you for entertaining me with your shipping adventures, maybe I'll be pirating a boat somewhere next year! Thank you Ruth Dennis – for being…you! The sheer bliss you exuded after handing in your thesis was true motivation. Thank you Lydia Reeves; my raconteur who keeps be laughing for hours. You have truly been my rock over the last few years. Thank you Lewis Barron for not understanding our science discussions and being a lifeline to the outside world. Thank you Laura and Patrick Collins-Moreno for the house parties, thank you Alessandra and Andrea for welcoming me into the dolce vita and thank you Rawan, Sal and Omar for the many wonderful brunches – thank you all!

ABBREVIATIONS

Acetylcholine	**ACh**
Acetylcholinesterase inhibitors	**AChEI**
Adenosine Triphosphate	**ATP**
Adenylate Cyclase	**AC**
Alanine	**Ala/A**
Arginine	**Arg/R**
Aspartic acid	**Asp/D**
Benzyl Quinolone Carboxylic Acid	**BQCA**
Chinese Hamster Ovary	**CHO**
Clozapine	**CLOZ**
Clozapine-N-oxide	**CNO**
Cyclic Adenosine Monophosphate	**cAMP**
Cysteine	**Cys/C**
Designer Receptor Exclusively Activated by Designer Drug	**DREADD**
Extracellular Loop	**ECL**
Fluorescent energy transfer	**FRET**
Forskolin	**FRSK**
G protein-coupled receptor kinases	**GRKs**
Glycine	**Gly/G**
Guanine nucleotide (G protein)-coupled receptor	**GPCR**
Guanine Triphosphate	**GTP**

Guanosine Diphosphate	**GDP**
Hoechst's Nuclei Stain	**H33342**
Human Embryonic Kidney	**HEK**
Inositol 1,4,5-trisphosphate	**IP3**
Intracellular Loop	**ICL**
LargeBiT (NanoLuc)	**LgBiT**
Medial Prefrontal Cortex	**mPFC**
Messenger Ribonucleic Acid	**mRNA**
Metabotropic Glutmate Receptor	**mGluR**
Mitogen Activate Protein Kinase	**MAPK**
Monod-Wyman-Changeux	**MWC**
Muscarinic Acetylcholine Receptor	**mAChR**
Muscarinic Acetylcholine	**mACh**
N, desmethylclozapine	**NDMC**
NanoLuc Luciferase	**NanoLuc**
Negative Allosteric Modulator	**NAM**
Neutral Allosteric Modulator	**NAL**
N-methyl-D-aspartate	**NMDA**
Norepinephrine	**NE**
Phosphatidylinositol 3' kinase	**PI3K**
Phosphoinositol-1,4,5-biphosphate	**PIP2**
Phospholipase A2	**PLA2**
Phospholipase C	**PLCβ**

Positive Allosteric Modulator	**PAM**
Proline	**Pro/P**
Protein Kinase A	**PKA**
Protein Kinase C	**PKC**
SmallBiT (NanoLuc)	**SmBiT**
Transmembrane domain	**TM**
Tyrosine	**Tyr/Y**
β2-adrenergic receptors	**β2-AR**
β-arrestin 2	**β-ARR2**
γ-aminobutyric acid	**GABA**
1,2-diacylglycerol	**DAG**
2-Chloro-N^6-cyclopentyladenosine	**CCPA**
3-amino-5-chloro-6-methoxy-4-methylthieno[2,3-b]pyridine2-carboxylic acid cyclopropylamide	**LY2033298**
((3-((1*S*,2*S*)-2-hydroxycyclohexyl)-6-((6-(1-methyl-1*H*-pyrazol-4-yl)pyridin-3-yl)methyl)benzo[*h*]quinazolin-4(3*H*)-one)	**BQZ12**
3-[4-(Hexyloxy)-1,2,5-thiadiazol-3-yl] -1,2,5,6-tetrahydro-1-methylpyridine oxalate	**Xanomeline**
4-[(4,5-Dihydro-3-isoxazolyl)oxy]-N,N,N-trimethyl-2-butyn-1-aminium iodide	**Iperoxo**
5’-(N-Ethylcarboxamido)adenosine	**NECA**

Chapter 1

GENERAL INTRODUCTION

1.1 G Protein-Coupled Receptors

1.1.1 General Overview

G protein-coupled receptors (GPCRs) belong to a large family of signalling proteins that mediate cellular responses to most hormones, metabolites, cytokines, and neurotransmitters (Shoichet and Kobilka, 2012). About 800 GPCRs have been identified in humans, ~350 non-sensory GPCRs mediate signalling by ligands that range in size from small molecules to peptides to large proteins (Lander *et al.*, 2001), these non-sensory receptors modulate several signalling processes involved in behaviour, blood pressure regulation, cognition, immune response, mood, smell, and taste (Allen and Roth, 2011). Over 30% of the pharmaceutical market caters to drugs that target GPCRs for therapeutic alleviation from disease (Santos *et al.*, 2017). Despite this clinical success, there is still the need to develop drugs that are more efficacious and remove off-target effects. A fundamental property of most of these approved drugs for GPCRs is where they bind to the receptor: the orthosteric-binding site. This is due to the highly conserved orthosteric sites of GPCRs, particularly in muscarinic acetylcholine receptors (mAChRs) as investigated here. This issue is exacerbated by the extreme diversity of GPCRs as these receptors are expressed in a multitude of tissues, as well as, their activation by a wide range of endogenous and exogenous ligands. Currently, there are great efforts being made in drug discovery to improve therapies (Chang and Bruchas, 2014), for example, by advancing the selectivity of drugs by using allosteric modulators, or by using new approaches to understand the relevance of GPCR signalling pathways in pathophysiology, such as chemogenetic technologies (Wootten, Christopoulos and Sexton, 2013).

1.1.2 Classification of GPCRs

In the past, various attempts were made to categorize GPCRs based on their ligand binding properties or physiological functions. A commonly used, and now widely, accepted classification uses sequence homology and functional properties to group all GPCRS in classes A-F (Attwood and Findlay, 1994; Kolakowski, 1994), shown in Table 1.1. The rhodopsin/β-adrenergic receptor family (family A), the secretin receptor

family (family B), the metabotropic glutamate receptor family (family C) and the frizzled/smoothened receptor family (family F) are all expressed in humans. The largest of these by far is family A, followed by family B. Family D and E are not expressed in man (Table 1.1).

CLASS	ATTRIBUTION
A	Rhodopsin-like family
B	Secretion receptor family
C	Metabotropic receptor family
D	Fungal mating pheromone receptor family
E	Cyclic AMP secretion receptor family
F	Frizzled/Smoothened receptor family

Table 1.1: ***Classification of GPCRs in families****. Receptors are grouped together dependent on homology and functional properties.*

GPCRs for which the endogenous ligand is still unknown are termed "orphan" receptors (Kolakowski, 1994). While Family A-F is the most widely used GPCR classification system, an alternative classification system was developed (Fredriksson *et al.*, 2003), which illustrated that most of the human GPCRs can be divided in five main families; known as the GRAFS-system (Table 1.2). The main difference between the two classification systems is that the latter further subdivides the Rhodopsin family into the four groups α, β, γ, δ and the further division of family B into the Secretin family and the Adhesion family (Fredriksson *et al.*, 2003; Bjarnadóttir *et al.*, 2006).

CLASS	ATTRIBUTION
G	Glutamate Family
R	Rhodopsin Family
A	Adhesion Family
F	Frizzled/Taste2 Family
S	Secretin Family

Table 1.2: ***Classification of GPCRs using the GRAFS-system.***

1.1.2.1 Class A GPCRs

Family A/Rhodopsin is the largest and best characterised family of GPCRs and contains ~700 receptor proteins, from a total of approximately 800 genes that encode for human GPCRs, which also include olfactory and light activated receptors (Lagerström and Schiöth, 2008). This family group can be divided further, into the four groups (α, β, γ and δ), based on their respective endogenous ligand. The α-group include receptors activated by amines such as histamine, dopamine, serotonin, muscarinic and adrenergic ligands. Peptide receptors are included in both the β- and γ-group, the latter of which comprises opioid, angiotensin and somatostatin receptors are as examples. Finally, purines and proteases and the olfactory ligands bind the δ-group (Lagerström and Schiöth, 2008).

1.1.2.2 Class B GPCR

The class B/Secretin family GPCRs comprises fifteen receptors in humans (Hoare, 2005). These GPCRs are characterised by an N-terminal extracellular domain which forms an α-helix and four β-strands that are stabilised by conserved disulphide bridges between conserved cysteine residues. Peptides bind both to this region, which governs peptide selectivity and affinity, and within the TM bundle to activate the receptor (Fredriksson *et al.*, 2003; Lee, Booe and Pioszak, 2015).

Adhesion receptors differ from Secretin-like receptors in their N-terminal architecture, which contains several domains that play an important role in the specificity of receptor ligand binding interactions (Bjarnadóttir *et al.*, 2006; Lagerström and Schiöth, 2008) and contain GPCR photolytic (GPS) domains, which the Secretin-like receptors lack (Hoare, 2005). In addition, adhesion receptors bind extracellular matrix molecules rather than peptide hormones (Lagerström and Schiöth, 2008).

1.1.2.3 Class C GPCRs

Family C/ Glutamate GPCRs consists of 22 human proteins that include the metabotropic glutamate receptors (mGluRs), the γ-aminobutyric acid receptor B (GABAB) and the calcium-sensing receptor (CaSR) (Fredriksson *et al.*, 2003). Similar to class B, class C have a large N terminal extracellular domain. At around 600 amino acids this is a large two lobed structure, named the “venus flytrap” domain, which

forms the ligand binding site for the small molecule activators such as amino acids and calcium ions (Cao *et al.*, 2009; Chun, Zhang and Liu, 2012). Although oligomerisation is a generally debated characteristic of the GPCR family in general (Milligan, Ward and Marsango, 2019), class C receptors are distinguished by being obligatory homo- or heterodimers, a characteristic that influences their structural integrity, trafficking and signalling (Ferré *et al.*, 2014). Two Family C GPCRs, although not complete structure, have been crystallised to date, mGlu1R and mGlu5R, both crystallised with allosteric modulators (Doré *et al.*, 2014; Wu *et al.*, 2014).

1.1.3Structural Characteristics of Class A GPCRs

GPCRs share a common three-dimensional structure of seven α-helical hydrophobic TM1-7 domains, connected to 3 intracellular (ICL 1-3) and 3 extracellular (ECL1-3) loops (Fig 1.1). This structure is flanked by an extracellular amino-terminus (N-terminus) and an intracellular carboxyl tail (C-terminus) (Palczewski *et al.*, 2000). While the structural architecture of the TM region is largely conserved, the diversity in GPCR sequences are most notable in the ECL and ICL regions. This is evident in the capacity GPCRs have to interact with a wide range of ligands that vary in size, shape and physicochemical properties (Basith *et al.*, 2018). Electron cryo-microscopy of 2D crystals of bovine rhodopsin suggested that the TM helices are arranged in a counter-clockwise formation with TM3 tilted towards the centre of the helical bundle (Unger and Schertler, 1995; Lee, Booe and Pioszak, 2015). This orientation was proposed from the first crystal structure of rhodopsin (Palczewski *et al.*, 2000), and confirmed by later structures (Ren *et al.*, 2016). An additional amphipathic helix (helix 8) is found, mainly with class A GPCRs, at the end of TM7 and through palmitoylation bonds with the lipid membrane lies parallel to the cytoplasmic face of the plasma membrane (Kirchberg *et al.*, 2011). The orthosteric ligand–binding site is a pocket in the extracellular side of the receptor TM region formed principally by TM3, TM5, TM6, and TM7 (Weis and Kobilka, 2018b).

In addition to the orthosteric binding pocket for small molecules within the TM domains, it has been shown that the extracellular loops, especially ECL2 can have a crucial role in ligand recognition, access and selectivity (Dror *et al.*, 2011; Kruse *et al.*,

2012; Zhang, Zhou and Cao, 2015; Emtage *et al.*, 2017). A distinctive feature of the extracellular region is the presence of disulphide bridges that contribute to receptor stability. The most highly conserved disulphide bridge, in most GPCR structures, is found connecting a cysteine residue at the top of TM3 with a cysteine in ECL2 (Wheatley *et al.*, 2012). This disulphide bridge tethers TM3 to ECL2 influencing receptor stability and integrity that limits receptor conformational changes (Venkatakrishnan *et al.*, 2013). The flexibility of the ECL controls the type of ligand that a GPCR can bind, and therefore its function as a whole. For example, lipophilic ligands that bind Class A GPCRs and conserved across the muscarinic family of receptors, may access the orthosteric site via sideways entry through the membrane, because a tyrosine "lid" (Tyr3.33, Tyr6.51, Tyr7.39 and Tyr7.43; using the Ballesteros-Weinstein numbering system (Ballesteros and Weinstein, 1995)). This lid, present in mAChRs, is formed by the TM domains, the N-terminus and ECL2 prevents direct entry from the extracellular fluid (Burger *et al.*, 2018). Other receptors, designed to bind hydrophilic ligands, have a different structure to their ECL2 in which the orthosteric site is only partially covered allowing entrance to the binding pocket (Venkatakrishnan *et al.*, 2013). The varying degrees of occlusion of the orthosteric binding site therefore affects the kinetics of ligand access and contributes to selectivity (Kruse *et al.*, 2012; DeVree *et al.*, 2016), for example, the difference between β1AR and β2AR whose binding sites are highly conserved (Latorraca, Venkatakrishnan and Dror, 2017).

Another key feature of the GPCR architecture is the presence of kinks in TM5-7, caused by the interruptions in the intrahelical hydrogen bonding at conserved proline residues (Pro5.50, Pro6.50, and Pro7.50 in β2-AR) (Weis and Kobilka, 2018b). This feature has been shown to be vital for the interaction between ligand binding and the global changes in conformation that is induced to achieve the active state. This is because the kinks lower the energy barrier allowing for greater conformational changes, as compared to TM3 which is straight with no kinks required to form the core of the receptor (Venkatakrishnan *et al.*, 2013). This network of kinks make contacts between TM3 (residues 3.32, 3.36) and TM6 (6.48, 6.51) and TM7 (7.39) forming the ligand binding "cradle"/binding site (Isberg *et al.*, 2015). Tyr6.48 on TM6 is part of the CWxP motif, which is critical during receptor activation, cause a kink in the intracellular

end of the TM6 helix so that it moves outwards from TM3 and towards TM5 (Bhattacharya, Hall and Vaidehi, 2008). The CWxP motif therefore links the conformation changes at the ligand-binding site to the intracellular conformational change.

Intracellularly the structure-function relationship changes into transducing the extracellular stimuli into an intracellular signalling pathway. It has been shown that ICL3 contains the major contact sites for the C-terminus to interact with the Gα subunit of the G protein (Cai, Itoh and Khorana, 2001; Hu *et al.*, 2010). Crystal structures of a GPCR with a Gα subunit C-terminal peptide confirmed the interaction of C-terminus of G protein with a GPCR (Scheerer *et al.*, 2008; Choe *et al.*, 2011). Further discussed in section 1.1.4.

It has also been shown that the TMs of GPCR can dictate whether these receptors signal as a homomer, heteromer or higher order oligomers (Ferré *et al.*, 2014). Interaction with TM4 and TM5, as well as, TM1 and TM7 have been identified as the possible dimerization interfaces (Mondal *et al.*, 2013; Ploier *et al.*, 2016; Dijkman *et al.*, 2018). The conformation GPCRs adopt can influence their intracellular signalling. This is most commonly known for the class C GPCRs, which from constitutive homo- or heteromers (Kniazeff *et al.*, 2011), however has also been identified in class A (Siddiquee *et al.*, 2013; Corriden *et al.*, 2014) and class B GPCRs (Harikumar *et al.*, 2012; Schelshorn *et al.*, 2012).

The physiological kinetics of the transition from the inactive state to an active state has been heavily investigated. Rhodopsin was found to have an activation time of 1-2ms (Lohse, Maiellaro and Calebiro, 2014). Fluorescent energy transfer (FRET) studies have also been able to show that a number of class A GPCRs (α2-adrenergic, β1-adrenergic and M2- and M3-muscarinic receptors) can activate within 30-50ms (Hoffmann *et al.*, 2005; Rochais *et al.*, 2007; Maier-Peuschel *et al.*, 2010; Vilardaga, 2011). GPCRs that function as a dimer, like the metabotropic glutamate receptor 1 (mGluR1) haven shown intra- and inter-subunit kinetics of 50ms and 30ms, respectively (Hlavackova *et al.*, 2012).

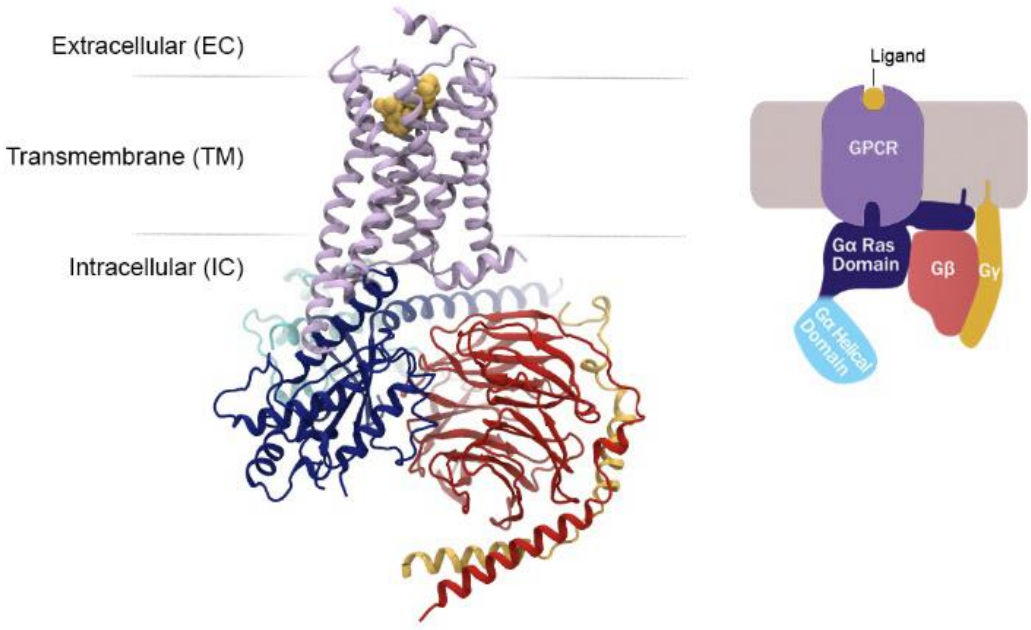


Figure 1.1: ***Structure of a 7 transmembrane G protein coupled receptor interacting with the G protein complex.***

1.1.4Activation Mechanisms of GPCRs

Historically, it was envisaged that GPCRs existed as a two-state model; inactive until an agonist bound inducing the receptor into an active conformation, which triggered a single G-protein type to initiate an intracellular signalling pathway. This was an idea based on using rhodopsin as a model receptor; however, the techniques used could not provide sufficient insights into receptor activation dynamics (Park, Lodowski and Palczewski, 2008). Additionally, it has been found that rhodopsin does not act in a stereotypical manner because of the cis-trans isomerisation of a tethered ligand (retinal) after photon absorption (Scheerer *et al.*, 2008; Choe *et al.*, 2011), and the way different retinal isomers stabilise the inactive and active states. It is now recognised that GPCR activation at a structural level is more complex than this. Receptor activation occurs across a spectrum of structural conformations (Manglik *et al.*, 2015; Latorraca, Venkatakrishnan and Dror, 2017) and that a single GPCR can activate multiple G-protein subtypes (Flock *et al.*, 2017), alongside other effectors, such as arrestins. Structurally distinct ligands have been shown to confer different receptor configurations through differential interaction with amino acids within the

binding site (Wess *et al.*, 2008). These ligand-specific conformational changes may then be responsible for differential activation of intracellular signalling pathways.

Upon ligand binding, class A GPCRs show the most prominent structural rearrangements at the intracellular coupling interface of TM5-7 with TM6, relative to TM3, rotating and swinging 14Å exposing the G-protein binding interface; while TM5 and TM7 having been shown to rotate inward (Rasmussen *et al.*, 2011). These movements occur due to ligand binding to the extracellular regions pulling them inwards, which subsequently moves the intracellular loops (Venkatakrishnan *et al.*, 2013). Movement of TM3, 5 and 6 play a vital role for downstream signalling. These helices facilitate the binding of effector proteins by creating the intracellular face of the receptor and thus the intracellular binding pocket for G proteins (Fig. 1.2).

The CWxP motif, conserved across the mAChRs, working in conjunction with the outward movement of the intracellular ends of TM6 (Glu6.30) away from TM3 (Arg3.50) and results in the breaking of the DRY motif "ionic lock", particularly Asn1.50 (TM1) and Asp2.50 (TM2); Arg3.50 (TM3). This causes a kink in the intracellular end of the TM6 helix so that it moves outwards from TM3 and towards TM5(Bhattacharya, Hall and Vaidehi, 2008). This goes on to form the G-protien binding site and interacts directly with the bound Gαs subunit (Weis and Kobilka, 2018a). However, with new data from crystal structures the importance of the DRY motif is now in question, because it is has shown "unbroken" within activated structures of β2-ARR (S. G. F. Rasmussen, Choi, *et al.*, 2011) and G protein bound β2-AR (Rasmussen *et al.*, 2011). In contrast, the mAChRs (and opioid) crystal structures show that there is no interaction involving this Arg3.50, instead a conserved Arg in ICL2 forms a salt bridge with Asp3.49 of the DRY motif in TM3 (Haga *et al.*, 2012; Kruse *et al.*, 2012). Alanine mutation of Asp3.49 and Tyr3.51 was shown to cause significantly reduced ligand efficacy and receptor expression, while alanine mutation of Asn2.39 resulted in normal ligand-binding properties (Huang *et al.*, 1999). Therefore, it is thought that Asn2.39 either directly stabilises the active conformation of the receptor, or engages in direct interaction with the G protein, while Asp3.49 and Tyr3.51 are thought to be critical for

maintaining a receptor conformation that will bind the ligand (Abdul-Ridha, Lane, Mistry, Laura López, *et al.*, 2014; Mahoney and Sunahara, 2016).

Another conserved motif, NPxxY, in TM7 also participates in forming the G protein-binding site. This motif does not directly bind the G protein, but is essential for formation the active conformation. In the inactive receptor, a hydrophobic barrier of TM2, TM3 and TM6 separates a water mediated hydrogen bond within the receptor TM domains and the DRY motif. The breakage of the hydrogen bond allows TM7 to rotate which in turns breaks the NPxxY interaction with helix 8 and connects the DRY motif to the cytoplasmic end of TM3 (Weis and Kobilka, 2018b).

Gα proteins are able to interact with the activated receptor through the C-terminal α helix, this structure determining the Gα selectivity, that binds to the newly opened TM3, TM5 and TM6 intracellular structures (Hamm *et al.*, 1988; Lambright *et al.*, 1994; Oldham and Hamm, 2008; Semack *et al.*, 2016). It has been found that across the number of G proteins expressed, residues that make contact with the α-subunit are found the cytoplasmic ends of TM2, TM3, TM5, TM7 and ICL2, ICL3 and TM8. Residues that make contacts to the G protein β-subunit are found in the cytoplasmic end of TM1, ICL1 and helix 8. Thus, virtually the whole receptor cytoplasmic face may be involved in coupling to any given G protein, with the exception of residues in TM4 (García-Nafría and Tate, 2019). The Gα C terminus alone constitutes 76% of the atoms making contact in the GPCR/G protein interface in the β2-AR-G_s crystal structure (Rasmussen *et al.*, 2011). Critically, the last three residues of the Gα C terminus are important for selective G protein activation (Conklin *et al.*, 1993). Three hot spot residues have been identified ($G\alpha_s$/$G\alpha_q$-Gln-384/Leu-349, Gln-390/Glu-355, and Glu-392/Asn-357) that together determine differential signalling through Gs- (see section 1.1.4.1.2) and Gq- (see section 1.1.4.1.1) coupled pathways (Semack *et al.*, 2016). This group was able to show that by swapping these residues, either individually or in combination, switches the agonist-stimulated G protein interaction in live cells.

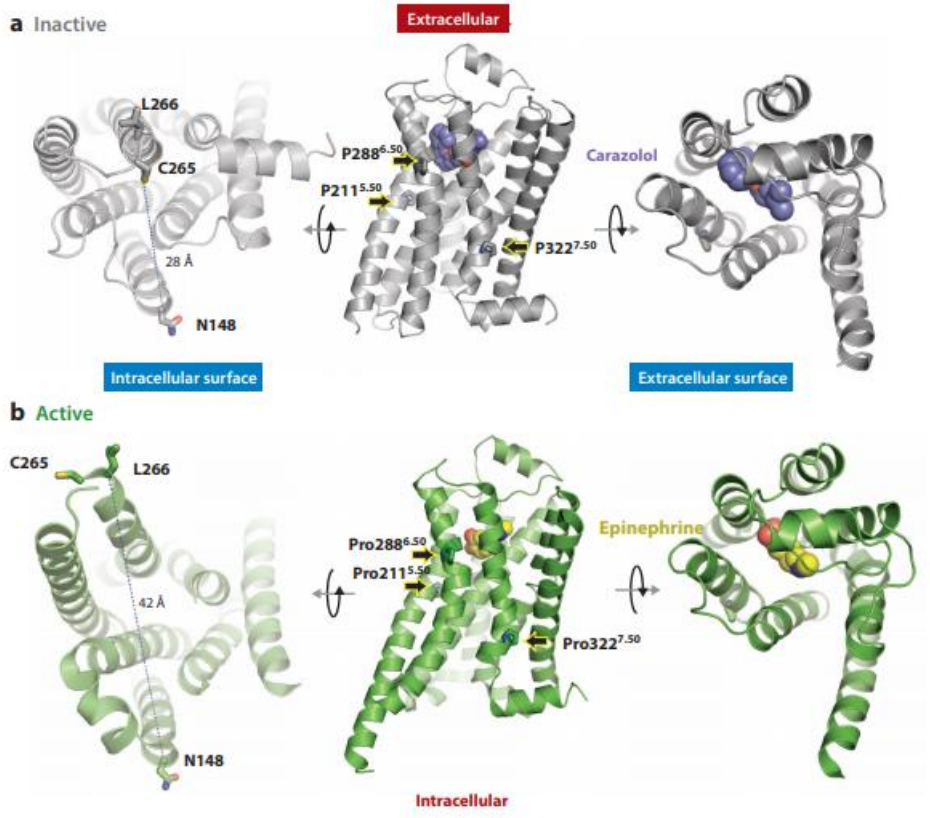


Fig 1.2: ***GPCR structure indicating the movement that occurs during receptor activation.*** *A) The inactive structure of β2-adrenergic receptor bound to carazolol and B) the active state of β2-adrenergic receptor bound to adrenaline. Highlighted are the conserved prolines and comparing active to inactive structures it can be seen that there is an opening of the G protein pocket upon receptor activation. Image taken from* (Weis and Kobilka, 2018b) .

1.1.4.1 G-protein dependent signalling

There are two principal classes of G proteins – the small monomeric class which are comprised of 3 main branches Ras, Raf and Rap which act as GTPases (Cherfils and Zeghouf, 2013) and the larger heterotrimeric G proteins. GPCRs activate heterotrimeric G proteins, utilising them as key molecular switches that transduce extracellular stimuli from the cell surface receptors, into cells and directly interact with intracellular signalling pathways (Milligan and Kostenis, 2009). A heterotrimeric G protein comprises of three separate subunits: Gα-, β- and γ-subunits. The α subunits of heterotrimeric G proteins are classified into four subfamilies based on the

homology of their amino acid sequences: Gq/11, Gs, Gi/o and G12/13. The Gβ and Gγ subunits remain tightly bound to one another as a constitutive heterodimer, and due to lipid modifications at their C-terminal are tethered to the inner leaflet of the plasma membrane (Escribá *et al.*, 2007). When inactive, these subunit are complexed together with Gα bound to guanosine diphosphate (GDP). Once activated, following ligand binding, the GPCR can activate its cognate G protein through the exchange of GDP for guanosine triphosphate (GTP). This causes the dissociation of Gα-GTP from the Gβγ complex. G protein activation is reversed through the hydrolysis of GTP to GDP at the Gα subunit, facilitated by the intrinsic GTPase activity of the Gα subunit in a self-limiting signalling process. A single receptor is capable of activating a large number of G proteins in this manner, which leads to the amplification of this signal to induce further cascades of secondary messengers.

The X-ray crystal structure of the β1 subunit in complex with Gαi1 revealed a bivalent interaction between Gα and Gβ, but no direct contact between Gα and Gγ (Wall *et al.*, 1995a; Sondek *et al.*, 1996), shown in Fig. 1.3. They were able to show the Gα subunit consists of an amino-terminal α helix, that connects to the Gβ subunit, followed by a Ras-like GTPase domain that control the subunit's conformation dependent on nucleotide binding. The GTPase domain has three flexible loops, named switch regions 1-3, whose conformations are dependent upon GDP or GTP binding. The helical domain contains six helices and is unique to the G protein subunit (Oldham and Hamm, 2008). Additionally, an independent domain was identified that forms the binding site for nucleotides and contributes amino acid involved in GTP hydrolysis. Later studies have shown receptor-mediated GDP release occurs by allosteric conformational changes of the C-terminus of Gα linked to the cytosolic core of the activated GPCR (Du *et al.*, 2019).

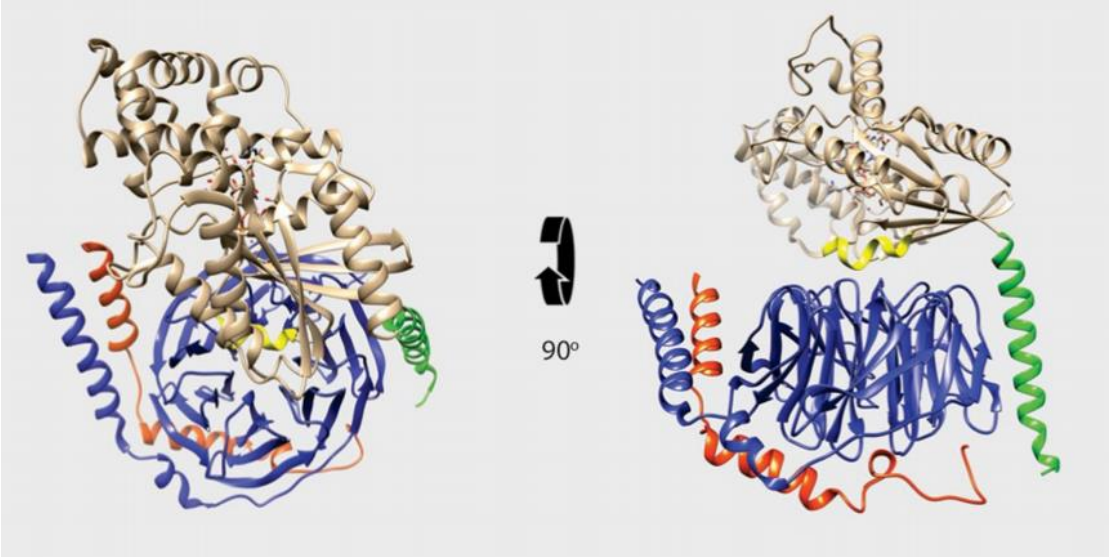


Figure 1.3: ***G-protein heterotrimer****. Ribbon diagram of the structure of the Gαi1β1γ2 heterotrimer; the Gβ subunit is shown in blue while the Gγ is shown is in red. The amino-terminal helix of Gαi1 is in green and the switch 2 helix of the Ras-like domain in Gαi1 is in yellow, with the remainder of Gαi1 shown in beige. Image taken from (Smrcka and Fisher, 2019a).*

G-protein β subunits are prototypical members of the WD40 repeat protein family (Neer *et al.*, 1994). WD40 repeat proteins have no known catalytic activity, but instead are involved in protein–protein interactions. As a WD40 protein, Gβ subunits fold into the characteristic toroid-like structure with 7 blades comprised of 4 antiparallel β sheets (Garcia-Higuera *et al.*, 1998). Binding of the Gβγ subunit complex has been shown to form constitutive dimers that have a number of unique characteristics. First, the dimer connects through an amino-terminal α helix of the Gβ, absent in other WD40 repeat proteins, through coiled-coil interaction with the γ subunit (Wall *et al.*, 1995b; Lambright *et al.*, 1996). The Gγ subunit is modified by prenylation and so determines the membrane association of the G protein by the dimer (Smrcka, 2008; Smrcka and Fisher, 2019b).

Mutagenesis studies have shown that deletion of the amino terminus of the Gα subunit prevents the formation of a stable complex with Gβ (Neer, Pulsifer and Wolf, 1988; Denker, Neer and Schmidt, 1992). GDP release results in a conformation change in the Gα subunit altering the switch 2 region of the Ras-like domain that connects with the β subunit toroid (Sprang, 1997). This reduces the already low affinity Gα has for Gβγ (Sarvazyan, Remmers and Neubig, 1998) resulting in the

subunit's dissociation. The Gα5 helix moves away from the nucleotide binding site allowing GTP to enter the binding site (Sprang, 2016). There have been reports that some G protein heterodimers do not always dissociate, and that the interaction between the Gα subunit amino-terminal can be associated with the Gβγ subunit during G protein activation (Galés *et al.*, 2006; Alvaro and Thorner, 2016). Interestingly, several recent cryo-EM structures of class B GPCRs have revealed contacts between regions of the C-terminal tail of the GPCR and Gβ subunits (Liang *et al.*, 2017, 2018; Zhang *et al.*, 2017; Zhao *et al.*, 2019).

In a recent structure of Rhodopsin, Gαiβγ2 was shown to bind between the Gα and Gβ subunits however, the authors highlight the fact no mutagenic studies evaluated the significance of these interactions; therefore, mechanistic studies are still required (Tsai *et al.*, 2019). Three main concepts as to the function of this interaction predict G proteins may bind to inactive receptors in order to increase specificity and improve coupling efficiency. The first suggests that the Gβ interaction with the C-terminus of the inactive receptor facilitates the interaction with receptor and the bound GDP (Galés *et al.*, 2006). Or, that the Gβ subunit remains transiently associated the C-terminus to facilitate the binding of downstream effectors which are within proximity of the receptor (Kan *et al.*, 2014). Finally, it has been shown that Gβγ is able to promote downstream signalling complexes in the Golgi apparatus potentially mediating signal transduction within the cell (Dupré *et al.*, 2009).

A recent discovery showed synthetic constructs comprising the Ras-like domain of Gα subunits, coined mini G, are capable of binding activated receptors in the absence of Gβγ, but are not capable of nucleotide exchange (Carpenter and Tate, 2016; Nehmé *et al.*, 2017; Wan, Okashah, Inoue, Nehmé, Carpenter, C. G. Tate, *et al.*, 2018). Two GPCRs have been crystallised with a partner G protein, utilising the mini Gs (Carpenter *et al.*, 2016) or mini Go (Tsai *et al.*, 2018), and have been comparable to structures determined by cryo-EM. The mini G proteins have a molecular weight less than 30kDa and recapitulate the receptor binding surface of the full length Gα. The main advantages of using mini-G proteins is the potential to use them in high-

throughput structure determination to stabilise active receptor states, in the absence of Gβγ subunits.

1.1.4.1.1 Gαq signalling

The Gαq subunit engages the phospholipase C (PLCβ) pathway in which phosphatidylinositol 4,5-trisphosphate (PIP2) is hydrolysed into inositol 1,4,5-trisphosphate (IP3) and 1,2-diacylglycerol (DAG) (Rhee, 2001). IP3 diffuses through the cytosol to bind to IP3 receptors releasing calcium from intracellular stores, while membrane-associated DAG activates protein kinase C (PKC), which in combination with intracellular calcium, further increases calcium release (Fig. 1.4) (Hall, 2000).

Recently the cryo–electron microscopy structure of M1 mAChR in complex with G11 (closely related to Gq) was described (Maeda *et al.*, 2019). In the active M1 mAChR, as compared to inactive, there is the outward movement of TM6 and a tilt of TM5 allowing the C-terminal helix of the α-subunit of the G protein to bind. The α5 helix and Ras domain of G11 are rotated ~15° away from TM5, as compared to M2 mAChR in complex with Go (Maeda *et al.*, 2019). It has been predicted that the rotational shift of M1-G11 may be due to strong interactions between ICL2 and the G protein. One distinctive feature discovered was the extended TM5 helix that interacts with the β6 strand and α4 helix of Gα11 interface, as well as, a polybasic cluster, of 11 residues, in the C-terminus that interacts with the G protein (Maeda *et al.*, 2019). These new structures highlight the importance of the TM5/TM6/α5 interface in G-protein selectivity determination in mAChRs.

1.1.4.1.2 Gαs signalling

When the Gαs subunit is activated, the enzyme adenylate cyclase is in turn activated. This catalyses the conversion of adenosine triphosphate (ATP) into cyclic adenosine monophosphate (cAMP), resulting in increased cytosolic cAMP levels. Four molecules of cAMP are required for binding to the cAMP-dependent protein kinase (Protein Kinase A; PKA). When PKA is activated, it acts by phosphorylating proteins at specific serine and/or threonine residues (Fig. 1.4).

A comparison between the structure of the inactive β2- adrenergic receptor (ARR) and the nucleotide-free β2-AR Gαs complex revealed ICL2 forms an α-helix and engages the hydrophobic pocket formed by the aN/b1 hinge, b2/b3 loop and F376 at α5 helix of the Gαs subunit. The outward movement of TM6 provides a space in the cytosolic core of the β2-ARR formed by ICL2 and TM3, 5 & 6 in which the C-terminus of Gαs can insert (Rasmussen *et al.*, 2011; Carpenter *et al.*, 2016; García-Nafría and Tate, 2019). In comparison to other G proteins, Gαs was shown to have the greatest movement in TM6 (at α2-ARR and β2-ARR), with the difference of 10Å from opsin coupled to mini-Go which showed the smallest TM6 movement (Carpenter *et al.*, 2016). Interestingly, there is a significant difference in the pattern of engagement of Gαs in Class A GPCRs compared to Class B GPCRs. In Class B GPCRs, the major interaction is between TM3 and the α5 helix of the α-subunit, with the equivalent number of interactions between H8 and the β-sheet of the β-subunit. However, it must be remembered that all these trends are based on only very few structures and this pattern may change, as more structures are determined (García-Nafría and Tate, 2019).

1.1.4.1.3 Gαi/o signalling

Gαi (1, 2, 3 isoforms), Go (A and B isoforms), Gz, two transducins (rod and cone), and gustducinare in the same subfamily of G proteins and it is usually assumed that if a receptor couples to Gαi then it will also couple similarly well to Gαo (García-Nafría and Tate, 2019). Most GPCRs preferentially couple to the Gαi family, and this subunit is the most abundantly expressed heterotrimeric G protein in most cell types (Draper-Joyce *et al.*, 2018). Gαi activation is associated with the inhibition of Gαs-induced AC signalling, and thus a reduction in cAMP levels intracellularly (Fig.1.4) (Bradley *et al.*, 2016). The Gαi subunit has also been implemented in activation of Rho signalling (Hirshman and Emala, 1999; Chiba, Sakai and Misawa, 2001), however the effects seen may actually be due to the G protein independent signalling of the βγ dimer (Thomas and Hoffman, 1996; Taussig and Zimmermann, 1998).

The structure of activated opsin was found using the mini Go (Tsai *et al.*, 2018). It was found that the active state structure was identical to the sixteen other structures of the active state of rhodopsin (Kang *et al.*, 2015). It therefore appears

that the ligand-bound receptor can adopt a thermodynamically stable conformation that is relatively unchanged upon G protein coupling (Tsai *et al.*, 2018; García-Nafría and Tate, 2019). It has been shown that in 5HT1b receptor bound to rhodopsin, the α5 helix of Gαo interacts with the TM6 of the receptor with fewer interaction with TM3, TM5 and Helix 8. The Gαi does not have this bias towards TM6 but tends to form a similar number of interactions with TM6 and Helix 8. In contrast, Gαi coupled to MOR acts as involved far more interaction sites with the receptor than with rhodopsin (García-Nafría and Tate, 2019).

1.1.4.1.4 Gα12/13 signalling

The Gα12/13 family are involved in cell proliferation and morphology. This α-subunit family interact with Rho guanine nucleotide exchange factors (RhoGEFs) that are thought to mediate these processes (Fig. 1.4) (N. Sugimoto *et al.*, 2003). The exact interaction sites of the Gα12/13 to the GPCR remains unclear, although it has been shown that the C-terminus of the G protein attenuates angiotensin (AT1), thrombin, and sphingosine-1-phosphate (S1P2/3) activation (Aragay *et al.*, 1995; Naotoshi Sugimoto *et al.*, 2003). The N-terminal short sequences of the G12 family, where G12 and G13 have low amino acid sequence homology, determines the selectivity of the G protein's coupling to receptors (Yamaguchi, Katoh and Negishi, 2003). Many GPCRs are reported to simultaneously couple to more than one G protein at one time (Hermans, 2003), and Gαq, especially, is thought to additionally couple to G12 and/or G13 (Riobo and Manning, 2005; Zhang *et al.*, 2006). Thus, it is complicated to evaluate the signalling of G12 or G13 with much specificity.

1.1.4.1.5 Gβγ subunit signalling

Early studies indicated only Gα-subunits were the only signalling molecule of the G protein subunits. However, it was shown that Gβγ regulate potassium channels (Fig. 1.4) and identified this heterodimer as a signal transducer as well (Logothetis *et al.*, 1987). Interestingly, it has been suggested that inhibition of Gβγ-dependent recruitment of GRK2 may be beneficial in heart disease patients, by preventing the desensitisation of β-arrestin (Campbell and Smrcka, 2018). Additionally, inhibition of Gβγ-regulated GRK2 activation reduced the desensitisation of α2-ARs, which occurs due to upregulation of GRK2 in heart failure (Kamal *et al.*, 2014).

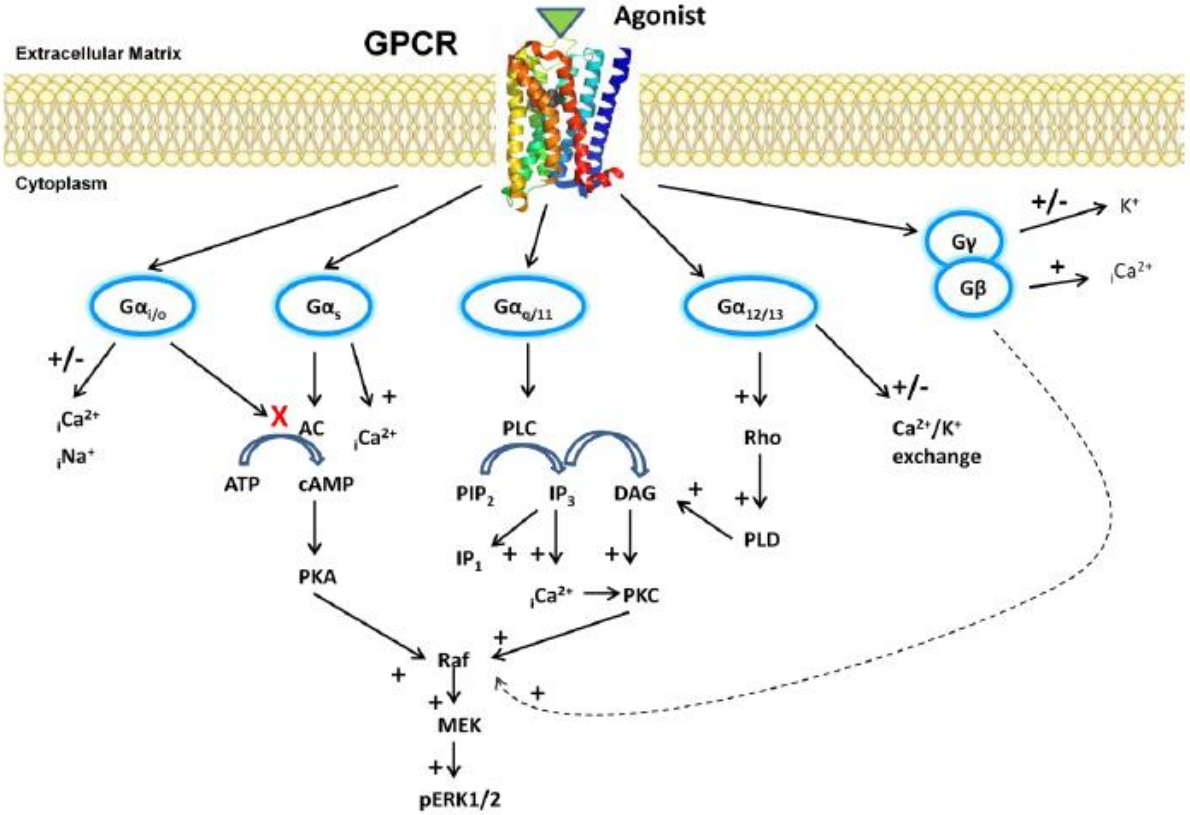


Figure 1.4: ***G protein dependent intracellular signalling pathways.*** *Gαi/o activation is associated with the inhibition of Gαs-induced adenosine 3',5'-cyclic monophosphate (CAMP) signalling, and thus a reduction in protein kinase C (PKC) activation. Gαs activation is associated with the increase in cAMP and the activation of the PKA that influences kinase cascades further downstream. Gαq activation engages the phospholipase C (PLC) pathway in which phosphatidylinositol 4,5-trisphosphate (PIP2) is hydrolysed into inositol 1,4,5-trisphosphate (IP3) and 1,2-diacylglycerol (DAG). IP3 then goes on to increase intracellular levels of calcium. G12/13 activation activates Rho signalling and further increases in DAG.*

1.1.5Termination of G protein signalling by β-arrestins

GPCR G protein signalling is terminated through the process of receptor desensitisation and internalisation (Fig. 1.5). This highly regulated process allows for high levels of spatial and temporal control of GPCR signalling. Heterologous desensitisation occurs independently of ligand binding, for example, shown to act via PKC in the M1 mAChR *in vivo* and *in vitro* (Uchiyama *et al.*, 1990; Haga *et al.*, 1996). PKC acts by phosphorylating sites on the ICL3 and C-terminus of the M1 receptor, specifically Thr354, Ser356, Ser451, Thr455 and Ser457 (Haga *et al.*, 1996). Homologous desensitisation, on the other hand, depends upon ligand-activated receptors and is mediated by β-arrestins. Similarly to homologous desensitisation, key serine and threonine residues of the C-terminus and intracellular loops are vital connection points, and are phosphorylated by G protein-coupled receptor kinases (GRKs) (Luttrell and Lefkowitz, 2002). GRK2 and GRK3 for example, are recruited to the plasma membrane by the active released Gβγ subunits of the G protein. Subsequently, β-arrestins bind the receptors due to their increased affinity for agonist occupied GPCRs in their phosphorylated conformation (Bayburt *et al.*, 2011; Vishnivetskiy *et al.*, 2011). It has been shown that in hippocampal neurones endogenous GRK6 regulates the phosphorylation-dependent desensitisation of M1 mAChRs, whereas GRK2 acts via phosphorylation-dependent and independent methods (Willets *et al.*, 2004; Willets, Nahorski and Challiss, 2005). Binding of β-arrestin to the activated receptor occurs via a phosphate sensor on β-arrestin that interacts with the phosphorylated C-terminus or IL3 of the receptor, while a conformational sensor recognises the agonist-induced active conformation of the receptor's core (Shukla *et al.*, 2013). Crystallography of mouse visual arrestin showed TM7 and helix 8 of the activated receptor recruits arrestin. This induces a conformational change, where the N- and C-terminus of arrestin rotates opening a cleft that binds the IL2 domain of rhodopsin (Kang *et al.*, 2015).

Once bound, β-arrestins sterically block G protein-receptor coupling (Krupnick *et al.*, 1997), therefore terminating any G protein mediated intracellular signalling

cascades. Biochemical data suggests the phosphorylated receptor is guided toward the polar core of β-arrestin, allowing the negatively charged phosphate to interact with the positive Arg169 of the β-arrestin-1 (Palczewski *et al.*, 1991; Vishnivetskiy *et al.*, 2000; Gurevich and Gurevich, 2006). The C-terminus of arrestin is then released allowing arrestin to act as a molecular scaffold by binding to components of the endocytic machinery (Goodman *et al.*, 1996). β-arrestin binds clathrin, dynamin and the β2-adaptin subunit of the AP-2 adaptor protein with high affinity forming a bond between the receptor-bound arrestin complex and the clathrin endocytic machinery. This engagement occurs through a number of binding motifs found on β-arrestin. The LIEFD motif on the C-terminus of arrestin binds clathrin (Kang, Tian and Benovic, 2014), while AP-2 binds via the C-terminal ([D/E]xxFxx) motif (Owen, Collins and Evans, 2004). These accessory protein sequester the receptor inside clathrin coated pits (Han *et al.*, 2001). Internalised receptors, influenced by the receptor's association with β-arrestin (Kendall and Luttrell, 2009), either undergo rapid dissociation from β-arrestin and recycling back to the receptor membrane (Class A GPCRs) or receptor degradation (Class B GPCRs) (Pavlos and Friedman, 2017).

It has been shown that receptor with greater affinity for β-arrestin2, such as β2-ARs, rapidly dissociate from each other following internalisation and re-sensitise to be recycled back to the plasma membrane (Kendall and Luttrell, 2009). Those receptors with equal affinity for β-arrestin1 and β-arrestin2 remain in complex (Luttrell and Lefkowitz, 2002), which after endosome sorting are slowly recycled or degraded by lysosomes (Kendall and Luttrell, 2009). This receptor downregulation functions to decrease the proportion of receptors at the plasma membrane thereby controlling the duration and magnitude of receptor-dependent intracellular signalling.

Arrestins are also capable initiating distinct signalling pathways, independently to G protein signalling (Luttrell *et al.*, 1999). β-arrestins scaffold mitogen-activated protein kinases , including extracellular signal-regulated kinase (1/2) (ERK1/2) in a distinct mechanism to that of G proteins. The β-ARRs act by sterically inhibiting G protein interaction with the activated receptor, thus removing G protein-dependent activation of ER (Smith and Rajagopal, 2016). Further sequestering ERK, β-ARRs also

scaffolds upstream in the kinase cascade including Raf-1 and MEK1 (Luttrell *et al.*, 2001).

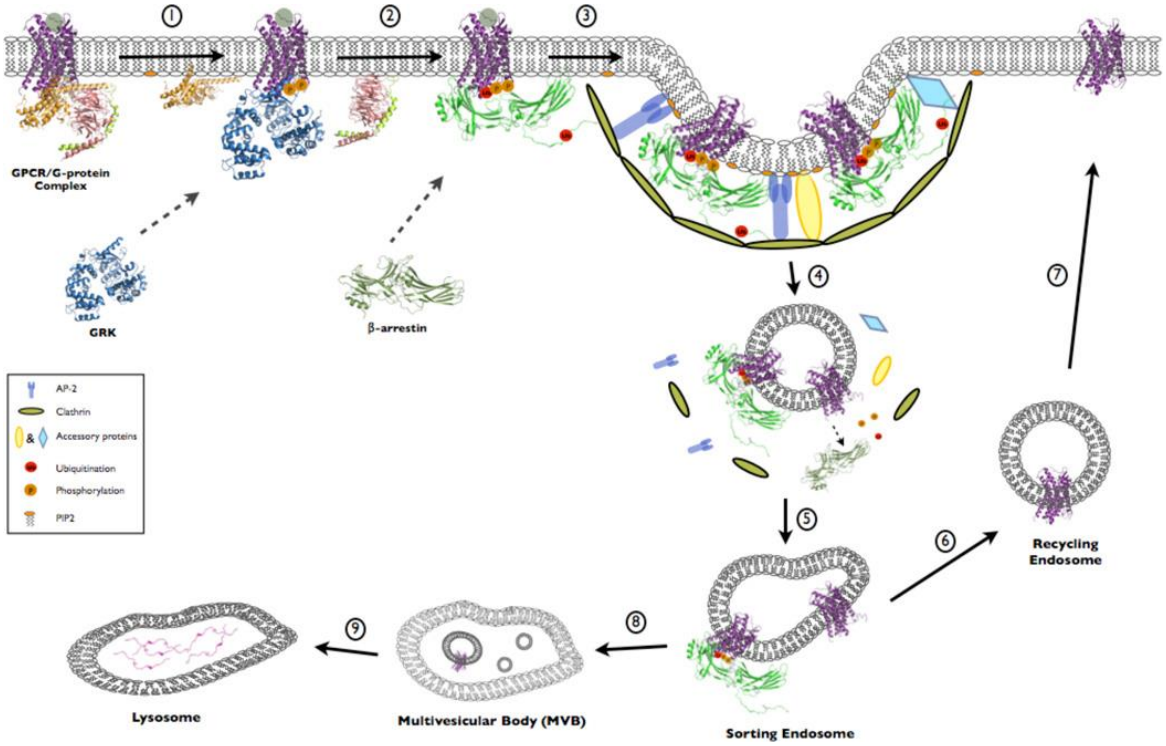


Figure 1.5: ***Agonist binding to a GPCR leads to a conformation change within the GPCR helical domains.*** *G protein coupled receptor kinases (GRKs) are recruited and phosphorylate key serine or threonine residues on the C-terminus of the receptor. This allows β-arrestin to bind, and in turn sterically blocks the G protein from coupling to the GPCR. β-arrestin acts as a scaffold for the receptor to be internalised and sequestered into the cell to either dissociate from the arrestin and recycle to the cell membrane or to be recycled and degraded. Image from* (Tian, Kang and Benovic, 2014).

1.2 Receptor Pharmacology

1.2.1Ligand Affinity

The equation to describe the interaction between a ligand and its receptor to form agonist ligand-receptor complex ([LR]) was first described, by deriving the Hill-Langmuir equation from the law of mass action (Hill, 1909, 1910). The equation is able to describe the complex concentration [LR], at equilibrium, as a functional total receptor concentration (R_T), concentration of ligand ([L]) and the ligand dissociation constant (K_D); the concentration of drug required to occupy 50% of the receptors.

$$[LR] = \frac{Rt\ [L]}{[L] + K_D}$$

1.2.2Ligand Efficacy

Agonist drugs not only have affinity for the receptor, but also the ability to initiate a conformational change to activate it and produce a response in a concept known as efficacy. Typically, the actions of agonists are measured using concentration-response curves to define their maximal effects (R_{max}) and potencies (EC_{50}, the concentration of agonist to produce 50 % of its R_{max}) (Figure 1.6). Agonists with sufficiently high efficacy may produce the maximum system response without occupying all the receptors. Low efficacy agonists have lower ability to shift the receptor equilibrium between inactive R to active R* states after binding. In some circumstances, low efficacy agonists can be revealed by their inability to produce the same R_{max} as a reference "full agonist", in which case they are described as partial agonists.

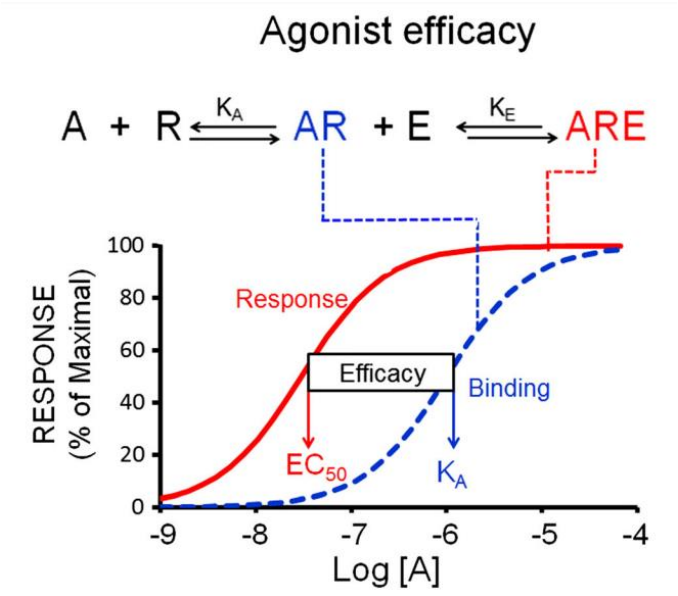


Figure 1.6: ***Agonist efficacy describes the initiation of a conformation change that activates a receptor to produce a response.*** *The agonist-bound receptor complex (AR) interacts with response elements (E) in the cell (for example G proteins). This equation describes that it is these new ARE complexes that cause the cellular response. Agonist efficacy is determined by the extent to which the agonist converts the receptor to an active conformation to engage downstream signalling within the cell (K_E). Since K_E also depends on the system's properties (including signal amplification) as well as efficacy, the concentration of agonist to produce 50 % maximal response (EC_{50}) can be much lower than that for 50 % receptor occupancy (K_A). Figure taken from* (Kenakin, 2016).

1.2.3 Receptor occupancy and its relation to affinity and efficacy

The concentration-response curve allows measurement of the maximum response and potency of a ligand in terms of R_{max} and EC_{50} within a functional assay. However, these measurements are not true affinity (K_D) or efficacy values and actually determine the ability of the ligand-receptor to initiate downstream signalling in a system-dependent manner (Lisa A. Stott, Hall and Holliday, 2016). Stott *et al.* highlight system parameters such as cell type, receptor expression levels, accessory proteins and signalling endpoints that significantly contribute to the functional response. Therefore, it is necessary to compare values across a range of different assay systems. One highly consequential parameter is receptor reserve. Agonists with high efficacy often produce the system's maximum response without the need to occupy all the receptors (Figure 1.5), leading to higher potencies (EC_{50}) compared to affinity (K_D). Equally, low efficacy can be obscured by signal amplification (Rang, 2006; Strange, 2009). Assays with high receptor reserve, such as reporter gene assays, display partial and full agonist as achieving the same R_{max} value because the low efficacy agonist can occupy proportionately more receptors and thus, appear equally efficacious to the high efficacy agonist (Lisa A. Stott, Hall and Holliday, 2016).

A further consideration in understanding G protein coupled receptor (GPCR) pharmacology is that the active conformation of the receptor is stabilised both by the agonist drug, and by the binding of the effector. Thus, the binding of the agonist is allosterically enhanced by the binding of the G protein to the receptor, for example, leading to the detection of high affinity (LRG) and low affinity (LR) receptor conformations for the agonist in binding experiments. This behaviour is described by the ternary complex model, which is considered in the context of allosteric ligands in section 1.4.2.2.

1.3 Muscarinic Acetylcholine Receptors

1.3.1General Overview

The muscarinic acetylcholine receptors are a family of five closely related class A GPCRs. The five different subtypes (M1-M5) are encoded by CHRM1-CHRM5, which are highly conserved throughout evolution and across species and receptor subtype (Hammer *et al.*, 1980; Bonner *et al.*, 1987; Caulfield, 1993).

The mAChR family can generally be subdivided into two groups based on their preference for G protein coupling efficiency. M1, M3 and M5 couple predominately to Gq/11 proteins upon ligand activation of the receptor (section 1.1.4.1.1). These receptors can be viewed as activators of signalling pathways that result in increased intracellular calcium release. M2 and M4 show preference for Gi/o protein coupling that acts as an inhibitory mechanism reducing cAMP signalling (section 1.1.4.1.3) (Caulfield and Birdsall, 1998; Wess, 2003). mAChRs are found in the peripheral nervous system, primarily on parasympathetic autonomic effector cells, as well as, in the ganglia and endothelial cells of blood vessels. These receptors are also highly expressed within the central nervous system (CNS). Structures such as the hippocampus, cortex and thalamus have high densities of muscarinic receptors (Tiwari *et al.*, 2013).

The endogenous ligand for mAChR is acetylcholine (ACh) (Picciotto, Higley and Mineur, 2012). ACh is a fast-acting neurotransmitter at the neuromuscular junction and in the autonomic ganglia (Changeux, 2010). ACh has been described to act more as a neuromodulator within central cholinergic neurotransmission due to its role in modulating neuronal excitability, triggering presynaptic release of neurotransmitters, and coordinating the firing of groups of neurones (Wonnacott, 1997; Rice and Cragg, 2004; Zhang and Sulzer, 2004; Kawai, Lazar and Metherate, 2007). Specifically, ACh can alter the firing of neurones on a rapid time scale which results in direct cholinergic activation, and thus has been implicated to play a role in memory and learning (Letzkus *et al.*, 2011). Specifically, ACh signalling has been shown to improve the "signal-to-noise" ratio in a learning paradigm *in vivo,* which had a positive enhancement on learning outcomes (Yu and Dayan, 2005). Another model showed

ACh reinforces neuronal signalling pathways and cortical activity during learning, thereby enhancing sensory learning and improving memory retrieval (Hasselmo, 2006).

1.3.2 Localisation of mAChRs in the Brain

The M1 mAChR subtype is the predominant receptor in all major areas of the forebrain, including the hippocampus, cerebral cortex, corpus striatum and thalamus, representing up to 60% of total receptors expressed (Levey, 1996; Volpicelli and Levey, 2004). The M1 knockout (KO) mice demonstrated increased locomotor activity associated with cognitive deficits and impairments in long-term potentiation (Miyakawa *et al.*, 2001). Further studies in KO animals show a series of cognitive deficits and impairments in long-term potentiation, indicating that the M1 subtype is physiologically linked to multiple functions such as synaptic plasticity, neuronal excitability, neuronal differentiation during early development, and learning and memory (Roth and Krochmal, 2018). Cortical M1 receptors localise post-synaptically in all layers of cortical pyramidal cells, with layers II, III and VI showing enriched expression (Galvin, Arnsten and Wang, 2018).

M2 mAChRs are expressed abundantly in non-cholinergic neurones projecting to the hippocampus and neocortex (Eglen, 2012). In the caudate-putamen, M2 mAChRs act as inhibitory modulator to dopaminergic terminals, and have been implicated as a target for disorders associated with excessive dopamine neurotransmission such as schizophrenia (Rasmussen *et al.*, 2001). Studies in M2 mAChR deficient mice indicate these receptors mediate cognitive and bipolar depressive disorders due to their involvement in hippocampal cholinergic neurotransmission (Cannon *et al.*, 2011; Jeon *et al.*, 2015).

The majority of M3 mAChRs are expressed in the hypothalamus (Levey *et al.*, 1994; Oki *et al.*, 2005). M3 KO mice consistently show a dwarf phenotype (Wettschureck *et al.*, 2005) due to a significant decrease in hormone secretion necessary for normal growth patterns and bone mass (Gautam *et al.*, 2008). KO mice also show reduced food intake and thus lower body weight (Yamada *et al.*, 2001).

As opposed to M1 mAChRs, M2 and M3 subtypes are located primarily in the periphery such as in the heart, smooth muscle, gastric system and salivary glands (Abrams *et al.*, 2006).

M4 mAChR is co-localised with dopamine receptors in the corpus striatum (Eglen, 2012). There is less known about the relevance of this subtype due to the overlapping expression pattern with the M2 but has been shown to be involved in the regulation of dopamine release in neurones (Zhang *et al.*, 2002). M4 mAChR deficient mice have been shown to exhibit locomotor activating and an enhancement of D1 dopaminergic effects (Gomeza *et al.*, 1999).

M5 mAChRs predominately express in the pars compacta of the substantia nigra and the ventral tegmental area (Levey, 1993; Felder *et al.*, 2000). Both areas relate to dopaminergic innervation of the limbic system. These brain regions are well known to be involved in the reward system of drugs of abuse (Berizzi *et al.*, 2016).

1.3.3Therapeutic potential in the CNS

1.3.3.1 Alzheimer's Disease

Alzheimer's Disease (AD) is the most commonly diagnosed form of dementia and currently affects approximately 35 million individuals worldwide (Foster *et al.*, 2014). AD is a progressive neurodegenerative disease that is characterised by a host of cognitive deficits, including impairments in learning and memory. Additionally, the disease causes behavioural disturbances, anxiety, depression, and psychosis (Desai and Grossberg, 2005). Age is the primary risk factor for AD, and the disease usually presents in individuals over the age of 60 years. The hallmarks of AD pathology are the accumulation of amyloid-beta (Aβ) peptide aggregates (neurotic plaques) and hyperphosphorylated tau protein (neurofibrillary tangles) (Hardy and Higgins, 1992; Tanzi and Bertram, 2005; Pakaski and Kalman, 2008).

It has been reported that in AD brains there is a reduction of ACh synthesis, as well as, a significant loss of cholinergic neurones and the malfunctioned cholinergic neuronal and axonal signalling (Jiang *et al.*, 2014a). There is strong evidence to

suggest that the cholinergic system is not only effected by AD, but due to its disordered signalling, plays an interconnected role in the formation of Aβ plaques. Aβ is derived from β-amyloid precursor protein (APP), through sequential cleavages by β- and γ-secretases. APP is cleaved by β-secretase (BACE1) to generate sAPPβ and the membrane bound APP C-terminal fragment-β (Thinakaran and Koo, 2008). This membrane bound APP can be further cleaved to generate Aβ and APP intracellular domain. The activation of M1 mAChRs has been shown to enhance sAPPα and reduces Aβ production (Jones *et al.*, 2008). PKC, activated by M1 mAChR, promotes the activity of α secretase and trafficking of APP to the cell surface. Therefore, with the loss of M1 mAChRs in the brain there is an increase in APP in neurones and promotes brain Aβ plaque pathology as shown in numerous mouse models of AD (Davis *et al.*, 2010).

The current primary treatment for AD are acetylcholinesterase inhibitors (AChEIs), such as galantamine, donepezil, tacrine and rivastigmine (Reichman, 2003). These drugs aim to potentiate cholinergic signalling by reducing enzymatic degradation of ACh in the synaptic cleft (Birks, 2006; Muñoz-Torrero, 2008). These treatments have been found to be efficacious in improving cognitive and psychiatric symptoms, however there are a number of cardiovascular and gastrointestinal side effects mediated by peripheral AChRs (Foster *et al.*, 2014). This is also a common limitation to potential new therapeutics targeting the orthosteric site due to mAChRs level of sequence conservation, highlighted in Table 1.3.

ORTHOSTERIC AGONIST	POTENTIAL ROLE IN AD	LIMITATIONS
XANOMELINE	Improves cognition and reduces psychotic symptoms in both preclinical and clinical studies.	Failed during Phase II clinical test due to dose dependent side effects - nausea and diarrhoea.
TALSACLIDINE	Enhances non-amyloidogenic processing of APP and decreases CSF Aβ level in AD patients	Discontinued due to side effects - sweating and salivation.
AF102B	Reverses cognitive impairments at low dose and reduces CSF Aβ in AD patients. The first drug to have shown such effects in human patients.	Discontinued due to side effects – gastrointestinal diaphoresis, confusion, diarrhoea, and asthenia.
AF267B	Improves cognitive function, decreases Aβ, hyperphosphorylated tau, and BACE1 levels in AD mice.	Inactive in clinical trial and discontinued due to peripheral side effects.
WAY-132983	Enhances performance memory and cognition in animal models.	Discontinued due to peripheral side effects.

Table 1.3: ***M1 mAChR orthosteric agonists based drugs for AD treatment.*** *A number of orthosteric drugs have been designed with the promise of therapeutic success in ALZ patients. However, due to off-target effects in the periphery such drugs had to be discontinued* (Jiang *et al.*, 2014b).

1.3.3.2 Schizophrenia

Schizophrenia (SZ) is a severe and debilitating psychiatric disease that affects approximately 1% of the population (Bhugra, 2005). Patients experience three classical symptom clusters: positive symptoms, negative symptoms and cognitive impairments (Stępnicki, Kondej and Kaczor, 2018). Current treatments include typical (haloperidol and chlorpromazine) and atypical (risperidone and clozapine) antipsychotics, which act on the dopaminergic system (Foster *et al.*, 2014). These

treatments are not very effective and show little to no efficacy in addressing cognitive impairments (Foster, Jones and Conn, 2012; Hüfner, Frajo-Apor and Hofer, 2015).

Multiple lines of evidence suggest that increasing cholinergic signalling, through both muscarinic and nicotinic AChR activation could be beneficial in SZ. Post-mortem studies of SZ patients have shown a decrease in mAChR expression levels in a number of brain regions (Crook *et al.*, 2000; Katerina *et al.*, 2004). Non-selective muscarinic antagonists induce symptoms associated with SZ in healthy humans and exacerbated existing symptoms in SZ patients (Osterholm and Camoriano, 1982; Tandon *et al.*, 1991; Melancon *et al.*, 2013). On the other hand, increasing cholinergic signalling using AChEI can improve cognitive performance (Feldman *et al.*, 2007). Specifically, the M1 mAChR is suggested to play a role in schizophrenia (Wess, Eglen and Gautam, 2007; Scarr *et al.*, 2013; Andrew C Kruse *et al.*, 2014). In patients with SZ, compared to age-matched controls, post-mortem binding sites showed decreased levels of M1 in the prefrontal cortex, caudate putamen, hippocampus and superior temporal gyrus (Dean *et al.*, 2002; Katerina *et al.*, 2004; Deng and Huang, 2005; Dean, Copolov and Scarr, 2016). This result was correlated with increased efficacy of Gαq/11 coupling to M1 mAChR (Salah-Uddin *et al.*, 2009), indicating adaptive changes of the receptor. It was also shown that these changes in M1 mAChR levels were not found in patients with bipolar disorder or major depression (Katerina *et al.*, 2004), thus M1 mAChR may have a specific role in SZ over general neuropsychiatric disorders.

The M1/M4 preferring agonist xanomeline (Table 1.3) progressed the furthest in clinical development. Although designed as a treatment for AD, the phase II trial failed to reach statistical significance in improving cognitive abilities, however the study showed a robust therapeutic effect on psychotic symptoms (Bodick, Offen, Levey, *et al.*, 1997; Bodick, Offen, Shannon, *et al.*, 1997). Xanomeline was then tested with SZ patients, and showed improvements in both the positive and negative symptoms, as compared to the placebo group. Therapeutic effects of xanomeline were statistically significant after one week of treatment as opposed to the multi-week delay observed with typical antipsychotics (Shekhar *et al.*, 2008). Adverse effects, particularly

gastrointestinal-related, were observed with xanomeline that caused it to be removed from general clinical use.

1.3.3.3 Parkinson's Disease

Finally, Parkinson's Disease (PD) is another therapeutic area where M1 mAChR signalling has been implicated. PD is a neurodegenerative disorder with symptoms related to movement: muscular rigidity, bradykinesia and a lack of balance (Noyce and Bandopadhyay, 2017). This is caused by the death of dopaminergic neurones projecting from the pars compacta of the substantia nigra to the caudate putamen that target cholinergic interneurones (Gibb and Lees, 1991; Paulus and Jellinger, 1991). The gradual decrease in dopaminergic signalling results in unregulated striatal acetylcholine signalling producing the movement disturbances (Ding *et al.*, 2006; McKinley *et al.*, 2019). Disturbances in cholinergic signalling also produces dementia in addition to the Parkinson's disease. Post-mortem (Ruberg *et al.*, 1982) and neuroimaging studies (Asahina *et al.*, 1998), were able to show there were increased levels of cortical muscarinic receptors in patients' with PD (Katzenschlager *et al.*, 2002). Recent studies have identified M1 mAChR to play a role in the disease. It was found the M1 mAChRs were significantly reduced in the caudate from people with Parkinson's disease (Piggott *et al.*, 2003). The M1-selective antagonist VU0255035 partially reversed some movement disturbances (akinesia and catalepsy) in rats (Xiang *et al.*, 2012). Treatment of PD is still in need of improvement, unfortunately it is not possible to use AChEI to combat the PD-related dementia, as this would exacerbate the motor symptoms (Wess, Eglen and Gautam, 2007).

1.4 Allosteric Modulation of GPCRs

1.4.1General Overview

Allosteric modulation (AM) was first described following studies that highlighted the fact enzymes possessed distinct binding pockets with differing affinities for ligands (Jacob and Monod, 1961; Monod, Changeux and Jacob, 1963; Monod, Wyman and Changeux, 1965). Monod *et al.*, were able to show enzymes possess two or more different binding sites, which were topographically distinct, and once substrates bind

underwent global conformational changes that altered the biological activity of the protein (Monod, Changeux and Jacob, 1963; Monod, Wyman and Changeux, 1965). This field of research has expanded over time, with allosteric sites being identified throughout the GPCR receptor family. Now, the term allosteric is related to any binding site on a receptor that is topographically distinct to that of the endogenous orthosteric binding site (Kenakin and Miller, 2010; Canals *et al.*, 2012a; Melancon *et al.*, 2012; Christopoulos, 2014; Changeux and Christopoulos, 2016). In fact, allostery has also been identified in ligand-gated ion channels, voltage-gated ion channels, nuclear hormone receptors and receptor tyrosine kinases (Changeux and Christopoulos, 2016).

Theoretically, any binding pocket in a protein that is topographically distinct from the orthosteric site can be regarded as a latent allosteric site. However, pure allosteric modulators (no efficacy at the receptor) do not compete with the orthosteric ligand, as the two ligands do not have overlapping binding sites (Zhang *et al.*, 2010; Wootten, Christopoulos and Sexton, 2013). Allosteric modulators act by promoting a conformational change in the receptor that manifests in changes in the affinity and/or efficacy of the orthosteric-bound ligand. In this way, allosteric modulation can directly activate or inhibit receptor signalling. Moreover, allosteric binding sites are generally less evolutionally conserved than orthosteric sites (Yang *et al.*, 2012; Lu *et al.*, 2014), therefore they have the potential to act as receptor subtype selective compounds and reduce off-target toxicity (Nickols and Conn, 2014; Hauser *et al.*, 2017).

1.4.2Allosteric Binding Models

The mAChRs have at least one allosteric site located in an extracellular vestibule (ECV) of the receptor, 15Å above the orthosteric site (Fig. 1.7). Numerous allosteric modulators that bind at this ECV site have been identified (Shirey *et al.*, 2009a; Yang *et al.*, 2010; Kruse *et al.*, 2013). The M2 mAChR has been crystallised with the PAM LY2119620, which was able to show the ECV allosteric site was surrounded by TM2, TM6 and TM7 and ECL2 (Gannon and Millan, 2012; Kruse *et al.*, 2013). Mutation of the M1 mAChR at W7.35 or Y45.51 of the ECL2 inhibits the PAM BQCA to bind or its highly M1-selective parent BQZ12 (Abdul-Ridha *et al.*, 2014).

The determination of allosteric binding sites has successfully improved understanding of how these ligands function (Thal *et al.*, 2016). However, there is still a significant amount of work required to fully understand the structure-function of the allosteric site within GPCRs, and little is known about specific aspects of protein design that can predict effective allosteric regulation. Biological data is still required to investigate the effects on affinity/efficacy and probe dependence. A number of mathematical models aim to quantify the effects of allosteric binding and its cooperativity to the orthosteric ligand, and are able to sub-categorise a number of allosteric ligands.

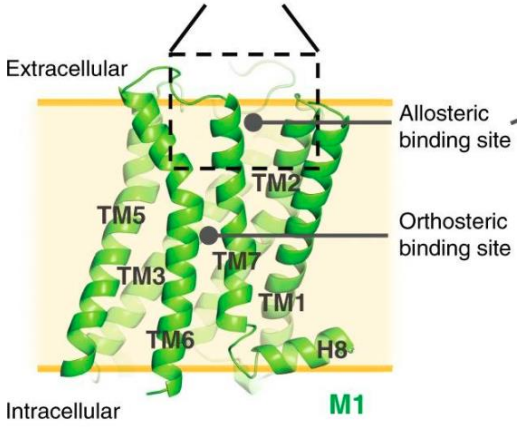


Figure 1.7: ***M1 mAChR structure indicating the position of the allosteric binding site, above the orthosteric binding site.*** *The common M1 allosteric binding site is proposed to the extracellular vestibule of this GPCR.*

1.4.2.1 Monod-Wyman-Changeux Model

The classical Monod-Wyman-Changeux (MWC) model explained allosteric modulation as the binding of either orthosteric or allosteric ligand eliciting a reversible conformational change on the receptor that favours the topographically distinct ligand to bind. This MWC model was first used to assess the allosteric interactions of haemoglobin within its four subunit complex, to account for the co-operative effects of oxygen binding to each subunit (Monod, Wyman and Changeux, 1965). This model assumes the two different ligands (e.g. oxygen molecules) bind without having direct interactions with each other (Kenakin and Miller, 2010). The allosteric modulator induces its allosteric effects via conformational change in a reversible manner.

1.4.2.2 Allosteric Ternary Complex Model

Simultaneous binding of both ligands can be described by the allosteric ternary complex model (Christopoulos and Mitchelson, 1997; Christopoulos and Kenakin, 2002). Under this model, allosteric ligands have the ability to promote conformational changes in the receptor that alter the affinity of the orthosteric-bound ligand. These changes can be positive (PAMs; positive allosteric modulators) which enhance orthosteric ligand affinity for the receptor, or negative (NAMs; negative allosteric modulators) which decrease orthosteric ligand affinity (Fig 1.8). There are also neutral allosteric ligands (NALs), which bind the allosteric site but do not affect orthosteric ligand's activity. This reciprocal binding is known as ligand cooperativity (May *et al.*, 2007), and is highly dependent on the chemical properties of the allosteric ligand, thus can differ widely between the receptor and ligand being investigated (Jakubík *et al.*, 1997; Congreve, Oswald and Marshall, 2017).

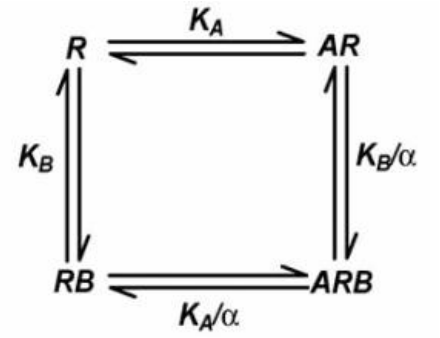


Figure 1.8: ***The Allosteric Ternary Complex Model*** *describes a receptor (R) and orthosteric ligand's (A) interaction in the presence or absence of an allosteric modulator (B). Receptors and orthosteric ligand can bind to from AR complex, with a dissociation constant K_A. Alternatively, the allosteric modulator can bind with the receptor to from RB; K_B. These two complexes can now bind the third component to form a stimulating ternary complex ARB. Cooperativity is denoted by α and can be positive α>1 (PAM) or negative α<1 (NAM). Image taken from* (Canals *et al.*, 2012a).

The idea of the cooperativity factor, which is a measure of both the magnitude and direction of the allosteric effect, explains that the orthosteric ligand can modulate the binding of the allosteric ligand in the same manner and extent as the allosteric towards the orthosteric site. However, this model assumes the allosteric site is only a non-overlapping site to that of the orthosteric. This is at odds to the presumed

mechanism for many ECV modulators, in that they provide steric hindrance of the orthosteric ligand to the extracellular environment due their binding location above the orthosteric binding site (Bindslev, 2013).

However, this model also assumes that the binding of the allosteric ligand only modulates the affinity of the orthosteric ligand (Gregory, Sexton and Christopoulos, 2007). Logically, the conformational change may also be able to alter signalling efficacy, in addition to or independently of affinity, and biological data proves this and shows allosteric modulators can also have their own intrinsic efficacy (Kenakin, 2007). To account for such, the allosteric two state model was designed (D. A. Hall, 2000).

1.4.2.3 Allosteric Two State Model

This model describes the allosteric ligand effects on affinity, efficacy and the ability to modulate orthosteric ligands across active and inactive receptor states (Fig 1.9). Thus, this particular model provides a way to describe the wide array of allosteric modulator effects on receptor binding and functional properties (Gregory, Sexton and Christopoulos, 2007). Advantageously, this model allows for investigation of allosteric agonism at a receptor that is not occupied by an orthosteric ligand (Keov, Sexton and Christopoulos, 2011), however this model remains more of a theoretical modelling system as a number of the parameter are experimentally difficult to measure. In addition GPCRs do not exist within a strict two-state model, active vs. non-active, and can adopt a multitude of conformations (Urban *et al.*, 2007)

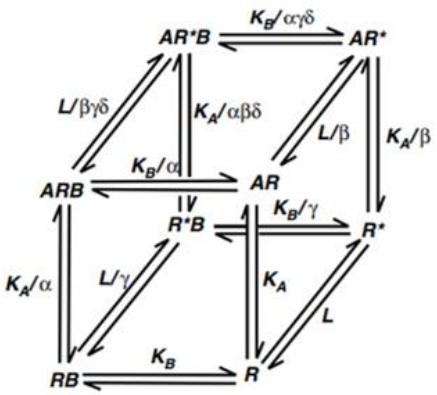


Figure 1.9: ***The allosteric ternary complex model was expanded to encompass inactive (R) vs active (R*) receptor conformational states.*** *The isomerisation of*

receptors between states is denoted by L, α denotes binding cooperativity, δ denotes the activation cooperativity and intrinsic efficacy of the orthosteric (β) and allosteric (γ) ligands. Image taken from (Canals *et al.*, 2012a)

1.4.3M1 mAChR Allosteric Modulators

The first generation of M1 mAChR allosteric modulation included AC-42 (Langmead *et al.*, 2006; Spalding *et al.*, 2006). This first-generation allosteric modulator was an important tool in cell-based assay; however, a lack of physiochemical properties did not allow this to progress into animal models. Second-generation allosteric modulators are more suitable for *in vivo* investigations, and now include allosteric agonists and PAMs. Further optimisation identified VU6004256 which was shown to attenuate prefrontal cortical cognitive defects in a NMDAR mouse model (Grannan *et al.*, 2016). Moreover, the M1 mAChR PAM VU0453595 was able to restore impaired long-term depression in the prefrontal cortex, following NMDAR antagonism (Ghoshal *et al.*, 2016). It was also shown that VU0486846 displayed high potency in a working memory evaluation on wild-type mice, which was able to overcome the cognitive defects seen by the antipsychotic risperidone (Rook *et al.*, 2018). In mice with scopolamine-induced cognitive deficits, the M1 PAM PQCA, was able to improve memory and spatial working memory, as well as, cerebral blood flow which is often limited in conditions such as AD and ischemic brain injury (Uslaner *et al.*, 2013).

In fact, three highly selective M1 PAMs, MK-7622, VU-319, and TAK-071, have been advanced to clinical testing in patients with cognitive disorders (see ClinicalTrials.gov Identifiers NCT01852110, NCT03220295, and NCT02769065). Therefore, it is clear that allosteric modulators, particularly those selective for M1 mAChR, are a promising target to develop new therapeutics for diseases related to cognitive decline.

1.4.3.1 BQCA is a promising M1 mAChR allosteric modulator

Benzyl quinolone carboxylic acid (BQCA) has been highlighted as a selective allosteric modulator, which has been shown to be a valuable tool in *in vivo* and *in vitro* studies (Ma *et al.*, 2009). It has previously been suggested that BQCA behaves according to

the MWC model at the M1 mAChR (Canals, Sexton and Christopoulos, 2011; Canals *et al.*, 2012b). For example, BQCA exhibited positive cooperativity with orthosteric agonists and negative cooperativity with antagonists/inverse agonists expected to promote the inactive receptor conformation (Canals *et al.*, 2012a; Abdul-Ridha *et al.*, 2013a). BQCA has been shown to play a role in the improvement of cognitive function in mice models by increasing the firing rate of neurones (Shirey *et al.*, 2009b), reversing hippocampal deficits due to a non-selective antagonist (Ma *et al.*, 2009; Chambon *et al.*, 2012) and can overcome amphetamine-induced memory disruptions (Gould *et al.*, 2015).

BQCA has been shown to bind within the ECV site and is separated from the orthosteric binding site by a shelf of aromatic residues (Abdul-Ridha, López, Keov, David M Thal, Mistry, Sexton, Lane, *et al.*, 2014). The residues that were predicted to form the BQCA binding pocket were identified in the ECL2 (Y179), TMII (Y85) and TMVII (W4007.35). Residues that abolished BQCA cooperativity with carbachol were found by alanine substitution of F182 (ECL2), E397 and E401 (TMVII) (Abdul-Ridha, López, Keov, David M Thal, Mistry, Sexton, Lane, *et al.*, 2014). W400 was the only residue that alanine substitution resulted in a complete loss of modulation of carbachol binding and cooperativity. Equivalent residues have been implicated in the binding of several allosteric ligands, including gallamine at the M1 mAChR (Marquer *et al.*, 2011), gallamine at M2 mAChR (Voigtländer *et al.*, 2003; Huang *et al.*, 2005) and LY2033298 at M4 mAChR (Nawaratne *et al.*, 2010). Newer M1 mAChR allosteric modulators PF-06767832 (Davoren *et al.*, 2016), VU6004256 (Grannan *et al.*, 2016) and MIPS1780 (Mistry *et al.*, 2016) have also verified the importance of this allosteric binding site and its residues. It was shown that the Y82$^{2.61}$A mutation reduced binding cooperativity with these modulators in the presence of [^{3}H]NMS but not ACh, indicating this residue's importance in antagonist cooperativity but not with the agonist (E Khajehali *et al.*, 2018).

The aromatic residues that neighbour the allosteric site form cation-π interactions with the allosteric modulator (Dror *et al.*, 2013). These aromatic residues strength the cation-π interactions and enhance the binding affinity of the allosteric ligand.

Specific mutations of selective residues have been shown to have differential sensitivity in the reduction it produces in affinity or cooperativity (E Khajehali *et al.*, 2018). Thus, it has been suggested that although there is a common shared allosteric site, the differences between allosteric modulators depends on their adoption of different poses within the site.

1.4.4Bitopic Ligands

The number of models that aim to quantify allosteric modulation suggest that allosteric modulators can be further subdivided based on their behaviours. For example, whether they influence affinity or efficacy, whether they act as allosteric agonists or antagonists or whether they function as an allosteric ligand (no efficacy at the receptor) or dualistically (influencing the orthosteric ligand while having their own intrinsic activity) (Digby *et al.*, 2012).

There are an increasing number of M1 mAChR bitopic ligands, including TBPB, GSK1034702 and VU0357017. TBPB has been shown to act as a selective M1 agonist able to potentiate NMDA signalling in rat hippocampal neurones, promotes amyloid processing and elicits antipsychotic-like behaviour in rodent models of schizophrenia (Jones *et al.*, 2008). TBPB is interesting as the mutated M1 DREADD receptor (see section 1.4) did not show a difference in this bitopic ligand's binding affinity or potency, as compared to the wild type receptor (Keov *et al.*, 2014). It has been suggested that TBPB is capable of activating the M1 mAChR at a binding site that is subtly distinct from prototypical orthosteric ligands (Sophie J. Bradley *et al.*, 2018).

GSK1034702 interacts in a bitopic manner at the M1 mAChR (Sophie J. Bradley *et al.*, 2018), and has been implicated to improve memory encoding during a double-blind, placebo-controlled study using the nicotine abstinence model of cognitive dysfunction (Nathan *et al.*, 2013). However this group also reported gastrointestinal adverse effects, thus GSK1034702 is not a superior ligand as it has not been able to overcome the activation of peripheral mAChRs. Radioligand binding and functional studies have shown that TPBP and GSK1034702 have structural similarities, highlighting the need for further investigation into bitopic ligands (Sophie J. Bradley *et al.*, 2018).

The compound VU0357017 has been shown to have high levels of M1 mAChR subtype selectivity, excellent blood brain barrier penetration and high *in vivo* efficacy (Decker and Holzgrabe, 2012). VU0357017 has been shown to displace [^{3}H]-NMS binding to the orthosteric site of M1–M5 receptors at high concentrations (Digby *et al.*, 2012). This bitopic ligand also shows robust efficacy *in vivo* ameliorating scopolamine-induced deficits during a rodent contextual fear conditioning (Lebois *et al.*, 2010).

1.4.5Advantages of using allosteric modulators

Allosteric modulators have several distinct advantages over orthosteric ligands that bind the traditional binding site of a receptor. Allosteric modulators have a high level of selectivity, due to their lack of conserved binding sites between receptor subtypes (Bridges and Lindsley, 2008).Allosteric modulators have a spatiotemporal basis in their specificity. Pure allosteric ligands do not have their own intrinsic efficacy, thus can only elicit a receptor to signal when the orthosteric ligand is present. This is particularly useful when the spatiotemporal pattern of orthosteric ligand is critical. For example, the physiological temporal pattern of ACh being released from the presynaptic neurones might be retained in the presence of the allosteric modulator, but with the magnitude of response adjusted. A similar principle underlies the use of AChE inhibitors to modulate cholinergic signalling in AD, but receptor targeted AMs would generate greater selectivity. When in combination with the orthosteric ligand, allosterics can exert their cooperative actions by fine-tuned modulation of the receptor's function rather than simply turning "on and off" receptor signalling (Wootten, Christopoulos and Sexton, 2013). This adds to the increased safety of these drugs, as this fine modulation will mitigate against an overdose of the allosteric drug (Wenthur *et al.*, 2014). The cooperativity between orthosteric and allosteric ligand also produces a beneficial ceiling effect of receptor response. An allosteric modulator without intrinsic efficacy depends upon the orthosteric ligand to produce a biological effect. Therefore, the additional of a PAM or NAM will only have a saturable effect on the receptor's binding or function setting a biological limit depending on the orthosteric ligand bound. (Keov, Sexton and Christopoulos, 2011; Kenakin, 2012a).

Thus receptor signalling can achieve its biological signalling ability but within a range that is still safe for patients.

Another benefit of using allosteric ligands as therapeutics may be exploit different probe dependency profiles across receptor subtypes for greater selectivity. The high dependence on cooperativity between orthosteric and allosteric ligand at one receptor adds another layer of selectivity within the receptor's signalling activation (Felder *et al.*, 2018). For example, if an allosteric site to be conserved across subtypes of a receptor, the magnitude and direction of the allosteric effect may still be different because the cooperativity with the bound orthosteric ligand varies (Valant *et al.*, 2012). A recent paper has been able to describe a "cryptic binding" pocket for allosteric modulators (Hollingsworth *et al.*, 2019) with structural similarities observed across receptor subtypes and closely related receptors (Kruse *et al.*, 2012, 2013; Dror *et al.*, 2013; Thal *et al.*, 2016, 2018). This finding raises the question as to how certain allosteric modulators are able to achieve subtype selectivity. This group used the M1 mAChR allosteric modulator BQZ12, which has been shown to be a highly subtype-selective PAM (Abdul-Ridha, Lane, Mistry, Laura López, *et al.*, 2014; Christopoulos *et al.*, 2016). This specific PAM was chosen as the M1 mAChR crystal structure does not appear to allow for a bound pose of BQZ12 that matches existing mutagenesis data (Abdul-Ridha, Lane, Mistry, Laura López, *et al.*, 2014; Abdul-Ridha, López, Keov, David M Thal, Mistry, Sexton, Robert Lane, *et al.*, 2014). Nor is it clear how M1 mAChRs allosteric modulators achieve such level of subtype selectivity (Mistry *et al.*, 2013; Davoren *et al.*, 2016; Beshore *et al.*, 2018; Sako *et al.*, 2019). Hollingsworth (2019) was able to show that the allosteric site of the M1 mAChR had a dynamically changing the allosteric binding site, in which Y2.64 rotates away from ECL2 to form a hydrogen bond with E7.36. E7.36 then rotates towards the allosteric site. These movements resulted in a secondary binding pocket adjacent to TM2 and ECL2, which the group referred to as the cryptic pocket. Following investigation across the M1-4, it was shown that M1 mAChR selectivity may occur due to the temporal pattern of the opening of the cryptic pocket. The M1 mAChR cryptic pocket was open 50.2% of the time, whereas the same pocket on M2, M3 and M4 were open for 0.4%, 3.4% and 4.3% of the time, respectively.

1.5 Astrocytes

1.5.1General Overview

In the CNS, there are two main type of cells: neurones and glial cells. Astrocytes are a class of glial cells that are highly heterogeneous in form and function, and demonstrate high levels of phenotypic plasticity (Zhou, Zuo and Jiang, 2019).

An astrocyte possesses a small soma and several thick processes that extend from the cell body to form numerous fine processes, in a morphology known *in vitro* as either stellate or protoplasmic astrocytes (Volterra and Meldolesi, 2005). Unlike neurones, astrocytes do not have axons or dendrites, and they are not electrical excitable and therefore do not generate action potentials. Astrocytes possess a number of GPCRs that not only allow the cell to receive information from synaptic transmission but also contribute to neuronal modulation by second messenger induced release of gliotransmitters (Parpura *et al.*, 1994; A Araque *et al.*, 1999a; Parpura and Zorec, 2010). Gliotransmitters such as glutamate, ATP, d-serine and taurine are secreted by astrocytes and regulate synaptic activity (Martin-Fernandez *et al.*, 2017; Tan *et al.*, 2017; Van Horn *et al.*, 2017).

The fundamental function of astrocytes is to sustain homeostasis throughout the CNS, (Eroglu and Barres, 2010; Perea, Sur and Araque, 2014; Bazargani and Attwell, 2016a). However, astrocytic control of the CNS is far more wide reaching than just this. Astrocytes have also been implicated in lactate production and turnover, regulation of the brain's microcirculation, regulation of the extracellular space volume, circadian rhythm and sleep, systemic energy homeostasis, memory and learning, reproduction and respiration to name but a few (Verkhratsky and Nedergaard, 2018).

Due to astrocytes' overarching importance to the CNS they have therefore been implicated in a number of diseases (Zhou *et al.*, 2019). It has been shown that alterations in astrocyte-derived signals may lead to the synaptic dysfunction in psychiatric disorders (Koyama, 2015), neurodevelopmental syndromes (Sloan and

Barres, 2014), epilepsy (Robel *et al.*, 2015), and neurodegenerative disorders (Ben Haim *et al.*, 2015).

1.5.2The Tripartite Synapse Allows Bidirectional Communication between Neurone and Astrocyte

Astrocytes tile the CNS, ensheathing neuronal synapses with their fine processes. Protoplasmic astrocytes are also in direct contact with blood vessels through a specialised cellular compartment called the end-foot (Foo *et al.*, 2011). In the cortex, a single astrocyte can ensheathe 4-8 neuronal somata and make contact with an estimated 300-600 neuronal dendrites (Halassa *et al.*, 2007). Thus, the extent astrocytes contribute to synaptic transmission, and this functional significance, is extremely wide reaching.

Astrocytes are able to control a large number of CNS processes through their role within, what has been termed, the "tripartite" synapse (A Araque *et al.*, 1999b). The concept of the tripartite synapse describes the bidirectional communication between the extrasynaptic astrocytes and the presynaptic and postsynaptic neurones (Dityatev and Rusakov, 2011). All five mAChRs subtypes have also been shown to be expressed in human and murine astrocytes (van der Zee *et al.*, 1993). Early studies show astrocytes express functional M1 mAChRs whereas M3 receptors were identified at an mRNA level (Murphy, Pearce and Morrow, 1986; André, Santos and Koulakoff, 1994), and as explained above, these receptors signal through the PLC-InsP3 pathway. Additionally, α-adrenergic receptor have been found in astrocytes *in vitro* and *in vivo* (Hertz *et al.*, 2010). The α1- adrenergic receptors elicit their activation through PLC and IP3 resulting in calcium release from the ER. These receptors are activated by endogenous adrenergic agonists, as well as, by norepinephrine released from neuronal varicosities following stimulation of locus coeruleus (Ding *et al.*, 2013).

Neurotransmitters released during synaptic activity can bind to and activate Gq-coupled GPCRs present on co-localized astrocytes leading to the receptor

mediated increases in intracellular calcium levels (Cornell-Bell *et al.*, 1990; Dani, Chernjavsky and Smith, 1992). In turn, it has been suggested that the outcomes of astrocyte calcium signalling may modulate downstream neuronal circuit activity (Guerra-Gomes *et al.*, 2018). However, the precise signalling pathways regulating these events are not fully characterised and there is a need for more evidence connecting increases in calcium signalling leading directly to astrocyte-dependent alterations in neuronal activity (Bazargani and Attwell, 2016b). However, one group was able to show, using the trace amines tyramine or octopamine in Drosophila, that once secreted from neurones these molecules could directly bind to their corresponding GPCR expressed in astrocytes (Ma *et al.*, 2016). Furthermore, the authors showed activation of the Oct-Tyr GPCR stimulated calcium increases that triggers astrocyte to secrete ATP which the bound to adenosine receptors expressed on dopaminergic neurones. This provides direct evidence of the tripartite synapse *in vivo*. Interestingly, the astrocytic calcium responses were linked to those elicited by norepinephrine-induced activation of α1 adrenergic receptors in mice (Paukert, Agarwal, Cha, Van A. Doze, *et al.*, 2014), suggesting a relevance across species.

1.5.3Spatiotemporal Dynamics of Calcium Signalling Within Astrocytes

Astrocytes are not electrically excitable cells however they have calcium excitability based on variations in intracellular calcium concentrations (Cornell-Bell *et al.*, 1990; Charles *et al.*, 1991). Astrocytes display both spontaneous calcium signals (Nett, Oloff and McCarthy, 2002; Parri and Crunelli, 2003; Tang *et al.*, 2015), and effector-activated calcium signals (Perea and Araque, 2005a; Asada *et al.*, 2015). Astrocyte calcium signalling is highly varied and can be seen as spontaneous oscillations, single calcium transients or repetitive transients/spikes (Nett, Oloff and McCarthy, 2002). The different temporal and spatial patterns of intracellular calcium signalling depends on how the calcium signal is generated; either by calcium release from the internal calcium stores in the endoplasmic reticulum (ER) (Perea and Araque, 2005b), or by calcium entry from the extracellular space (Parri, Gould and Crunelli, 2001; Aguado *et al.*, 2002; Nett, Oloff and McCarthy, 2002). It is still unknown whether the

spatiotemporal variability of these calcium signals is associated with different physiological functions.

The IP3-dependent release of subcellular blips of calcium can summate in a process where calcium-induced calcium release (CICR) occurs from internal stores, which triggers a calcium wave to occur that spreads throughout the cell. One hypothesis was that the frequency of this calcium spiking related to the strength of the stimulus applied to astrocytes from the synapse (Berridge, Bootman and Roderick, 2003). However, when further investigated, it was demonstrated that the relationship between the interval of agonist addition and agonist concentration was a more robust parameter for understanding the differences in stimulus strength and the intracellular calcium response induced (Thurley *et al.*, 2014). In fact, astrocytes would not be able to produce a calcium response that matches the temporal pattern of the neurotransmitter as it signals too quickly (Croft *et al.*, 2016). It is therefore of interest to understand the different temporal patterns of calcium intracellular signalling within astrocytes, and how these calcium events related to the astrocytic function and its bidirectional communication with neurones.

A number of studies that focused on the kinetics of neuronal activation of astrocytes, and the subsequent astrocytic calcium release concluded that the onset latency of several seconds between neuronal activity and the calcium response meant that these two cells were not coupled in their communication. However, recently it was discovered that there are microdomains within the astrocytic processes that only had an onset latency of 100ms as compared to neuronal activity (Stobart *et al.*, 2018). Both the plasma membrane and the ER contain several families of calcium channels that allow the flow of calcium into the cytoplasm. Calcium influx from extracellular sources occurs through voltage gated calcium channels (VGCC), especially L-type (Codazzi, Teruel and Meyer, 2001; Parri, Gould and Crunelli, 2001; Zeng *et al.*, 2009). Recent *in vivo* imaging of calcium activity within astrocytes has been able to show a spatiotemporal hierarchy of calcium signalling. The location-dependent generation of calcium signals was studied by using a knockout of the IP3 receptor 2 (IP3R2), which abolished the majority of calcium transients although it was interesting that it had a

lower effect on calcium signals in the astrocytic processes (Srinivasan *et al.*, 2015; Stobart *et al.*, 2018). Additionally, the removal of extracellular calcium significantly reduced the frequency of calcium in the astrocytic processes but only had a minor effect on calcium signals in the soma (Srinivasan *et al.*, 2015). From this, it was shown that fast calcium fluctuations in the astrocyte's processes allow for fast extracellular calcium influx through VGCCs (Di Castro *et al.*, 2011; Bindocci *et al.*, 2017). Whereas, larger calcium events, resulting from CICR, are slower and IP3-dependent (Bindocci *et al.*, 2017).

Astrocytic calcium signals are not always a local event and can spread throughout the cell and even an astrocyte population, from neighbouring astrocyte to astrocyte. In compartments that contain internal calcium stores, calcium waves occur via the diffusion of calcium and IP3 which evokes intracellular amplification through CICR (Golovina and Blaustein, 2000). Whereas, the astrocytic processes are capable of producing strong calcium signals by calcium transport from the extracellular space, and propagate calcium waves via diffusion (Rusakov, 2015). Calcium waves that spread throughout the population are a result of IP3 diffusing through gap junctions eliciting further release of calcium from neighbouring cells (Fujii, Maekawa and Morita, 2017).

1.5.4Reactive Gliosis Is a Morphological Process That Allows Astrocytes to Protect the CNS

Reactive gliosis describes a response of astrocytes to brain or spinal cord trauma, injury, infection, stroke, neurodegenerative disease. Gliosis is a multi-stage process, where astrocytes dramatically change their morphology and function to provide a defence mechanism to the injured brain that aims to control inflammation and the blood-brain barrier's integrity (Pekny and Pekna, 2016). Likewise, it has been shown that reactive astrocytes are able to isolate non-injured tissue, through the gliosis process, which supports regeneration of the damaged neuronal tissue (Burda, Bernstein and Sofroniew, 2016).

The significant morphological variations seen in astrocytes, during the reactive gliosis process, are a result of a changing cytoskeleton however; the exact process of how this occurs is less well known. Reactive astrocytes are seen to have prominent hypertrophy, altered ramifications and outgrowths of particularly long processes (Myer, 2006; Schiweck, Britta J. Eickholt and Murk, 2018). It has been shown that the astrocyte's morphology, and reactive "status", is dependent on its distance from the site of injury. For example, astrocytes in the vicinity of a focal lesions have been shown to have a more prominent stellate shape, while orienting themselves towards the site of injury with long processes extending out (Kanemaru *et al.*, 2013). This group showed that the morphological changes in the astrocytes reduced with distance from the legion. It has also been shown that astrocytes close to the lesion cannot reverse their reactivity, whereas those further from the injury are able to return to their normal state (Bardehle *et al.*, 2013). The astrocyte irreversibly altered form a glial scar that is normally considered resistant to treatment or regenerative processes following traumatic brain or spinal cord injuries (Cregg *et al.*, 2014).

The actin cytoskeleton has been implemented in controlling hypertrophy and alterations in the astrocyte's morphological changes. It has been shown that inhibition of the actin-nucleating Arp2/3 complex increased cell body size and the number of long processes in reactive astrocytes (Murk *et al.*, 2013). Inactivation of Arp2/3 complex was also shown to accelerate the hypertrophy of *in vitro* astrocytes, in a model of stroke, whereas over-activating the complex suppressed the cell body expansion (Murk *et al.*, 2013). It has also been shown that reactive astrocytes switch from Rac1 and Arp2/3-dependent networks towards a RhoA-dependent organisation of actin (John *et al.*, 2004; Renault-Mihara *et al.*, 2017). Signalling through receptors such as β-adrenergic receptors activates PKA and inhibits the ROCK-RhoA signalling pathway (Schiweck, Britta J. Eickholt and Murk, 2018).

All three subtype of the β-adrenergic receptors (β1-3) have been identified in astrocytes *in vitro* and *in vivo* (Liu *et al.*, 1992; Mantyh *et al.*, 1995; Catus *et al.*, 2011). All three subtypes signal via Gαs and thus increase the intracellular concentration of cAMP within astrocytes (Hertz *et al.*, 2004). Intracellular cAMP activates PKA and

phosphorylates substrates that control metabolism, cell proliferation, gene transcription and has implicated in functions such as learning and memory (Horvat and Vardjan, 2019; Reuschlein *et al.*, 2019; Zhou, Ikegaya and Koyama, 2019).

In contrast to astrocytes *in situ,* cultured astrocytes acquire a flat, epithelioid morphology. However, the *in situ* phenotype can be partially recovered in an actin-dependent, cAMP-led process known as stellation (Racchetti, D'Alessandro and Meldolesi, 2012; Vardjan, Kreft and Zorec, 2014). Activation of the β-AR by noradrenaline has long been known to alter astrocytes to a process-bearing morphology (Shain *et al.*, 1987; Bicknell *et al.*, 1989), however the exact mechanism is still elusive. One group was able to show that the actin cytoskeleton network was reorganised after application of the cAMP analogue dibutyryl cAMP (dBcAMP) (Baorto, Mellado and Shelanski, 1992). This actin breakdown was accompanied by a decrease in phosphorylation regulatory light chain of myosin (MLC), which may give mechanistic insight into the process of stellation (Baorto, Mellado and Shelanski, 1992). Profilins are small proteins involved in actin dynamics. The knockdown of Profilin 2a was shown to abolish the stellation obseverved by forskolin-treated astrocytes (Schweinhuber *et al.*, 2015). Finally, a study was able to support cAMP-led stellation using FRET to show β-AR agonists increased intracellular cAMP, and that after an hour of stimulation astrocytes had decreased their cross-sectional area by 10% (Vardjan, Kreft and Zorec, 2014).

1.6 Chemogenetic DREADDs

1.6.1General Overview

The importance of GPCRs in terms of their therapeutic potential has highlighted the need to study and selectively understand their function and link receptor activation to consequent physiological responses. Designer receptors exclusively activated by designer drugs (DREADDs) (Armbruster *et al.*, 2007), are engineered muscarinic GPCRs that aim to provide a tool that elicits receptor-selective activation. DREADDs contain mutations, within the orthosteric site of mAChRs, at two strictly conserved amino acid residues: Tyr3.33Cys and Ala5.46Gly (described further in Chapter 3). Discovered using a directed molecular evolution approach in yeast, it has been shown that these

two mutations allow the receptor to be activated by clozapine-N-oxide (CNO), while simultaneously reducing the binding of the endogenous ligand ACh (Armbruster *et al.*, 2007). CNO is a pharmacologically inert metabolite of clozapine, the antipsychotic therapeutic, and has been shown to penetrate the CNS while having favourable pharmacokinetics in mice (Bender, Holschbach and Stöcklin, 1994) and humans (Jann, Lam and Chang, 1994). It has been verified that DREADDs still show the same G protein coupling preference (Gq, and Gi) as their non-mutated parent muscarinic receptors (Guettier, Gautam, Scarselli, Ruiz de Azua, *et al.*, 2009a). Moreover, DREADDs express in cells with low constitutive activity in the absence of CNO (Armbruster *et al.*, 2007).

1.6.2Advantages of Using DREADDs for Selective Receptor Activation

DREADDs offer a gain of control over GPCR signalling that allows for a system in which CNO can be administered non-invasively, without specialised equipment, that is both safe in humans and readily distributed throughout the CNS (Sternson and Roth, 2014).

Furthermore groups have employed inducible expression technology and tissue-specific promoters in order to greater control of spatial receptor expression and activation (Alexander *et al.*, 2009; Garner *et al.*, 2012). This is advantageous over optogenetic manipulations, as there is no need to implant an optic fibre. Systemic administration of CNO allows a number of DREADD-expressing brain areas to be investigated at one time, whereas optogenetic activation is limited to the area in proximity to the optic fibre. The fact DREADD signalling makes use of the cells' intrinsic G protein signalling cascade allows for intracellular endpoint molecules to be activated in an intrinsic manner, and thus maintaining a level of physiological relevance. Gq-DREADDs have been used to specifically activate astrocytic signalling (Agulhon *et al.*, 2013; Bull *et al.*, 2014; Scofield *et al.*, 2015b; Martin-Fernandez *et al.*, 2017). It has been shown that Gq-DREADD activation by CNO shows IP3-mediated calcium mobilisation which closely mimic physiological patterns produced by ACh (Durkee *et al.*, 2019).

1.7 Aims of This Thesis

Targeting muscarinic receptors, such as the M1 subtype, with orthosteric or allosteric ligands, has significant therapeutic potential for future treatment of CNS disorders. However, we know little about how these ligands affect the function of glial cells in the CNS, or indeed the overall contribution that muscarinic receptors make to astrocyte saptiotemporal signalling and long-term effects such as reactive gliosis. In part, investigations are made more challenging in primary cells by the complex array of different receptor subtypes responsive to individual neurotransmitters. The use of designer muscarinic receptors (DREADD) provides an opportunity to isolate spatiotemporal responses in such cells from a clearly defined receptor subtype. However, for DREADDs to be a suitable model system, a good understanding of how accurately their orthosteric and allosteric pharmacology represents their cognate muscarinic receptor is required.

The purpose of this thesis was to provide novel evaluation of M1-DREADD receptor pharmacology in recombinant systems, and ultimately to explore the use of these receptors in studying key aspects of astrocyte signalling. After design and synthesis of the constructs described in Chapter 3, the effects of a range of orthosteric ligands and the prototypical positive allosteric modulator BQCA was examined in depth in CHO and HEK293 cells (Chapter 4). In addition to routine measurements of intracellular calcium signalling, new kinetic signalling assays were developed, based on luciferase complementation technology, to examine DREADD recruitment of mini Gq and arrestin proteins. Further, we identified fluorescent ligands for the M1-DREADD receptor for the first time and demonstrated their applicability in binding assays. Finally, Chapter 5 describes the attempts to establish the DREADD receptor system in primary astrocytes, both as a system to understand calcium-signalling dynamics, and through a morphological stellation assay, to explore the interplay between cAMP and calcium pathways that may be relevant in reactive gliosis.

Chapter 2

MATERIALS AND METHODS

2.1 Materials

2.2.1 Laboratory Reagents

2.1.2.1 Molecular biology reagents

pcDNA 3.1 neo(+) vector, Super Optimal broth with Catabolite repression (S.O.C) medium, optiMEM, Lipofectamine 2000 and Lipofectamine LTX, all oligonucleotide primers and the selection antibiotic zeocin were from Invitrogen (Paisley, UK). The GenElute^{TM} gel extraction, PCR purification, miniprep kits, amplicillin and neomycin (G418 sulphate) were purchased from Sigma Aldrich (St. Louis, MO, U.S.A), as were Luria Bertani (LB) media and agar. The maxiprep kit was purchased from QIAGEN (Hilden, Germany). Fast alkaline phosphatase, T4 DNA ligase, pJET cloning kit, and all restriction enzymes were obtained from Thermo Fisher Scientific (Loughborough, UK). The 1kb DNA ladder was purchased from New England Biolabs (Ipswich, MA, U.S.A.). Additional molecular biology reagents were generally purchased from Sigma Aldrich (St. Louis, MO, U.S.A.).

2.1.2.2 Fluorescent dyes and indicators

Hoechst 33342 nuclear stain dye was purchased from Thermo Fisher (Loughborough, UK). Membrane impermeable SNAP-Surface Alexa Fluor 488 was obtained from New England Biolabs (Ipswich, MA, USA), Fluo-4 AM, Fluo-5F AM, Calcein AM and Pluronic F-127 were all purchased from Invitrogen (Paisley, UK).

2.1.3Tissue Culture Reagents

Media solutions were made up for the individual cell type (Table 1.1). Media solutions were kept at 4^{o}C for a maximum of 6 weeks.

Cell Type	Media Composition
CHO K1 (CCL-61)	Dulbecco's modified Eagle's medium (DMEM; Thermo Fisher (Loughborough, UK)): Ham's F-12 (1:1) + 10% heat inactivated foetal calf serum (FCS; Sigma Aldrich (St. Louis, MO, U.S.A))
HEK293T (CRL-3216)	DMEM – high glucose (4500mg/L glucose and sodium bicarbonate, L-glutamine (2.5mM) without sodium pyruvate) + 10% FCS
Primary Rat Astrocytes	DMEM – high glucose (10% FCS, 50ng ml^{-1} L-proline (Sigma Aldrich; St. Louis, MO, U.S.A) and 100 units ml^{-1} penicillin and 100µg ml^{-1} streptomycin (Thermo Fisher; Loughborough, UK))

Table 2.1: Cell media composition to maintain relevant cell types during tissue culture procedures. Different Dulbecco's modified Eagle's medium with differing cellular supplements necessary for the different cell types.

Phosphate buffered saline (PBS) and trypsin were purchased from Sigma Aldrich (St. Louis, MO, U.S.A.). Tissue culture plasticware was from Fisher Scientific (Loughborough, UK). Flat bottom, black-sided 96-well imaging plates (655090) and flat bottom, white sided 96-well imaging plates (655073) were both purchased from Greiner Bio One (Stonehouse, UK). Sterile 6-well plates (3516) were purchased from Corning Costar (NY, U.S.A.).

2.1.4Pharmacological Compounds

Acetylcholine, atropine, benzyl quinolone carboxylic acid, carbachol, iperoxo, oxotremorine-M and VU0357017 were purchased from Sigma Aldrich (St. Louis, MO, U.S.A.). Clozapine, clozapine-N-oxide, forskolin, N-desmethylclozapine, pilocarpine, prazosin, propanolol and xanomeline were purchased from Tocris Bioscience (Avonmouth, Bristol, UK).

Compounds were stored as single-use aliquots diluted in dimethyl suphoxide (DMSO; Invitrogen, Paisley, UK) at -20^{o}C except for acetylcholine that was made fresh on the day of the experiment.

2.1.4.1 Fluorescent Ligands

Fluorescent ligands **I**, **II**, **III**, **IV** and **V** (stock concentrations 10mM in DMSO, kept in amber vials) were generously donated from Max Keller's lab in the University of Regensburg synthesised by Dr. Andrea Pegoli and Dr. Xueke (Coco) She.

2.2 Methods

Molecular biology techniques were employed in order to create SNAP-tagged or LgBiT SNAP-tagged versions of the M1 and M1-DREADD constructs, which are required for pharmacological investigation of the effects of allosteric modulators and the chemogenetic DREADDs. It was first necessary to mutate the M1-WT cDNA to produce the chemogenetic DREADD version that will be required in the pharmacological studies in Chapter 4. Ligation techniques were used to introduce C-terminal tagged LgBiT and/or N-terminal SNAP-tagged of the M1-WT and M1-DREADD constructs to allow visualisation of these receptors in following experiments. Cell culture techniques allowed these constructs to be expressed in both recombinant cells and primary astrocytes.

2.2.1PCR Protocol

Polymerase Chain Reaction (PCR) is a process in which defined DNA sequences can be amplified in order to increase their concentration, and can also be used to insert desired mutations into a sequence of DNA. The initial step starts when a double stranded template DNA is heated and denatured to give single stranded DNA. The temperature is then decreased to allow annealing of the primers to the template. The annealing temperature varies depending on the primer used but are typically 5°C less than the melting temperature of the primer to allow specific primer hybridisation. The reaction is warmed to the optimal temperature for an extension step to be performed (optimally approximately 1.5min is given per kbp) whereby a thermostable DNA polymerase synthesises a new complementary DNA strand from the primer sequence in a 5' to 3' direction. This cycle of denaturation, annealing and elongation is repeated multiple times, with the newly synthesised fragment DNA (containing the region to be amplified) now also acting as the template DNA, allowing for exponential expansion.

Following completion of all cycles, the amplified DNA is cooled and held at 4°C. PCR was carried out using a thermocycler block (Mastercycler gradient, Eppendorf, UK).

2.2.2Mutagenesis to Create the M1-DREADD Construct

Mutagenesis was carried out using the "quickchange" approach to sequentially introduce the two point mutations Y160C and A196G and create the M1-DREADD receptor (Armbruster *et al.*, 2007)(Genbank Ref: NM_000738, from www.cdna.org; Missouri S&T Resource Centre). This was achieved using two sets of complementary primers designed to introduce the two point mutations (Table 2.2).

The buffer utilized for the PCR reaction was 10X Accuzyme buffer, while Accuzyme was used as the enzyme (Bioline, London, UK). The initial first two steps of the reaction; 94°C for 30sec then 60°C for 1min, are known as a "HotStart" protocol, which prevents the enzyme amplifying non-specifically bound primer sites which can occur as the PCR solution is initially warmed. The subsequent steps are conducted at 68°C for 8min for 16 cycles. This enables the enzyme to amplify the entire plasmid DNA (~ 7kbp) in both directions from the complementary mutagenesis primers.

After the PCR protocol was completed, 20µl samples were treated with the restriction enzyme DpnI for 2hr at 37°C. DpnI can only cleave methylated DNA (i.e. the original template cDNA); leaving solely the unmethylated mutated DNA intact as a circular plasmid for efficient transformation (see section 2.2.5).

hM1-Y106C Fwd primer	CCTCTGGCTGGCCCTGGACTGTGTGGCCAGCAATGCC
hM1-Y106 Rev primer	GGCATTGCTGGCCACACAGTCCAGGGCCAGCCAGAGG
hM1-A196G Fwd primer	GGCACAGCCATGGCTGGCTTCTACCTCCCTGTCACAGTC
hM1-A196G Rev primer	GACTGTGACAGGGAGGTAGAAGCCAGCCATGGCTGTGCC

Table 2.2: The two pairs of mutagenesis oligonucleotides used in order to add the two point mutations needed to produce the hM1-DREADD receptor. The sequences are complementary to the hM1 amino acid sequence except for one amino acid which is required for the mutagenesis to occur. The point mutations are shown in yellow, with "TGT" used to form the Y106C mutation and "GGC" to form the A196G mutation.

2.2.3PCR Amplification of M1-WT and M1-DREADD Constructs

In order to create the M1 and M1-DREADD receptors with an N-terminal SNAP-tag, PCR amplification of the M1 and M1-DREADD cDNA was carried out. Primers were designed to remove the start (ATG) codon and preserve the stop codon. The forward primer also contained a BamHI restriction site and the reverse primer contained an XhoI restriction site (Table 2.3). These restriction sites are used in following steps to ligate (see section 2.2.4) the receptor in frame into the SNAP p3.1neo(+) vector containing an N-terminal 5HT3 signal sequence and the SNAP-tag between KpnI and BamHI sites (Watson, Brown and Holliday, 2012a), see Chapter 3.

To construct the N-terminal SNAP-tagged and C-terminal LgBiT tagged (Dixon *et al.*, 2016; Wan, Okashah, Inoue, Nehmé, Carpenter, C. G. Tate, *et al.*, 2018) M1 and M1-DREADD receptor fusion proteins, PCR amplification of the cDNA constructs was carried out as explained above. However, a different reverse primer was required to remove the STOP codon and add an in frame XhoI site (Table 2.3). These products were ligated into LgBiT SNAP pc3.1neo(+) vector (provided by Dr. N. Holliday, University of Nottingham), in which the large fragment of nanoluciferase is placed

between the XhoI and XbaI sites of the vector. Final vector maps and further details can be found in Chapter 3.

hM_1 BamHI Fwd primer	TAT AAA GGA TCC AAC ACT TCA GCC CCA CCT GCT GTC
hM1 XhoI Rev primer	TAT AAA CTC GAG GCA TTG GAG GGA GGG AGT GCG GTG A
LgBiT M1 XhoI Rev primer with no STOP	TAT AAA CTC GAG GCC AGA TCC GCA TTG GAG GGA GGG AGT GCG GTG C

Table 2.3: ***The oligonucleotide primers used in order to add flanking restriction sites on the hM1 constructs.*** *The BamHI restriction site for the forward reading primer and XhoI restrictions site for reverse primer are shown underlined. The blue highlighted sequence shows the complementary sequence to that of the hM1 nucleotide sequence. The yellow highlight indicates the STOP codon, whereas for the LgBiT primer a short linker (highlighted in green) separates LgBiT domain from the final Cys in the M1 sequence.*

2.2.4PCR Fragment Subcloning into pJET1.2 Vector

The PCR products of the M1 constructs containing the restriction sites were first subcloned into the pJET1.2/blunt vector in order to accelerate the process of colony screening and amplify the DNA via minipreps (see section 2.2.1.9). Principally subcloning improves the subsequent digestion of the BamHI / XhoI restriction sites flanking the PCR product, which otherwise are located close to the end of the DNA fragments (not ligated into pJET1.2) and may be inefficiently cleaved. The blunt ended cloning also acted as a form of protection to the newly added “sticky end” restriction sites. When restriction digested inserts are passed through gel electrophoresis the matrix-like agarose gel can cleave these small, unsupported nucleotides from the DNA construct thus reducing ligation efficiency. Therefore, this initial blunt ended cloning step overcame this before the restriction digest occurred to produce “sticky ends” for ligation into SNAP pcDNA3.1(+)neo vector. The pJET1.2/blunt vector also contains a lethal restriction enzyme gene for *E Coli* (*eco471R)* that is disrupted by ligation of a DNA insert into the cloning site. As a result, only bacterial cells with recombinant plasmids are able to form colonies. This positive selection pressure accelerates the screening of properly ligated colonies.

To form a ligated product, 2µg of pJET1.2/blunt vector (3.0kbp) was mixed with 1µg of uncut PCR (approx. 1.5kbp, 1: 1 molar ratio) product before T4 DNA ligase and

its appropriate buffer was added into a total volume in 20µl ddH_20, before being heated at 22^oC for 30mins. The subclones of M1-DREADD and M1-WT constructs were subsequently transformed into DHα5 cells (see section 2.2.5), grown up on ampicillin-resistant agar plates and purified via miniprep. They were then screened using restriction enzymes and gel electrophoresis (section 2.2.3). The PCR derived DNA constructs were then sequenced and if correct, ligated into fresh SNAP/LgBiT SNAP pcDNA3.1(+)neo vectors (section 2.2.4).

2.2.5Restriction Digest

Restriction enzymes cleave double stranded DNA by hydrolysis of the phosphodiester bonds between nucleotides within highly specific recognition nucleotide sequences (typically 4 – 8 base pairs). Generally, DNA for preparative and diagnostic digests was cut via a double digest using two different restriction enzymes, flanking either end of the inserted DNA. The same enzyme pair were used to digest the vector DNA in order to complement the insert fragment. This was possible because the enzymes chosen produced complementary 'sticky ends', whereby an overhang stretch of unpaired nucleotides was left following digestion (see Table 2.4). The 'sticky ends' are complementary and differ for the enzymes chosen, so can subsequently be joined together in only one orientation by T4 DNA ligase to increase the likelihood of correct orientation between insert and vector sequences.

Restriction Enzymes	Restriction sites
BamH I	5'…G↓ GATCC…3' 3'…CCTAG↑ G…5'
Xho I	5'…C↓ TCGAG…3' 3'…GAGCT↑ C…5'

Table 2.4: ***Indication of the amino acid sequence recognised and cut by restriction enzymes.*** *Arrows indicate where the BamHI and XhoI restriction enzyme cut their short recognition sequence.*

When performing a restriction digest, 2µg of cDNA (in a total volume of 50µl) was added to a sterile 0.5ml Eppendorf tube along with 2µl of 10x fast digest buffer (supplied with enzyme; Thermo Fisher, Loughborough, UK) and digested with 1µl of each restriction enzyme. This reaction was incubated for 1hr at 37°C, followed by

5min at 80°C and 20min at 65°C to heat inactivate the restriction enzymes. Digested DNA was then identified and isolated using gel electrophoresis (Section 2.2.3).

2.2.6Visualisation and Isolation of DNA Using Agarose Gel Electrophoresis

Gel electrophoresis is a technique used to separate DNA fragments. At a molecular level, the gel is a matrix of agarose molecules. DNA has a negative charge because of the phosphate groups in their sugar-phosphate backbone, so when a current is passed across the gel the DNA moves through the matrix towards the positive pole. All DNA molecules have the same amount of charge per mass, thus gel electrophoresis of DNA fragments separates them based on size with smaller fragments travelling faster through the gel, allowing distinct DNA bands to be visualised. Ethidium bromide is a chemical agent that intercalates into DNA and when exposed to ultraviolet light fluoresces, allowing DNA to be visualised as discrete bands on the gel.

A gel was prepared by dissolving 1% agarose (Sigma Aldrich) in TBE buffer (89mM Tris HCl,89mM Boric acid, 2mM disodium EDTA (ethylenediaminetetraacetic acid); pH 7.6) and heating for 10mins at 56^{o}C in order to dissolve the agarose. The mixture was allowed to cool before the addition of ethidium bromide (0.1µg ml^{-1}). The gel was then left to set, prior to being placed into an electrophoresis tank and covered entirely with TBE buffer. DNA samples were mixed with blue loading buffer (0.25% w/v bromophenol blue, 50% v/v glycerol in TBE) and loaded, with 5µl of 1kb DNA ladder (Promega, WI, U.S.A) as a molecular weight marker. The gel was run at 70V for 45mins until sufficient separation of the DNA bands was achieved. DNA was visualised using an UV light box (Syngene GVS-30 transilluminator) and the DNA band of the correct size excised. Representative gels showing a the M1 constructs within the pcDNA3.1(+)neo vector used throughout this thesis and the DNA bands obtained following their restriction digestion can be seen in Chapter 3. Gel images were taken on the GENE flash (Syngene Bio Imaging).

2.2.7Gel Extraction of DNA

DNA fragments separated by agarose gel electrophoresis were isolated using a gel extraction kit. This method of DNA purification is a silica gel-based method, which uses column chromatography. The excised gel containing the correct DNA fragment was weighed in a sterile Eppendorf and 3 gel volumes of gel solubilisation solution was added before subsequently being heated for 10 min at 60°C. The chaotropic salts in the solubilisation solution disrupt the structure of the water molecules surrounding the DNA, creating a hydrophobic environment that facilitates DNA binding to the silica of the spin column whilst other contaminants are washed away. One gel volume of isopropranol was then added to the solubilised gel solution to increase specific binding of the DNA to the column. Column preparation solution was added to the binding column and centrifuged for 1 min at 14,000rpm. The solubilised gel solution was then added and centrifuged for 1 min at 14,000rpm binding the DNA to the silica filter of the column. A solvent based wash solution, containing 70% ethanol, was added to remove any contaminants without affecting DNA binding (DNA does not dissolve in ethanol solution). A further 2min centrifuge at 14,000rpm removed excess ethanol. The DNA was then diluted into 40µl ddH_2O and a 1min centrifugation at 14,000rpm allowed for the collection of the DNA in solution.

2.2.8Ligation into pcDNA(+)neo Vector

The final stage to produce the M1 and M1-DREADD recombinant plasmids was to ligate the constructs into the SNAP pcDNA3.1(+)neo vector or the LgBiT SNAP pcDNA3.1(+)neo vector (full plasmid maps available in Chapter 3). Vector DNA (2µg) was double digested with respective digest enzymes (see Table 2.1) for 2hrs at 37°C, followed by 5min at 80°C and 20 min at 65 C to heat inactivate the restriction enzymes. This was then treated with Fast Alkaline Phosphatase (100mM Tris-HCl (pH 8.0 at 37°C), 50mM $MgCl_2$, 1M KCl, 0.2% Triton X-100 and 1 mg/mL BSA; Thermo Fisher); 2µl alkaline phosphatase and 2µl alkaline phosphatase buffer for 30mins at 37°C then 10mins at 75°C (Table 2.4). Alkaline phosphatase treatment is necessary to remove phosphate groups from the ends of linearised plasmid DNA in order to prevent recircularisation during ligation. The vector DNA was purified using a PCR clean up kit,

which follows a similar silica-based method to remove contaminants as explained in section 2.2.3. Vector DNA was eluted into 40µl ddH_2O.

The constructs and vector, having been digested by respective restriction enzymes, were ligated together. The T4 DNA ligase enzyme catalysed the formation of covalent phosphodiester linkages, which forms permanent bonds between the nucleotides.

The digested insert and vector were ligated together in a 3:1 insert: vector molar ratio. For all preparations it was assumed that an 80% yield of DNA was achieved from the gel purification process and was thus the total insert amount in 50µl gel purified sample was calculated from this equation, given 2µg originally digested:

$$= 2\mu g \times (insert\ size \div total\ original\ plasmid\ size) \times 0.8$$

50ng of vector DNA was deemed optimal for use in ligations to produce single circular plasmids, therefore assuming 50ng of vector contains x moles, and the following equation was used to calculate the correct amount of insert DNA required:

$$Insert\ required\ (ng) = 3 \times \left(50 \div \left(\frac{vector\ size}{insert\ size}\right)\right)$$

Positive and negative ligations were set up in 0.5ml Eppendorf tubes, with ddH_2O added in place of insert to the negative control.

2.2.9Transformation of Component Cells with DNA Constructs

Transformation is the process of introducing plasmid DNA into E coli cells. Cells can be treated with β-mercaptoethanol and a heat shock process to increase membrane permeability and allow the bacterial cells take up DNA. The heat shock process and calcium phosphate transform E. Coli to competent cells. Antibiotic selection allows cells with DNA inserted into the vector, containing the antibiotic resistant gene, to be expanded and the DNA concentration to be increased.

Agar plates were produced using 35g of Luria Bertani (LB) agar powder (Sigma Aldrich) dissolved in 1L of ddH_20 that was sterilised by autoclaving. The mixture was

allowed to cool and ampicillin (final concentration 75µg ml^{-1}) was added before being poured into Petri dishes and allowed to set.

For transformation of ligations, high efficiency 'Top 10F' competent E Coli cells (Thermo Fisher) aliquots were gently thawed on ice and 25µl of cell suspension per transformation was added to pre-chilled Eppendorf tubes. 2µl of ligation solutions were added to the cells and incubated for 30mins on ice. Heat shock was applied for precisely 30secs at 42°C, to facilitate uptake of DNA by the competent cells, then returned to the ice. 200µl of S.O.C medium was then added to the cells and incubated for 1hr at 37°C while being shaken at 225rpm. 50µl of this solution was then spread over an agar plate.

For more routine propagation, competent DH5α cells of lower efficiency (Thermo Fisher) were transformed with a similar protocol albeit with the addition of β-mercaptoethanol as an initial step. This is a reducing agent that increases the efficiency of transformations by inactivating surface nucleases and making the cell wall permeable to nucleic acids. DH5α cells aliquots were thawed on ice and 50µl of cell suspension per transformation was added to pre-chilled Eppendorf tubes. While still on ice, 1.5µl β-mercaptoethanol (from 1.4M stock) was then added to each tube and incubated for 10min. 2µl of a ligation reaction was added and incubated on ice for 30min. Following this, the same protocol for heat shock was carried out, with the difference of 400µl LB broth being added to the cells and 200µl of the subsequent solution spread on the agar plate after the 1hr incubation.

For both competent cell lines, after being spread on the agar plates, colonies were grown overnight at 37°C. The next day 4 individual colonies were picked, from each transformation, and each inoculated in 5ml of LB broth containing the appropriate selection antibiotic (75µg ml^{-1} ampicillin) for 16hrs at 37°C while being shaken at 225rpm.

2.2.10 MiniPrep

Minipreps allow diagnostic isolation of plasmid DNA from small (1 – 5 ml) cultures of transformed *E Coli* colonies. Minipreps were performed using a GenElute Plasmid Miniprep Kit (Sigma-Aldrich) according to the manufacturer's instructions. The

transformed cells were collected by centrifuging 3ml of LB broth or S.O.C. medium, with the transformed cells, for 5mins at 4,000rpm. The pellet was then resuspended in a chilled hyperosmotic sucrose resuspension buffer containing RNase that degrades RNA in the preparation. Cells were then lysed in alkaline sodium dodecyl sulphate (SDS)/sodium hydroxide containing buffer which is a detergent used to solubilises the lipid bilayer of the cells. This strong base disrupts the hydrogen bonds intrinsic to DNA base pairing of chromosomal DNA, denaturing it into single stranded DNA. However, the supercoiled nature of the plasmid DNA means it is not irreversibly affected. This solution was then neutralised with a potassium acetate (KOAc) buffer to precipitate the denatured cellular debris and genomic DNA, while keeping the plasmid DNA in solution. This was then centrifuged for 10mins at 14,000rpm to form a pellet of the cell debris and any other containments. The spin column was loaded with 500µl of the column preparation solution and was centrifuged for 30sec at 12,000rpm, before adding the supernatant containing the plasmid DNA and again spinning this onto the silica filter for 30sec at 12,000rpm. The filter was then washed with an ethanol containing solution that dissolves residual salts and removes any remaining contaminants. Excess ethanol was removed by a further 2min centrifugation at 14,000rpm. The DNA was dissolved in 100µl of ddH_20 and collected after a 1min spin at 12,000rpm.

Isolated DNA was digested with restriction enzymes and gel separated to ensure the plasmid DNA contained the appropriate receptor inserts following ligation; as appropriate samples were also sent to the sequencing lab of the University of Nottingham, for example to verify the presence of the desired mutation.

2.2.11 MaxiPrep

If after screening the miniprep contains the correct plasmid DNA, it is necessary to further expand the DNA for future experiments. This was achieved using a MaxiPrep kit (QIAGEN) according to the manufacturer's instructions. Many of the buffer solutions are of a similar composition to those used in the miniprep kit.

To initiate the exponential phase of bacterial growth, 20µl of the stored miniprep bacteria was added to 5ml of fresh LB broth containing 75µg ml^{-1} ampicillin and

incubated for 7hrs at 37°C while being shaken at 225rpm. The entirety was then added to 120ml of sterile LB broth containing ampicillin (75µg ml^{-1}) and grown overnight at 37°C while being shaken at 225rpm.

The next day, the cells were collected by centrifuging the LB broth for 15mins at 4°C at 4,000rpm. The pellet was resuspended in 10ml of the hyperosmotic sucrose solution containing RNase, and then lysed for 3mins to break down the cell membranes. A neutralisation solution was added to separate the debris and genomic DNA from the plasmid DNA in solution. A chaotropic salt solution, to promote DNA binding to silica, was added to the QIAGEN tip and allowed to pass through via gravity flow. The neutralised solution and debris aggregate were added to a QIAGEN column with the lysate being pushed through a filter into the prepared QIAGEN tip, which was then allowed to pass through via gravity flow. This filter was washed twice with an ethanol containing solution, then the plasmid DNA was eluted in Buffer QF. The plasmid DNA was precipitated from this solution using isopropanol and then centrifuged for 60mins at 4°C and at 4,000rpm. The resulting pellet was then ethanol precipitated to further concentrate and purify the eluted DNA. The pellet was resuspended in a 1:10 ratio of 300 µl TE (10mM Tris HCl, 0.1mM EDTA; pH 8.0) to sodium acetate (NaOAC; 30µl) and 2.2 volumes of chilled ethanol (100%). This was centrifuged for 10mins at 14,000rpm then 200µl of chilled ethanol (70%) was added and centrifuged for 5mins at 14,000rpm. The pellet was allowed to air dry before being resuspended in TE. DNA concentration and purity were determined using a spectrophotometer (BioPhotometer, Eppendorf) with absorbance read at 260nm (the wavelength at which double stranded DNA absorbs light). This absorbance was converted to a DNA concentration using the calibration for double stranded DNA (1 AU = 50 ng / ml). Protein peak absorption was also measured at 280nm, and the ratio between these two values (260/280nm) indicated the purity of the sample DNA. A ratio between 1.7-1.9 is indicative of relatively pure double stranded DNA. The remaining DNA was stored as a stock DNA concentration of 1µg/µl in TE buffer.

2.2.12 DNA Sequencing

The sequences of all engineered DNA were verified for any alterations that may have been incorrectly introduced and that restriction sites and mutations purposely introduced were present (Chapter 3). The T7 forward and bGH reverse sequencing primers were used for all constructs. All sequencing was undertaken by the DNA sequencing laboratory at the University of Nottingham.

2.2.13 Cell Culture

2.2.13.1 Recombinant Cells

Chinese Hamster Ovary K1 (CHO-K1) cells were used to express the SNAP-tagged M1 and SNAP-tagged M1 DREADD constructs. For NanoBiT experiments to investigate the recruitment of β-arrestin2 or mini G proteins, the SNAP-M1/M1-DREADD – LgBiT constructs were transfected into Human Embryonic Kidney 293T (HEK 293T) cells that stably expressed either the SmBiT114-miniGsq71 mini G protein, or the SmBiT114-tagged β-arrestin2 using zeocin-resistant expression plasmids, see Chapter 4 for more details (Dixon *et al.*, 2016; Wan, Okashah, Inoue, Nehmé, Carpenter, C. G. Tate, *et al.*, 2018). Mini Gq and mini β-arrestin2 NanoBiT cell lines were prepared previously by members of the Holliday group.

HEK293T cell lines were grown in DMEM supplemented with 10% FBS, while CHO K1 cells were cultured in DMEM : Ham's F12 media (1:1) containing 10 % heat inactivated FBS, in 75cm^2 tissue culture (T75) flasks at 37°C and 95% O_2/5% CO_2. Medium was supplemented with maintenance concentrations of the appropriate antibiotic required for the transfected constructs in that cell line (see Table 2.2). Cells were grown to 70-80% confluency prior to passaging to prevent cell detachment. In order to remove residual FCS, which can deactivate trypsin, cells were washed with PBS then incubated with 1ml trypsin (Lonza Wokingham Ltd). Trypsin is a serine protease that facilitates cell detachment by hydrolysing proteins that enable cells to adhere to the culture flask. Cells were removed from the flask by washing again with 10ml DMEM and collected into a universal 30ml tube for centrifuging. For cell passaging, a cell suspension was added to a T75 flask at a ratio of 1:5 or 1:10 with

maintenance concentrations of the appropriate antibiotic (see table 2.5). For experiments, 100µl cell suspension was loaded onto a haemocytometer and the number of cells within a 1mm^2 area counted (25 x 0.04mm^2 squares totalling 0.1µl volume). The average number of cells per ml was calculated by multiplying the number of cells by 10,000. This cell suspension was then diluted in an appropriate volume of DMEM to give the required cell density (densities indicated in section 2.3). CHO K1 cells lines were loaded directly into wells of the relevant 96 well assay plate. For the HEK cell lines and primary astrocytes, the wells of an appropriate plate were pre-coated with poly-D-lysine (HEKs) or poly-L-lysine (astrocytes), respectively (10 µg ml^{-1} in double distilled H_2O; filter sterilised using a 0.2µm filter) for 30min at room temperature before being aspirated and washed with DMEM prior to cell loading. Cells were seeded the day before experimentation.

	CHO K1 cells	**HEK293T cells**
Neomycin (G418)	0.2mg ml^{-1}	0.2mg ml^{-1}
Zeocin	-	50µg ml^{-1}

Table 2.5: The maintenance concentrations of antibiotics used during the cell culture of stably transfected CHO K1 and HEK293T cells. Neomycin (G418) was used to select for the CHO SNAP M1-/M1-DREADD cells, whereas zeocin was used to maintain the selection pressure for the HEK LgBiT SNAP mini G and βARR-2 cells.

2.2.1.1 Astrocytes

Primary astrocyte cells were cultured from neonatal rat cortices, with the dissection performed by Zoe Smith (University of Nottingham). Briefly, dissection of the animals was carried out in a flow hood under sterile conditions. After cervical dislocation and decapitation, the cortex was collected in dissection buffer (DMEM high glucose, 10% FBS) and kept ice cold. Subsequently, the dissection media was replaced with papain (20U/ml) in glial media. Papain is a cysteine protease that acts by breaking down connective tissues within the brain tissue. The tissue was then incubated for 40min at 37°C with 5% CO_2. After papain treatment, tissue was resuspended in 10ml of glial media supplemented in DNase to dissociate cells into a single cell solution before centrifugation for 6mins at 2,000rpm. The supernatant containing dissociated cells

was collected, and the pellet resuspended in glial medium with DNase for two further rounds of titration and centrifugation. The total volume of supernatant, containing the astrocytes, had a final centrifugation for 6mins at 2,000rpm to collect the cells within a pellet. The cells were resuspended in 10ml of media and filtered through a cell strainer, before being transferred to T75 flasks. Flasks were incubated at 37°C with 95% O_2/5% CO_2 for 14 days before use and kept for a maximum of a further 2 weeks, with media being replaced every 14 days.

2.2.14 Transfection

2.2.14.1 Stable Transfection in Recombinant Cells

Stable transfection is the process of introducing DNA into a eukaryotic cell's genome. Stable transfections were conducted using Lipofectamine and either the CHO K1 or the HEK293T cell lines to generate mixed populations. Cells were grown to 70% confluence in T25 flasks and the media replaced with 1.2 ml OptiMEM. Mixtures of 2µg DNA in 200µl OptiMEM and 18 µl Lipofectamine in 200µl OptiMEM, were prepared separately and then combined to allow Lipofectamine:DNA complexes to form over 30mins at room temperature. At the end of the incubation, a further 800µl OptiMEM was added to the DNA-lipofectamine reaction, which was then mixed by vortexing. The entire 1.2 ml DNA-lipofectamine mixture was then added to the T25 flask of cells and left for 24 h at 37°C and 95% O_2/5% CO_2.

After transfection, cells were plated into T75 flasks in medium containing the selection concentrations of the relevant antibiotic (0.8mg ml^{-1} G418), and passaged for 10-14 days over which resistant colonies develop and were expanded. The resistant mixed population was then dilution cloned. Following trypsinisation, cells were diluted into two populations of either 10 cells/mL or 100 cells/mL and plated at 200µL/well of a 96-well flat-bottomed culture plate. Empty wells and those with multiple cells were identified and marked for discard. It is essential to ensure that a cell line is grown from a monoclonal cell colony to ensure that resulting cells have a uniform level of transfection and thus receptor expression for future experiments. Cells were allowed to grow for another 4 days or until 70% confluent, then trypsinised

and transferred to a 6-well flask for further cell expansion, as well as, 100µL being transferred to a 96-well plate. Once the 96-well plates were 80% confluent they were then washed with HBSS (25mM HEPES, 10mM glucose, 146mM NaCl, 5mM KCl, 1mM $MgSO_4$, 2mM sodium pyruvate, and 1.3mM $CaCl_2$ (Sigma Aldrich, pH7.4), dissolved in double distilled (dd)H_2O and kept at 4^oC) and replaced with HBSS containing cell impermeable SNAP surface AF488 (0.2µg ml^{-1}) and incubated for 30mins at 37°C. This was washed with HBSS then incubated with Hoechst's (H33342) (2µg ml^{-1}) nuclear dye in HBSS and incubated for 20 mins at room temperature. Plates were read using the Ultra IX with positive colonies identified by the levels of SNAP-tagged receptor level expression at the cell membrane. The nuclear stain helped identify individual cells. Positive clones were pelleted from T75 flasks then prepared for liquid nitrogen long term storage by being resuspended in freezing media (FCS containing 10% DMSO) and placed in cryovials. Cells were then placed in a Mr Frosty (Thermo Fisher) that contained isopropyl alcohol allowing the cells to be cooled 1°C per minute, preventing cell damage. After 24hrs cryovials were transferred to the liquid nitrogen dewars.

2.2.14.2 Lipofectamine LTX Transfection of Astrocytes

For astrocyte transfection Lipofectamine LTX was used. In this transfection method the main advantage was complete growth media could be used during the process which yielded better cell viability and a reduction in reactive astrocytes during the transfection process. Transfections were carried out with Lipofectamine LTX Reagents according the manufacturer's instructions. Cells were grown on 22mm round coverslips coated in poly-L-lysine in a 6-well plate at a concentration of 2.5 x 10^5 per well. The next day, or when cells had reached 80-90% confluency, 2.5µg DNA in 500µl OptiMEM was added directly to 2.5µl PLUS Reagent (1:1 ratio to DNA). This was gently agitated to ensure thorough mixing and incubated for 15mins at room temperature. For each transfection, 7.5µL of Lipofectamine LTX was added into the diluted DNA solution, mixed and incubated for 25mins at room temperature to allow DNA-Lipofectamine LTX complexes to form. DMEM was removed from the wells and replaced with 2ml fresh complete growth and 500µl of the DNA-Lipofectamine LTX was added directly to the astrocytes. Transfections were incubated for 18hrs at 37°C

and 95% O_2/5% CO_2. Coverslips were read using the Olympus IX inverted microscope (10x, 0.25NA; Olympus, Toyoko, Japan) with positive cells being identified by the levels of SNAP-tagged receptor level expression at the cell membrane (method in section 2.2.10.1). A pcDNA3.1 vector expressing Green fluorescent protein (GFP) was used as a transfection control, which can be detected using 488nm wavelength excitation.

2.2.14.3 Electroporation Transfection of Astrocytes Using Nucleofector™ Technology

Electroporation was also investigated as a method of astrocyte transfection. Electroporation is a physical transfection method that permeabilises the cell membrane, by applying an electrical pulse, to promote DNA to move into the cell. Nucleofector™ technology is designed to use a cell-specific combination of electrical parameters which enables transfection of primary cells that have traditionally been difficult to transfect via more traditional methods. Transfections were carried out with proprietary Nucleofector reagents and devices according the manufacturer's instructions (Lonza Wokingham Ltd (Wokingham, UK)). Cells were grown to 90% confluency in a T75 flask, with the aim to have 1.5-2 x 10^6 cells available for each transfection. Cells were washed with PBS before being trypsinized and collected by centrifugation for 12mins at 1,000rpm. The astrocytes were resuspended in 100µl Nucleofector reagent (+ supplement 1, Lonza), and then 3.5µg DNA per transfection was added. This cellular mixture was then added to a Nucleofector cuvette, ensuring all the solution was located between the two metal plates with no bubbles present, and then placed in the Nucleofector device and run on recommended programme T-20. The cuvette was flooded with 500µl of DMEM and subsequently 100µl was added to a poly-L-lysine coated 22mm round coverslip in a 6-well plate. The cells were then covered with 2ml DMEM and incubated for 24-36hrs at 37°C and 95% O_2/5% CO_2.

2.3 Assays

2.3.1Calcium Mobilisation Assay

Fluorescent calcium dyes are small molecules based on an aminopolycarboxylic group, which is a calcium chelator, with a high affinity for Ca^{2+} ions (Tsien, 1980). These dyes are esterified to produce a lipophilic molecule that enables entrance into the cell. Once within the intracellular environment, cellular esterases free the carboxyl groups and allow for calcium binding. These dyes are suitable for plate-based assays, allowing for the quick and easy exploration of Gq-mediated signalling from the M1 receptor. The dyes used in the current studies can be found in Table 2.6.

	Fluo-4 AM	**Fluo-5F AM**
K_D value	335nM	2.3µM
excitation/emission wavelength (nm)	494/506	494/515

Table 2.6: Comparison of the intracellular calcium dyes Fluo-4 AM and Fluo-5F AM. The K_D value and the label's excitation and emission wavelengths define the dynamic range of intracellular calcium concentrations over which the calcium dyes will respond.

CHO K1 cell lines expressing either SNAP-hM1-DREADD or SNAP-hM1 receptors were seeded onto 96 well clear flat bottomed black sided plates at 30,000 cells/ml the day prior to the assay being incubated in DMEM: F-12 media at 37°C/5% CO_2. On the day of the experiment, cells were incubated with *100*µL/well of Fluo-4 (2.5 µM *Fluo-4 AM in* 0.2% Pluronic F-127 and 1% DMSO *and 2.5mM probenecid* dissolved in cell-specific DMEM with 10% FCS) loading medium *for 45 minutes at* 37°C/5% CO_2. Fluo-4AM loading medium was made immediately before experimentation and shielded from the light in order to protect Fluo-4 AM fluorescent properties. Pluronic F-127, used as part of the both the Fluo-4 AM and Fluo-5F AM loading medium, is a nonionic detergent useful for solubilizing hydrophobic dye molecules to further facilitate cell loading (Granados, Soriano and Saavedra-Molina, 1997). Probenecid inhibits secretion of the deesterified Fluo-4 AM by cellular anion transporters (Silverman, Locovei and Dahl, 2008). Cells were washed twice with HBSS, and the media replaced with 100µl HBSS, before being placed onto a FlexStation 3 Microplate Reader (Molecular Devices, San Diego, U.S.A.). Automated liquid handling within the plate reader delivered ligands in either a single or dual ligand addition

protocol. Single additions were carried out by adding 20µl of ligand in HBSS from a round-bottom 96-well compound plate onto the cells at 15sec. Dual ligand additions occurred with ligands being added at 15sec then 75sec. Ligand compound plate concentrations (at 6x or 7x final assay concentration) were correctly calculated to adjust for the dilution factor once added to the cells in the well. Single ligand additions were carried out after a baseline reading of 15secs, whereas for dual additions, the secondary ligand was added 60 second after this initial addition. The total fluorescent read was taken over 165secs. All readings were measured with an excitation wavelength of 480nm and Fluo-4 fluorescence was collected at 525nm with a cut-off at 515nm.

Fluo-5F AM was designed to detect intracellular calcium levels in the 1µM - 1mM range that would saturate the response of Fluo-4 AM. Fluo-5F AM can be excited by 488nm and remains suitable for microscopy and plate screen applications (Table 2.3) (Thomas *et al.*, 2000; Paredes *et al.*, 2008). Astrocytes were loaded for 30mins, at room temperature, with 1µM of the calcium indicator Fluo-5F AM (1µM Fluo-5F AM in 0.2% Pluronic F-127 and 1% DMSO) in the standardised imaging buffer (135mM NaCl, 3mM KCl, 10mM HEPES, 15mM D-Glucose, 1mM $MgSO_4$ and 2mM $CaCl_2$, dissolved in ddH_2O; pH 7.6). This was made immediately before experimentation and shielded from the light in order to protect Fluo-5F AM fluorescent properties. Cells were then transferred to standarised imaging buffer for a further 30mins to allow de-esterification of the accumulated Fluo-5F AM. The mounted coverslip was then transferred to the stage of an Olympus IX70 inverted microscope (10 × 0.25 NA). Ligands were added by manual displacement of the bath solution with excess buffer containing the ligand. Using an ORCA-ER camera (Hamamatsu, Germany) Fluo-5F AM fluorescence was detected following excitation at 470/20 nm (exposure 100ms, bining 4x4) with emission detected through 535/50 nm band pass filter. Camera and shutter were controlled by Micromanager software.

2.3.2SNAP-tagged Receptor Internalisation

The use of the cell impermeable SNAP surface 488 allows receptor internalisation of activated receptors to be selectively investigated. The receptors of interest have the

SNAP-tag fused to the N-terminus of their GPCR structures, allowing this impermeable dye bind irreversibly. This is then exploited after receptor activation and internalization, where fluorescence can be tracked intracellularly.

Cells were seeded on black imaging plates at 20,000 cells per well the day before the experiment. On the day, cells were incubated for 30min in 0.1µM membrane impermeable SNAP-surface-488, in complete media, at 37°C/5% CO_2. Plates were then washed with HBSS before increasing concentrations of test ligands were added to the cells, to produce concentration response curves. After a 30min incubation with the ligands, cells were fixed for 15min with 3% paraformaldehyde (in PBS) at room temperature, shielded from the light. Cells were then washed with PBS before 2µg ml^{-1} H33342 nuclear stain was incubated with the cells for 15min. The IX Ultra confocal plate reader (Molecular Devices, San Diego, U.S.A.) was then used to image 4 sites per well, using a Plan Fluor 40x Na0.6 extra long working distance objection at 405nm (H33342) and 488nm (SNAP) excitation.

2.3.3Fluorescent Ligand Binding Assays

The use of fluorescent ligands provides an opportunity to investigate receptor-ligand interactions using equilibrium and kinetic binding studies (Briddon, Kellam and Hill, 2011), for example by using live cell imaging to directly visualise the binding of such ligands in living cells. CHO K1 cell lines expressing SNAP hM1-DREADD were seeded onto 96 well flat bottomed black sided plates at 25,000 cells/ml the day prior to the assay being incubated at 37°C/5% CO_2. A Plan Fluor 20 x NA 0.6 extra-long working distance air objective with a pinhole set to 4 was used to image one central site per well collecting images of H33342 stained nuclei (405 nm excitation) and Cy5-fluorescent ligand binding (633 nm excitation). Laser powers and gains were kept constant for all experiments.

2.3.3.1 Fluorescent Ligand Binding Assays

On the day of the experiment, cells were washed in HBSS + H33342 (2µg ml^{-1}) + 0.1% BSA. To evaluate specific binding cells were incubated with increasing concentrations of the relevant fluorescent ligand (**III**), while non-specific binding was calculated by

adding 10μM of the antagonist atropine across the range of increasing concentrations of **III**.

2.3.3.2 Fluorescent Ligand Competition Assay

To determine competition binding between **III** and test ligands, cells were again washed in HBSS + H33342 (2μg ml^{-1}) + 0.1% BSA and incubated with 10nM of the relevant fluorescent ligand and increasing concentrations of the test ligand (e.g. clozapine derivatives) concentrations. 10μM of atropine was used to define non-specific binding. Plates were incubated at room temperature, while being shielded from the light, for 1hr and imaged at this 1hr time point. Alternatively, time course data was taken at 10min intervals over 1hr. Images of wells were taken on the IX Ultra (Molecular Devices, San Diego, U.S.A.) confocal plate reader without a wash step. Images were compared between including a wash step and without a wash step. It was found that without a wash step images were sufficient for analysis, without high levels of background fluorescence, with the advantage of maintaining equilibrium conditions that wash steps remove due to increased ligand dissociation (Sridharan *et al.*, 2014).

2.3.4Nano Luciferase Complementation Assay

NanoBiT is a complementation reporter assay that can be utilised for quantitative investigation of signalling kinetics by monitoring the protein-protein interaction between GPCRs and their effectors, under relevant physiological conditions (see Chapter 4) (Dixon *et al.*, 2016; Wan, Okashah, Inoue, Nehmé, Carpenter, C. G. Tate, *et al.*, 2018). NanoBiT assays were used to investigate the recruitment of a mini Gq protein (mini Gq71; Wan et al 2018; Nehme et al 2018) or β-arrestin-2 (βARR-2) (Reyes-Alcaraz *et al.*, 2018) recruitment to the M1 receptor, and its DREADD equivalent. As described in more detail in Chapter 4, the Large BiT (LgBiT; 17.6 kDa) and Small BiT (SmBiT; 1kDa) nanoluciferase fragments, were respectively fused to the M1 receptor and to either the mini G protein or βARR2. Upon receptor recruitment of these downstream proteins, the SmBiT and LgBiT fragments associate to form functional luciferase, and with addition of the substrate furimzaine produce a luminescent signal.

HEK cell lines expressing either LgBitSm114 M1 or M1-DREADD mini Gq or LgBitSm117 M1 or M1-DREADD βARR2 were seeded onto poly-D-lysine coated 96 well clear flat bottomed white sided plates at 40,000 cells/ml the day prior to the assay being incubated at 37°C/5% CO_2. Cells were washed twice with HBSS + 0.1% BSA, then 1µM Nano-Glo furimazine (Promega (Madison, WI, USA)) in HBSS + 0.1% BSA was then added to each well (final volume 50µl). In the case of allosteric modulator pre-treatment, BQCA (10µM) was added to this solution and incubated for 5min before being added to plates. Luminescence readings were taken on a PHERAstar FS microplate reader (BMG Labtech, Ortenberg, Germany) in a 37°C heated compartment. Basal luminescence was measured over three 2-minute cycles, and then ligands were added rapidly in 10µl at 6x final assay concentrations, before luminescence reading for a further 25 min at 2 min intervals.

2.3.5Astrocyte Stellation Assay

Calcein AM is a fluorescent dye and is commonly used within viability assays, as only living cells have the functional esterases to cleave the lipophilic acetomethoxy groups to release fluorescent calcin. However, it is additionally useful as a general fluorescent dye which is permeable and present throughout the cytoplasm of the cell allowing for the morphological features of the astrocytes to be visualised under 488nm excitation. This is a fast and simple method to assess the morphological changes of the astrocytes, without the need for lengthy immunocytochemical protocols. As with the Fluo-4 AM/-5F AM dyes, Calcein is suitable for use in a high-throughput 96-well format.

Astrocytes were loaded into poly-L-lysine coated flat-bottomed, black sided 96-well plates at 10,000 cells/ml the day prior to the assay and were incubated at 37°C/5% CO_2. The next day, M_1 receptor ligands were diluted to appropriate concentrations and loaded directly into the well of the astrocytes covered with DMEM; the plates were then incubated for 3hrs at 37°C/5% CO_2. After this time, cells were loaded with 1µM Calcein AM for 30mins at 37°C/5% CO_2. Cells were then washed twice with the standardised astrocyte buffer and read on the IX Ultra confocal plate reader. A Plan Fluor 20 x NA 0.6 extra-long working distance air objective with

a pinhole set to 4 was used to image once central site per well. A 488nm (GFP) laser excitation was used. Laser powers and gains were kept constant for all experiments.

2.4 Data analysis

2.4.1 Calcium Mobilisation Assay

Changes in cellular calcium concentration are a universal mechanism for signal transduction, and can thus give information on the potency and relative efficacy (as maximal response) for agonists at a target receptor. Fluorescence readings, taken in either duplicate or triplicate, from the calcium indicator Fluo-4 AM were used to fit calcium concentration response curves, performed using GraphPad Prism 7.04 (GraphPad software, San Diego CA, U.S.A.), using pre-programmed equations. Concentration response curves were plotted as peak increase over the basal read over the time frame of the experiment, taken as $\Delta F/F_{basal}$. In the case of dual addition, fold change was taken from the time course from the addition of the second ligand to endpoint. Data was normalised as 100% to the top concentration of the maximal response for the relevant reference agonist used: Acetylcholine with the M1-WT cell lines and clozapine-N-oxide (CNO) with the M1-DREADD cell lines, and 0% set to vehicle. Responses were fit as defined by the following equation:

$$Response = \frac{Rmax\ [\mathrm{A}]}{[\mathrm{A}] + \mathrm{EC50}}$$

Where Rmax is the maximal agonist response, [A] is the concentration of agonist, EC50 is the concentration of agonist which produces a half maximal effect and n is the Hill slope.

Responses were defined as agonist pEC_{50} values (concentration of ligand that produces half maximal response i.e. the potency; expressed as –log EC50; pEC50) and Rmax values (the maximum response), as mean ± standard error of the mean (SEM) to show pooled data from 5 individual experiments, performed in either duplicate or triplicate.

2.4.2 Receptor Internalisation

Receptor internalisation was assessed using stably transfected cell lines that expressed either the SNAP M1-WT or SNAP M1-DREADD. Receptors were labelled

with SNAP surface 488, and acquired using the IX Ultra confocal plate reader then analysed using an automated granularity algorithm (MetaXpress, Molecular Devices). This provided quantitative data reflecting the intensity of intracellular fluorescence. All images acquired were 16-bit greyscale without saturation, meaning the fluorescence intensity within pixel is represented as a number from 0 (black) to 65535 (white). Fluorescent "pits" of SNAP-labelled receptors were identified with a diameter of 2-3µm and nuclei at 3 – 7µm which allowed the analysis to generate a pit count per cell (analysis is similar to that shown in section 2.4.5).

2.4.3NanoBiT Complementation Assay

Luminescence readings from the NanoBiT LgBiT and SmBiT complementation were used to fit concentration response curves, performed using GraphPad Prism 7.04 (GraphPad software, San Diego CA, U.S.A.), using pre-programmed equations. Concentration response curves were plotted as fold change from peak over the basal read at a set time point, to show pooled data from 5 individual experiments, performed in either duplicate or triplicate. Concentration response curves were taken at an early peak (3min) time point and a sustained (25min) time point. NanoBiT experiments were normalised as 100% to the top concentration of the maximal response induced by the relevant reference agonist used: ACh with the M1-WT cell lines and CNO with the M1-DREADD cell lines or iperoxo when comparing orthosteric ligands and 0% set to vehicle. Concentration response curves were fit with the same equation as in section 2.4.1. Responses were defined as agonist pEC_{50} values and R_{max} values, as mean ± standard error of the mean (SEM).

2.4.4Time Course of Stimulation

Time course data from the calcium mobilisation experiments or NanoBiT experiments were plotted as arbitrary fluorescence or luminescence units, respectively, against time in Prism 7.04. Time courses included basal readings of 15sec for CHO calcium experiments or 6min for HEK NanoBiT experiments before ligand addition and subsequent responses.

2.4.5Fluorescent Binding Studies

Images were acquired using the IX Ultra confocal plate reader and were analysed using an automated granularity algorithms (MetaXpress, Molecular Devices) to provide quantitative data reflecting the intensity of fluorescent ligand binding (Liu *et al.*, 2016). All images acquired were 16-bit greyscale without saturation, meaning the fluorescence intensity within pixel is represented as a number from 0 (black) to 65535 (white). Granules were identified between a diameter of 1-3µm and a threshold for grey level count was set according to the total (positive) and non-specific (atropine, negative) images on the day of the assay. The algorithm also identified nuclei of 6 – 10µm in diameter which allowed the analysis to generate a granule count per cell.

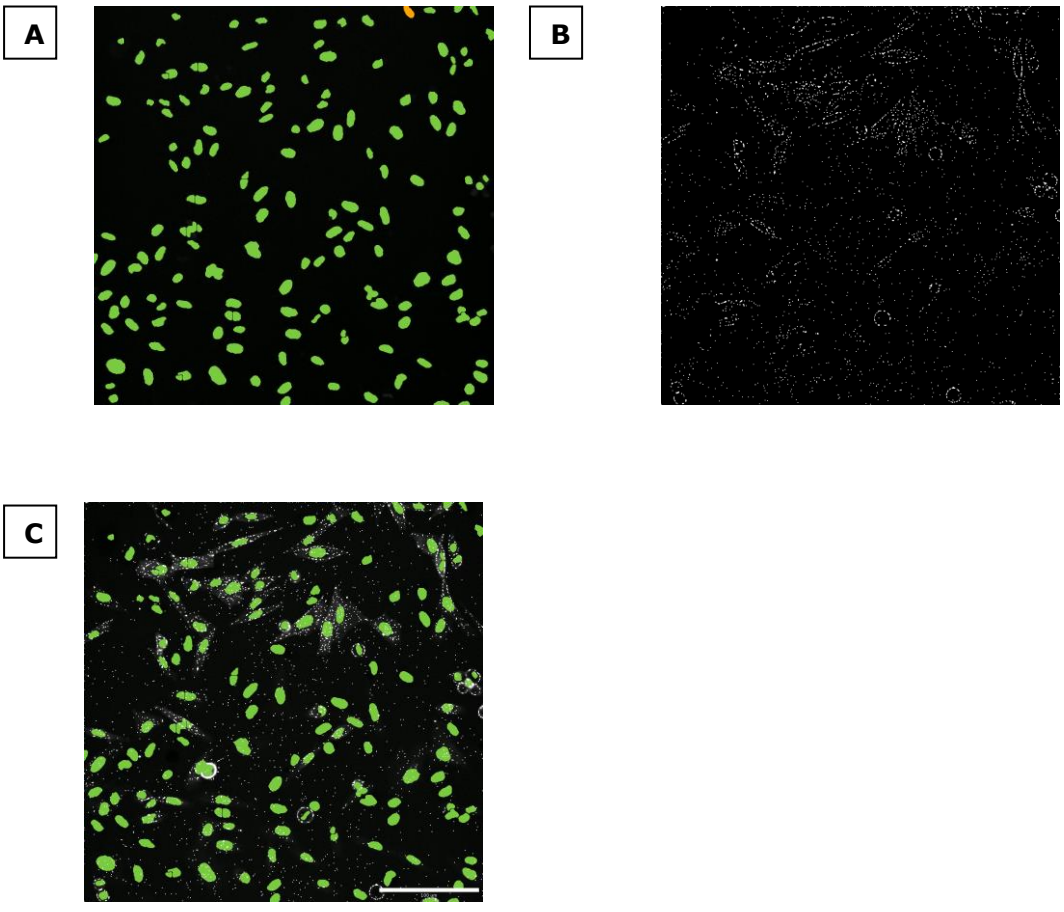


Figure 2.1: Representative granularity analysis. Representative images of fluorescence binding analysis. (A) Shows H33342 stained nuclei identified by the algorithm; identified nuclei of 6-10µm in diameter (B) Fluorescent granules identified by the algorithm; identified 1-3µm (C) Overlay of analysis against cells labelled with III, grey-scale.

In saturation binding studies total and non-specific binding data at different fluorescent ligand concentrations were globally fitted to a one-site model with the following equation:

$$Total\ Binding = \left(\frac{Bmax\ [L]}{[L] + KD}\right) + (NS\ [L]) + Background$$

$$Non - Specific\ binding = (NS\ [L]) + Background$$

The K_D value is the equilibrium dissociation constant, the ratio koff / kon of the rate constants for association (k_{on}) and dissociation (k_{off}), and representing the concentration of fluorescent ligand required to occupy 50 % of the receptor population. B_{max} represents the total concentration of receptors in the assay. [L] is the concentration of the fluorescent ligand and NS is the slope of the linear non-specific binding background.

In competition binding studies, individual experiments were carried out in duplicate and normalised to the fluorescence ligand binding in the absence of competing ligand (total, 100%) and in the presence of 10µM atropine (non-specific, 0%). Inhibition curves were fitted using Graphpad Prism and the equation:

$$Response = \frac{Rmax\ [\mathrm{A}]}{[\mathrm{A}] + \mathrm{IC50}}$$

Where Rmax is the maximal agonist response, [A] is the concentration of agonist, IC50 is the concentration of agonist that produces a half maximal inhibition and n is the Hill slope.

From which pIC_{50} values could be determined (-log concentration of unlabelled ligand that produces half-maximal inhibition). All experiments are shown as the pooled data of 3-5 experiments carried out in duplicate ± SEM.

Next, IC50 values were converted to Ki values using the Cheng-Prusoff equation (Yung-Chi and Prusoff, 1973):

$$Ki = \frac{IC50}{1 + \frac{[L]}{Kd}}$$

Ki is the affinity of the test ligand, IC_{50} is the concentration of the test compound that inhibits 50% of the fluorescent ligand binding (**III**), [L] is the concentration of **III** and K_D is the affinity of **III** as calculated by saturation binding.

2.4.6Astrocyte Stellation

Astrocytes are notoriously heterogenous and pleomorphic. It is therefore somewhat subjective when manually assessing their stellate morphology, however, morphological changes between a protoplasmic flat and a stellate or process-bearing appearance can be profound. To circumvent human bias when manually assessing stellate morphology, all experiments were blinded during cell counting. A stellation index with the following constraints was followed in order to standardise the selection of stellate astrocytes: cells must have at least 2 cell processes extending from the main body of the cell, forming a process-bearing appearance with the cytoplasm shrinking towards the nucleus. The percentage of stellate cells from the total cell number within a 96-well plate was calculated and data were fitted from pooled data from 5 individual experiments carried out in duplicate (~1000 cells counted).

2.4.7Single Cell Calcium Response

For an individual cell, the pattern of calcium spiking in response to ligand addition can be determined using a calcium indicator such as Fluo-5F AM. Image files were viewed in ImageJ, and cells were manually selected using TimeSeries Analyzer V3 plugin (open source). This software was used to define regions of interest (ROI) centred on individual cells in order to measure cytosolic calcium release; with ROI height and width set as 5x5. A multi measure function was used to determine the mean Fluo-5F AM fluorescent value of each individual cell over the 300s time course. This data was analysed using a bespoke script called "calcium GUI", written by Dr. Wayne Croft (University of Nottingham), in MetaXpress R2015b (The MathWorks, Inc., Natick, MA, U.S.A). Mean fluorescence intensity of pixels falling within each ROI were quantified and expressed as the ratio of fluorescence at time *t* divided by mean intensity from a 60sec window prior to the first increase in stimulus concentration (F/F_{basal}). Values were taken as the percentage of cells which responded over the threshold set to 1.4x increase over basal (ΔF) and the area under the curve (AUC) values were determined from the fluorescence traces (Chapter 5). Individual representative calcium traces of fluorescence intensity fluctuations were also taken. Data was fitted from pooled data from at least 5 individual experiments, performed in duplicate.

2.5 Statistical analysis

2.5.1Concentration Response Curves

Normal distribution was verified then statistical analysis between two independent groups was performed using Student's unpaired *t*-test. For analysis of more than two independent groups, a one-way analysis of variance (ANOVA) followed post-hoc by Dunnett's test was used. Statistical significance was defined * P < 0.05, **P < 0.01, ***P <0.001 and NS – not significant.

2.5.2Stellation Analysis

Normal distribution was verified then statistical analysis was performed on more than two independent groups using a one-way ANOVA followed by Dunnett's post hoc test. Statistical significance was defined * P < 0.05, **P < 0.01, ***P <0.001 and NS – not significant.

2.5.3Single Cell Calcium Analysis

Normal distribution was verified then then statistical analysis was performed using a one-way ANOVA by Dunnett's post hoc test. Statistical significance was defined as *P<0.05, **P < 0.01, ***P <0.001 and NS – not significant.

Chapter 3

GENERATION OF M1-WT AND M1-DREADD EXPRESSION VECTORS FOR FUNCTIONAL STUDIES

3.1 Introduction

The DREADD chemogenetic system was originally designed to control neuronal signalling pathways, with the Gq-DREADD typically used to activate neuronal signalling and firing while Gi-DREADD inhibits adenylate cyclase and attenuates neuronal activity and neurotransmitter release (B. N. Armbruster *et al.*, 2007). DREADDs also achieve a greater level of selectivity when investigating the function of mAChR subtypes *in vivo* which have highly conserved amino acid sequences within their orthosteric binding sites. It has been shown that mutation of Ala5.46Gly at the M1 mAChR causes a decrease in ACh affinity, potency and signalling efficacy (Allman *et al.*, 2000). This was exploited by (B. N. Armbruster *et al.*, 2007) to create the DREADD receptor in which ACh has reduced affinity for the M1 mAChR while simultaneously increasing the affinity of clozapine-N-oxide (CNO) for the receptor. Armbruster *et al.* were able to show Tyr3.33 and Ala5.46 were highly conserved across the five mAChR subtypes and that two point mutations (Tyr3.33Cys and Ala5.46Gly) produced the M1-DREADD receptor in which CNO now acted as a high potency agonist. Molecular docking of CNO into the X-ray structure of the M3 mAChR demonstrated that this molecule makes contact with both Tyr3.33 and Ala5.45 residues (Andrew C. Kruse *et al.*, 2014), and this was supported by the crystal structure of the M1 mAChR confirming the importance of these residues (Thal *et al.*, 2016). This does not give much explanation as to why CNO lacks affinity at the WT mAChR; however, it has been suggested that the Tyr3.33Cys mutation causes a conformational rearrangement of the aromatic Tyr that alters CNO binding to increase its affinity at the DREADD receptor (Thal *et al.*, 2016). It has also been suggested that the TM5 Ala5.46Gly mutation increases the flexibility of this transmembrane and enables CNO-specific inward movement within the orthosteric site (Wess, Nakajima and Jain, 2013). Together these mutations may also allow the stabilisation of an active DREADD receptor conformation by CNO necessary for its agonist response. These two amino acid mutations are therefore imperative for the formation of a functional and selective DREADD system.

In order investigate the pharmacodynamics of ligand binding and the subsequent intracellular signalling pathways of the DREADD receptor activation; it was necessary to produce a WT M1-mAChR for comparison in key assays. The endogenous ligand,

ACh, binds to the orthosteric binding site located within the extracellular third of the core of the seven-transmembrane domain (Burger *et al.*, 2018). The TM3 region has been identified as particularly important in both binding and activation mechanisms (Venkatakrishnan *et al.*, 2013), with ACh interacting with TM3-7 regions and ECL2 (Haga *et al.*, 2012; Kruse *et al.*, 2012). The DREADD Tyr3.33Cys mutation is located on TM3 supporting this location's importance of the Tyr3.33 residue for ACh binding. Detailed pharmacological comparison between the M1-WT and M1-DREADD receptors is needed to truly decipher the advantages of using the DREADD system as a highly selective and controlled biological tool able to overcome the issues in drug promiscuity between mAChR subtypes due to their highly conserved orthosteric sites.

Fluorescence microscopy is an invaluable tool for the visualisation of protein function and pharmacological investigations in living cells. Until recently, the most common ways to label receptors for investigation were antibody based detection of native or epitope-tagged receptors (e.g. FLAG-tagged; Holliday et al 2007), or fusion of the receptor to a C-terminal fluorescent protein such as green fluorescent protein (GFP) or yellow fluorescent protein (YFP) (Day and Davidson, 2009; Uno *et al.*, 2015). Fluorescent protein fusions in particular allow direct visualisation of labelled proteins (Cormack, 1998; A. A. T. Johnson *et al.*, 2005), for example, in order to follow ligand directed receptor trafficking in living cells (Tarasova *et al.*, 1997). However, there are some limitations, for example, the positioning of the GFP-tag on the C terminal regulatory domain of the GPCR may influence signalling and function (Hanazono *et al.*, 1997; Haseloff *et al.*, 1997; Liu *et al.*, 1999; Palmer and Freeman, 2004). Furthermore newly synthesised proteins, as well as those at the cell surface, are fluorescent and therefore effect GFP detection levels (Sample, Newman and Zhang, 2009). Thus, more flexible labelling strategies have now been developed to allow time-dependent labelling and expand the range of fluorophores (for example for the latest advances in imaging techniques, such as super resolution microscopy). These include the use of Halo-tag or SNAP/CLIP-tag protein fusions (Erdmann *et al.*, 2019).

The SNAP-tag is a modified form of the 20-kDa monomeric DNA repair enzyme, human O^6-alkylguanine-DNA-alkyltransferase (AGT). The SNAP-tag can be specifically labelled with fluorescent synthetic O^6-benzylguanine (BG) derivatives, resulting in a

stable bond between the tag and the target probe (Keppler, Kindermann, *et al.*, 2004; Keppler, Pick, *et al.*, 2004; Macias-Contreras, He and Zhu, 2018). Using fluorescence microscopy in conjunction with SNAP-tag technology has allowed for investigations into the spatiotemporal aspects of GPCR signalling *in vivo* (Farrants *et al.*, 2018), internalisation (Levoye *et al.*, 2015), intracellular signalling pathways (Foster and Bräuner-Osborne, 2017; Jensen *et al.*, 2017) and receptor-ligand interactions (Haruki, Gonzalez and Johnsson, 2012; Mie *et al.*, 2012).

There are a large number of commercially available BG-conjugated substrates, allowing effective and specific labelling of the target protein within different cellular systems and assays in order to fit experimental requirements. The SNAP-tag can be fused to the intracellular C-terminus or extracellular N-terminus of the target protein (Keppler, Pick, *et al.*, 2004). For GPCRs, positioning of the SNAP-tag at the N terminus (following a signal sequence peptide to ensure correct receptor folding and maturation) is generally desired (Juillerat *et al.*, 2003; Uttamapinant *et al.*, 2010; Tabor *et al.*, 2016). This places the label extracellularly, and so in combination with membrane impermeant variants of the BG-fluorescent dyes (such as SNAP surface AF488), allows labelling of the cell surface receptor population selectively, for example, to study ligand induced internalisation (Kilpatrick, Humphrys and Holliday, 2015; Levoye *et al.*, 2015). N-terminal SNAP-tagged receptors also preserve the native intracellular signalling and regulatory domains (Bosch *et al.*, 2014) and typically the label does not interfere with small molecule ligand binding sites that reside within the transmembrane domain bundle (Farrants *et al.*, 2018).

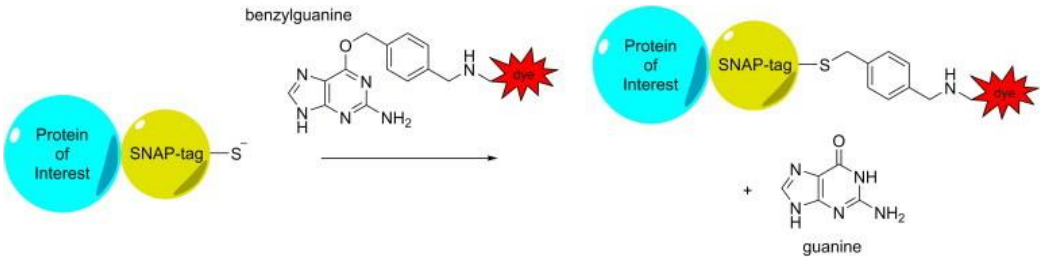


Figure 3.1: In a suicide reaction, the 20 kDa SNAP-tag removes the benzyl group, which is linked to a fluorophore (e.g. Alexa Fluor 488 dye), from its benzylguanine (BG) substrate and transfers it onto a cysteine residue within its active site, thereby covalently and irreversibly linking a fluorophore to the SNAP-tagged. Image taken from (Bosch et al., 2014).

Aims

This chapter outlines the generation of SNAP-tagged human M1 receptor constructs and expressing cell lines, and the generation of the DREADD variant of this receptor. First, we aimed to mutate the human M1 cDNA to form the hM1-DREADD receptor by making the substitutions Y106C and A196G. Secondly, we aimed to fuse an extracellular N-terminal SNAP-tag to the hM1 and hM1-DREADD constructs by ligating the receptor cDNAs in frame with the SNAP pcDNA3.1(+)neo vector. Finally, SNAP-tagged hM1-WT and hM1-DREADD constructs with a C-terminal LgBiT motif were constructed for use in NanoBiT luciferase complementation assays, described in Chapter 4.

3.2 Results

3.2.1Design of desired SNAP-tagged pcDNA3.1(+)neo vectors

The pcDNA3.1(+)neo mammalian vector was chosen as the foundation for the DNA constructs engineered in this chapter. This vector contains a cytomegalovirus (CMV) region, which is a potent promoter that is strongly expressed in mammalian cell lines and allows for a high level of receptor expression. A polyadenylation signal (bovine growth hormone, bGH poly A) allows for receptor expression in eukaryotic cells and the forward-reading T7 promoter and reverse-reading bGH priming sites permit the resultant DNA to be sequenced. Sites of antibiotic resistance that enable the selection of both transformed bacterial cells (ampicillin) and transfected mammalian cell lines (neomycin) were also present within the vector (Figure 3.2).

The hM1-DREADD or hM1 receptor cDNA were ligated into a pcDNA3.1(+)neo vector containing either the SNAP-tag fused to the extracellular N-terminus of the M1 receptor (Fig 3.2, A) or both the extracellular SNAP-tag and intracellular C-terminal LgBiT (Fig 3.2, B) (Dixon *et al.*, 2016). The SNAP-tagged pcDNA3.1(+)neo was previously produced by the Nick Holliday (University of Nottingham) by adding an N-terminal 5HT3 signal sequence and SNAP-tag between KpnI and BamHI sites of the multiple cloning site (MCS) of the vector (Watson, Brown and Holliday, 2012b). The

large fragment of Nano luciferase was placed downstream of the SNAP-tag between the XhoI and XbaI restriction sites of the SNAP-tagged pcDNA3.1(+)neo vector by members of the Holliday group (University of Nottingham).

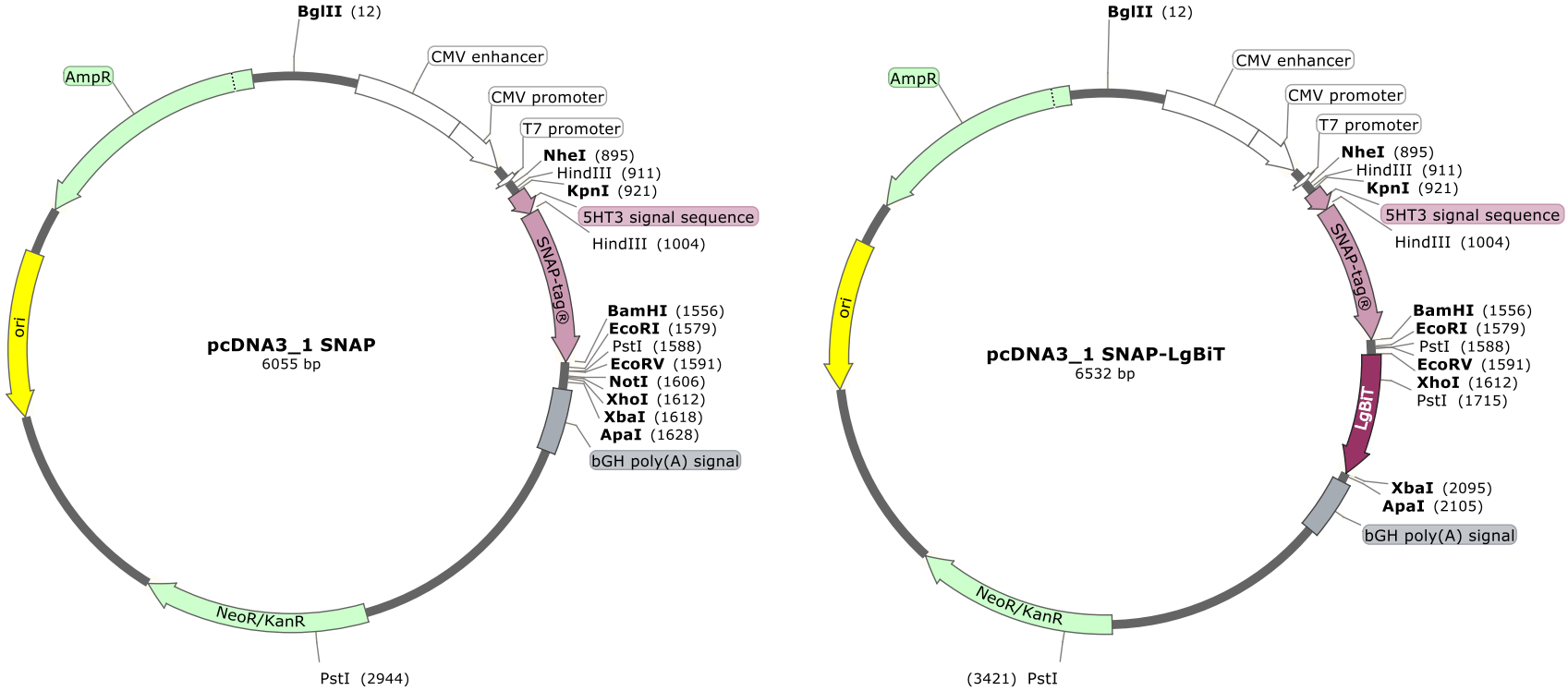


Figure 3.2: ***The vector map showing the SNAP-tagged and LgBiT SNAP-tagged pcDNA3.1(+)neo vector previously made by the Holliday Lab, used for the cloning of the M1 constructs****. Visible is the SNAP-tag present between KpnI and BamHI restriction sites with the 5HT3 signal sequence located directly upstream. The ampicillin and neomycin resistances allow for transformed bacterial selection and mammalian transfection selection, respectively. (A) The SNAP-tag is flanked on either side by the forward reading T7 promoter and the reverse bGH poly(A)signal which are utilised for DNA sequencing of the constructs. (B) The SNAP-tag and LgBiT construct are now flanked by the CMV and T7 promoter (5') and bGH poly (A) signal (3'). The fusion between the receptor and LgBiT includes a 5 amino acid linker (Gly Ser Gly residues, followed by the XhoI site).*

3.2.2Site Directed Mutagenesis to form the hM1-DREADD Receptor

First, it was necessary to mutate the human M1 receptor (Genbank Ref: NM_000738) with the two point mutations (Y106C and A196G) in order to produce the hM1-DREADD construct required in later experiments. These mutations were carried out sequentially using the Quikchange approach (section 2.2.1.1), in which annealing primers substituted the nucleotides necessary to make the relevant amino acid changes in hM1. During PCR mutagenesis, the primers bind to the hM1 construct at the same forward and reverse positions within the pcDNA3.1(+)neo vector, and the polymerase amplifies the entire pcDNA3.1(+)neo vector sequence. PCR amplified DNA is unmethylated, and so can be enriched in the reaction prior to transformation, by DpnI digestion, which degrades the methylated wild type template DNA. Description of the primer design and sequences is given in section 2.2.1.1 and 2.2.1.2.

3.2.3Introducing Restriction Sites to Flank the hM1 Constructs to Allow Ligation within the SNAP-tagged pcDNA3.1(+)neo Vectors

Next, it was necessary to add BamHI and XhoI restriction sites which flanked the hM1 and hM1-DREADD constructs to allow for ligation in frame within the SNAP-tagged pcDNA3.1(+)neo vector . This was carried out during the PCR amplification of the two M1 constructs using primers with one of each of the restriction sites present in the forward or reverse primer sequences. Within the primer design it was also necessary for the “ATG” start codon to be removed to allow the SNAP-tag to fuse to the N-terminal of the M1 constructs, while preserving the STOP codon at the end of the receptor (see section 2.2.1.2).

For ligation into the LgBiT SNAP-tagged pcDNA3.1(+)neo vector, the same forward primer was used however the reverse primer was designed to remove the STOP codon and add an in frame XhoI restriction site. The XhoI reverse primer incorporated a short linker after the end of the M1 sequence Gly-Ser-Gly (highlighted in blue, Table 2.3), before the XhoI site and between the interface of the LgBiT sequence. This space gave a small separation between the LgBiT domain and the potential palmitoylation site (final Cys in the M1 sequence) that may be lipid modified and attached to the posttranslational modifications of the receptor (Chini and Parenti, 2009; Naumenko and Ponimaskin, 2018). There is no STOP codon to allow in frame fusion of the expressed receptor sequence to the C terminal LgBiT tag after ligation into the LgBiT SNAP pcDNA3.1(+)neo vector. As described in section 2.2.2 blunt ended PCR products were first subcloned into the pJET1.2 plasmid, prior to excision with BamH1 and XhoI and cloning into the relevant pcDNA3.1 vector (section 2.2.4) to create the final expression constructs (Figure 3.3).

3.2.4Ligation into Desired Vectors to Achieve Recombinant Plasmids

The final stage to produce the hM1 recombinant plasmids was to ligate the constructs into the SNAP pcDNA3.1(+)neo vector (Fig 3.6) or the LgBiT SNAP pcDNA3.1(+)neo vector (Fig 3.3).

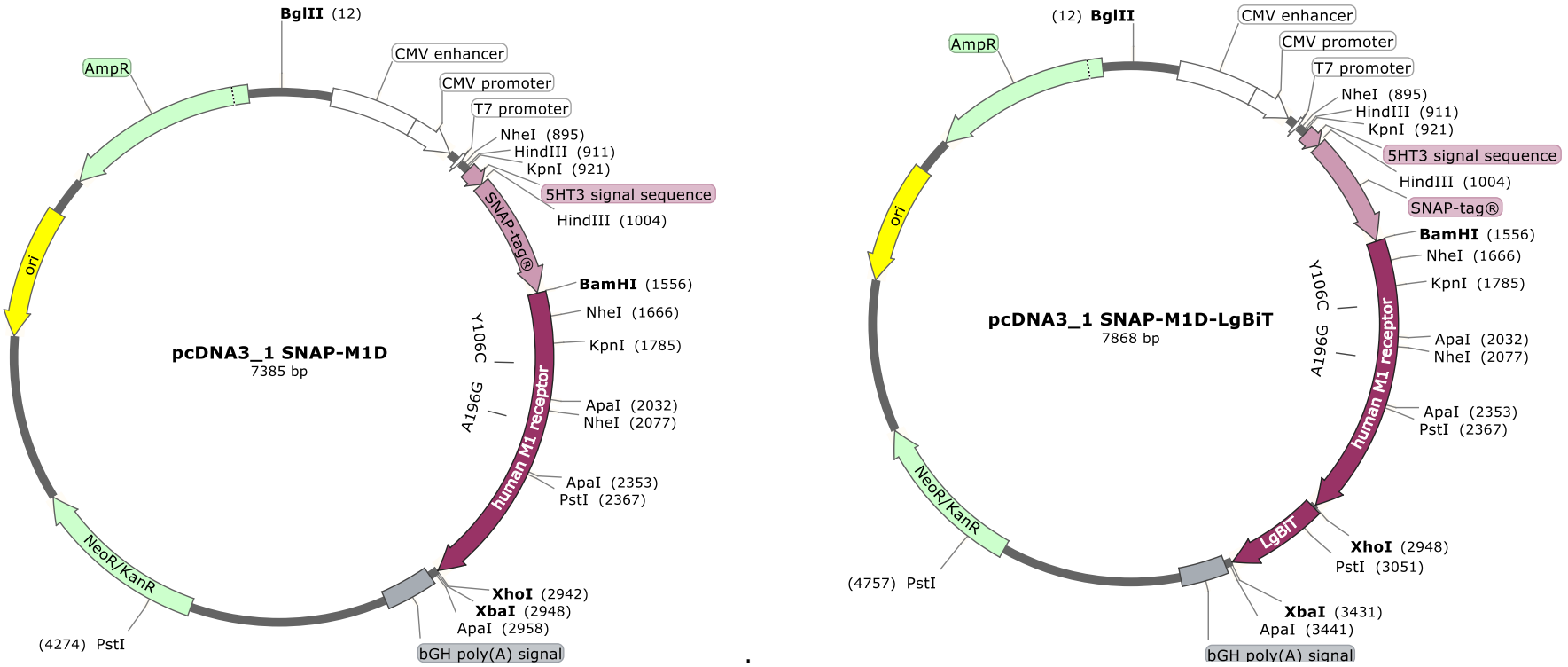


Figure 3.3: ***Vector maps showing human M1 receptor cloned into respective pcDNA3.1(+)neo vectors.*** *(A) Human M1-DREADD cloned between the SNAP-tag and the bGH poly (A) sequence (B)* ***human*** *M1 receptor cloned between the SNAP-tag and LgBiT sequence. The two point mutations for the M1-DREADD receptor is shown as Y106C and A196G.*

3.2.5Restriction Digests Verfies the hM1 Constructs are Present within the LgBiT SNAP-tagged pcDNA3.1(+)neo Vector

After ligation, constructs were transformed into *E.Coli* component cells are expanded through mini and maxi-preps before the DNA was extracted and restriction digested by respective enzymes. Figure 3.4 shows the gel electrophoresis from the resultant restriction digest, confirming the LgBiT SNAP-tagged pcDNA3.1(+)neo vector and hM1/hM1-DREADD insert were present and of the correct size with the inserts being 1.2 kb and the SNAP-tagged vector seen at 6kb. Three restriction digests were carried out: KpnI + BamHI releases the SNAP tag and results in three bands; ~7kb, 635bp and 229bp, XhoI + BamHI releases the receptor resulting in two bands; 6.5kb and 1.4kb and XhoI + Xba cuts the LgBiT and produces two bands; 7.4lb and 483bp.

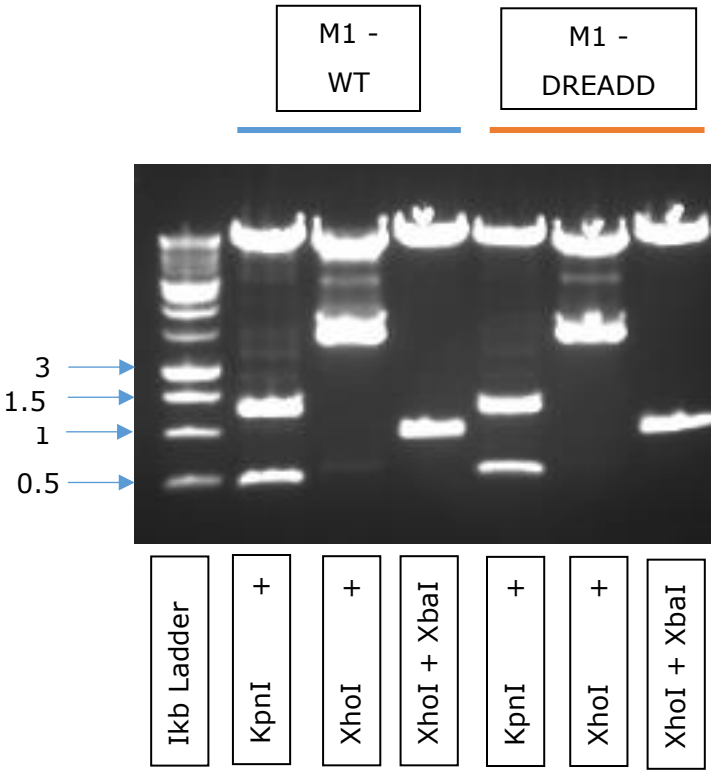


Figure 3.4: The gel electrophoresis from the resultant restriction digest, confirming the LgBiT SNAP-tagged pcDNA3.1(+)neo vector and hM1 insert were present and of the correct size with the inserts being 1.2 kb and the SNAP-tagged vector seen at 6kb.

3.2.5DNA Sequencing

A sample of each construct shown in the figures above was sent for DNA sequencing to verify the insert of interest contains the correct nucleotide sequence, is in frame with the N and C terminal tags, and without unexpected mutations introduced by PCR. Examples of this analysis are given below.

3.2.5.1 The Interface between the 5HT3 Signal Sequence and SNAP-tag within the Vector

The positioning of the signal sequence and SNAPtag was verified in the pcDNA3.1(+) SNAP vector. The KpnI restriction site was identified upstream of the Kozak site for translation and 5HT3 signal sequence, which was used to insert this construct into the pcDNA3.1(+)neo vector. This sequence interfaces with the start of the SNAP-tag amino acid sequence (DKDC motif); with an intervening HindIII restriction site (Fig 3.5).

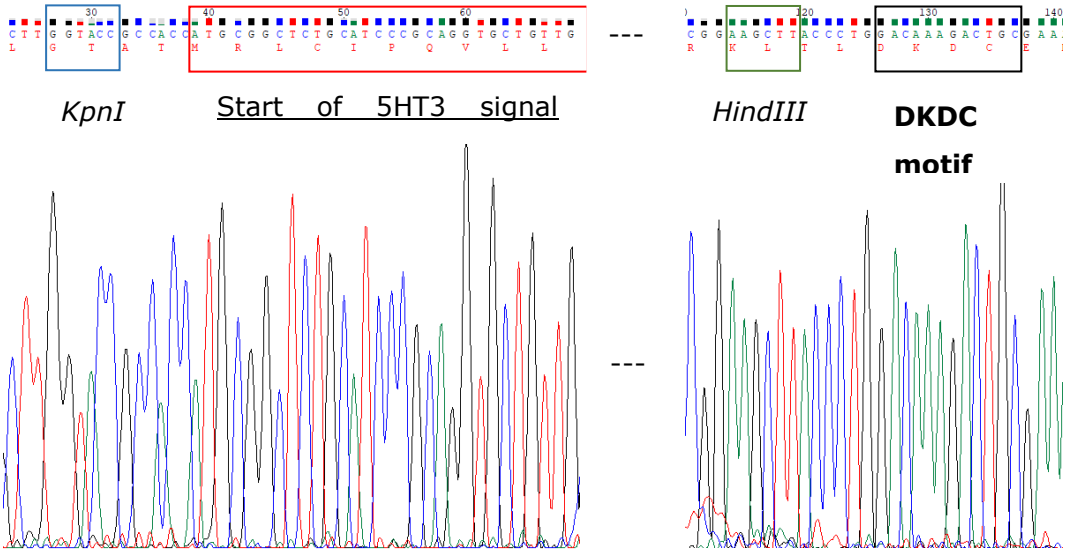


Figure 3.5: Sequence identification using Chromas software to investigate DNA sequence of the SNAP-tagged pcDNA3.1(+) vector (generated from the T7 promoter primer), utilising the DNA sequence from the maxiprep of M1 and M1-DREADD. The KpnI restriction site (blue box, shown in italics) is shown up stream of the 5HT3 signal sequence (red box, underlined). The HindIII restriction site (green box, shown in italics) is shown at the end of the 5HT3 signal sequence that interfaces with the DKDC epitope motif indicative of the start of the SNAP-tag sequence (black box, bold).

3.2.5.2 The Interface between the SNAP-tag and the Human M1 Receptor Sequence

DNA sequencing showed the successful addition of the M1 constructs within the SNAP-tagged pcDNA3.1(+)neo vector. The amino acid sequence confirms the M1 construct is downstream of the SNAP-tag, separated by the BamHI restriction site added during PCR amplification by specifically designed primers (Fig 3.6).

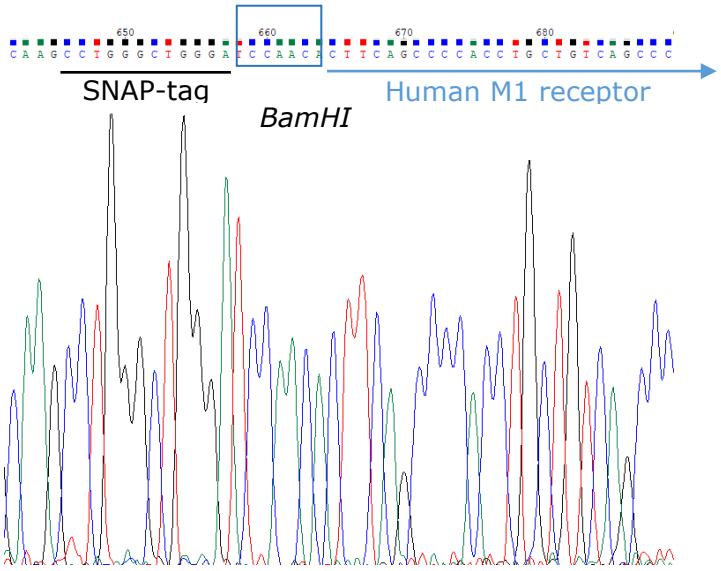


Figure 3.6: DNA sequencing in Chromas (pcDNA3.1 neo SNAP M1, T7 promoter primer) shows the in frame fusion of the SNAP-tag and M1 receptor sequence, with intervening BamH1 site.

3.2.5.3 Identification of the Two DREADD Point Mutations within the Human M1 Construct

The nucleotide sequences comparing the WT M1 construct to the sample that underwent the "Quick change" mutagenesis confirms the two mutations were successfully added to the hM1-DREADD sequence. The DNA sequence shows the successful Y106C mutation, in which the WT shows the "TAT" codon which correlates to tyrosine, while the mutated sequence shows "TGT" which correlates to cysteine. The second mutation successfully introducing an A196G mutation to the hM1 sequence is present where "GCC" has been altered to "GGC" (Fig 3.7). The position of each of these single point mutations were verified by using BLAST sequence alignment) against the hM1 cDNA (Genbank reference NM_000738).

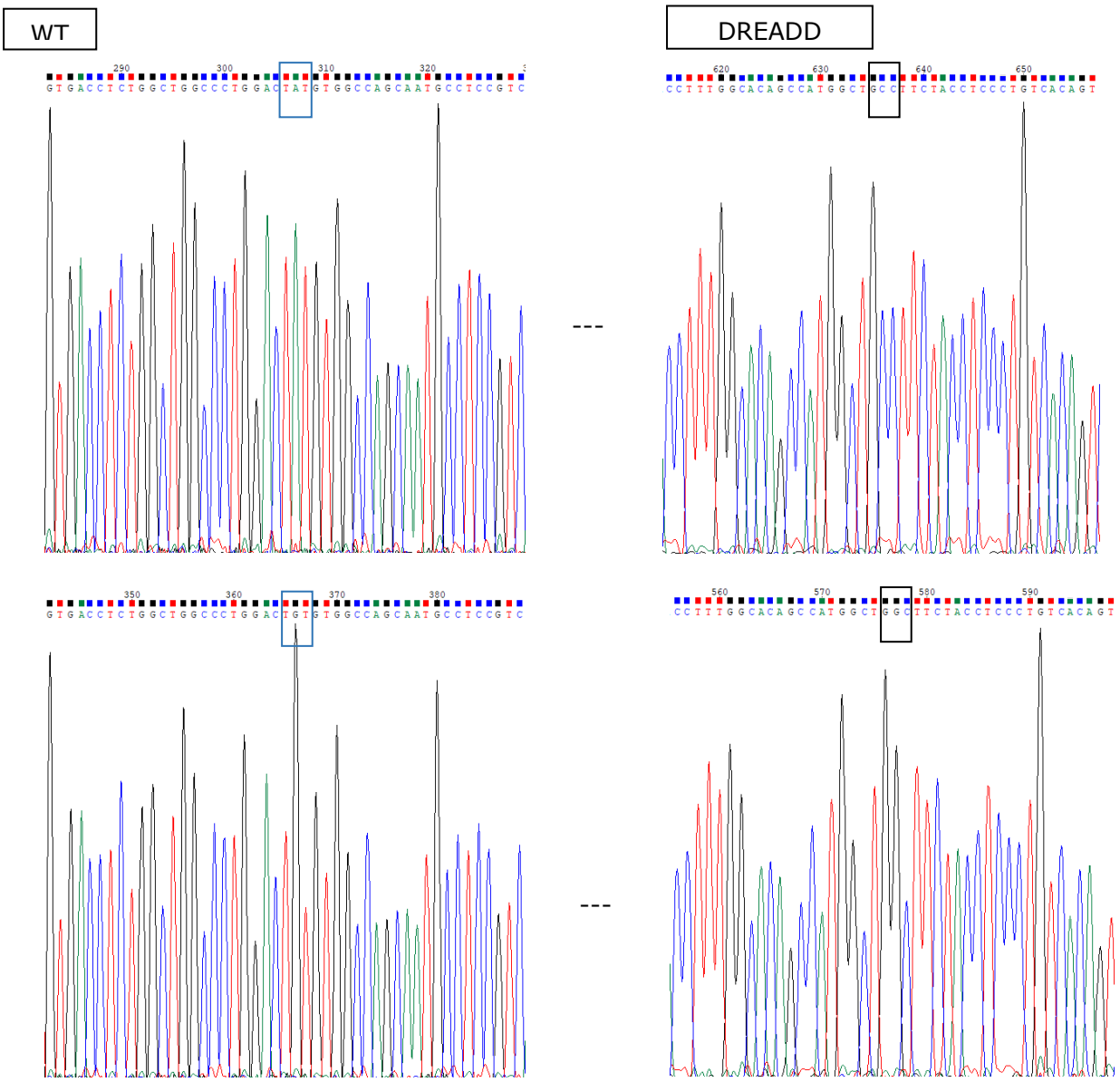


Figure 3.7: DNA sequencing shown in Chromas identifies the successful point mutations added to the human M1 construct to form the hM1-DREADD. The first mutation shown on the left is the Y106C where the Tyr "TAT" has been mutated to the Cys "TGT" (highlighted in the blue boxes). The second mutation, shown on the right, is the A196G mutation where Ala "GCC" has

3.2.5.4 In Frame Fusion of the M1 Receptor with the C-Terminal LgBiT Tag

Finally, DNA sequencing of pcDNA3.1neo SNAP-M1-LgBiT constructs confirmed the correct nucleotide sequence in the interface between the hM1 constructs and the LgBiT motif separated by the 5 amino acid linker (Fig 3.8). The two DREADD mutations were also verified but are not shown as they are indicated in section 3.2.5.3.

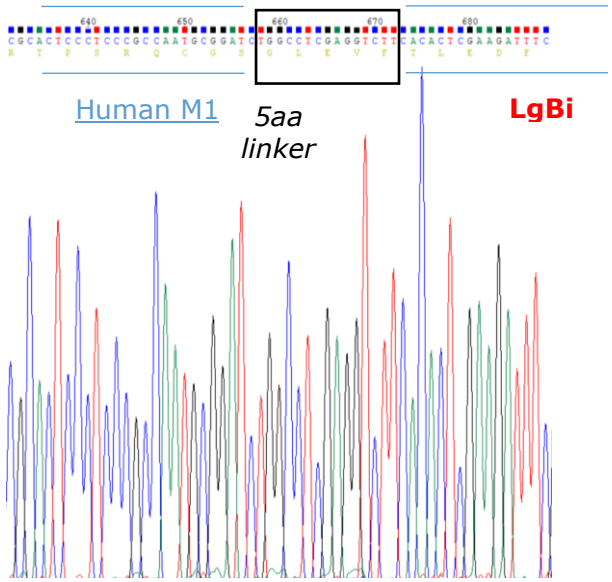


Figure 3.8: ***DNA sequence shown in Chromas verifying the interface of the human M1 sequence and LgBiT motif.*** *The 5 amino acid (aa) linker is present (black box, italic lettering) before the start of the downstream intracellular C-terminal LgBiT motif (red lettering, bold) present in both the hM1 and hM1-DREADD construct ligated into the LgBiT SNAP pcDNA3.1(+)neo vector, shown in SNAP-M1-LgBiT using bGHRev.*

3.2.6Development of Stably Transfected SNAP-M1 and SNAP M1-DREADD Cell Lines, and Verificantion of Recetor Expression by SNAP-Labelling

CHO K1 cells were transfected with the SNAP M1-WT or SNAP M1-DREADD constructs, and the LgBiT counterparts, using Lipofectamine and cell lines were selected via the dilution cloning selection method, as described in section 2.2.9.1. Clones were screened by labelling cell surface SNAP-tagged receptors using the fluorescent cell

impermeable substrate SNAP surface AF488 (Fig. 3.9). From this screen, clones were chosen which had a high level of cell membrane expression and were expanded for further investigation (Chapter 4). It was shown that SNAP M1-WT receptors were internalised after receptor activation, however when this process was compared with SNAP-labelled M1-DREADD receptors it appears this is reduced (Fig. 3.10). It may be that the comparison between the two cell lines masks the internalisation seen in the M1-DREADD, in the future a reference drug may be useful to determine a more accurate level of internalisation. If the graphs were normalised to their own ligand (ACh for WT and CNO for DREADD) internalisation would always be at 100% and thus nuance between receptor levels would not be seen either. It may be that additional clones should have been screen not only for the SNAP-labelled receptor expression but also for their internalisation profile. For both cell lines the M1 allosteric modulator BQCA was shown to act as PAM for internalisation of these receptors.

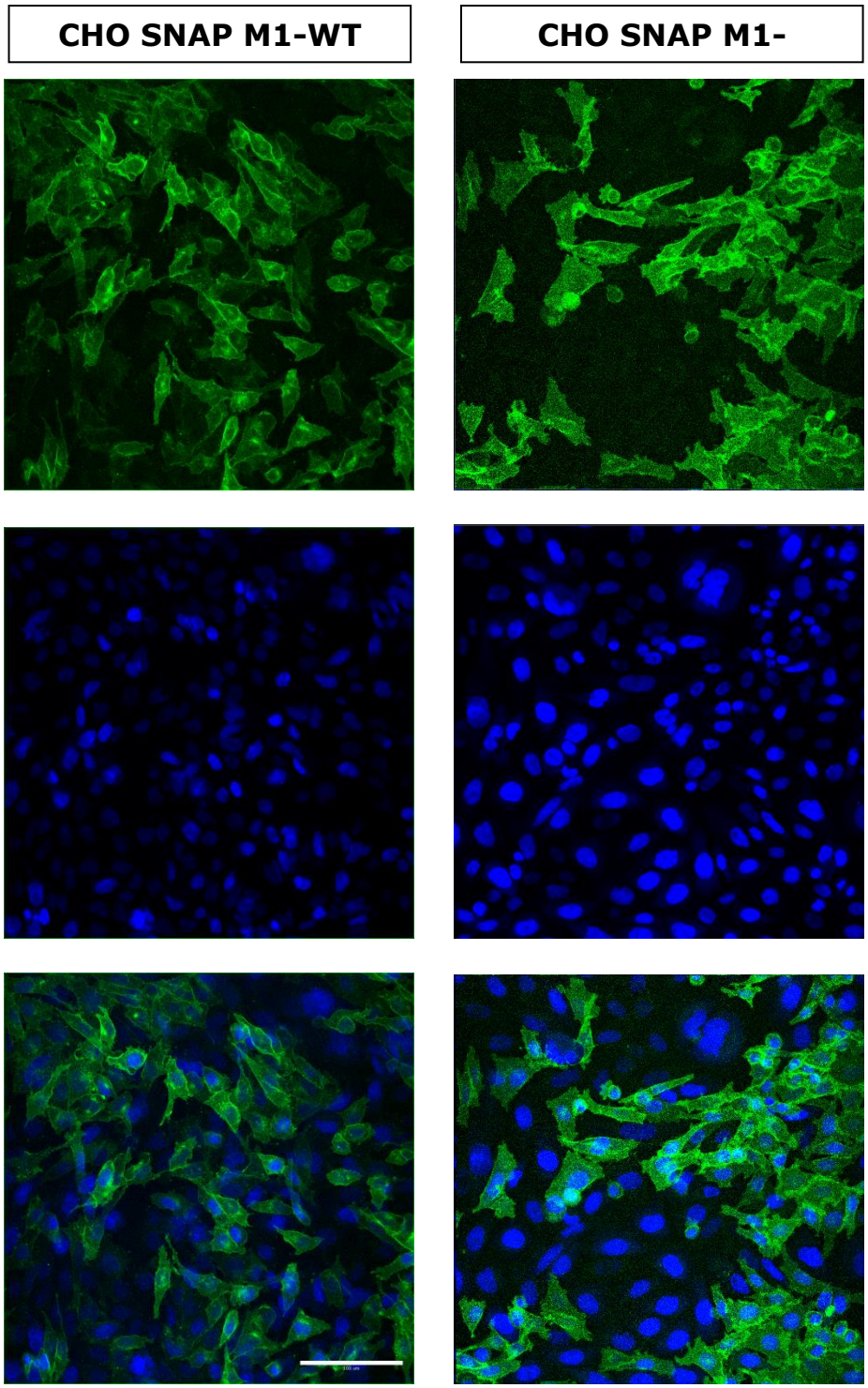
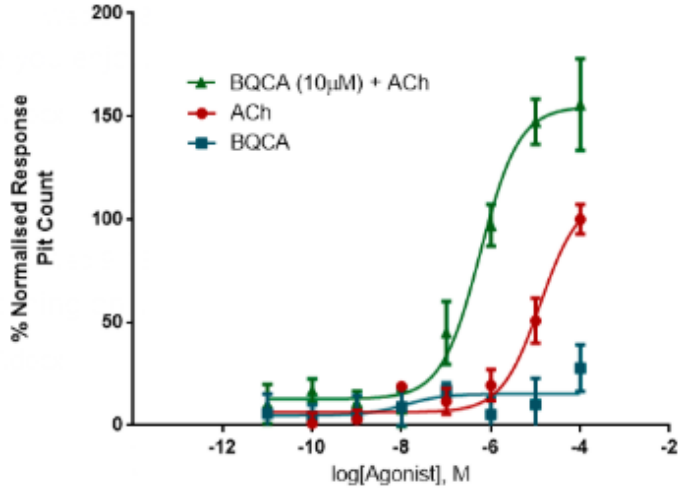


Figure 3.9: ***Representative images of CHO K1 cells expressing SNAP-tagged constructs.*** *Cell surface expression of SNAP-M1 and SNAP-M1 DREADD receptors in stably transfected cell lines. Cells were labelled with impermeable SNAP surface AF488 (0.2μM, 37°C, 30 min) and H33342 nuclear dye prior to imaging on a confocal platereader (IX Ultra), scale bar indicates 100μm..*

A



B

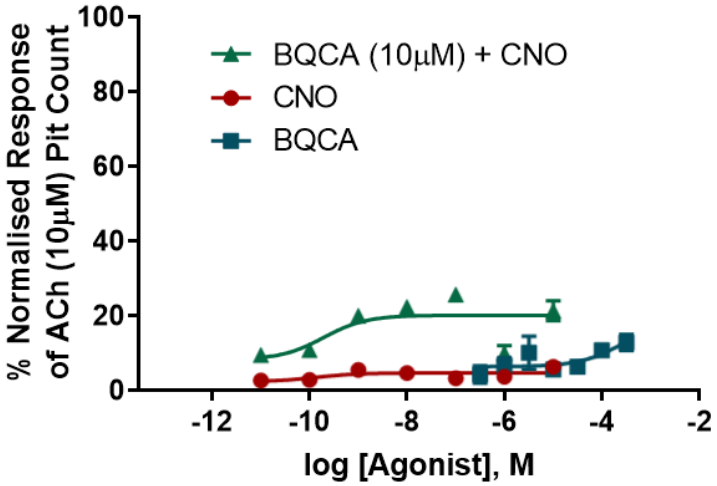


Figure 3.10: ***SNAP-tagged M1-WT and M1-DREADD receptor Internalisation.*** *CHO M1-WT (A) and M1-DREADD (B) expressing cells were labelled with SNAP surface 488 and internalised "pits" were analysed using a granularity algorithm. Cells were incubated with either the endogenous ligand ACh, for M1-WT, or CNO, for M1-DREADD receptors, and the effects of the allosteric modulator BQCA (10μM) on receptor internalisation was measured. Data was normalised to 10μM ACh (100%) at the M1-WT receptor and vehicle was used as 0%. ACh was used as a reference level of internalisation to compare between the two receptors. Values shown are mean ± SEM of 3 experiments carried out in duplicate.*

3.3 Discussion

In this chapter, the WT hM1 and hM1-DREADD constructs were successfully ligated within the SNAP-tagged pcDNA3.1(+)neo vectors and the LgBiT SNAP-tagged pcDNA3.1(+)neo vectors, and expressed as stable cell lines. The two constructs were generated by PCR amplification, with point mutations engineered within for the DREADD receptor and in combination with cloning methods expressed in the desired vector. Both constructs were verified using a number of restriction digests to confirm the correct DNA band size. DNA sequencing was able to confirm the correct nucleotide sequence and in frame fusion of the receptor and SNAP or LgBiT tags. SNAP-tag labelling using SNAP-surface Alexa Fluor 488 confirmed the plasma membrane localisation of both SNAP-M1 and SNAP-M1DREADD receptors in clonal stably transfected CHO cell lines. These constructs will be integral to characterise the pharmacology and investigate the effects of allosteric modulators within the DREADD chemogenetic system in the following chapters.

Chapter 4

INVESTIGATION OF ALLOSTERIC MODULATION OF RECOMBINANT M1-DREADD RECEPTORS USING CALCIUM MOBILISIATON, COMPLEMENTATION AND FLUORESCENT LIGAND BINDING TECHNIQUES

4.1 Introduction

As discussed in chapter 1, the M1 muscarinic receptor is a compelling molecular target due its role in a number of neurodegenerative diseases, including Alzheimer's disease (Wess, 2004; Shinoe *et al.*, 2005; VanDeMark *et al.*, 2009). There have been many efforts in identifying receptor subtype-selective compounds in order to find efficacious drugs with reduced off-target effects (Eglen, Choppin and Watson, 2001). However, due to highly conserved orthosteric sites shared between mAChR subtypes this has not translated into successful therapeutics so far (Fisher, 2000). Recent pharmacological advances are less reliant on ligands that bind the orthosteric site and aim to target M1 binding, and its subsequent signaling pathways, with higher spatiotemporal selectivity (Bradley and Tobin, 2016). New tools include the use of allosteric modulators that have less conservation between binding sites (Presland, 2005; Conn, Christopoulos and Lindsley, 2009). These modulators may also exhibit bias between the signaling pathways they can activate, therefore adding further selectivity to these tools (Gao and Jacobson, 2013). In addition transgenic expression of DREADD receptors provide an opportunity to probe the functional role of specific muscarinic receptor subtypes in physiology and disease models (Wess, Nakajima and Jain, 2013; Roth, 2016).

4.1.1 Allosteric Modulation Used to Improve Spatiotemporal Control of Receptor Signalling

Allosteric ligands function by promoting a change in the bound receptor's conformational state, either stabilising or inhibiting the active conformation, and can induce additional conformational states that are not achieved when the orthosteric ligand alone is bound (Kruse *et al.*, 2013). The cooperativity between allosteric and orthosteric ligand can induce the increase or decrease of affinity and/or efficacy at the orthosteric binding site. It has been shown that a number of PAMs, including BQCA and some highly related compounds, have their own intrinsic allosteric agonism, predominately function through the enhancement of orthosteric affinity, and exhibit positive cooperativity towards ACh but negative cooperativity towards the antagonist [^{3}H]NMS (Elham Khajehali *et al.*, 2018). With the M1 common allosteric binding site

being 15Å above the orthosteric site, allosteric modulators are also able to sterically interfere with the entry or exit of a ligand from the orthosteric site altering its function at the receptor (Thal *et al.*, 2016).

The allosteric modulator BQCA and the bitopic ligand VU0357017 were chosen as examples to investigate allosteric modulation at the M1 DREADD receptor in this chapter. BQCA, which has been shown to bind at the common allosteric binding site (Elham Khajehali *et al.*, 2018), is an exemplary tool to investigate M1 allostery. In fact, later generations of PAMs, intended to have optimised allosteric properties, have been shown to bind and function, through comparable interactions in the allosteric site, as BQCA (Elham Khajehali *et al.*, 2018; van der Westhuizen *et al.*, 2018). Recently, the novel tacrine-BQCA bitopic hybrid was produced, designed with BQCA as an M1-selective compound and tacrine as a acetylcholine esterase inhibitor, with potential dual benefits for AD patients (Hepnarova *et al.*, 2018). This highlights how allosteric modulators could be used in the future to selectively target receptor subtypes with disease ameliorating effects. However, it has also been shown that BQCA can also have M1-induced side effects, which are not seen in M1-KO animals (Kurimoto *et al.*, 2018). Kurimoto *et al.* (2018) highlighted the subtle differences in cooperativity between allosteric modulators and the effector orthosteric ligand. They were able to show an allosteric modulator with low cooperativity induces improvement in cognition without inducing diarrhoea, whereas the high cooperativity modulator resulted in the opposite effect. This demonstrates how titrating the "ceiling" effect of the modulator can be beneficial and supports the need for functional assays to be carried out in order to quantify the effects of an allosteric modulator.

VU0357017 is a bitopic ligand binding both the orthosteric and allosteric sites (Digby *et al.*, 2012). Despite not being a pure allosteric modulator, VU0357017 is still a useful tool to investigate due to its high level of selectivity towards M1 mAChR generated by allosteric site interactions, and its ease of crossing the blood brain barrier for *in vivo* investigations (Lebois *et al.*, 2011). VU0357017 was shown to reverse cognitive deficits induced by the mAChR antagonist scopolamine, in the hippocampus of rats (Lebois *et al.*, 2011). It was also shown that when administered

with a GABA allosteric modulator, bitopic VU0357017 had beneficial effects on head twitches in a behavioural mouse model of schizophrenia (Cieślik *et al.*, 2019). Another group was able to show a significant improvement in rates of extinction after cocaine administration in the presence of VU0357017 (Stoll *et al.*, 2018).

4.1.2 Probe and Species Dependency of Allosteric Modulation

The nature and extent of allosteric modulation depends on the orthosteric ligand present at the receptor, a concept known as probe dependence. Probe dependence describes a change in the degree of modulation an allosteric ligand can exert at a receptor dependent on which orthosteric ligand is bound (Kenakin, 2005). This is because an allosteric modulator stabilises or inhibits a particular conformation of the receptor, and this conformation is dependent on the interactions the orthosteric ligand has at its binding site, as well as the allosteric modulator's own preference for different receptor conformations (Kenakin, 2005). The potential for different active receptor conformations stabilised by orthosteric agonists underpins the ideas behind ligand bias (Lisa A Stott, Hall and Holliday, 2016), in which ligands are capable of modulating different subsets of signalling pathways from the same receptor. These ideas can be extended to the ability of allosteric modulators themselves to engender unique receptor conformations i.e. "biased modulation" (Kenakin and Christopoulos 2013; Christopoulos 2014).

The effects of the muscarinic allosteric modulator LY2033298 is an example of a ligand that exhibits strong probe dependence. It has been shown that LY2033298 acts as a PAM for ACh responses at the mACh M4 receptor, however when this allosteric modulator binds M2 it is able to modulate the signalling of oxotremorine-M but fails to show allosteric modulation in the presence of ACh (Valant *et al.*, 2012). It was also shown that LY2033298 showed robust potentiation of ACh and oxotremorine-M at M4 mAChR but the agonist xanomeline was only weakly affected (Leach *et al.*, 2010).

The extent of allosteric modulation can also vary dependent on the species of receptor investigated; a problem when considering the extrapolation of *in vivo* data

from animal models to man. For example, the adenosine A1-receptor was shown to have probe dependency between the human and rat receptor subtypes. The allosteric modulators PD81,723 and VCP171, were able to significantly enhance the binding affinities of 5'-(N-Ethylcarboxamido)adenosine (NECA) and 2-Chloro-N^6-cyclopentyladenosine (CCPA) at human A1 receptors. However, when using rat A1 receptors the allosteric modulator were unable to show a significant increase of the binding affinities for the orthosteric agonists (Cooper *et al.*, 2019).

4.1.3 New Insights into DREADD Receptor Pharmacology – Can DREADDs be Used to Study mAChR Allosteric Modulation?

Alongside allosteric modulators, DREADD receptors have also been developed with the aim of increasing the degree of specificity in which GPCR signalling can be studied (Roth, 2019). The M1 mAChR DREADD contains two point mutations of orthosteric site residues (Y106C and A196G) that reduces endogenous ACh binding, while potentiating the affinity of CNO (Armbruster *et al.*, 2007). DREADDs are potentially a useful tool to provide more insight of allosteric modulation *in vivo*. It is of interest to first understand whether the allosteric modulation of orthosteric ligands at DREADDs is altered due to the point mutations at these receptors. This chapter focusses on characterising this within recombinant cells. If this is the case, it may be that DREADDs can be used as a tool that allow for investigation into allosteric modulation while ensuring selective receptor activation. For instance, investigations of how allosteric ligands alter the cross-talk between astrocyte and neurone could be assessed by activating DREADD-expressing astrocytes, within the tripartite synapse, with CNO in the presence of an allosteric modulator. Although the delivery of CNO would not have the same spatiotemporal dynamics as ACh being released from the synapse would, any changes in astrocytic function could be investigated under a selective system in which the surrounding neurones should not be activated by CNO.

The strength of any system is to be able to use tools in parallel, with the aim of achieving a superior mode of action. By combining the DREADD's signalling specificity with the allosteric modulators' ability to control the spatiotemporal aspects

of ligand-receptor binding, the resultant system is one in which ligand-receptor binding kinetics, G protein and β-arrestin membrane recruitment, and calcium mobilisation can be accurately investigated and dynamically modified through allosteric modulation. However, due to the nature of allosteric modulation, and its cooperativity, any effect also depends on the orthosteric ligand binding. Thus, it cannot be assumed that the pharmacology of an allosteric modulator would be the same at the DREADD as it would for the WT receptor (Lane, Abdul-ridha and Canals, 2013). Additionally, there is potential for pathway dependent effects when comparing allosteric modulators at DREADDs compared to the WT receptor (Yeatman *et al.*, 2014). Therefore, the purpose of this study is to consider the effects of BQCA and VU0357017 at the M1-DREADD receptor, systematically comparing indicator measurements of Gq coupled calcium mobilisation, with novel assays to measure fluorescent ligand binding; mini G protein and arrestin recruitment.

The DREADD system was initially designed so that any receptor signalling pathways stimulated can only be attributed to the administration of CNO activating the expressed DREADD receptor. In reality, CNO is known to be metabolised to clozapine and N, desmethylclozapine *in vivo* (Structures shown in Fig. 4.1). This has been shown in mice (Guettier, Gautam, Scarselli, Ruiz de Azua, *et al.*, 2009b), rats (MacLaren *et al.*, 2016), monkeys (Raper *et al.*, 2017) and to a greater extent in guinea-pigs (Jann, Lam and Chang, 1994; Geula, 1998) and humans (Chang *et al.*, 1998). Manvich *et al.*, (2018) explain that the Guettier (2009) metabolite study in mice is widely cited due to the authors' conclusion that insignificant quantities of clozapine were found after CNO administration. However, with the evidence for relatively high levels of clozapine from other animal species this is a clear area where limitations may be introduced into studies. Clozapine is an atypical antipsychotic with a wide number of pharmacological targets, such as dopamine receptor antagonism (Meltzer, 1994). We therefore tested CNO alongside clozapine and N, desmethylclozapine at the M1-DREADD to identify whether DREADDs are more likely to be activated by these metabolites *in vivo*.

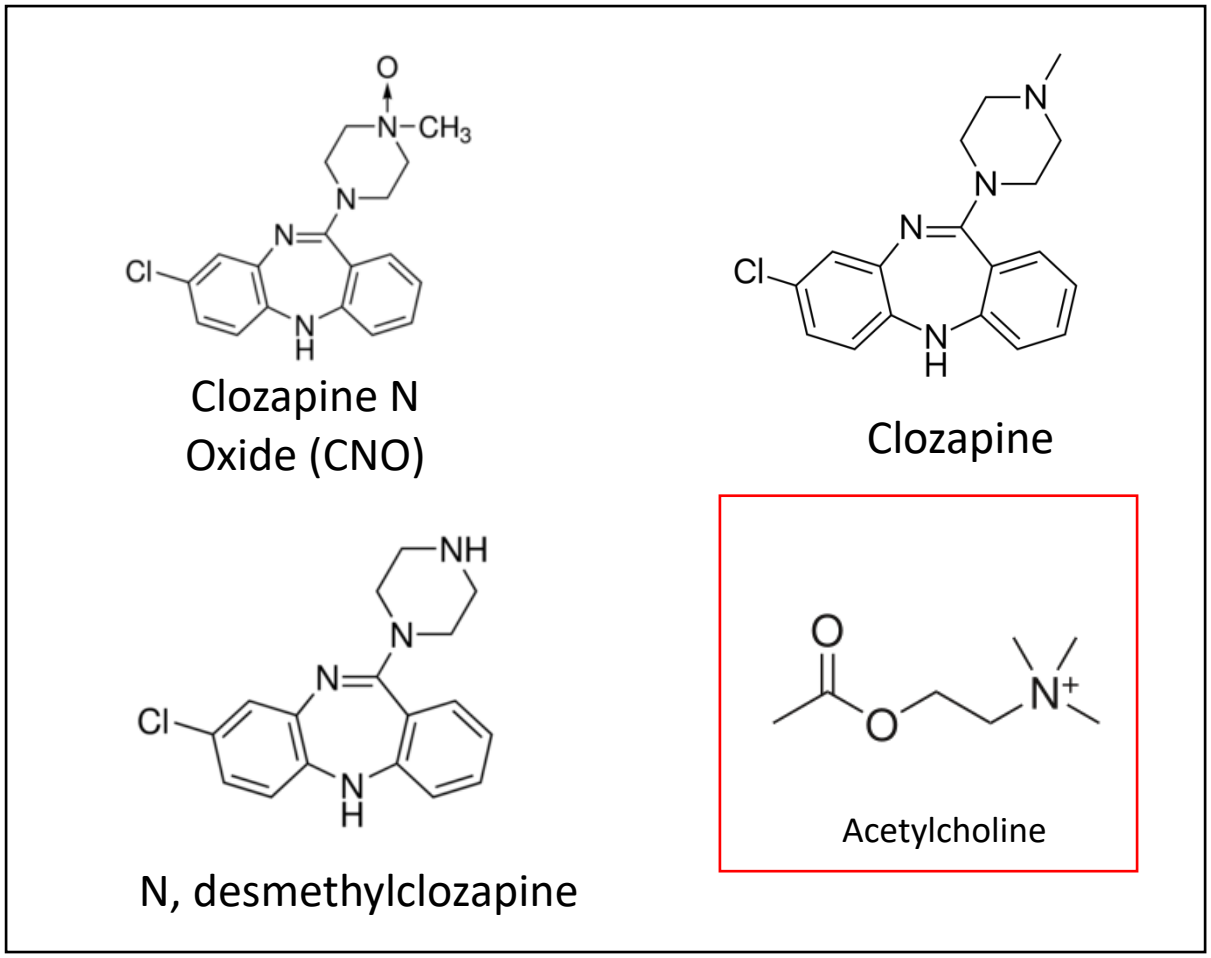


Figure 4.1: Structures of clozapine derivatives (black box) used within this study, in comparison to the endogenous ligand acetylcholine (red box).

4.1.4 The Use of Fluorescent Indicators to Measure M1-WT and M1-DREADD Receptor Calcium Signalling

To monitor M1-WT and M1-DREADD activation of calcium mobilisation by agonists, calcium-sensitive fluorescent indicator dyes were used in this chapter. When selecting a calcium indicator it is important to consider the dynamic range of such a molecule. The K_D corresponds to the concentration of calcium at which half the indicator molecules are bound with calcium, at equilibrium. Optimally, an indicator should be selected that has a K_D that is 0.1 - 10 X lower than the calcium concentration expected in the test cell to give the greatest dynamic (ΔF) fluorescent response (Paredes *et al.*, 2008). Non-equilibrium calcium responses can occur over a time period of seconds to minutes, dependent on the test cell type, therefore the kinetics of indicator binding

are also important to accurately measure the initial calcium increase (Paredes *et al.*, 2008). Calcium indicators can be ratiometric (increase and decrease fluorescence at different excitation waves length e.g. fura2) or single wavelength indicators (increase and decrease fluorescence at a single excitation e.g. Fluo4 which is excited at 488nm) (Paredes *et al.*, 2008). Ratiometric indicators allow for very accurate quantification of calcium concentration (Gupta *et al.*, 2009), overcoming issues such as dye leakage and photobleaching (Paredes *et al.*, 2008), however spectral overlap with other fluorophores is a common issue that can be mitigated by using single wavelength indicators (Lipp, Lüscher and Niggli, 1996).

Originally, calcium dyes were based on negatively charged chelators, such as EGTA and BAPTA (Tsien, 1980; Harrison and Bers, 1987). Calcium dyes based on salt structures or dextran conjugated structures are membrane impermeable and at times require invasive loading procedures, such as microinjection (Paredes *et al.*, 2008). To overcome this, acetoxymethyl (AM) ester-conjugated structures were developed. AM dyes are hydrophobic and therefore membrane permeable (Tsien, 1981). For example Fluo-4 (AM), allows for high-throughput ligand screening within a range of cell types and are relatively easy to use (Gee *et al.*, 2000). Once inside the cell, intracellular esterases cleave the AM group from the dye, trapping it within the cell, and allowing calcium to bind. The fluorescent signal is low in cells under resting conditions (intracellular calcium being in the nM range), but can be amplified more than 100-fold after receptor activation and intracellular calcium release (Caers *et al.*, 2014). The calcium responses produce data that allows for the identification of efficacious and potent ligands or allosteric modulators at the M1-DREADD receptor.

One final consideration necessary when analysing intracellular calcium studies, is that calcium is a secondary messenger and undergoes signal amplification dependent on a large number of regulatory mechanisms. One typical measurement used to analyse calcium signalling is the peak intracellular calcium response, which can occur at seconds - minutes following ligand addition depending on the test system. This intracellular calcium increase reflects a complex interplay between ligand affinity and binding kinetics, amplification in the signal pathway leading to calcium release,

and regulatory processes limiting receptor activation and intracellular calcium concentration (Thore *et al.*, 2005). As previously discussed, activation of Gq subunit induces the activation of PLC, which in turn produces IP3 molecules that are able to release calcium from the endoplasmic reticulum. Each molecule in this intracellular pathway is subject to feedback mechanisms that can affect the amplification of the calcium responses initiated at the receptor level (Putney and Tomita, 2012). It has been shown that PLC activity is enhanced by a positive feedback loop caused by calcium entering the cytoplasm, in which calcium is able to amplify both the initial and sustained receptor-activated PLC activity (Thore *et al.*, 2005). Moreover, cytosolic calcium increases the rate at which PLCβ can cleave PIP2 into IP3 molecules which go on to release calcium via IP3Rs (Siso-Nadal *et al.*, 2009). As a final example, it has shown that calcium entry into the cell via ionotropic and voltage-gate ion channels can sensitise IP3 receptors in such a way that subsequent activation of mGluR1s (Gq-coupled), expressed in neurones, produce increased calcium responses (Batchelor and Garthwaite, 1997).

Calcium amplification as well as signal cross-talk place limitations in discerning the spatiotemporal aspects of receptor signalling at the membrane (Werry 2003). These effects can obscure potential effects of orthosteric and allosteric ligands on receptor coupling to individual effectors such as G proteins (Koehl *et al.*, 2018) and β-arrestin (Reyes-Alcaraz *et al.*, 2018). Therefore, in addition to calcium mobilisation data, the aim of this study was to develop luciferase complementation (NanoBiT) assays to directly investigate the complementation of M1-WT and M1-DREADD receptors and the G protein mimetics and arrestins.

4.1.5 NanoBit complementation of mini G protein and β-arrestin2 to investigate intracellular signalling pathways

Techniques such as fluorescence resonance energy transfer (FRET) and bioluminescence resonance energy transfer (BRET) are able to produce a quantifiable signal that determines when proteins are within close proximity of each other (<100Å) (Dale *et al.*, 2019). This occurs by energy transfer from the luciferase donor to a

fluorescent acceptor resulting in a detectable emission (Stoddart *et al.*, 2016). These techniques have been adapted for use in receptor signalling assays, for example, FRET has been used to directly monitor the recruitment of fluorescently labelled β-arrestin (Jung *et al.*, 2017) or G proteins (Tian, Fürstenberg and Huber, 2017) to GPCRs. These are convenient "real time" GPCRs assays which accurately detect the kinetics of ligand binding to the receptor (Stoddart *et al.*, 2018). However, there are some limitations to these techniques. For example, G proteins exist as membrane-associated proteins and therefore do not change subcellular location once bound to the activated GPCR (Wan, Okashah, Inoue, Nehmé, Carpenter, C. G. Tate, *et al.*, 2018). This may cause high levels of background noise when receptor-G protein complexes are investigated using such techniques as FRET and BRET (Galés *et al.*, 2005; Hein *et al.*, 2005).

Mini G proteins are engineered GTPase domains of the Gα subunit (Carpenter and Tate, 2016; Nehmé *et al.*, 2017; Wan, Okashah, Inoue, Nehmé, Carpenter, C. G. Tate, *et al.*, 2018). It is possible to use these proteins, as well as β-ARR2, within complementation assays to investigate their recruitment to GPCRs. Complementation approaches enable the detection of protein-protein interactions in living cells and allow the detection of spatial localisation and binding dynamics at relevant, endogenous levels (Michnick *et al.*, 2011), as well as, receptor dimerisation (Kilpatrick, Humphrys and Holliday, 2015). Inactive fragments of a reporter protein (for example a fluorescent protein or luciferase) are brought together with their interacting protein partner and become reconstituted to generate activity which can be measured. (Rose, Briddon and Holliday, 2010).

The NanoBiT complementation assay is a quantification method to measure protein interactions at ligand-bound receptors at the cell membrane. Within our study, NanoLuc (LgBiT; 18kDa) was fused to the M1-WT and M1-DREADD, while the SmBiT (1kDa) was fused to either the mini G protein or β-arrestin2 (β-ARR2). The two "BiTs" have been designed to have low affinity for each other to allow physiologically relevant interactions to occur between the GPCR and the SmBiT-fused target proteins (Dixon *et al.*, 2016). This minimises the interference of the luminescent complex's own binding kinetics within the system. Once the GPCR is activated the SmBiT-fused

target proteins are recruited to the receptor, where in the presence of furimazine; a highly selective synthetic substrate (Hall *et al.*, 2012), the interaction with the LgBiT provides an rapid increase in the luminescence signal.

The data received from this assay allows for a real-time investigation into the interaction of the mini G, replicating G protein α-subunit binding, and β-arrestin2 with the M1 mAChR in its activated state. The luminescence response can be followed in in living cells with the interaction between LgBiT and SmBiT being rapid and reversible. The luminescence signal produced relates the kinetics of receptor-effector interaction directly, without amplification, and so the potencies (EC_{50}) and R_{max} values for orthosteric agonists, in the absence and presence of modulators, are closely related to the ability of the activated receptor to interact with each effector. GPCR intracellular signalling is multidimensional and there is considerable evidence showing that GPCRs operate with a level of promiscuousness towards G protein (Wettschureck and Offermanns, 2005) and β-arrestin binding, that can be influenced by the nature of the ligand (Wootten, Christopoulos and Sexton, 2013). NanoBiT technology allows ligand-determined signalling pathways to be investigated, and in conjunction with calcium mobilisation data, will allow for a deeper understanding of how allosteric modulation occurs at DREADDs (Kenakin, 2012b).

4.1.6 Novel Fluorescent Ligands to Investigate Ligand Binding at M1-DREADD Receptor

Functional studies, such as the calcium mobilisation assay outlined above, can report the potency and relative maximal responses of orthosteric ligands in the presence or absence of allosteric modulators. However, it is more difficult to determine the direct effect these modulators have on the ability of the orthosteric ligand to bind receptors, in these studies. The affinity of the orthosteric ligand in the presence of the allosteric modulators is important to determine, due to the cooperativity between orthosteric and allosteric ligand that determines the mechanism in which the allosteric modulator acts; altering affinity, efficacy or both.

Traditionally, affinity has been determined through direct assessment of ligand binding using radioligand studies. These studies provide measurements of

the equilibrium dissociation constant (K_D; the concentration of ligand that binds 50% of the target population) for the radioligand (saturation binding) or unlabelled competing ligands (competition binding). For example, the radioligand [^{3}H]quinuclidinyl benzilate ([^{3}H]QNB) has been used previously to study binding at the M1-DREADD receptor (Abdul-Ridha *et al.*, 2013a). Fluorescent ligands provide a useful alternative to radioligand binding, with greater safety, and allow direct monitoring and imaging in live whole cells. FRET and BRET techniques have been adapted for use in ligand binding assays, for example, FRET has been used to assess a fluorescent ligand interacting with a fluorophore-tagged GPCR. SNAP-tags (or CLIP- and Halo-tags) are commonly used, and have the advantage of membrane impermeable substrates that can only bind cell surface receptors, improving this technique's selectivity (Bosch *et al.*, 2014).

Fluorescent ligands are similarly able to investigate the affinity of receptor ligands by determining K_D – the equilibrium constant (Cottet *et al.*, 2011). Fluorescent ligands are composed of a pharmacophore; a known agonist or antagonist for the receptor of interest, a linker and a fluorophore. In this study, fluorescent ligands were generously donated from our colleagues in the University of Regensburg (Structures shown in Fig 4.2). Unlike radioligand studies, fluorescent ligands have not been used in M1-DREADD binding assays (at the time of writing); therefore, these novel ligands will offer a unique perspective into these receptors. The fluorescent ligands used in this study were designed against a pirenzepine-based pharmacophore, varying sizes of linkers and as a fluorophore, either sulphated or non-sulphated Cy5-related cyanine dyes which have an excitation emission at 650nm and an emission maximum of 670nm. Ligands were either designed as monovalent, or as bivalent ligands duplicating the pharmacophore (She *et al*. 2019, manuscript submitted).

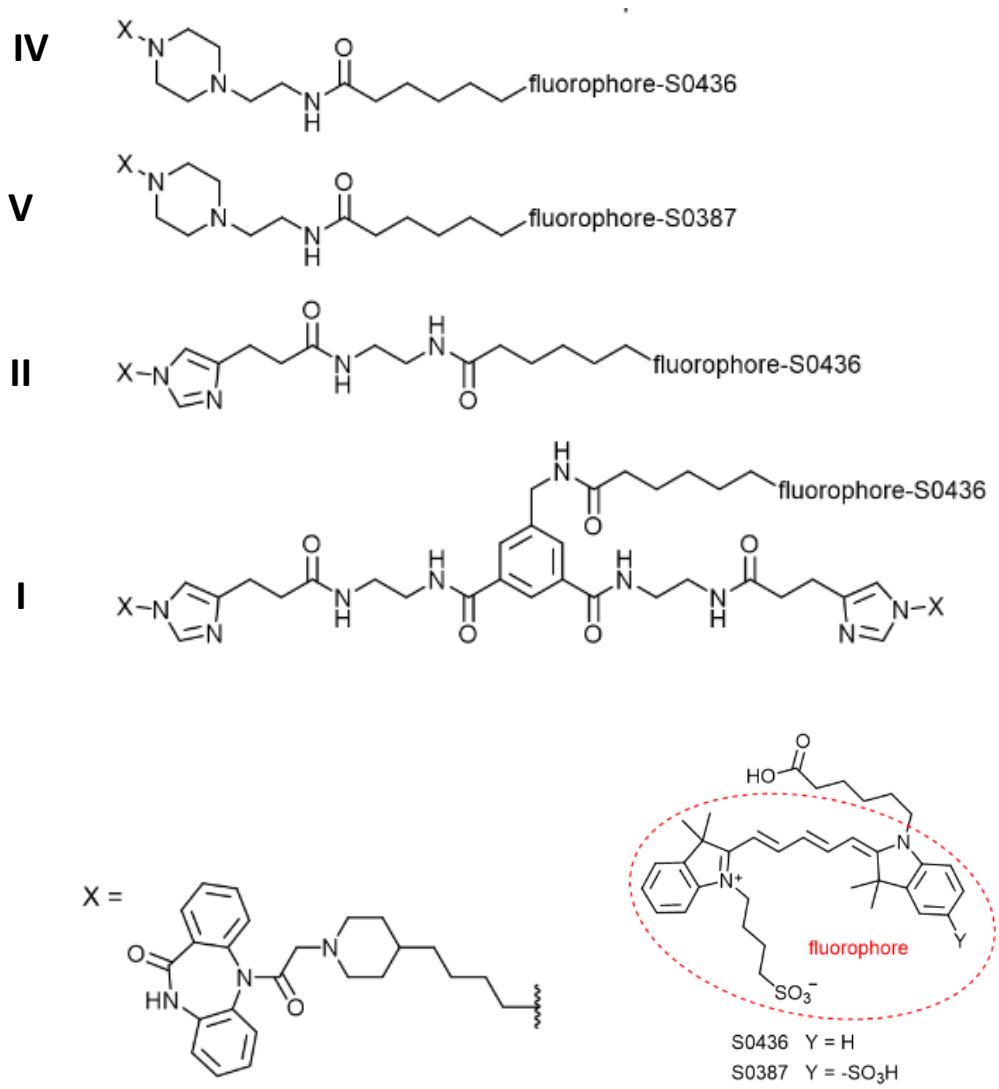


Figure 4.2: ***Structure of fluorescent ligands used in ligand binding studies****. The Max Keller Lab at the University of Regensburg provided these fluorescent ligands: Dr. Andrea Pegoli synthesised* ***I****,* ***II*** *and* ***III****, while Dr. Xueke She synthesised* ***IV*** *and* ***V****. The structure of* ***III*** *is the same as* ***II*** *but with a sulphated Cy5 fluorophore (S0387) compared to the non-sulphated structure of* ***II****. All fluorescent ligands have a pirenzepine-based pharmacophore and are Cy5-related cyanine dyes with an excitation wavelength of 650nm.*

Aims of this chapter

The aim of the chapter was to develop novel luciferase complementation and fluorescent ligand binding approaches to explore the pharmacology of the M1-DREADD receptor, in comparison to more routine calcium mobilisation assays. These assays were used first to consider orthosteric agonist pharmacology and the activity of CNO and the metabolites, clozapine and N, desmethylclozapine, at the M1-DREADD. Second, the activities of representative allosteric ligands (in particular BQCA) were explored, particularly in terms of their interactions with the fluorescent ligands investigated, and in modulating specific signalling pathways highlighted by the mini G protein and β-arrestin2 (β-ARR2) complementation assays.

4.2 Results

4.2.1 Initial Characterisation of the SNAP-tagged Muscarinic M1 Wild Type and DREADD Receptors in the Calcium Mobilisation Assay

Initial calcium mobilisation measurements were performed on non-transfected CHO K1 cells, in comparison to the CHO cell line stably transfected with the SNAP-human M1 receptor (Fig 4.3 A&B). The response to acetylcholine was compared with that to three test clozapine derivatives; clozapine, clozapine-N-oxide and N, desmethlyclozapine. Cells loaded with Fluo-4 AM, were treated with the ligands at increasing concentrations after a basal read of 15sec, and the subsequent calcium mobilisation response was read over 150sec on a FlexStation 3. The peak fold change of fluorescence from the basal reading was then used to produce concentration-response curves for each ligand.

As expected, the three clozapine derivatives (at up to 1μM failed to produce a calcium response in either CHO K1 WT or SNAP-M1 cells, suggesting they have no action on endogenous receptors in the cell line, and limited activity as agonists at the

M1-WT mAChR. Acetylcholine, as the endogenous ligand of M1 receptor, initiated a robust calcium response in CHO SNAP-M1 cells with pEC_{50} value of 6.32 ± 0.43 (n=3) (Table 4.1). At the highest concentrations, limited acetylcholine responses were also observed in CHO K1 wild type cells with an R_{max} value of 0.36 ± 0.02 (n=3) fold above basal.

In contrast, addition of clozapine derivatives elicited potent calcium responses in CHO SNAP M1-DREADD cells, in comparison to acetylcholine (Figure 4.3, C). The potencies of the clozapine derivatives (pEC_{50} values given in Table 4.1) were approximately 10,000 to 100,000 fold more potent than for acetylcholine at this receptor ($P < 0.001$, one way ANOVA followed by Dunnett's post test). Notably, clozapine itself was significantly more potent than CNO (Table 4.1; $P<0.05$, one way ANOVA followed by Dunnett's post test). CNO is metabolised into clozapine, within the body, therefore the fact clozapine can elicit a response has negative implications as to the use of CNO being a selective ligand to activate the DREADD receptors. All three clozapine derivatives were full agonists with comparable R_{max} values of 2.67 ± 0.28, 1.90 ± 0.22 and 2.29 ± 0.13 for clozapine, N-desmethylclozapine and CNO (Table 4.1). Maximal responses to CNO and N-demthylclozapine were significantly greater than to acetylcholine in this cell line ($P< 0.001$, one-way ANOVA analysis with a Dunnett's post hoc comparison).

Concentration response curve data reflected the peak change in fluorescence in response to the different agonists. Fig. 4.4 shows the full time course analysis for the response to the different clozapine derivatives, compared to acetylcholine, in the CHO SNAP M1-DREADD cell lines. Each agonist produced a relatively sustained increase in calcium over the 150sec time period, with faster onset kinetics at higher concentrations of agonist. However the peak increase to clozapine derivatives occurred more rapidly than for acetylcholine – at highest concentration of acetylcholine used (1mM), the peak response was not reached until ~ 50sec following addition (compared to a peak at 5 – 10sec following 1µM CNO).

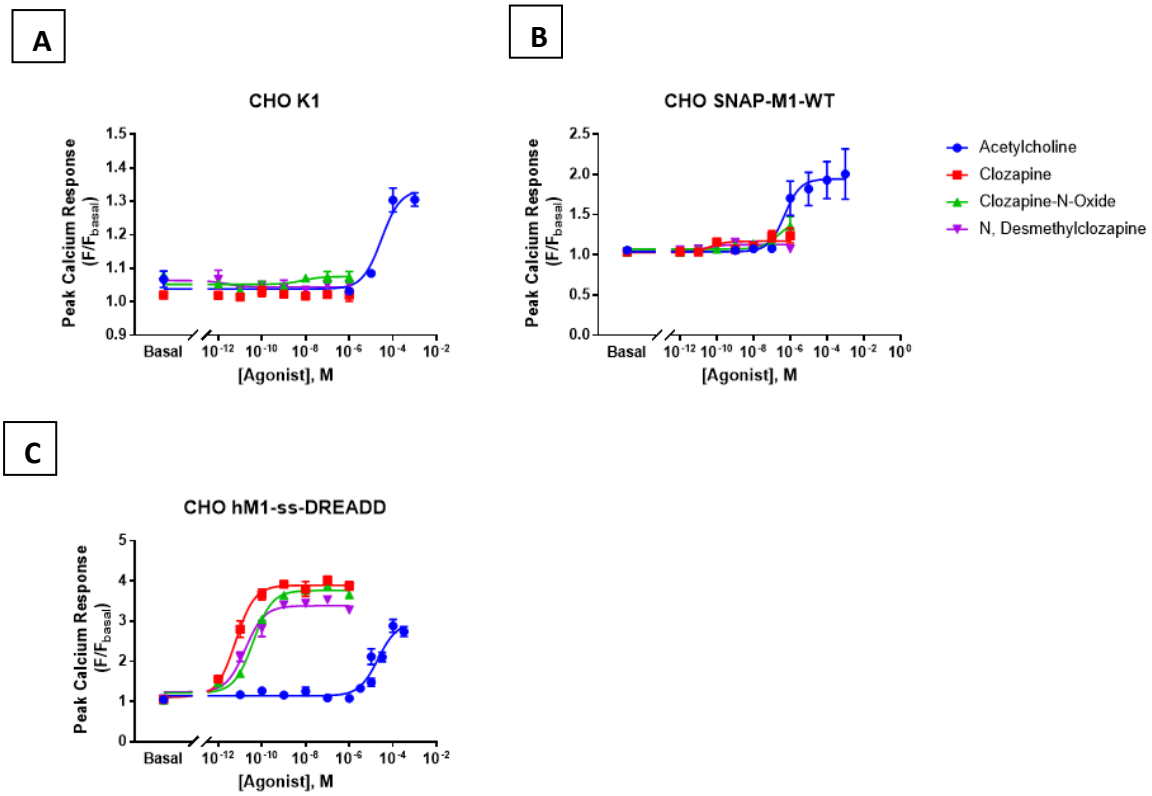


Figure 4.3: ***Calcium mobilisation in response to clozapine derivatives and acetylcholine in CHO K1 WT, M1-WT and M1-DREADD cell lines.*** *Cells were loaded with the calcium indicator Fluo-4 AM and fluorescence reads were taken on the FlexStation 3 plate reader in response to ligand addition at 15sec. Concentration-response curves reflect peak agonist induced changes in calcium mobilisation. A) Non-transfected CHO K1 cells (n=3), B) CHO SNAP M1 WT and C) CHO hM$_1$-ss-DREADD cells*

A

CHO K1	CHO K1 pEC_{50}	CHO SNAP hM1- WT pEC_{50}
Acetylcholine	6.01 ± 0.83	6.32 ± 0.43 ^{NS}
Clozapine	NE	NE
Clozapine N Oxide	NE	NE
N-desmethylclozapine	NE	NE

B

CHO SNAP hM1-DREADD	pEC_{50}	Fold change in potency (EC_{50} ratio)	R_{max} (change in F/F_{basal})	Fold difference in maximum response (R_{max} ratio)
Clozapine N Oxide	10.29 ± 0.13	1.00	2.29 ± 0.13	1.00
Clozapine	11.01 ± 0.16 *	5.24	2.67 ± 0.28 NS	1.17
N-desmethylclozapine	10.43 ± 0.26 NS	1.38	1.90 ± 0.22 *	0.83
Acetylcholine	5.10 ± 0.21 ***	$6x10^{-6}$	1.46 ± 0.15 ***	0.64

Table 4.1: ***pEC_{50} and R_{max} values for the clozapine derivatives and the endogenous ligand acetylcholine from the three different cell lines.*** *Data are mean ± SEM values of 3-5 independent experiments carried out in triplicate (see Figure 4.1 for concentration response curves). ND – no concentration dependent response. A one-way ANOVA was carried out with a Dunnett's post hoc comparisons (CNO as the reference ligand) compared pEC_{50} and R_{max} values; NS- not significant, P>0.05. * P < 0.05, or *** P < 0.001.*

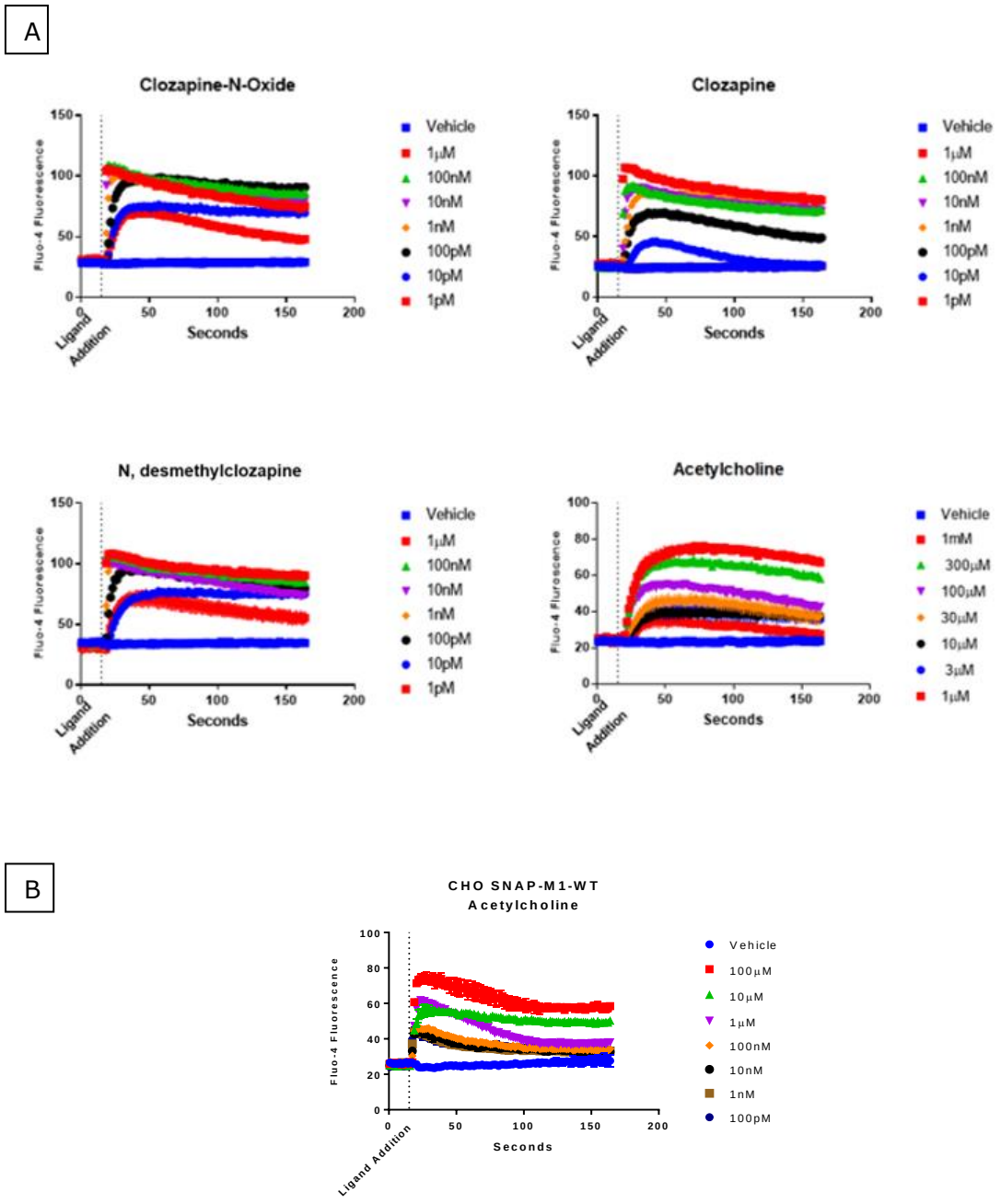


Figure 4.4: ***Representative time course plots of ligand-induced calcium mobilisation in CHO SNAP hM1-DREADD cells compared to CHO SNAP M1-WT cells.*** *Automated ligand addition was at 15sec, with a total fluorescence read time of 165sec on the Flexstation 3. (A) CHO SNAP hM1-DREADD cells in the presence of the clozapine derivatives and the endogenous ligand ACh with calcium mobilisation being shown by Fluo-4 fluorescence signal over time. (B) CHO SNAP M1-WT cells are shown in the presence of the ACh. Data are mean fluorescence of a representative experiment.*

4.2.2Characterisation of Orthosteric Ligand and Allosteric Modulator Effects on SNAP hM1-DREADD Induced Calcium Signalling

To characterise the SNAP M1-DREADD receptor pharmacology, the activities of a range of typical muscarinic ligands were first investigated in the calcium mobilisation assay, using CNO as the reference agonist (Figure 4.5; Table 4.2). The order of potency was CNO > iperoxo > oxotremorine-M > xanomeline = acetylcholine > carbachol = pilocarpine. One-way ANOVA analysis indicated that all ligands had a significant reduction in potency when compared to CNO ($P<0.001$). All ligands, with the exception of carbachol and pilocarpine ($P<0.001$), showed full agonist properties, with maximal responses comparable to that of CNO in producing a peak calcium response (Table 4.2). Time courses show rapid onset of calcium mobilisation for all ligands, with a transition from transient to sustained calcium responses with increasing concentration of ACh, oxotermorine-M, iperoxo and xanomeline. Transient responses were seen at higher concentrations of pilocarpine and carbachol, with these ligands having the lowest potency (Fig 4.6). It appears that only the full agonists, as compared to the partial agonists, elicited a sustained calcium response indicating that perhaps the maximal response had been reached within the system. In future experiments, it would be advantageous to use an ionophore, such as ionomycin, to calibrate the system and to verify the uppermost limits of the calcium response. This would then show if the response seen is a true sustained calcium response or whether the response is limited at the higher concentrations and therefore not showing the peak and decline seen in the partial agonists.

Then it was necessary to determine the effects of the two allosteric ligands, the modulator BQCA and the allosteric agonist VU0357017, in their own right to define any intrinsic activity before considering their actions on orthosteric ligands. Figure 4.5B, shows that BQCA was unable to produce a calcium response with increasing concentration up to 100µM. At the top concentration of 300µM BQCA calcium mobilisation was seen, with a change in F/F_{basal} of 0.87 ± 0.13 (Table 4.2). In contrast

VU0357017 did act as an agonist for M1-DREADD receptors (Figure 4.5, B), with a pEC_{50} of 4.75 ± 0.29 and an R_{max} value of 0.90 ± 0.16 (Table 4.2). Time courses indicated transient calcium mobilisation at the highest concentrations of VU0357017 and BQCA (Figure 4.7).

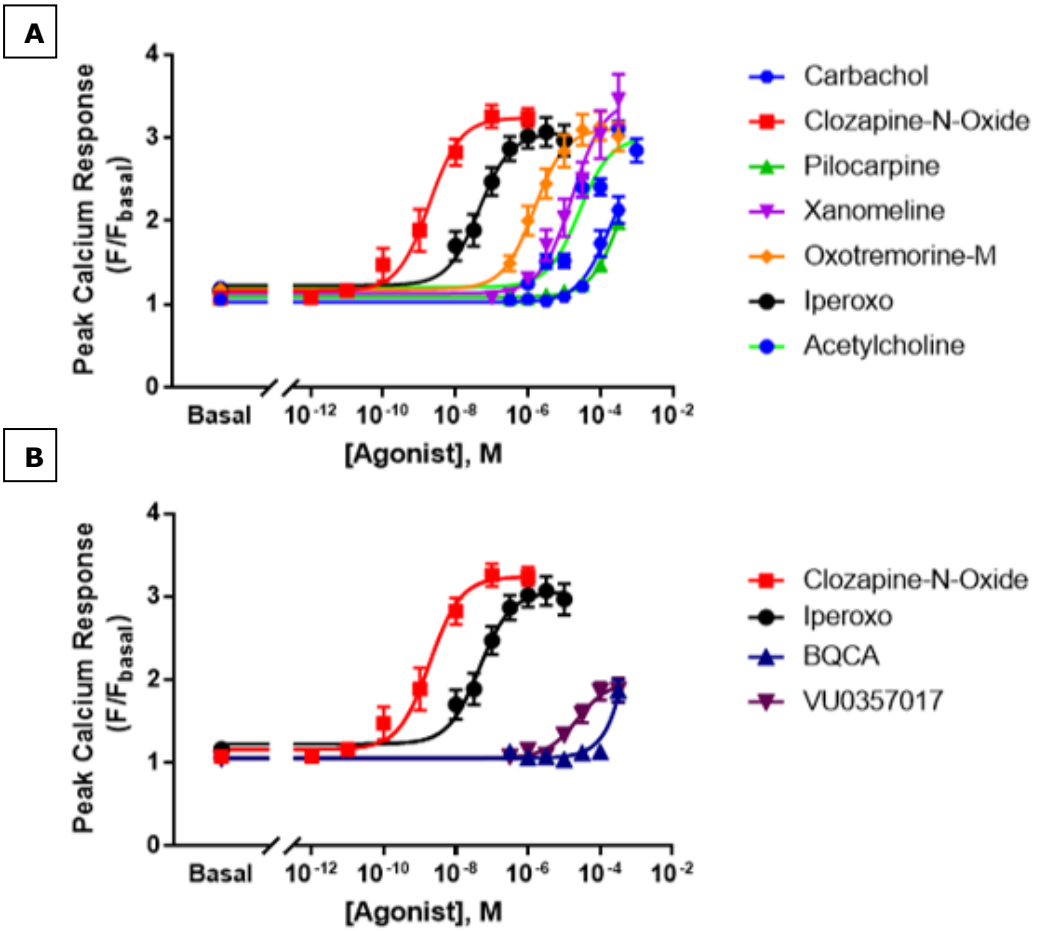


Figure 4.5: ***Concentration-response curves of representative M1 muscarinic ligands allosteric ligands CHO SNAP M1-DREADD cells.*** *Calcium mobilisation shown for (A) representative muscarinic ligands and (B) allosteric modulators. The peak agonist response was measured to construct the curves, after ligand addition at 15sec. Data points represent mean ± SEM of pooled experiments carried out in duplicate (n=5).*

Orthosteric Ligands	pEC_{50}	Fold change in potency (EC_{50} ratio)	R_{max} (change in F/F_{basal})	Fold change in maximal response (R_{max} ratio)
Clozapine-N-Oxide	8.73 ± 0.20	1.00	2.08 ± 0.11	1.00
Acetylcholine	4.59 ± 0.10 ***	$1.38x10^4$	1.81 ± 0.09 NS	0.87
Xanomeline	4.78 ± 0.08 ***	$0.89x10^4$	2.32 ± 0.19 NS	1.12
Oxotremorine-M	5.82 ± 0.08 ***	$0.081x10^4$	1.94 ± 0.08 NS	0.93
Carbachol	< 4.0 ***	$93.32x10^4$	1.08 ± 0.12 ***	0.52
Iperoxo	7.35 ± 0.15 ***	$0.0024x10^4$	1.83 ± 0.13 NS	0.88
Pilocarpine	< 4.0 ***	$23.44x10^4$	0.91 ± 0.09 ***	0.44
VU0357017	4.75 ± 0.29 ***	$0.95x10^4$	0.90 ± 0.16 ***	0.43
BQCA	NE	NE	0.87 ± 0.13 ***	0.42

Table 4.2: ***pEC_{50} and R_{max} values for the M1-muscarinic orthosteric and allosteric ligands at the CHO SNAP M1-DREADD receptor****. Data summarise the concentration response relationships in Figure 4.5, and values are mean ± SEM values of 5 independent experiments carried out in duplicate. NS, *** P < 0.001 represent the results of one-way ANOVA followed by Dunnett's post test, comparing pEC_{50} or R_{max} values for the indicated ligands to CNO.*

all

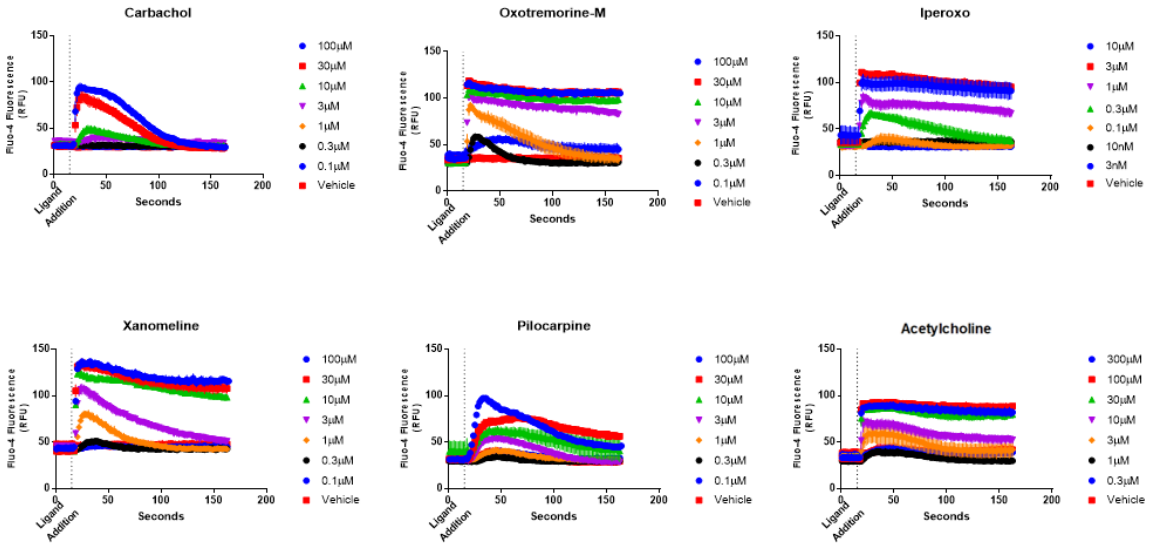


Figure 4.6: ***Representative time courses of muscarinic ligands at M1-DREADDs.*** *CHO SNAP M1-DREADD cells were loaded with Fluo-4 AM, and calcium mobilisation measured over a 165sec time course with ligand addition occurring at 15sec. Data is mean fluorescence ± range of a representative experiment carried out in duplicate.*

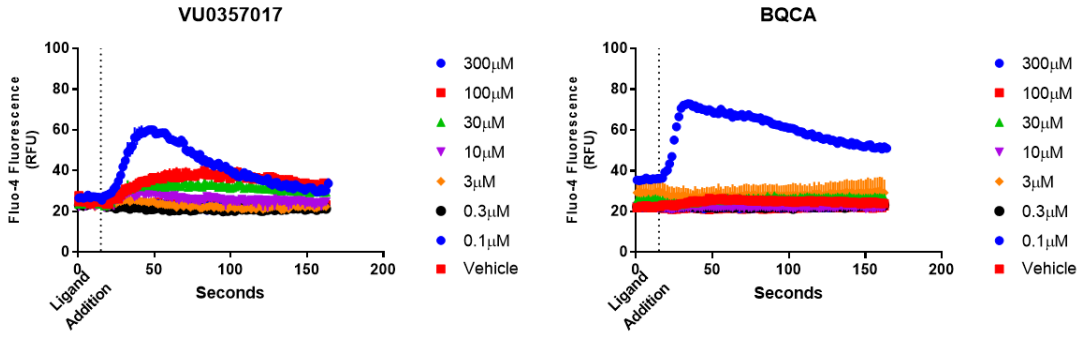


*Figure 4.7****: Representative kinetic plots for calcium responses to the allosteric ligands VU0357017 and BQCA in CHO SNAP hM1-DREADD cells.*** *Fluo-4 AM loaded cells were read in the FlexStation 3 over a 165sec time course with ligand addition occurring at 15sec after baseline. Data is mean fluorescence ± range of a representative experiment carried out in duplicate.*

4.2.3The Allosteric Effects of BQCA and VU0357017 on ACh and CNO Calcium Responses Mediated by the M1-DREADD Receptor

To test the allosteric action of different concentrations of VU0357017 and BQCA on orthosteric agonist calcium responses, a dual addition protocol on the Flexstation3 was used during the recording of Fluo-4 AM fluorescence in CHO M1-DREADD cells. VU0357017 or BQCA was added at the indicated concentration at 15sec, followed by ACh or CNO 60sec later.

The concentration response curves to ACh or CNO, in the presence of differing concentrations of VU0357017 are shown in Figure 4.8A and B. As expected VU0357017 itself had intrinsic agonist activity (Figure 4.9 & 4.10), producing a sustained increase in calcium signalling which is reflected in the orthosteric agonist concentration response data (expressed as the peak fluorescence change from the original experiment baseline). The apparent decline in CNO or ACh R_{max} in the presence of VU0357017 (Table 4.8) therefore reflected the elevated calcium mobilisation VU0357017 initiated prior to orthosteric ligand addition, confirmed by the time course data in Figure 4.8. There was no significant change in the CNO pEC_{50} in the presence of VU0357017, where this could be measured (Table 4.3). Subsequent experiments therefore focussed on the action of BQCA, which had limited intrinsic activity of its own in the calcium assay at concentrations less than 300µM.

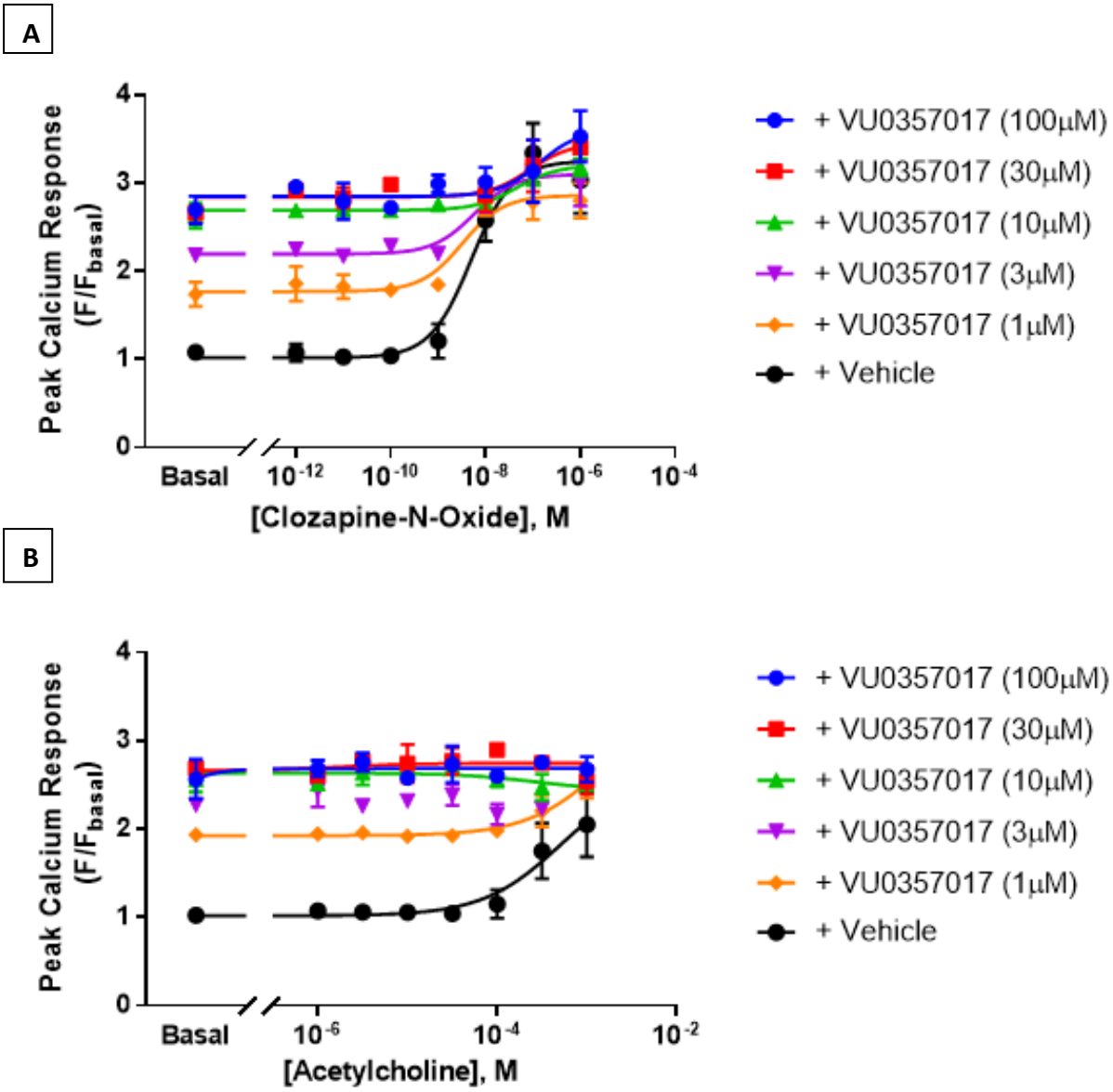


Figure 4.8: ***Calcium concentration response curves in CHO SNAP hM1-DREADD cells for CNO (A) and acetylcholine (B) in the presence of increasing concentrations of VU0357017.*** *VU0357017 was added at 15sec, followed by acetylcholine or CNO at 75 s. Data shown are mean ± SEM of pooled experiments, expressing the peak acetylcholine or CNO response as the fold change over the original baseline (n=3).*

Clozpaine-N-Oxide	pEC_{50}	Potency fold change (EC_{50} ratio)	R_{max} (change in $F/F_{VU0305717}$)	R_{max} fold change
+ 100µM VU0357017	NE	-	0.76 ± 0.22	0.32
+ 30µM VU0357017	NE	-	0.61 ± 0.15	0.26
+ 10µM VU0357017	NE	-	0.51 ± 0.06	0.22
+ 3µM VU0357017	8.24 ± 0.20	0.87	0.91 ± 0.08	0.39
+ 1µM VU0357017	8.49 ± 0.22	1.55	1.09 ± 0.10	0.47
+ Vehicle	8.30 ± 0.14	1.00	2.33 ± 0.14	1.00

Table 4.3: ***pEC_{50} and R_{max} values for CNO in the absence (vehicle) or presence of VU0357017 in stimulating calcium responses form CHO SNAP hM1-DREADD receptor****. pEC_{50} and R_{max} values were calculated as the peak CNO response over baseline fluorescence prior to CNO addition (change in $F_{VU0.357017}$). ND – pEC_{50} values could not be accurately determined. Values are mean ± SEM values of 3 independent experiments carried out in duplicate.*

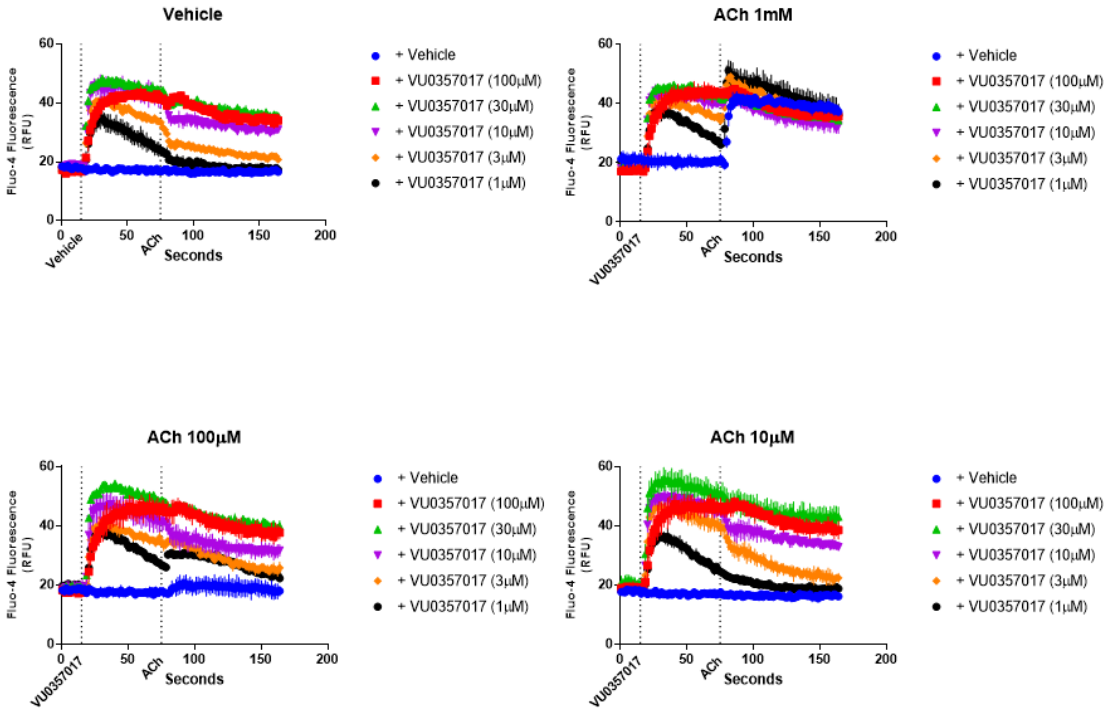


Figure 4.9: ***Representative calcium timecourses of ACh in the presence of bitopic ligand VU0357017****. Illustrating the effects of VU0357017 (added at 15sec) and acetylcholine (Ach; added at 75sec) in the dual addition protocol in CHO SNAP M1-DREADD cells. Data are mean ± range from a representative duplicate experiment.*

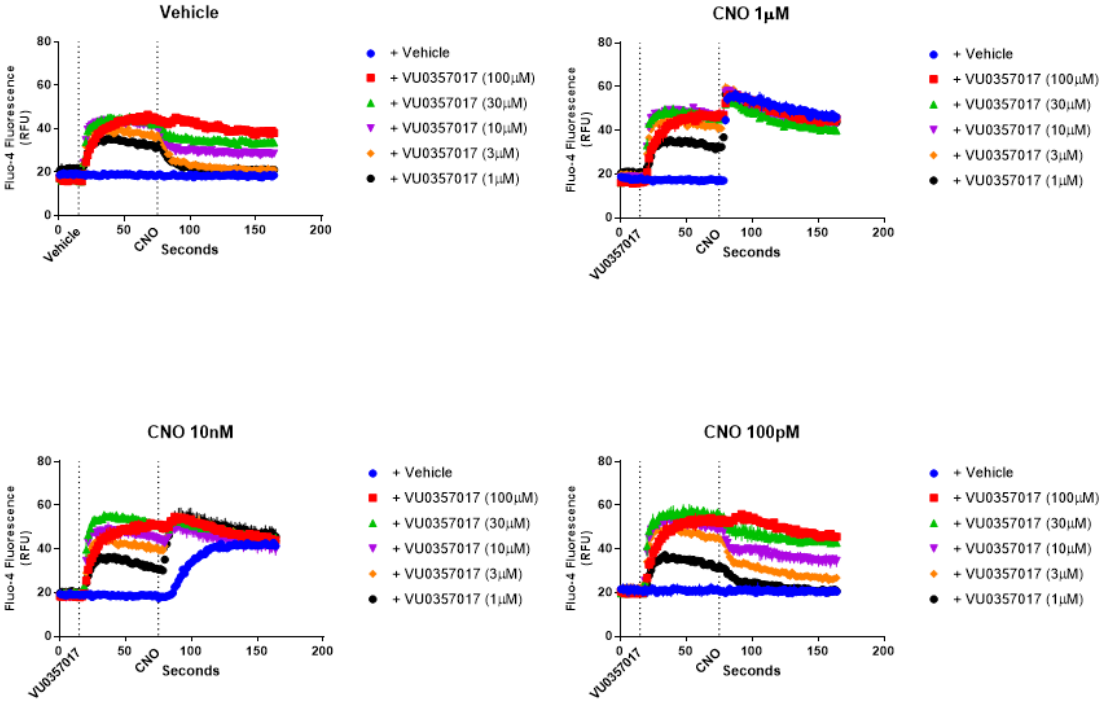


Figure 4.10: ***Representative calcium time course of CNO in the presence of VU0357017.*** *illustrating the effect of VU0357017 (added at 15sec) and clozapine-N-oxide (CNO; added at 75sec) in the dual addition protocol in CHO SNAP M1-DREADD cells. Data are mean ± range from a representative duplicate experiment.*

4.2.4Allosteric Modulation of DREADD Receptor Agonists by BQCA

The action of BQCA in combination with acetylcholine was first tested in the untransfected CHO K1 cell lines in order to exclude a potential modulatory effect on otherwise undetectable endogenous muscarinic receptor. However, acetylcholine in the presence of BQCA was unable to produce any calcium response in the CHO K1, with increasing BQCA concentrations up to 10µM (Fig. 4.11). This control experiment gives confidence that any allosteric effect elicited within our transfected CHO cell line is due to specific ligand-receptor interactions at the M1-DREADD receptor.

Next, the allosteric effect of different concentrations of BQCA at the M1-DREADD receptor was investigated with respect to acetylcholine, and the clozapine derivatives. As for the VU0357017 experiments, the modulator was added at 15sec, and the orthosteric agonist at 75sec, during continuous recording of Fluo4-AM measurements over 165sec. All responses are shown in reference to responses in the absence of BQCA. With increasing concentrations of BQCA a leftward shift was seen in the concentration response curves of acetylcholine (Fig 4.12, A). All concentrations of BQCA were able to produce a significant increase is acetylcholine's potency (pEC_{50}) at the M1-DREADD receptor, with the top concentration of BQCA (10µM) eliciting a 12-fold change in potency ($P<0.001$; one-way ANOVA). BQCA was also able to increase the maximum response to acetylcholine (R_{max}), at the higher concentrations of 10µM and 3µM ($P<0.001$, Table 4.4). At the top concentration of BQCA (10µM), there was a 1.4-fold increase in the maximum response.

The three clozapine derivatives were then investigated in the presence of increasing concentrations of BQCA. CNO and N,desmethylclozapine showed at least somewhat of a leftward potency shift with increasing concentrations of BQCA (Fig 4.12 B & C), however clozapine did not appear to show any change between in the presence or absence of BQCA. The fold increase in clozapine-N-oxide potency ranged from 5.89-fold in the presence of 0.1µM BQCA ($P<0.001$) to 93.3-fold increase with 10µM BQCA

(P<0.0001). An increase in CNO maximum response was also observed, but this was only significant in the presence of 10µM BQCA (P<0.01; Table 4.4).

The representative Fluo4-AM time course data (Fig. 4.13, 4.14, 4.15 & 4.16) confirmed that BQCA alone did not activate calcium mobilisation (15-75sec) in these experiments. Other than those reflecting the increase in agonist potency and R_{max} defined in the pooled concentration response curves, there were no significant differences apparent in the orthosteric agonist time courses. For example, maximal orthosteric agonist time courses in the absence or presence of BQCA were rapid in onset and relatively sustained over the 90sec recording time.

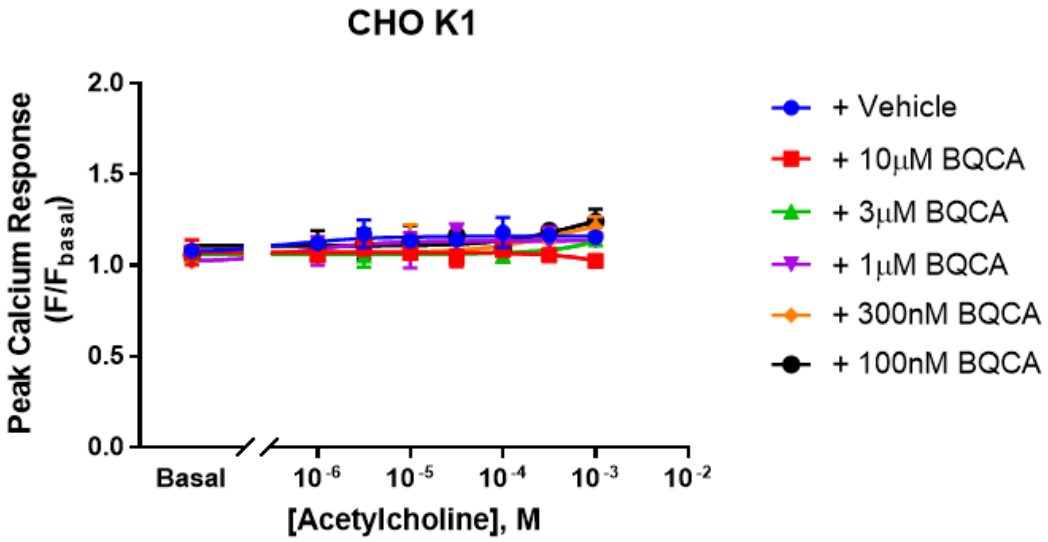


Figure 4.11: ***Concentration response curve for BQCA modulation of ACh at CHO K1 cells.*** *Peak calcium response for acetylcholine (added at 75sec) in absence or presence of increasing concentrations of BQCA (added at 15sec) at non transfected CHO K1 cells. Data are mean ± SEM for peak calcium responses, with experiments carried out in duplicate (n=3).*

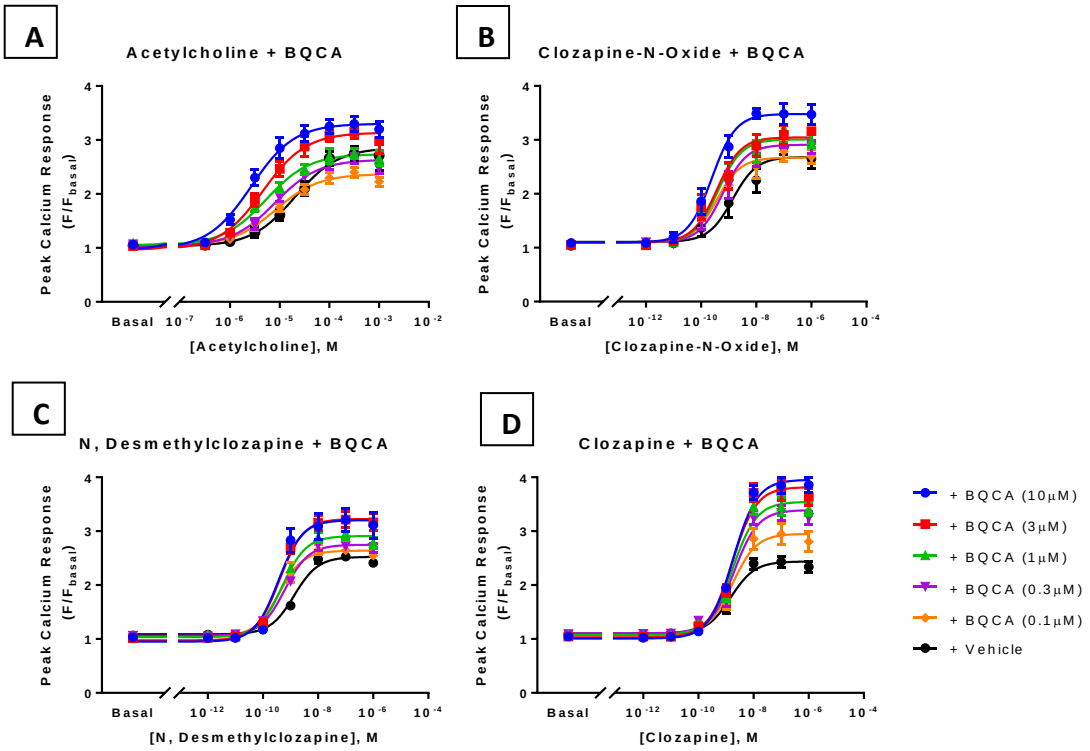


Figure 4.12: ***The allosteric effect of different BQCA concentrations on orthosteric agonist calcium responses in CHO SNAP M1-DREADD cells.*** *BQCA addition was made at 15s, and the orthosteric agonist at 75s during the Fluo4 recording on the Flexstation 3. Data are shown as mean ± SEM (as fold over initial basal read) of pooled experiments carried out in duplicate (n=5).*

	Ligand	pEC_{50}	Fold Change in Potency (EC_{50} ratio)	R_{max} (change in F/F_{basal})
Acetylcholine	+10uM BQCA	5.22 ± 0.09 ***	12.02	2.31 ± 0.12 **
	+3uM BQCA	4.95 ± 0.08 ***	6.46	2.30 ± 0.10 **
	+1uM BQCA	4.82 ± 0.09 **	4.79	1.71 ± 0.08 NS
	+0.3uM BQCA	4.61 ± 0.11 *	2.95	1.69 ± 0.09 NS
	+0.1uM BQCA	4.60 ± 0.10 *	2.88	1.39 ± 0.07 NS
	+Vehicle	4.14 ± 0.16	1.00	1.66 ± 0.19
Clozapine-N-oxide	+10uM BQCA	10.07 ± 0.09 ***	93.33	2.38 ± 0.11**
	+3uM BQCA	9.48 ± 0.10 ***	23.99	1.95 ± 0.11 NS
	+1uM BQCA	9.00 ± 0.10 **	7.94	1.91 ± 0.08 NS
	+0.3uM BQCA	8.96 ± 0.12 **	7.24	1.82 ± 0.12 NS
	+0.1uM BQCA	8.87 ± 0.11 **	5.89	1.57 ± 0.09 NS
	+Vehicle	8.10 ± 0.11	1.00	1.57 ± 0.07
N-desmethyl-clozapine	+10uM BQCA	9.43 ± 0.07 **	3.72	2.27 ± 0.08 ***
	+3uM BQCA	9.40 ± 0.09 **	3.45	2.11 ± 0.07 ***
	+1uM BQCA	9.30 ± 0.10 **	2.75	1.77 ± 0.07 **
	+0.3uM BQCA	9.21 ± 0.08 **	2.23	1.61 ± 0.05 NS
	+0.1uM BQCA	9.25 ± 0.09 **	2.45	1.51 ± 0.05 NS
	+Vehicle	8.86 ± 0.10	1.00	1.38 ± 0.05
Clozapine	+10uM BQCA	8.74 ± 0.06 NS	3.72	2.18 ± 0.09 ***
	+3uM BQCA	8.77 ± 0.08 NS	3.39	2.02 ± 0.08 ***
	+1uM BQCA	8.75 ± 0.08 NS	3.39	1.71 ± 0.07 **
	+0.3uM BQCA	8.71 ± 0.08 NS	2.45	1.52 ± 0.06 NS
	+0.1uM BQCA	8.76 ± 0.09 NS	1.07	1.48 ± 0.05 NS
	+Vehicle	8.83 ± 0.11	1.00	1.34 ± 0.06

Table 4.4: ***pEC_{50} and R_{max} values for acetylcholine, clozapine-N-oxide, N,desmethylclozapine and clozapine in the presence or absence (vehicle) of the M1-muscarinic allosteric modulator BQCA at the CHO SNAP hM1-DREADD receptor.*** *Values are mean ± SEM of experiments carried out in duplicate (n=5). * P < 0.05, ** P < 0.01, *** P < 0.001 one-way ANOVA analysis with a Dunnett's post hoc comparison, compared with ligand in the absence of BQCA.*

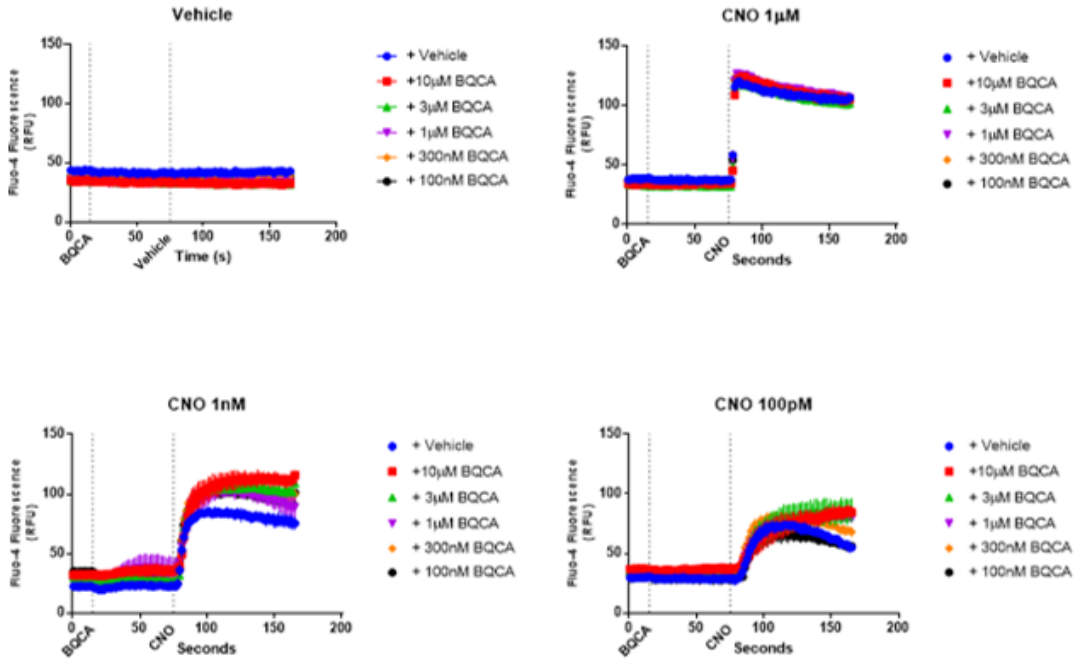


Figure 4.13: ***Representative time courses for CNO in the absence or presence of increasing concentrations of BQCA.*** *CHO SNAP M1-DREADD cells were loaded with Fluo-4 AM and fluorescence was read on the FlexStation 3 over 165sec. At 15sec BQCA was added, then 1min later CNO was added in log-fold differences. Values are mean ± range, for a representative experiment in duplicate*

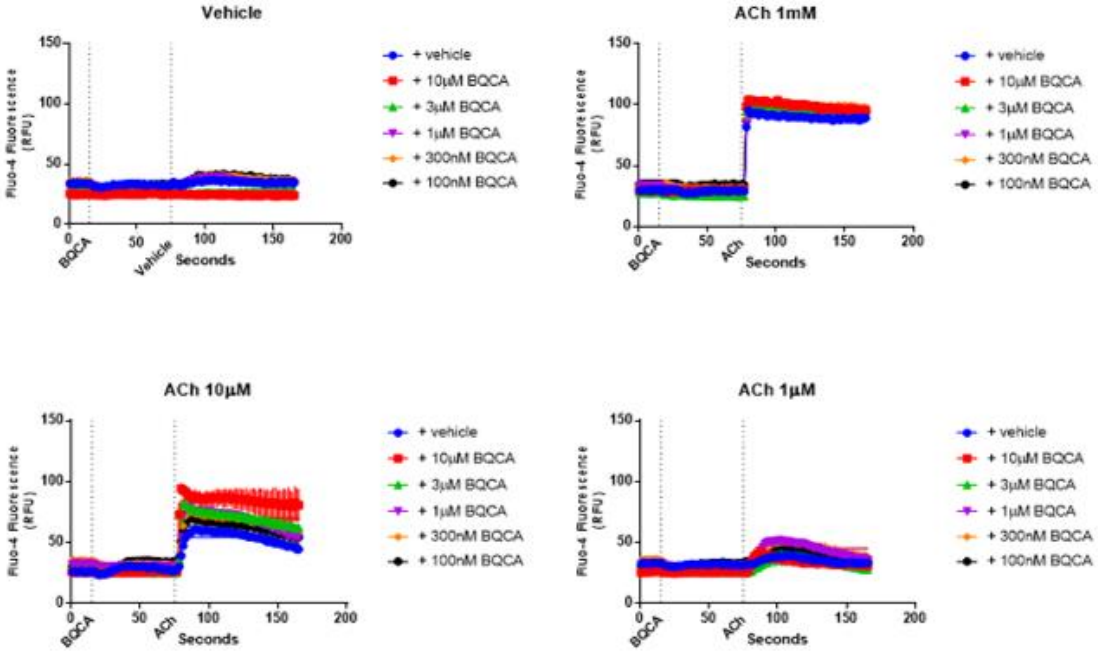


*Figure 4.14****: Representative timecourses for ACh in the absence or presence of increasing concentrations of BQCA.*** *CHO SNAP M1-DREADD cells were loaded with Fluo-4 AM and fluorescence was read on the FlexStation 3 over 165sec. At 15sec BQCA was added, then 1min later CNO was added in log-fold differences. Values are mean ± range, for a representative experiment in duplicate.*

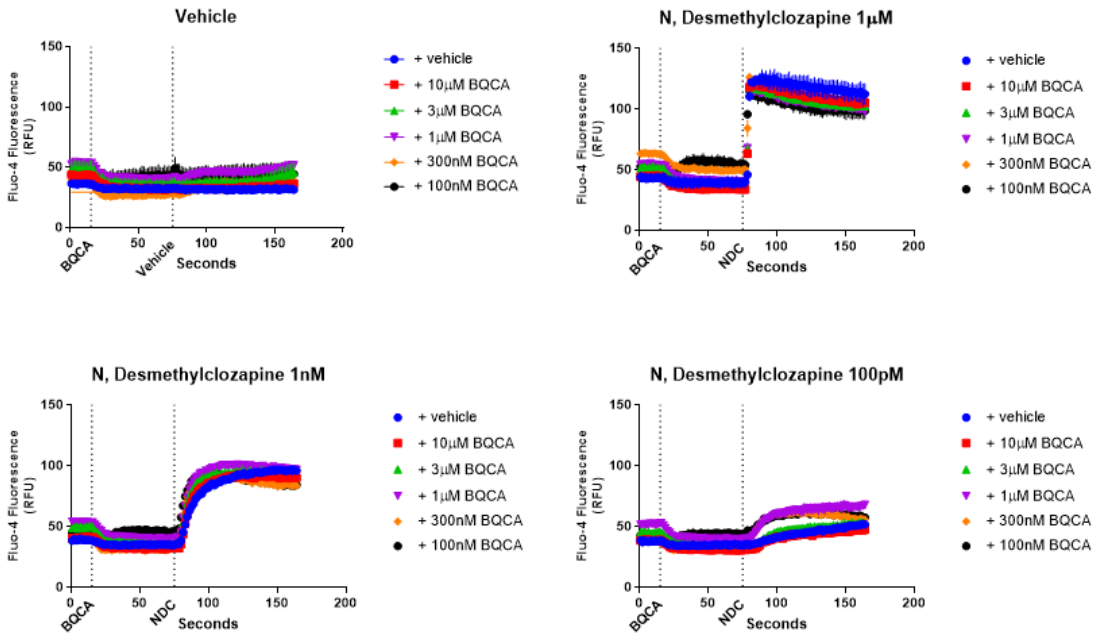


Figure 4.15: ***Representative time courses for N, desmethylclozapine (NDC) in the absence or presence of increasing concentrations of BQCA.*** *CHO SNAP M1-DREADD cells were loaded with Fluo-4 AM and fluorescence was read on the FlexStation 3 over 165sec. At 15sec BQCA was added, then 1min later CNO was added in log-fold differences. Values are mean ± range, for a representative experiment in duplicate.*

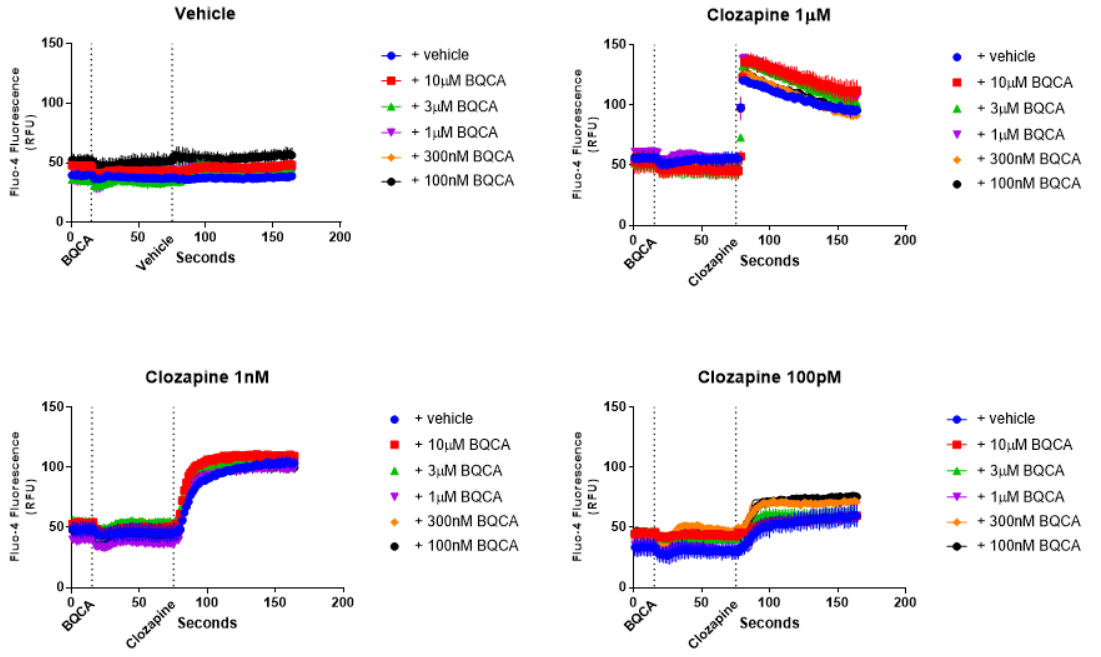


Figure 4.16: ***Representative time courses for clozapine in the absence or presence of increasing concentrations of BQCA****. CHO SNAP M1-DREADD cells were loaded with Fluo-4 AM and fluorescence was read on the FlexStation 3 over 165sec. At 15sec BQCA was added, then 1min later CNO was added in log-fold differences. Values are mean ± range, for a representative experiment in duplicate.*

4.2.5Evaluating Probe Dependence of BQCA in the CHO SNAP M1-DREADD System

Given BQCA was able to modify the acetylcholine calcium response at the M1-DREADD receptor, in addition to those of clozapine derivatives, it was then of interest to investigate the effect of BQCA on other muscarinic ligands in CHO SNAP M1-DREADD cells. Iperoxo, oxotremorine-M and xanomeline were selected, as they were able to produce a robust calcium response in the absence of the allosteric modulator (Fig. 4.17; pEC_{50} and R_{max} values are shown in Table 4.5). The allosteric modulator BQCA was able to increase the R_{max} value for all three agonists, the order of positive R_{max} modulation being greater for xanomeline > iperoxo > oxotremorine-M. The fold change of R_{max} of these drugs in the presence of 10µM BQCA as compared to vehicle was 3.72 ($P<0.001$), 2.74 ($P<0.01$) and 5.46 ($P<0.01$) for xanomeline, iperoxo and oxotremorine-M, respectively (Table 4.5). Interestingly, BQCA did little to alter the potency (pEC_{50} value) of the three orthosteric ligands (Fig 4.17). The fold change of EC_{50} of these drugs in the presence of 10µM BQCA as compared to vehicle for oxotremorine-M, xanomeline and Iperoxo, respectively are shown in Table 4.5. In terms of modulating the EC_{50} of these drugs, lower concentrations of BQCA had a slightly greater effect (Table 4.5). The largest EC50 changes were for iperoxo or oxotremorine-M, in the presence of 1µM BQCA, with a fold change of 13.80 and 9.12 respectively compared to vehicle.

It should be noted that the R_{max} of these drugs were much reduced from the original studies (Fig 4.5), in which R_{max} of 1.94 ± 0.08, 2.32 ± 0.19 and 1.83 ± 0.13 were obtained for oxotremorine-M, xanomeline and iperoxo respectively. In these studies, which were carried out at a later date, the R_{max} values were 0.73 ± 0.18, 0.74 ± 0.04 and 0.85 ± 0.14 for oxotremorine-M, xanomeline and iperoxo. Potentially, this might be a function of receptor loss over cell passage number and time from transfection (Hughes *et al.*, 2007). In future studies it would be useful to use an agent that induces calcium flux, such as ionomycin, at the end of the experiment as a measure of maximal calcium concentration within the experiment to verify the function of the cells especially over a number of cell passages.

Representative time courses supported the positive modulatory effects of BQCA on agonist potency (Fig. 4.18, 4.19 & 4.20). For iperoxo and xanomeline there was an indication that this effect was accompanied by a more rapid time to peak for the agonist response, as compared to xanomeline, as well as more sustained calcium mobilisation over the 90sec measured.

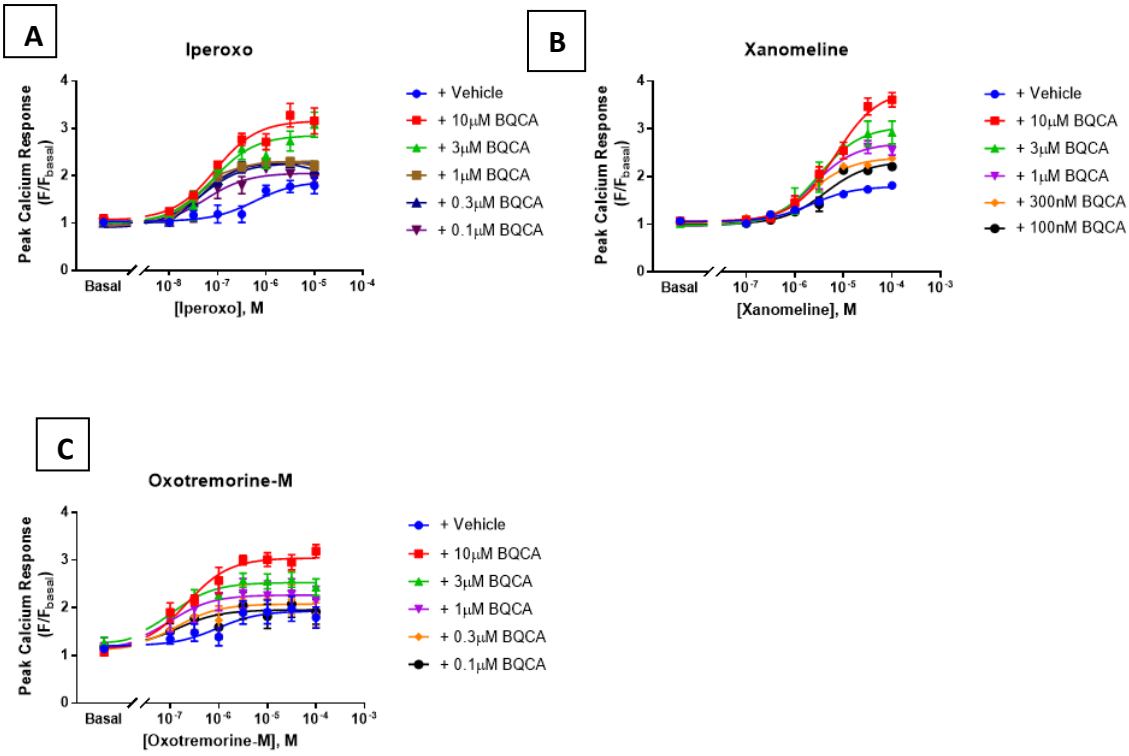


Figure 4.17: ***Concentration response curves of orthosteric ligands in the absence or presence of increasing concentrations of the allostereic modulator BQCA.*** *CHO SNAP M1-DREADD cells were loaded with Fluo-4 AM and fluorescence was read on the FlexStation 3 over 165sec. At 15sec BQCA was added, then 1min later, iperoxo (A), xanomeline (B) or oxotremorine-M (C) were added. Values are mean ± SEM for pooled experiments being carried out in duplicate (n=3).*

Iperoxo	pEC_{50}	Fold Change in Potency (EC_{50} ratio)	R_{max} (change in F/F_{basal})
+10uM BQCA	7.05 ± 0.13 *	6.46	2.09 ± 0.14 **
+3uM BQCA	7.09 ± 0.22 *	7.07	1.85 ± 0.23 **
+1uM BQCA	7.38 ± 0.12 **	13.80	1.37 ± 0.09 NS
+0.3uM BQCA	7.34 ± 0.11 **	12.59	1.36 ± 0.08 NS
+0.1uM BQCA	7.25 ± 0.13 *	10.23	1.10 ± 0.13 NS
+Vehicle	6.24 ± 0.20	1.00	0.85 ± 0.14
Xanomeline			
+10uM BQCA	5.17 ± 0.14 NS	0.41	2.75 ± 0.14 ***
+3uM BQCA	5.52 ± 0.16 NS	0.91	2.08 ± 0.13 ***
+1uM BQCA	5.60 ± 0.11 NS	1.09	1.74 ± 0.10 **
+0.3uM BQCA	5.66 ± 0.11 NS	1.26	1.37 ± 0.08 *
+0.1uM BQCA	5.60 ± 0.12 NS	1.09	1.32± 0.07 *
+Vehicle	5.56 ± 0.11	1.00	0.74 ± 0.04
Oxotremorine-M			
+10uM BQCA	6.56 ± 0.16 NS	3.39	2.00 ± 0.18 **
+3uM BQCA	6.96 ± 0.14 **	8.51	1.27 ± 0.14 NS
+1uM BQCA	6.99 ± 0.13 **	9.12	1.09 ± 0.20 NS
+0.3uM BQCA	6.86 ± 0.18 *	6.07	0.98 ± 0.20 NS
+0.1uM BQCA	6.83 ± 0.19 *	6.31	0.78 ± 0.20 NS
+Vehicle	6.03 ± 0.15	1.00	0.73 ± 0.18

Table 4.5: ***pEC_{50} and R_{max} values for iperoxo, xanomeline and oxotremorine-M in the presence of the M1-muscarinic allosteric modulator BQCA at the CHO SNAP hM1-DREADD receptor.*** *Values are mean ± SEM of experiments carried out in duplicate (n=3). NS, not significant; * P < 0.05, ** P < 0.01, *** P < 0.001; one-way ANOVA analysis was carried out with a Dunnett's post hoc comparison to compare statistical significance from ligand in the absence of BQCA.*

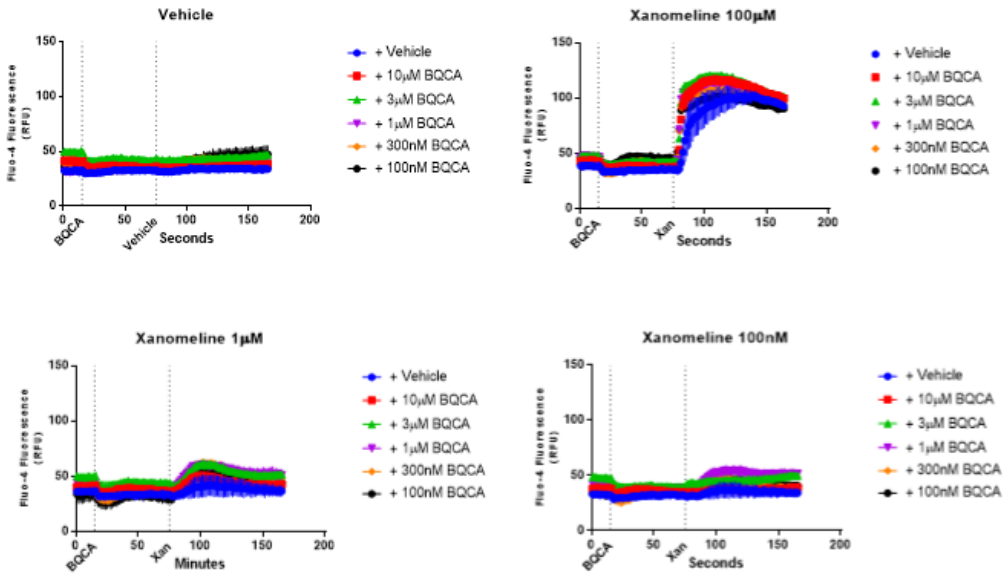


Figure 4.18: ***Representative timecourses for xanomeline in the absence or presence of increasing concentrations of BQCA.*** *CHO SNAP M1-DREADD cells were loaded with Fluo-4 AM and fluorescence was read on the FlexStation 3 over 165sec. At 15sec BQCA was added, then 1min later CNO was added in log-fold differences. Values are mean ± range, for a representative experiment in duplicate.*

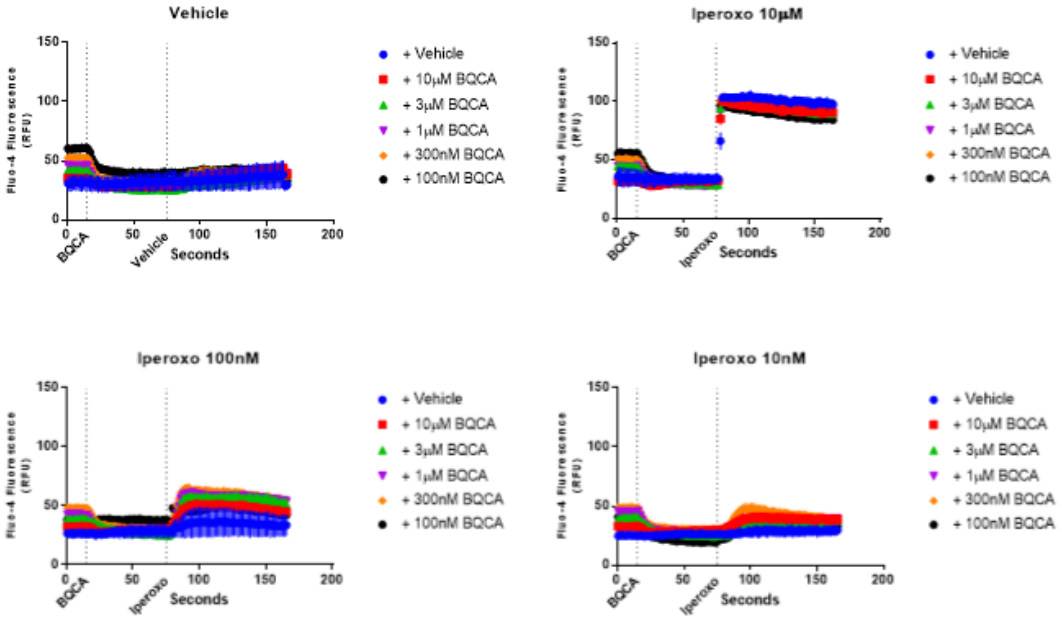


Figure 4.19: ***Representative timecourses for iperoxo in the absence or presence of increasing concentrations of BQCA.*** *CHO SNAP M1-DREADD cells were loaded with Fluo-4 AM and fluorescence was read on the FlexStation 3 over 165sec. At 15sec BQCA was added, then 1min later CNO was added in log-fold differences. Values are mean ± range, for a representative experiment in duplicate.*

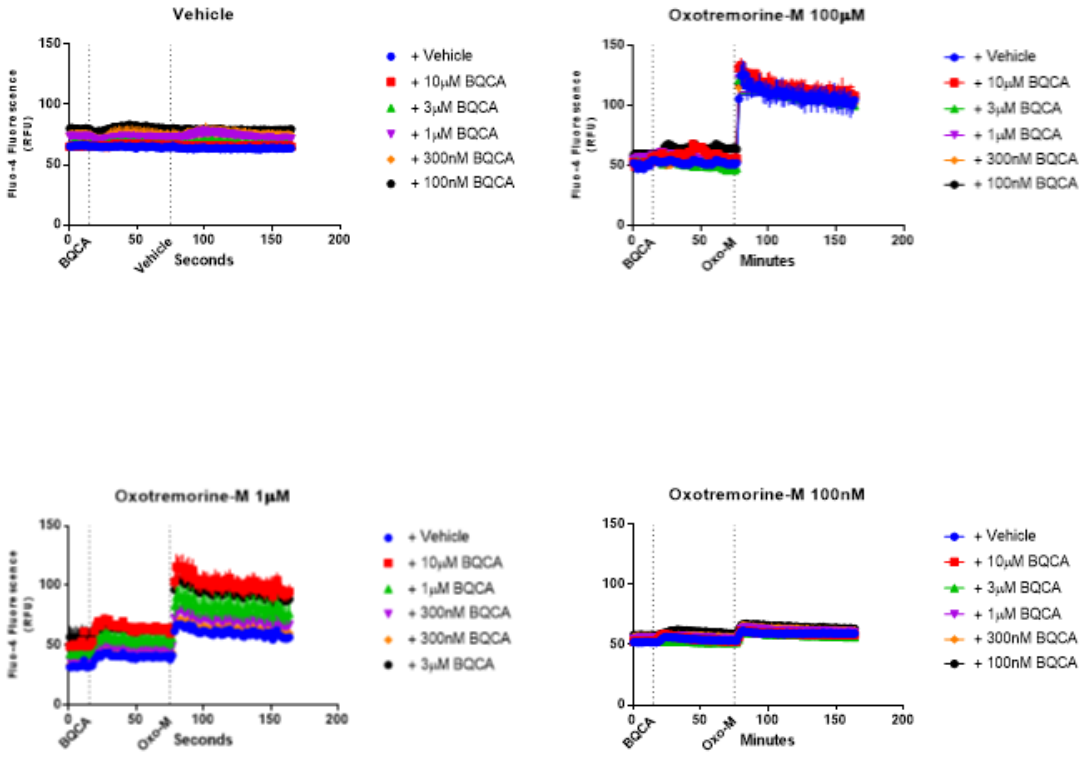


Figure 4.20: ***Representative timecourses for oxotremorine-M in the absence or presence of increasing concentrations of BQCA.*** *CHO SNAP M1-DREADD cells were loaded with Fluo-4 AM and fluorescence was read on the FlexStation 3 over 165sec. At 15sec BQCA was added, then 1min later CNO was added in log-fold differences. Values are mean ± range, for a representative experiment in duplicate.*

> Using Mini G protein and β-arrestin2 luciferase complementation assays to explore allosteric modulation of the M1-WT and M1-DREADD receptors

4.2.6Mini Gq and β-ARR2 Protein Recruitment by M1-WT, and the Effect of BQCA

In the HEK LgBiT SNAP M1 mini Gq cells, the panel of muscarinic receptor agonists each produced sustained increases in luminescence reflecting agonist dependent recruitment of the mini Gq protein (Fig 4.21). When analysing the time courses of the responses produced by orthosteric ligands and the clozapine derivatives, it can be seen that the orthosteric ligands produced a prolonged effect of the mini G being recruited to the M1 receptor. The agonists induced luminescence to rapidly rise within 3-7min, which was then sustained over the 25min time course without a decay of the signal occurring (Fig. 4.21). The clozapine derivatives had no effect of mini Gq recruitment to the M1 receptor (Fig 4.22).

To compare changes in potency and maximal response over time, agonist concentration response curves were constructed from the data at the 3min and 25min time points. The 3 minute time point was taken as peak response after ligand addition, while the 25 minute time point was used to investigate the sustained effect of complementation after ligand addition. Although not all drugs reached peak response by 3 minutes it was useful to have a consistent time point to compare across all drugs, in the future it may be of interest to investigate the difference between individual peak response compared to the set time point. Iperoxo ($P<0.001$; paired t-test) and ACh ($P<0.05$) showed significant increases in potency between the early and sustained time points (Table 4.6). There were no significant differences in potency at these two time points between the other orthosteric ligands. The muscarinic agonist panel produced a range of potency and maximal responses measuring the complementation of mini Gq. In rank order from the most potent (pEC_{50}) were Iperoxo > Acetylcholine

> Xanomeline > Oxotremorine-M > Carbachol > Pilocarpine (Fig. 4.23; Table 4.6). In comparison to the calcium mobilisation assay, there was also greater distinction in the maximal response R_{max} to each agonist (measured at 25 min following addition) - in terms of R_{max} values, the rank order from full to partial was iperoxo = acetylcholine > carbachol = oxotremorine-M > xanomeline > pilocarpine (Table 4.7).

To explore the effect of BQCA, this ligand was added with the furimazine substrate, 10 min prior to acetylcholine. It can be seen that BQCA is having its own effect without the orthosteric ligand being present, with luminesce increasing before time 0. The concentration of ACh appeared to determine the kinetic profile and shape of the curves, while BQCA positively modulates this effect while maintaining comparable kinetic plots as ACh in the absence of BQCA (Fig 4.24). At lower concentrations of ACh (<1µM) it can be seen that luminescence gradually decreased over the time course. Whereas with higher concentrations of ACh, especially 1mM, mini Gq complementation can be seen to be sustained with an initial increase over 4min after ligand addition (Fig 4.24).

Regarding the concentration response curves, interestingly, BQCA alone was able to produce mini Gq complementation at concentrations between 3 – 100 µM, below that observed to initiate a calcium response, and an R_{max} value of 93.51 ± 7.36% of 10µM iperoxo (Fig 4.24 & Table 4.8). The agonist effect of BQCA was evident in the elevated baselines for the ACh concentration response curves illustrated in Fig. 4.25. BQCA was added prior to the first plate read on the Pherastar, thus BQCA had time to initiate mini Gq complementation before the endogenous ligand was added after a 6min baseline read. For instance, while there was an apparent reduction in R_{max} values for ACh in the presence of 3µM BQCA as compared to in the absence of BQCA, this can be attributed to this BQCA concentration elevating the baseline roughly 50% compared to that of vehicle addition (Fig 4.25 and Table 4.8). When ACh was added in the presence of BQCA there was still an allosteric effect which induced an expected left-shift, indicating an increased potency for M1 receptor recruitment of mini Gq (Table 4.9).

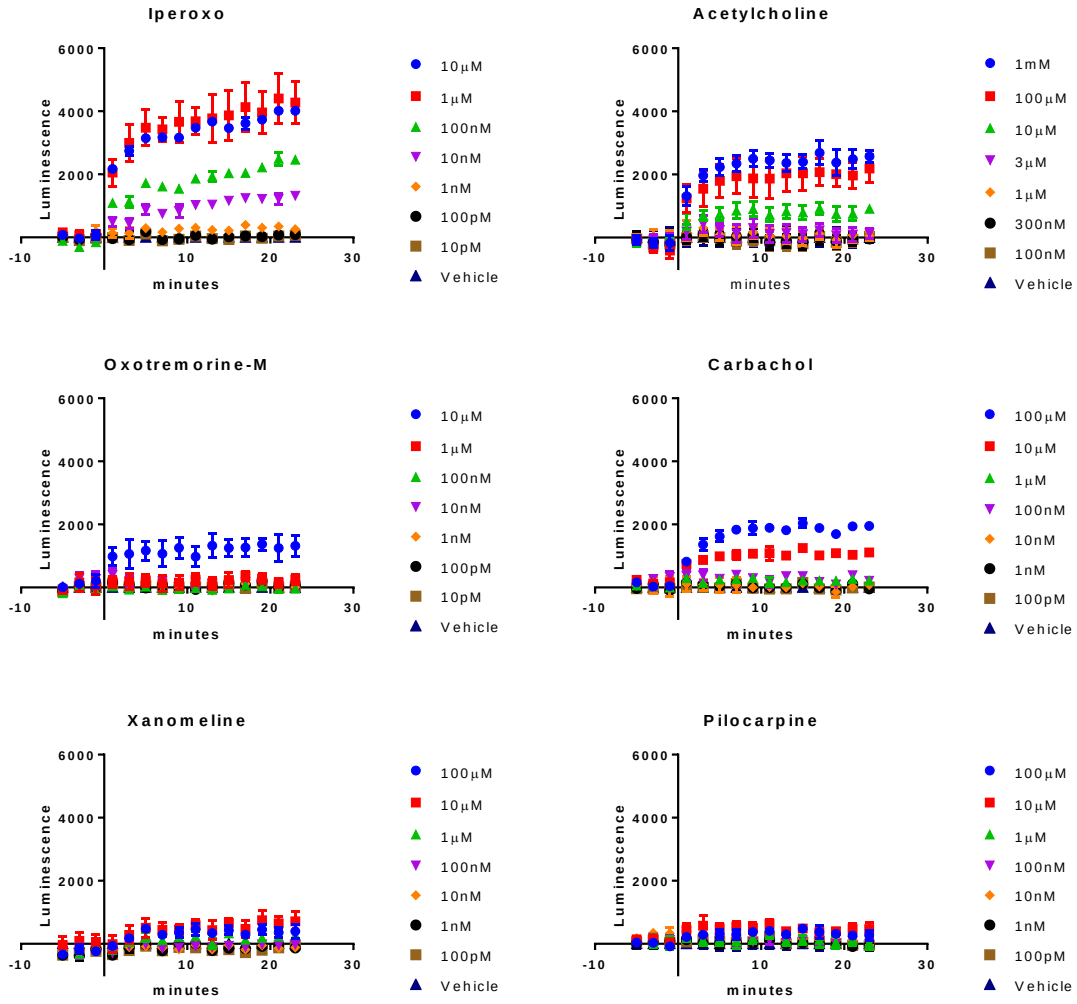


Figure 4.21: **Time course of the orthosteric ligand luminescence complementation responses in HEK LgBiT SNAP M1 mini Gq cells.** After furimazine incubation for 5 min, luminescence complementation was measured on the Pherastar over a 30min time course at 37°C. Ligands were added after an initial baseline read of 6 min. Values are arbitrary luminescence units representing mean ± range of a representative experiment carried out in duplicate.

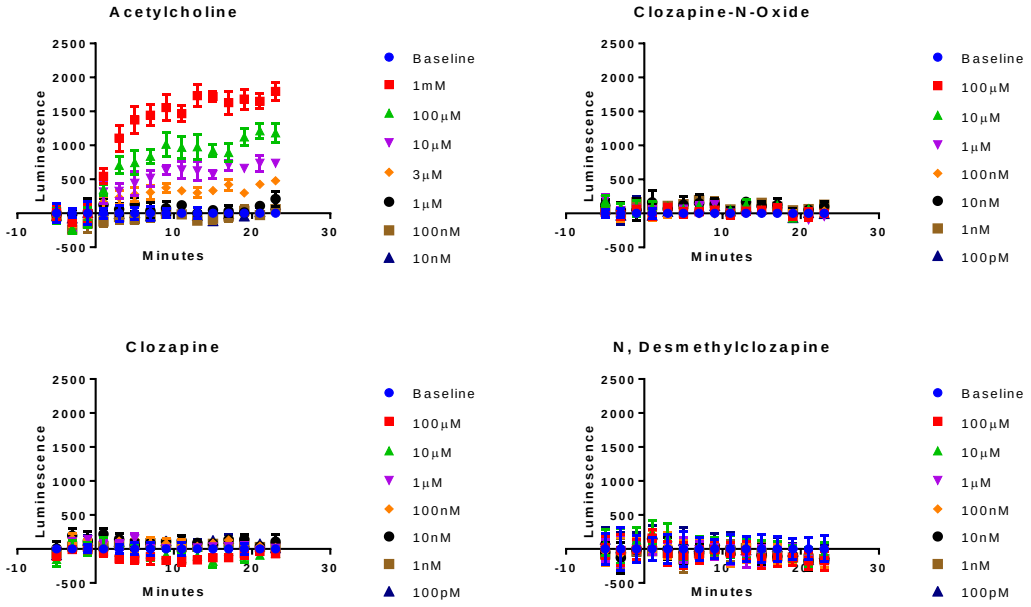


Figure 4.22: ***Timecourse of the clozapine derivatives and ACh, the endogenous ligand, luminescence complementation responses in HEK LgBiT SNAP M1 mini Gq cells.*** *After furimazine incubation for 5 min, luminescence complementation was measured on the Pherastar over a 30min time course at 37°C. Ligands were added after an initial baseline read of 6 min. Values are arbitrary luminescence units representing mean ± range of a representative experiment carried out in duplicate.*

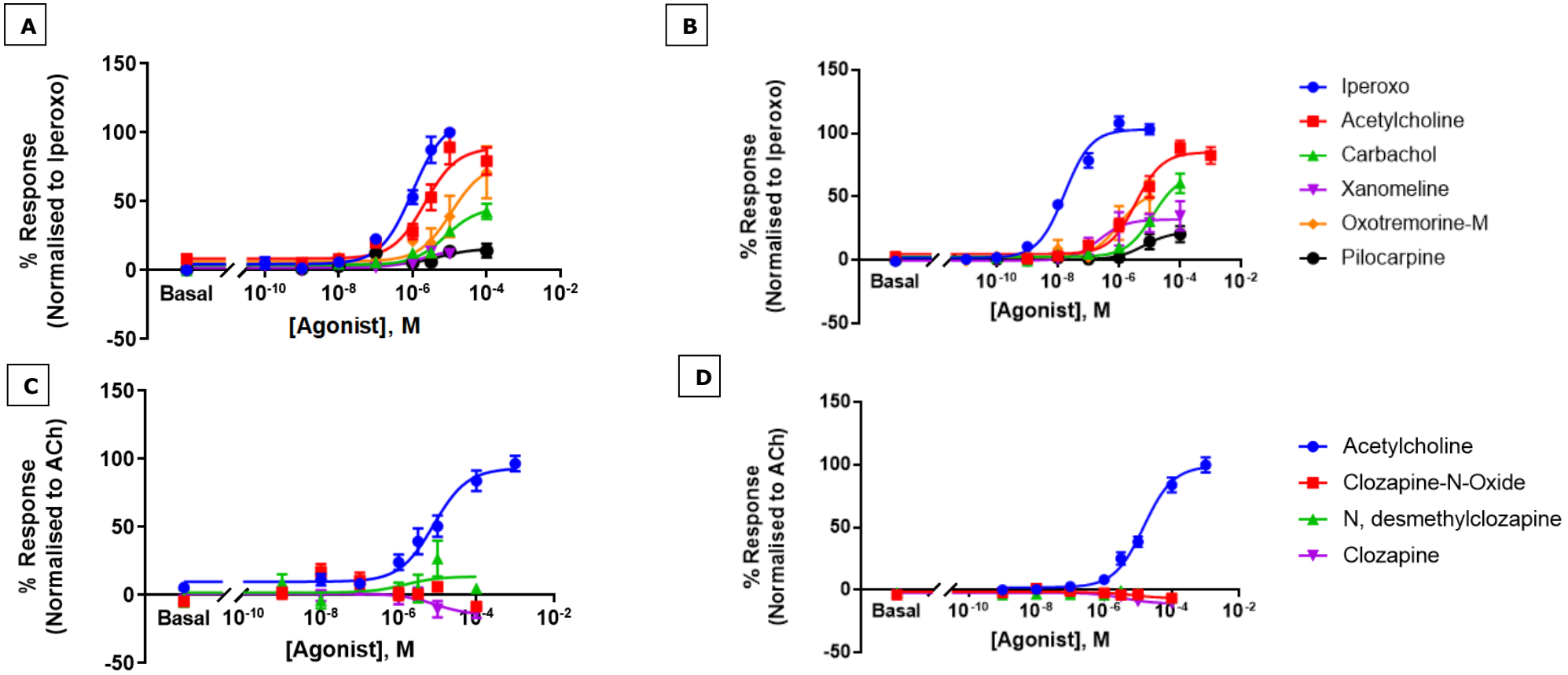


Figure 4.23: ***Monitoring mini Gq protein recruitment to the LgBiT SNAP M1 receptor in the NanoBiT complementation assay****. HEK LgBiT SNAP M1 mini Gq cells were loaded with luciferase substrate furimazine for 5min prior to recording luminescence on a Pherastar for 30 min at 37 C. After 3 basal readings (6 min), orthosteric agonists were added and concentration response curves were constructed at 3 min (A, C) and 25 min post addition (B, D). Luminescence values were normalised to the vehicle (0%) and 10uM iperoxo (100 %) response. (A) Concentration response curve of the orthosteric ligands at 3min and (B) at 25min. (C) Concentration response curve of the clozapine derivatives and the endogenous ligand ACh at 3min, normalised to the ACh response; and (D) 25min. Data are shown as mean ± SEM for pooled experiments carried out in duplicate (n=5)*

HEK M1 mini Gq	pEC_{50} 3min post ligand addition	pEC_{50} 25min post ligand addition
Acetylcholine	6.01 ± 0.09*	5.45 ± 0.13
Iperoxo	5.67 ± 0.15***	7.78 ± 0.07
Xanomeline	5.12 ± 0.12 ^{NS}	6.15 ± 0.39
Oxotremorine-M	5.76 ± 0.46 ^{NS}	5.99 ± 0.32
Carbachol	4.96 ± 0.20 ^{NS}	5.19 ± 0.34
Pilocarpine	5.29 ± 0.50 ^{NS}	4.89 ± 0.11

Table 4.6: ***Comparison between pEC_{50} values between 3min and 25min post ligand addition at the mini Gq in HEK LgBiT SNAP M1 cells.*** *A paired t-test was used to find statistical significance between the two difference time points: NS, not significant.*

HEK M1 mini Gq (sustained response)	pEC_{50}	Fold Change (F/F_{basal})	R_{max} (% of 10µM Iperoxo)
Iperoxo	7.78 ± 0.07	1.00	101.40 ± 3.13
Acetylcholine	5.45 ± 0.13***	213.80	80.41 ± 4.21
Xanomeline	6.15 ± 0.39***	42.66	32.54 ± 5.72
Oxotremorine-M	5.99 ± 0.32***	61.66	52.60 ± 10.04
Carbachol	5.19 ± 0.34***	389.04	65.31 ± 4.15
Pilocarpine	4.89 ± 0.11***	776.25	21.64 ± 4.01
BQCA	ND	ND	ND

Table 4.7: ***Comparison between pEC_{50} and R_{max} values for mini Gq complementation after equilibrium in HEK LgBiT SNAP M1 cells.*** *A one-way ANOVA analysis with Dunnett's post hoc analysis was used to find statistical significance when iperoxo was used as a reference ligand compared to the other orthosteric ligands; NS, not significant, or ** $P < 0.01$.*

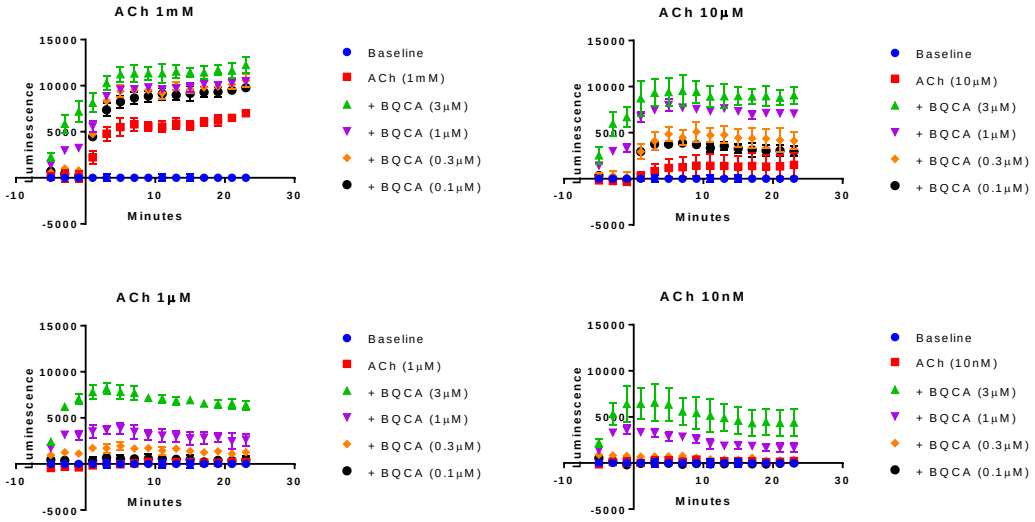


Figure 4.24: ***Time course of complementation responses in HEK LgBiT SNAP M1 mini Gq cells with acetylcholine in the presence of increasing concentrations of BQCA.*** *HEK LgBiT SNAP M1 mini GQ cells were loaded with luciferase substrate furimazine for 5min prior to recording luminescence on a Pherastar for 30 min at 37°C. Increasing concentrations of BQCA was then added and a basal read (6min) was taken before ACh was added at timepoint 0 (intercept of axes). Data was then taken over a time period of 25min to produce a kinetic plot. Values are arbitrary luminescence units representing mean ± range of a representative experiment carried out in duplicate.*

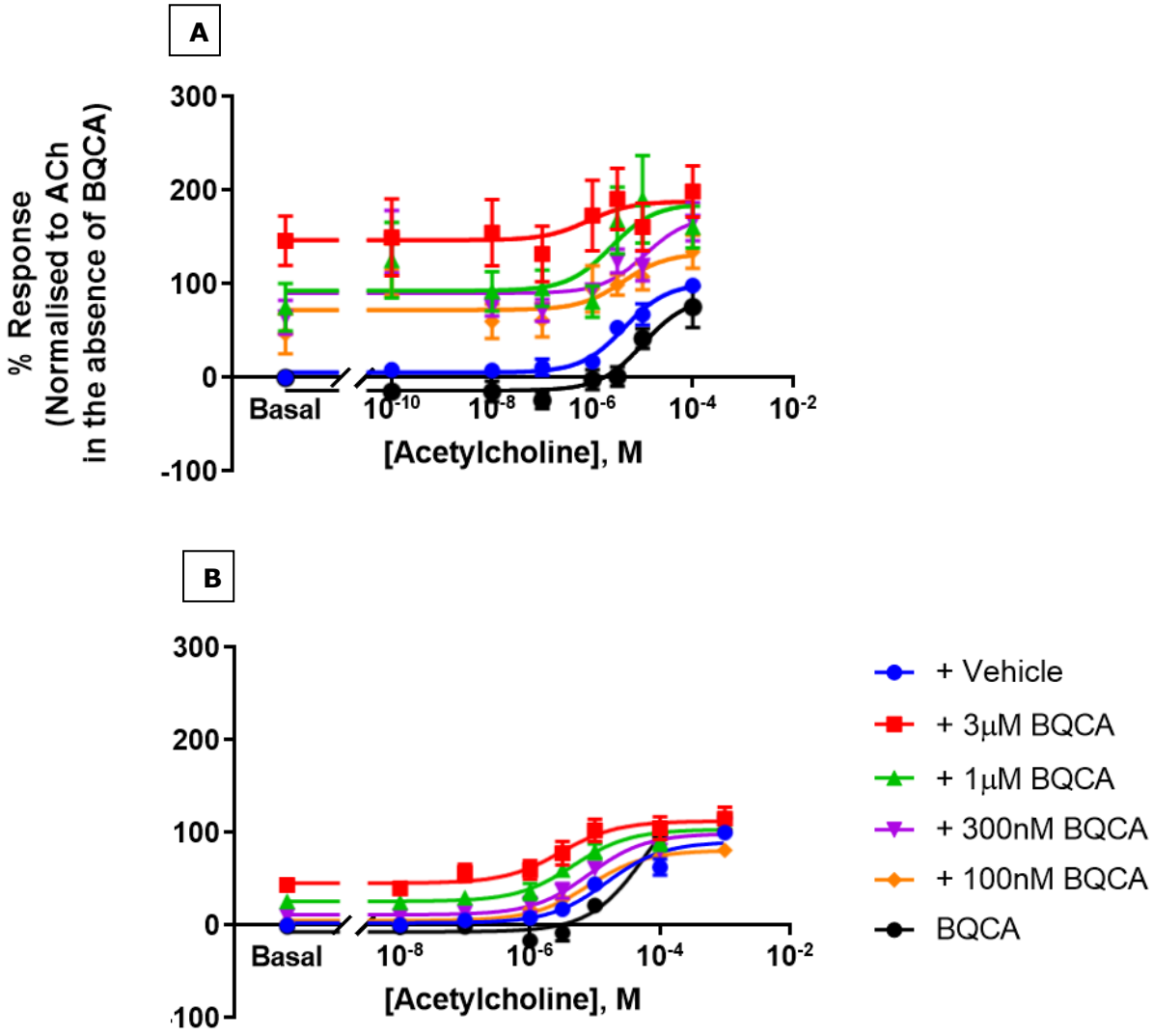


Figure 4.25: ***Monitoring mini Gq protein recruitment to the LgBiT SNAP M1 receptor in the NanoBiT complementation assay****. HEK M1 mini Gq cells were loaded with luciferase substrate furimazine for 5min, prior to recording luminescence on a Pherastar for 30 min at 37 C. Luminescence values were normalised to the vehicle (0%) and 100μM acetylcholine (100%) response. After 3 basal readings (6min), acetylcholine in increasing concentrations of BQCA was added and concentration response curves were constructed at 3 min (A) and 25 min post addition (B). Data are shown as mean ± SEM for pooled experiments (n=5).*

HEK M1 mini G + ACh	pEC_{50} 3min post ligand addition	pEC_{50} 25min post ligand addition
BQCA	4.99 ± 0.13	ND
+ 3µM BQCA	6.09 ± 1.40 ^{NS}	5.53 ± 0.25
+ 1µM BQCA	5.63 ± 0.50 ^{NS}	5.34 ± 0.15
+ 300nM BQCA	4.95 ± 0.40 ^{NS}	5.09 ± 0.12
+ 100nM BQCA	5.39 ± 0.60 ^{NS}	5.10 ± 0.11
+ Vehicle	5.37 ± 0.13	4.83 ± 0.12

Table 4.8: ***Comparison between pEC_{50} values between 3min and 25min post ligand addition at the mini Gq in HEK LgBiT SNAP M1 cells.*** *Peak calcium mobilisation was investigated with increasing concentrations of BQCA in the presence of ACh. A paired t-test was used to find statistical significance between the two difference time points: NS, not significant.*

HEK mini G + ACh (sustained response)	pEC_{50}	Fold Change in potency (EC_{50} ratio)	R_{max} (% 100µM acetylcholine response)
+ Vehicle	4.83 ± 0.12	1.00	87.50 ± 5.07
+ 3µM BQCA	5.53 ± 0.25 ^{NS}	5.01	67.03 ± 9.36
+ 1µM BQCA	5.34 ± 0.15 ^{NS}	3.24	77.68 ± 6.52
+ 0.3µM BQCA	5.09 ± 0.12 ^{NS}	1.82	87.56 ± 5.78
+ 0.1µM BQCA	5.10 ± 0.11 ^{NS}	1.86	75.70 ± 5.07

Table 4.9: ***Comparison between pEC_{50} values at equilibrium at the mini Gq in HEK LgBiT SNAP M1 cells.*** *Peak calcium mobilisation was investigated with increasing concentrations of BQCA in the presence of ACh. A one-way ANOVA, with Dunnet's post hoc, was used to find statistical significance with ACh alone used as a reference: NS, not significant.*

In the HEK LgBiT SNAP M1 βARR2 cells, the panel of muscarinic receptor agonists each produced a peak increase in luminescence reflecting a spike in agonist dependent complementation of the βARR2 protein over 4-8min, before a subsequent depletion in its interaction with the receptor (Fig 4.26). Statistical comparison between early recruitment (3min) and sustained recruitment (25min) of the βARR2 was not found to be significantly different (Table 4.10). This reflects the rapid peak of response and the slow decay of the luminescence signal over the 25min.

Concentration curves of the orthosteric agonists produced complementation responses that were comparable to the mini Gq complementation data, above. In rank order from the most potent to least (pEC_{50}) was iperoxo > xanomeline > acetylcholine > carbachol > pilocarpine > oxotremorine-M (Fig. 4.27). A pEC_{50} value was unable to be calculated for oxotremorine-M due to an incomplete sigmoidal concentration response curve. R_{max} values showed a rank order from highest being Iperoxo > Acetylcholine > Carbachol > Oxotremorine-M > Xanomeline > Pilocarpine (Table 4.10 & 4.11). There was no detectable βARR2 recruitment to the M1 receptor when the clozapine derivatives were applied (Fig 4.27 C & D).

In the presence of BQCA, time courses produced a rapid increase in luminescence over 6min, reflecting a spike in agonist dependent complementation of the βARR2 protein to the M1 receptor (Fig 4.28). The concentration response curves showed BQCA on its own could produce some recruitment of βARR2 protein and showed an R_{max} value of 30.4% compared to 100µM ACh. BQCA in the presence of ACh caused a left-shift of all concentration response curves, except in the presence of BQCA at 100nM. Additionally, with increasing BQCA concentrations there was a reduction in R_{max} values as compared to ACh in the absence of BQCA (Fig 4.29, Table 4.12 & 4.13).

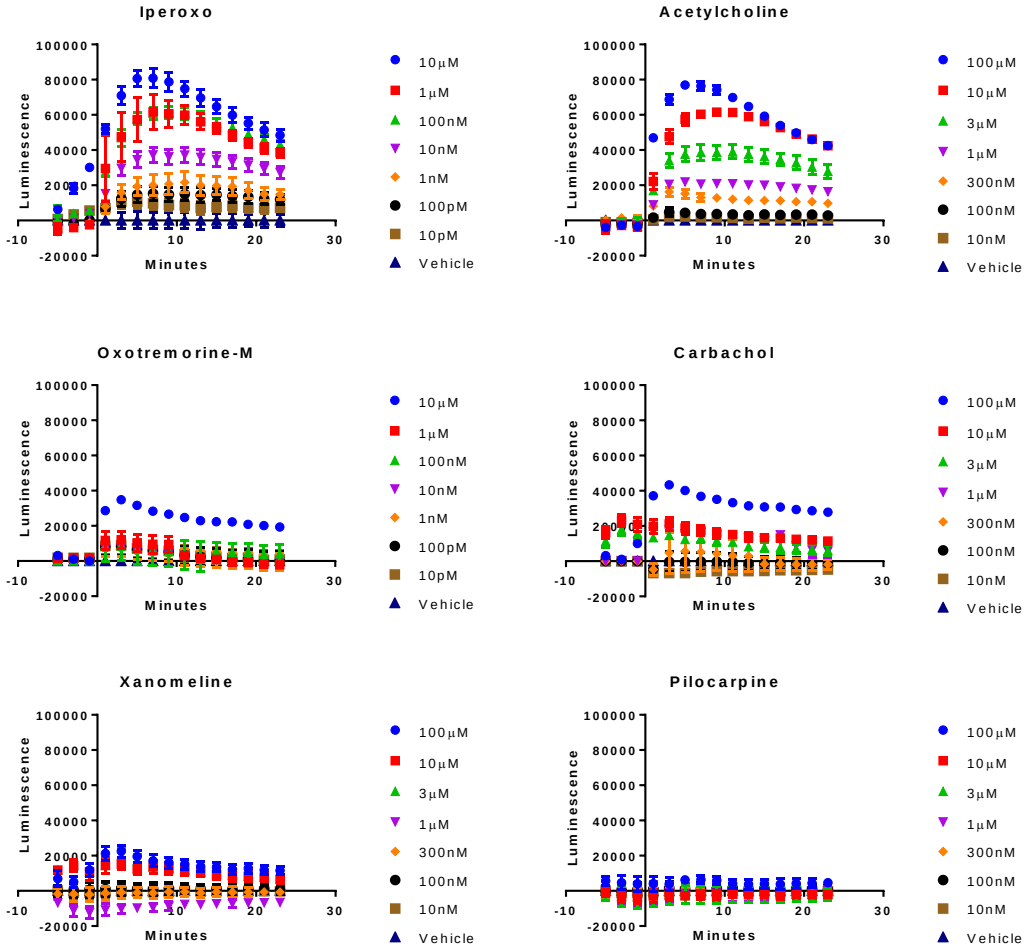


Figure 4.26: ***Time course of the orthosteric ligand luminescence complementation responses in HEK LgBiT SNAP M1 βARR2 cells****. After furimazine incubation of 5min, luminescence complementation was measured on the Pherastar over a 30min time course at 37°C. Ligands were added after an initial baseline read for 6min. Values are arbitrary luminescence units representing mean ± range of a representative experiment carried out in duplicate.*

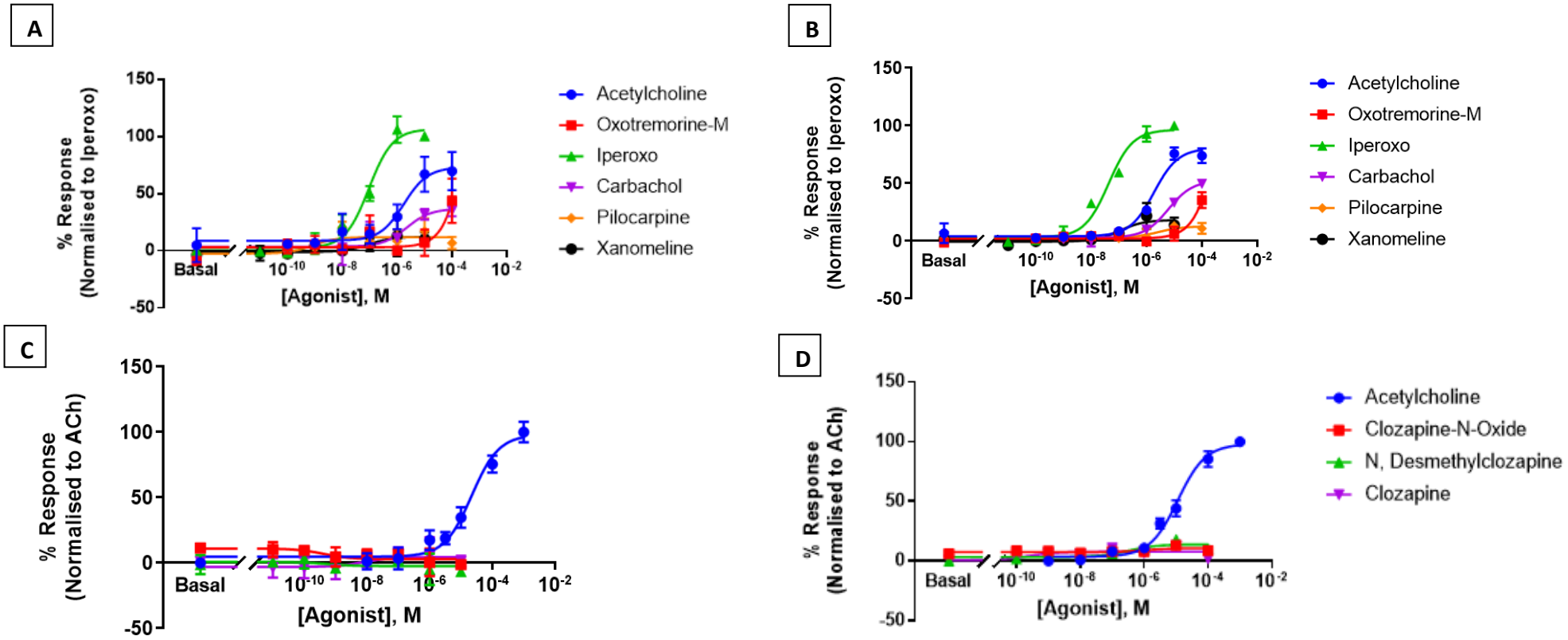


Figure 4.27: ***Monitoring βARR2 protein recruitment to the M1 receptor in the NanoBiT complementation assay****. HEK LgBiT SNAP M1 βARR2 cells were loaded with luciferase substrate furimazine for 5min, prior to recording luminescence on a Pherastar, for 30min at 37°C. After 3 basal readings, agonists were added at 6 min and concentration response curves were constructed at 3 min (A, C) and 25 min post addition (B, D). (A , B) Concentration response curve of the orthosteric ligands, values were normalised to the vehicle (0%) and 10uM iperoxo (100 %) response. (C, D) concentration response curve of the clozapine derivatives and the endogenous ligand, normalised to the 100μM ACh response. Data are shown as mean ± SEM for pooled experiments (n=5).*

HEK M1 βARR2	pEC_{50} (M) 3min post ligand addition	pEC_{50} (M) 25min post ligand addition
Iperoxo	7.03 ± 0.15 ^{NS}	7.78 ± 0.07
Acetylcholine	5.76 ± 0.20 ^{NS}	5.45 ± 0.13
Carbachol	5.65 ± 0.35 ^{NS}	6.15 ± 0.39
Xanomeline	7.03 ± 0.16 ^{NS}	5.99 ± 0.32
Oxotremorine-M	ND	ND
Pilocarpine	5.94 ± 0.16 ^{NS}	4.89 ± 0.11

Table 4.10: ***Comparison between pEC_{50} values between 3min and 25min post ligand addition at the βARR2 in HEK LgBiT SNAP M1 cells.*** *A paired t-test was used to find statistical significance between the two difference time points: NS, not significant.*

HEK M1 βARR2 (sustained response)	pEC_{50}	Fold Change in potency (EC_{50} ratio)	R_{max} (% 10μM Iperoxo Response)
Iperoxo	6.31 ± 0.12	1.00	99.42 ± 5.73
Acetylcholine	4.65 ± 0.10 **	45.71	81.58 ± 4.18
Carbachol	5.03 ± 0.09 **	19.05	53.69 ± 3.50
Xanomeline	5.57 ± 0.10 ^{NS}	5.50	19.47 ± 4.24
Oxotremorine-M	ND	ND	ND
Pilocarpine	5.94 ± 0.16 ^{NS}	2.34	ND
Pilocarpine	5.26 ± 0.11	11.22	10.22 ± 2.95

Table 4.11: ***Comparison between pEC_{50} and R_{max} values in equilibrium at the βARR2 in HEK LgBiT SNAP M1 cells.*** *A one-way ANOVA analysis with Dunnett's post hoc analysis was used to find statistical significance when iperoxo was used as a reference ligand compared to the other orthosteric ligands; NS, not significant, or ** P < 0.01.*

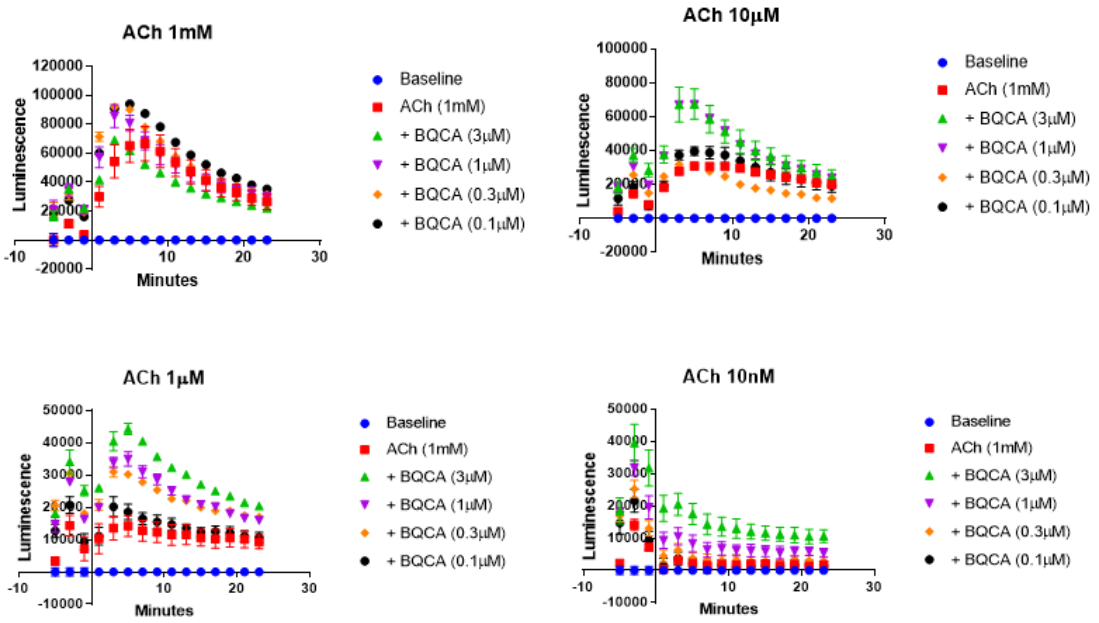


Figure 4.28: ***Time course of acetylcholine in increasing concentrations of BQCA in HEK LgBiT SNAPM1 βARR2 cells.*** *After furimazine incubation of 5min, luminescence complementation was measured on the Pherastar over a 30min time course at 37°C. Ligands were added after an initial baseline read of 6min. Values are arbitrary luminescence units representing mean ± range of a representative experiment carried out in duplicate.*

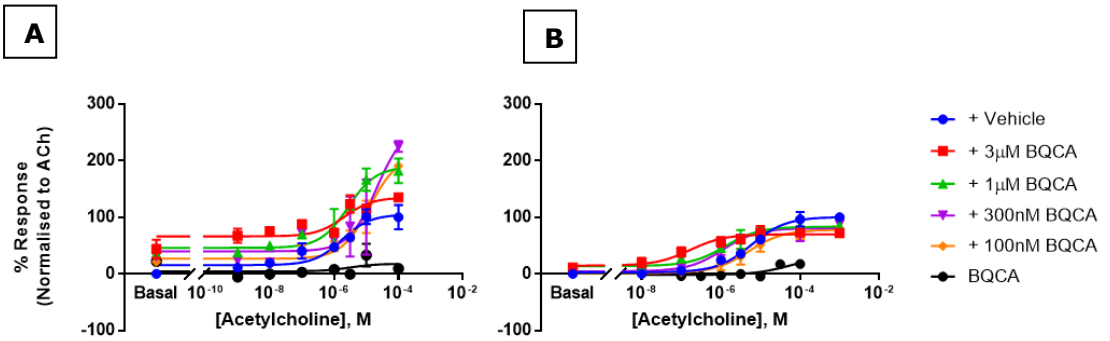


Figure 4.29: ***Monitoring βARR2 protein recruitment to the LgBiT SNAP M1 receptor in the NanoBiT complementation assay****. HEK LgBiT SNAP M1 βARR2 cells were loaded with luciferase substrate furimazine for 5min, prior to recording luminescence on a Pherastar for 30 min at 37 C. Luminescence values were normalised to the vehicle (0%) and 100µM acetylcholine (100%) response. After 3 basal readings (6min), acetylcholine in increasing concentrations of BQCA was added and concentration response curves were constructed at 3 min (A) and 25 min post addition (B). Data are shown as mean ± SEM for pooled experiments (n=5).*

HEK M1 βARR2 + ACh	pEC_{50} 2min post ligand addition	pEC_{50} 25min post ligand addition
BQCA	5.51 ± 1.14	4.38 ± 0.26
+ 3µM BQCA	5.69 ± 0.34 ^{NS}	5.53 ± 0.25
+ 1µM BQCA	5.57 ± 0.12 ^{NS}	5.34 ± 0.15
+ 300nM BQCA	4.68 ± 0.33 ^{NS}	5.09 ± 0.12
+ 100nM BQCA	4.89 ± 0.13 ^{NS}	5.10 ± 0.11
+ Vehicle	5.22 ± 0.10 ^{NS}	4.83 ± 0.12

Table 4.12: ***Comparison between pEC_{50} values between 3min and 25min post ligand addition at the βARR2 in HEK LgBiT SNAP M1 cells.*** *A paired t-test was used to find statistical significance between the two difference time points: NS, not significant.*

HEK M1 βARR2 + ACh (sustained response)	pEC_{50}	Fold Change in potency (EC_{50} ratio)	R_{max} (% 100µM ACh)
BQCA	4.38 ± 0.26 ^{NS}	0.15	30.41 ± 5.23
+ 3µM BQCA	6.78 ± 0.28 **	+36.31	55.41 ± 6.08
+ 1µM BQCA	5.90 ± 0.23 ^{NS}	+4.79	69.62 ± 8.11
+ 300nM BQCA	5.95 ± 0.19 ^{NS}	+5.37	76.35 ± 7.36
+ 100nM BQCA	5.23 ± 0.21 ^{NS}	+1.02	76.56 ± 8.98
+ Vehicle	5.22 ± 0.10	1.00	97.85 ± 5.49

Table 4.13: ***Comparison between pEC_{50} and R_{max} values for post ligand addition at the βARR2 in HEK LgBiT SNAP M1 cells.*** *A one-way ANOVA analysis with Dunnett's post hoc analysis was used to find statistical significance when CNO alone was compared to increasing concentrations of BQCA, as well as, BQCA on its own; NS, not significant, or ** P < 0.01.*

4.2.7Mini Gq and β-ARR2 Protein Recruitment by M1-DREADD, and the Effect of BQCA

In the HEK LgBiT SNAP M1-DREADD mini Gq cell line, the time course of ligand activated complementation of mini Gq was comparable to that of the M1-WT receptor. Following clozapine and its derivatives activation, luminescence rapidly reached R_{max} 4-8min after ligand addition. The complementation of mini G was then sustained over the time course without a decay of the signal occurring (Fig 4.30).

The orthosteric agonists at the M1-DREADD had greatly reduced effect on mini Gq recruitment, with only iperoxo producing any detectable response (Fig 4.31). The clozapine derivatives were identified as potent agonists. With pEC_{50} values indicating a rank order of clozapine > N, desmethylclozapine > CNO, with R_{max} values, normalised to the response of CNO, indicating all ligands to be full agonists with comparable efficacies (Fig. 4.32 & Table 4.15). There was a significant difference in pEC_{50} values for clozapine and clozapine-N-oxide between the early time point and at equilibrium. This reflects their slower onset of complementation (Fig 4.14).

When CNO was applied in the presence of the allosteric modulator BQCA there was a concentration-dependent positive allosteric effect, with an increase of R_{max} values as compared to CNO in the absence of BQCA (Fig. 4.33). There was a small left-shift of the concentration response curves but this was insignificant for all concentrations ($p<0.05$; Table 4.16 & 4.17). BQCA was unable to produce mini Gq complementation at the M1-DREADD cell line (Fig 4.34).

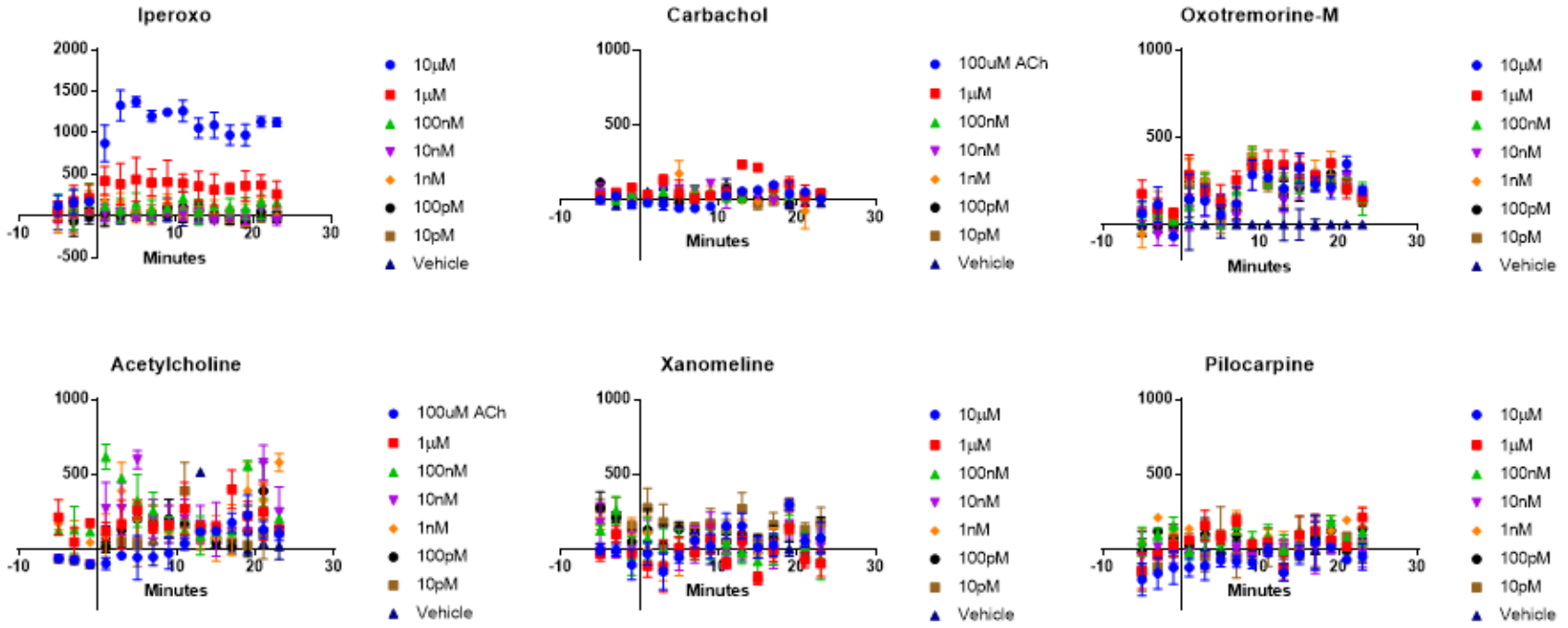


Figure 4.30: ***Time course of the orthosteric ligand luminescence complementation responses in HEK LgBiT SNAP M1-DREADD mini G cells.*** *After furimazine incubation for 5min, luminescence complementation was measured on the Pherastar over a 30min time course at 37°C. Ligands were added after an initial baseline read of 6 min. Values are arbitrary luminescence units representing mean ± range of a representative experiment carried out in duplicate.*

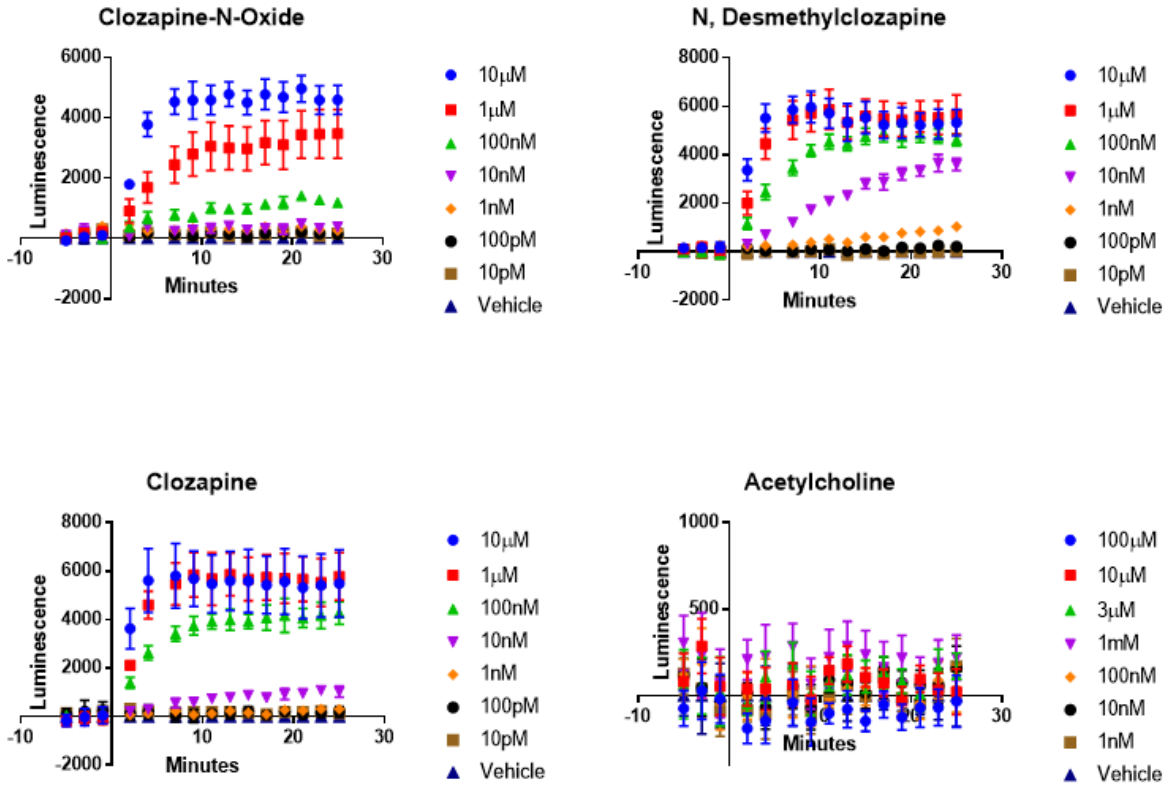


Figure 4.31: ***Timecourse of the clozapine derivatives and ACh, the endogenous ligand, luminescence complementation responses in HEK LgBiT SNAP M1-DREADD mini Gq cells.*** *After furimazine incubation for 5 min, luminescence complementation was measured on the Pherastar over a 30min time course at 37°C. Ligands were added after an initial baseline read of 6 min. Values are arbitrary luminescence units representing mean ± range of a representative experiment carried out in duplicate*

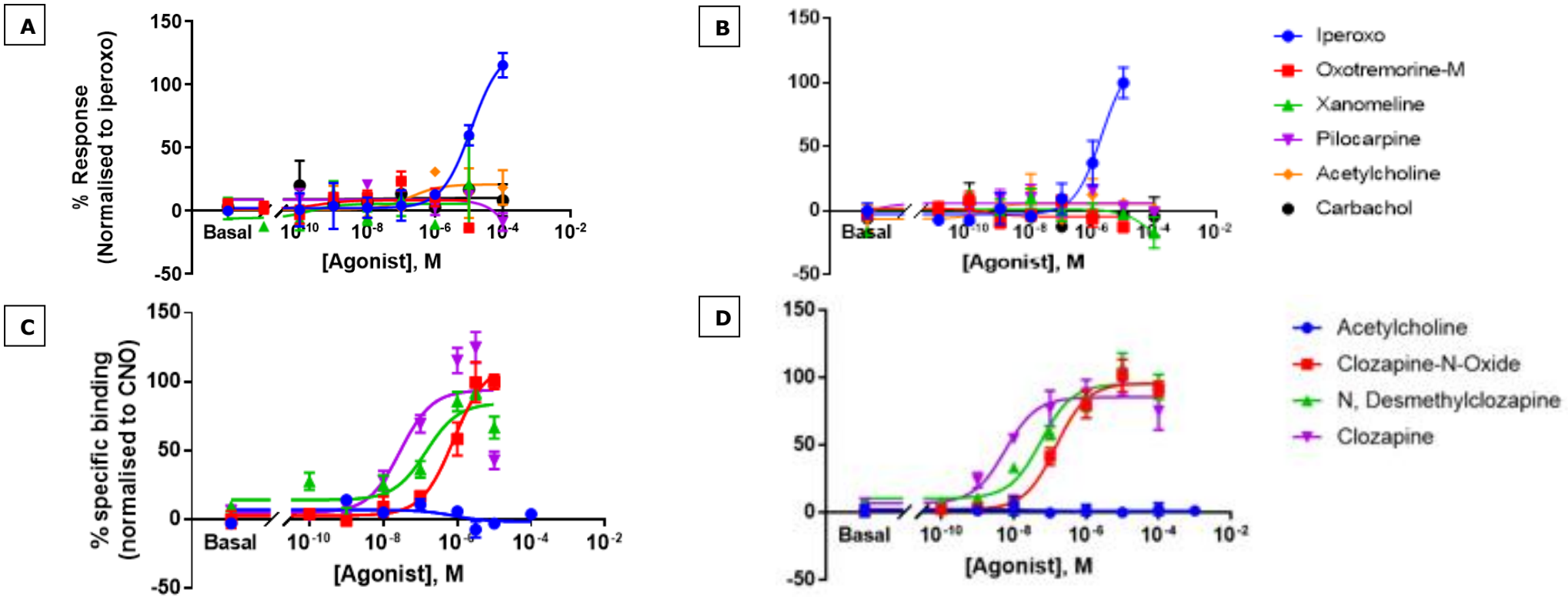


Figure 4.32: ***Monitoring mini G protein recruitment to the LgBiT SNAP M1-DREADD receptor in the NanoBiT complementation assay****. HEK LgBiT SNAP M1-DREADD mini G cells were loaded with luciferase substrate furimazine for 5min prior to recording luminescence on a Pherastar for 30 min at 37 C. After 3 basal readings (6 min) clozapine and its derivatives were added and concentration response curves were constructed at 3 min (A, C) and 25 min post addition (B, D). Luminescence values were normalised to the vehicle (0%) and (A, C) 10uM iperoxo (100 %) response or (B, D) 10μM CNO. Data are shown as mean ± SEM for pooled experiments carried out in duplicate (n=5).*

HEK M1-DREADD mini G	pEC_{50} 3min post ligand addition	pEC_{50} 25min post ligand addition
Clozapine-N-Oxide	6.09 ± 0.10 **	6.84 ± 0.10
Clozapine	7.53 ± 0.10 **	8.24 ± 0.11
N, desmethylclozapine	7.11 ± 0.11 NS	7.25 ± 0.09
Iperoxo	4.93 ± 0.10 NS	4.71 ± 0.09

Table 4.14: ***Comparison between pEC_{50} values between 3min and 25min post ligand addition at the mini Gq in HEK LgBiT SNAP M1-DREADD cells.*** *A paired t-test was used to find statistical significance between the two difference time points; NS, not significant; ** P<0.01.*

HEK M1-DREADD mini G (sustained response)	pEC_{50}	Fold change in potency (EC_{50} ratio)	R_{max} (% 1µM CNO response)	Fold change in efficacy (R_{max} ratio)
Acetylcholine	ND	ND	ND	ND
Clozapine-N-Oxide	6.84 ± 0.10	1.00	93.80 ± 5.12	1.00
Clozapine	8.24 ± 0.11 ***	25.12	85.60 ± 5.30	0.91
N, desmethylclozapine	7.25 ± 0.09 *	2.57	78.84 ± 7.21	0.84

Table 4.15: ***Comparison between pEC_{50} and R_{max} values post ligand addition at the mini Gq in HEK LgBIT SNAP M1-DREADD cells.*** *A one-way ANOVA analysis with Dunnett's post hoc analysis was used to find statistical significance when CNO was compared to clozapine and N, desmethylclozapine; *P<0.05 or *** P < 0.001.*

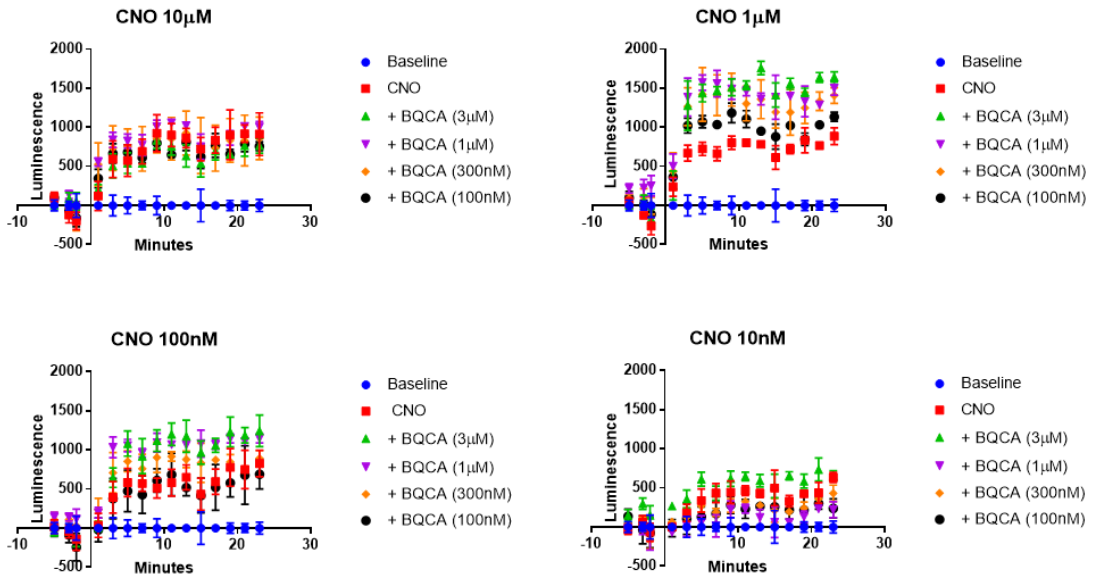


Figure 4.33: ***Time course of the CNO in the presence of BQCA luminescence complementation responses in HEK LgBiT SNAP M1-DREADD mini Gq cells.*** *After furimazine incubation for 5 min, luminescence complementation was measured on the Pherastar over a 30min time course at 37°C. Ligands were added after an initial baseline read of 6 min. Values are arbitrary luminescence units representing mean ± range of a representative experiment carried out in duplicate.*

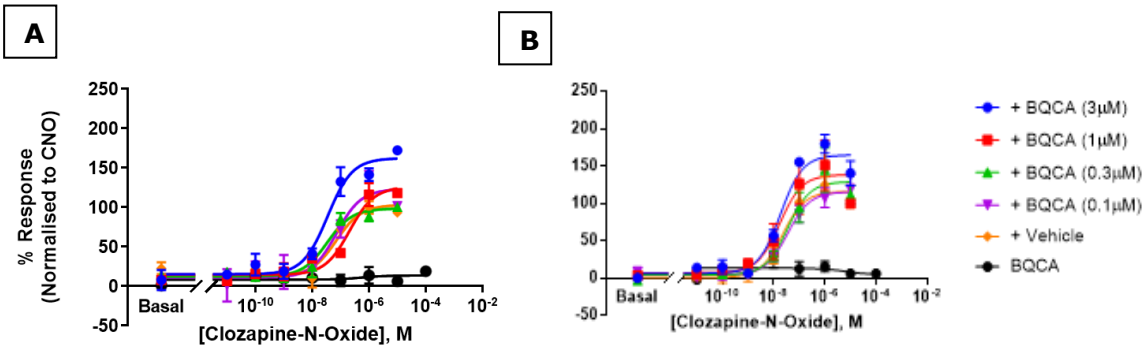


Figure 4.34: ***Monitoring mini G protein recruitment to the LgBiT SNAP M1-DREADD receptor in the NanoBiT complementation assay****. HEK LgBiT SNAP M1-DREADD mini Gq cells were loaded with luciferase substrate furimazine for 5min, prior to recording luminescence on a Pherastar for 30 min at 37 C. Luminescence values were normalised to the vehicle (0%) and 10µM CNO (100%) response. After 3 basal readings (6min), CNO in increasing concentrations of BQCA was added and concentration response curves were constructed at 3 min (A) and 25 min post addition (B). Data are shown as mean ± SEM for pooled experiments (n=5).*

HEK M1-DREADD mini G + CNO	pEC_{50} 3min post ligand addition	pEC_{50} 25min post ligand addition
+ Vehicle	7.49 ± 0.08 ^{NS}	7.53 ± 0.12
+ 3µM BQCA	8.36 ± 0.13 **	7.73 ± 0.11
+ 1µM BQCA	7.52 ± 0.12 ^{NS}	7.76 ± 0.13
+ 0.3µM BQCA	7.62 ± 0.09 ^{NS}	7.45 ± 0.09
+ 0.1µM BQCA	6.47 ± 0.19 **	7.45 ± 0.10

Table 4.16: ***Comparison between pEC_{50} and R_{max} values for post ligand addition in HEK LgBiT SNAP M1-DREADD mini Gq cells.*** *A one-way ANOVA analysis with Dunnett's post hoc analysis was used to find statistical significance when CNO alone was compared to increasing concentrations of BQCA, as well as, BQCA on its own; NS, not significant, or ** P < 0.01.*

HEK M1-DREADD mini G + CNO (sustained response)	pEC_{50}	Fold Change in potency (EC_{50} ratio)	R_{max} (% 10µM CNO response)
BQCA	ND	ND	ND
+ Vehicle	7.53 ± 0.12	1.00	108.32 ± 6.79
+ 3µM BQCA	7.73 ± 0.11 ^{NS}	1.58	158.20 ± 8.82
+ 1µM BQCA	7.76 ± 0.13 ^{NS}	1.69	131.22 ± 6.06
+ 0.3µM BQCA	7.45 ± 0.09 ^{NS}	0.83	124.85 ± 11.65
+ 0.1µM BQCA	7.45 ± 0.10 ^{NS}	0.83	110.91 ± 8.06

Table 4.17: ***Comparison between pEC_{50} and R_{max} values for post ligand addition in HEK LgBiT SNAP M1-DREADD mini Gq cells.*** *A one-way ANOVA analysis with Dunnett's post hoc analysis was used to find statistical significance when CNO alone was compared to increasing concentrations of BQCA, as well as, BQCA on its own; NS, not significant.*

In the HEK LgBiT SNAP M1-DREADD βARR2 cells, the panel of muscarinic receptor agonists were unable to induce an increase in luminescence in contrast to M1-WT (Fig 4.35). Clozapine and its derivatives showed peak luminescence 4-6min after ligand addition. Statistical comparison between early recruitment (3min) and sustained recruitment (25min) of the βARR2 was found to be statistically significant for iperoxo and clozapine (Table 4.18). This is reflects the slower peak seen in clozapine, for example, in comparison to N, desmethylclozapine that shows rapid onset and the slow decay of the luminescence signal over the 25min (Fig 4.19).

Concentration curves of clozapine and its derivatives produced complementation responses that were comparable to the mini Gq complementation data. Clozapine was shown to have a significantly greater effect than CNO ($P<0.001$), as did N, desmethylclozapine ($P<0.01$) (Table 4.36, C&D). There was no detectable βARR2 recruitment to the M1 receptor when the muscarinic ligands were applied (Fig 4.36, A&B).

In the presence of BQCA, time courses produced a rapid increase in luminescence over 6min, reflecting a spike in agonist dependent complementation of the βARR2 protein to the M1-DREADD receptor (Fig 4.37 & 4.38). The concentration response curves showed BQCA did not intrinsic activity at this receptor, however this may be a factor of normalisation against cells in the presence of CNO because in the time course it can be seen that luminesce increases when BQCA is present alone before CNO is added. BQCA in the presence of CNO caused positive allosteric modulation shown by a left-shift of all concentration response curves, which was significant at 3µM BQCA ($P<0.01$) (Table 4.20 % 4.21). It would be best to further investigate the effect of BQCA only at these cells, with special focus on the concentration response curve.

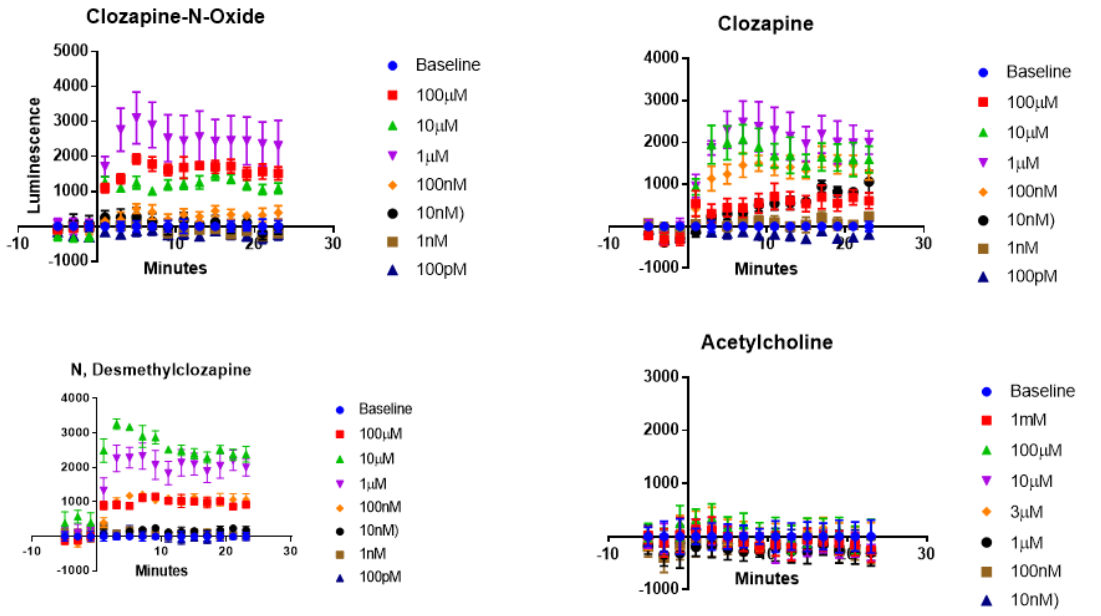


Figure 4.35: ***Timecourse of the clozapine derivatives and ACh luminescence complementation responses in HEK LgBiT SNAP M1-DREADD β-ARR2.*** *After furimazine incubation for 5 min, luminescence complementation was measured on the Pherastar over a 30min time course at 37°C. Ligands were added after an initial baseline read of 6 min. Values are arbitrary luminescence units representing mean ± range of a representative experiment carried out in duplicate.*

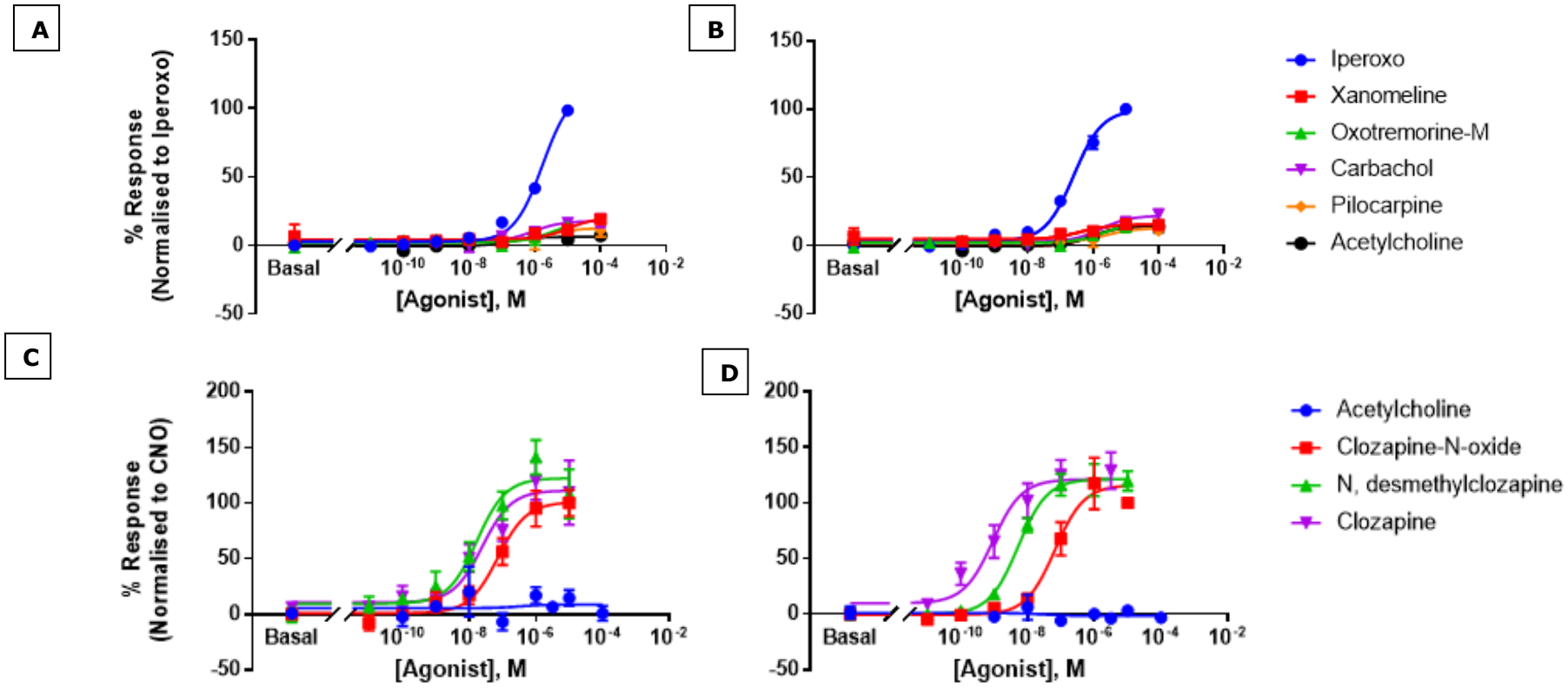


Figure 4.36: ***Monitoring β-ARR2 recruitment to the LgBiT SNAP M1-DREADD receptor in the NanoBiT complementation assay****. HEK LgBiT SNAP M1-DREADD β-ARR2 cells were loaded with luciferase substrate furimazine for 5min prior to recording luminescence on a Pherastar for 30 min at 37 C. After 3 basal readings (6 min), clozapine and its derivatives were added and concentration response curves were constructed at 3 min (A, C) and 25 min post addition (B, D). Luminescence values were normalised to the vehicle (0%) and (A, C) 10uM iperoxo (100 %) response or (B, D) 10μM CNO Data are shown as mean ± SEM for pooled experiments carried out in duplicate (n=5).*

HEK M1-DREADD βARR2	pEC_{50} 3min post ligand addition	pEC_{50} 25min post ligand addition
Clozapine-N-Oxide	7.18 ± 0.26 ^{NS}	7.07 ± 0.18
Clozapine	7.55 ± 0.19 **	8.67 ± 0.21
N,Desmethylclozapine	7.59 ± 0.39 ^{NS}	8.09 ± 0.13
Iperoxo	5.71 ± 0.10 **	6.59 ± 0.08

Table 4.18: ***Comparison between pEC_{50} values between 3min and 25min post ligand addition in HEK LgBiT SNAP M1-DREADD β-ARR2 cells.*** *A paired t-test was used to find statistical significance between the two difference time points; NS, not significant, ** P<0.01.*

HEK M1-DREADD βARR2 (sustained response)	pEC_{50}	Fold Change in potency (EC_{50} ratio)	R_{max} (% 1μM CNO Response)
Acetylcholine	ND	ND	ND
Clozapine-N-Oxide	7.07 ± 0.18	1.00	116.8 ± 10.77
Clozapine	8.67 ± 0.21 ***	+ 39.81	111.6 ± 10.54
N-Desmethylclozapine	8.09 ± 0.13 **	+ 10.47	121.6 ± 6.53

Table 4.19: ***Comparison between pEC_{50} and R_{max} values for post ligand addition in HEK LgBiT SNAP M1-DREADD β-ARR2 cells.*** *A one-way ANOVA analysis with Dunnett's post hoc analysis was used to find statistical significance bewteen CNO and the clozapine or N, desmethylclozapine; **P<0.01, ***P<0.001.*

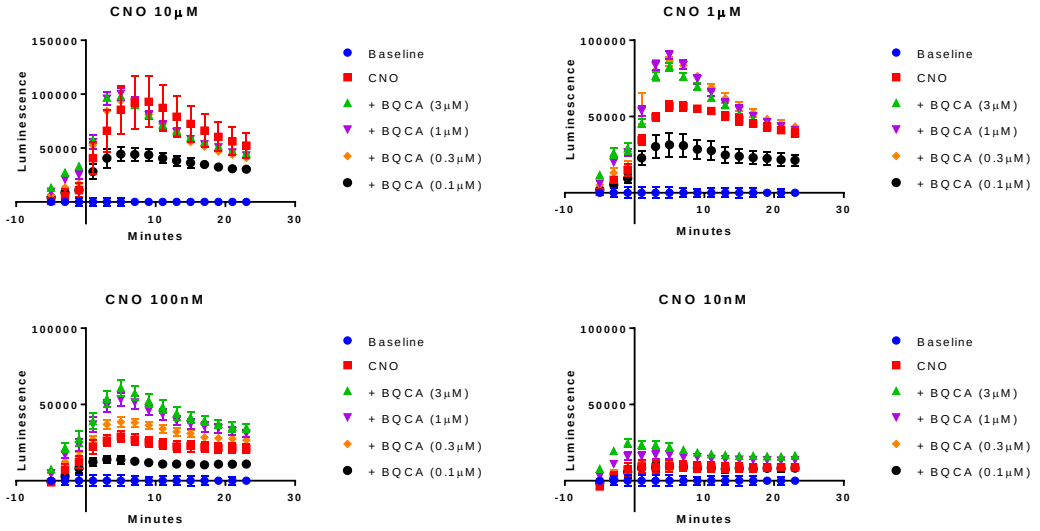


Figure 4.37: ***Time course of CNO in the presence of BQCA luminescence complementation responses in HEK LgBiT SNAP M1-DREADD β-ARR2 cells.*** *After furimazine incubation for 5 min, luminescence complementation was measured on the Pherastar over a 30min time course at 37°C. Ligands were added after an initial baseline read of 6 min. Values are arbitrary luminescence units representing mean ± range of a representative experiment carried out in duplicate.*

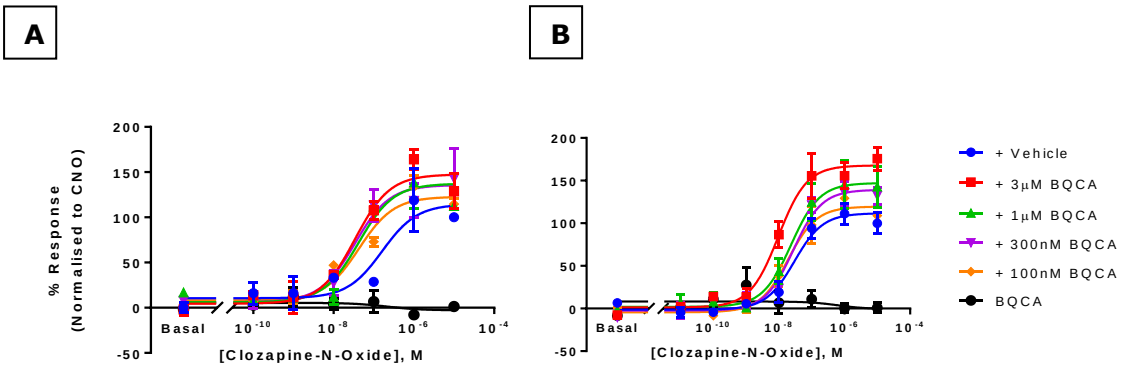


Figure 4.38: ***Monitoring β-ARR2 recruitment to the LgBiT SNAP M1-DREADD receptor in the NanoBiT complementation assay****. HEK LgBiT SNAP M1-DREADD βARR2 cells were loaded with luciferase substrate furimazine for 5min, prior to recording luminescence on a Pherastar for 30 min at 37 C. Luminescence values were normalised to the vehicle (0%) and 10µM CNO (100%) response. After 3 basal readings (6min), CNO in increasing concentrations of BQCA was added and concentration response curves were constructed at 3 min (A) and 25 min post addition (B). Data are shown as mean ± SEM for pooled experiments (n=5).*

HEK M1-DREADD βARR + CNO	pEC_{50} 3min post ligand addition	pEC_{50} 25min post ligand addition
+ 3μM BQCA	7.47 ± 0.21 *	8.02 ± 0.28
+ 1μM BQCA	7.38 ± 0.19 NS	7.63 ± 0.23
+ 0.3μM BQCA	7.47 ± 0.20 NS	7.56 ± 0.19
+ 0.1μM BQCA	7.37 ± 0.17 NS	7.72 ± 0.21
+ Vehicle	6.79 ± 0.25 ***	7.53 ± 0.10

Table 4.20: ***Comparison between pEC_{50} values between 3min and 25min post ligand addition in HEK LgBiT SNAP M1-DREADD β-ARR2 cells.*** *A paired t-test was used to find statistical significance between the two difference time points; NS, not significant; ** P<0.01.*

HEK M1-DREADD βARR + CNO (sustained response)	pEC_{50}	Fold Change in potency (EC_{50} ratio)	R_{max} (% 1μM CNO Response)
BQCA	ND	ND	ND
+ 3μM BQCA	6.78 ± 0.28 **	+ 36.31	55.41 ± 6.08
+ 1μM BQCA	5.90 ± 0.23 NS	+ 4.79	69.62 ± 8.11
+ 0.3μM BQCA	5.95 ± 0.19 NS	+5.37	76.35 ± 7.36
+ 0.1μM BQCA	5.23 ± 0.21 NS	+ 1.02	76.56 ± 8.98
+ Vehicle	5.22 ± 0.10	1.0	97.85 ± 5.49

Table 4.21: ***Comparison between pEC_{50} and R_{max} values for post ligand addition in HEK LgBiT SNAP M1-DREADD β-ARR2 cells.*** *A one-way ANOVA analysis with Dunnett's post hoc analysis was used to find statistical significance when CNO alone was compared to increasing concentrations of BQCA, as well as, BQCA on its own; NS, not significant.*

The Influence of BQCA on Ligand Binding at the M1-DREADD Receptor, Measured by Fluorescence Imaging

Finally, the novel pirenzepine-based fluorescent ligands were developed for muscarinic receptors (She *et al.* 2019, manuscript submitted) to investigate their suitability to develop a fluorescent ligand-binding assay for the M1-DREADD receptor. Then we were able to use these fluorescent ligands to determine the ligand binding properties of the clozapine derivatives and ACh in living CHO M1-DREADD cells, via competition binding studies, and explore how BQCA influenced these properties.

Initially, a range of fluorescent ligands were tested in order to determine their binding capabilities at the CHO M1-DREADD cells. Binding of the five different fluorescent ligands (10nM) to live CHO M1 DREADD cells, counterstained with the nuclear dye H33342, was visualised using a confocal imaging plate reader (IX Ultra; Fig 4.39). For each ligand, Cy5 fluorescence was detected labelling the plasma membrane, and some intracellular compartments, following 60 min incubation at room temperature. The subcellular distribution of fluorescence labelling was similar for each ligand, but **I**, **III** and **V** showed the brightest fluorescence at the concentration used. In each case, co-incubation of the cells with 100µM atropine (to determine non-specific binding) displaced the fluorescent ligand labelling, demonstrating specific binding to the M1 DREADD receptors. Following this initial characterisation, **III** was selected as the ligand to continue further in this study due to its brightness and specificity of plasma membrane labelling.

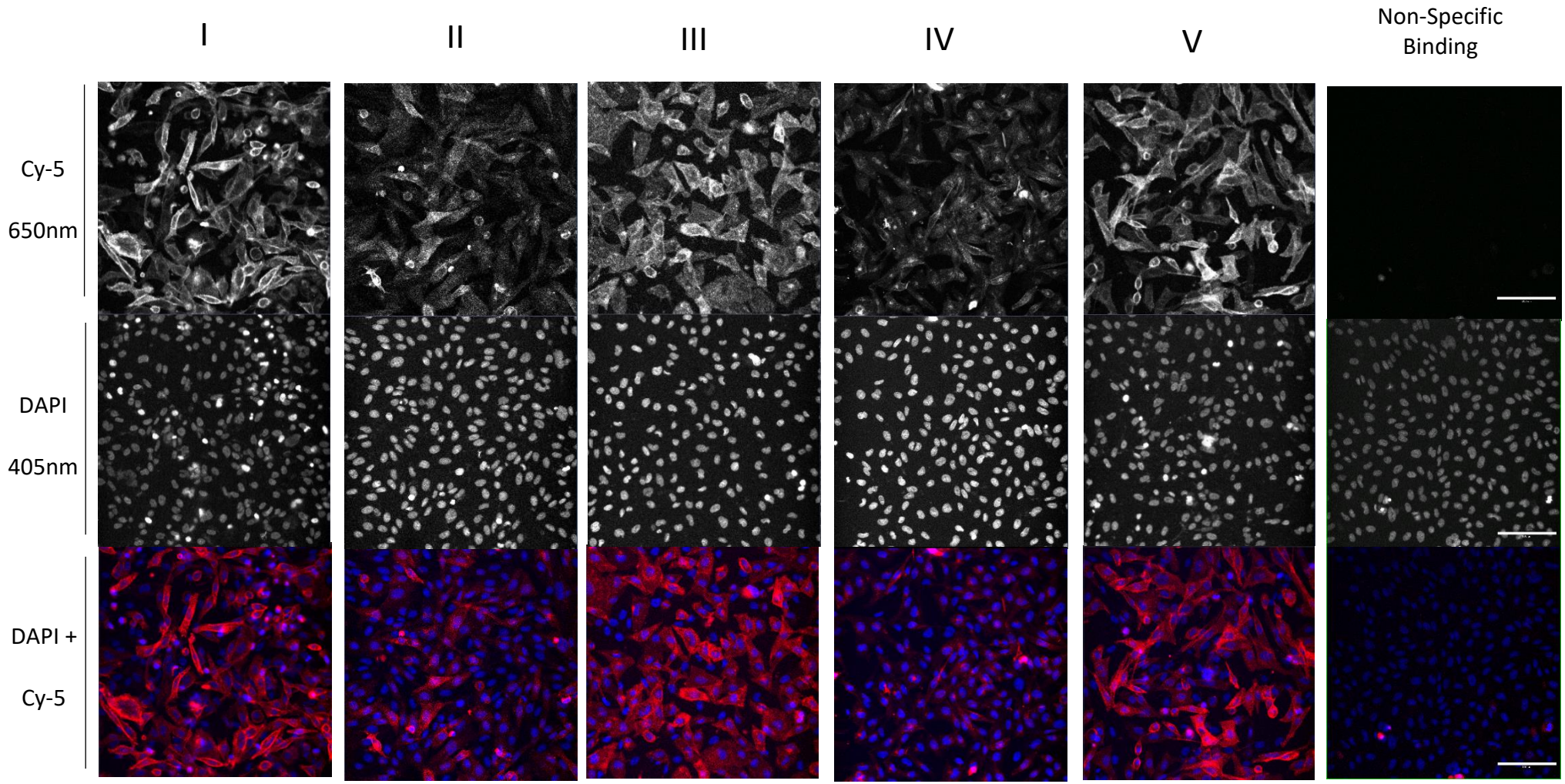


Figure 4.39: Binding of Regensburg fluorescent ligands (10nM) to live CHO SNAP hM_1-DREADD cells visualized on an IX Ultra confocal plate reader. Fluorescent ligands were incubated for 60min in HBSS containing the nuclear dye Hoescht 33342, in the dark, at room temperature; cells were then imaged without removal of the free ligand. Non-specific binding was evaluated in the presence of 100μM atropine. Ligand binding was visualised using Cy5 excitation / emission settings, and H33342 staining via 405nm excitation (DAPI). I, II and III were synthesised by Dr. Andrea Pegoli, while IV and V were synthesised by Dr. She Xueke from the University of Regensburg.

4.2.8Determining the Functional Properties of Fluorescent Ligand III

To examine whether **III** had its own intrinsic activity at the M1-DREADD receptor we first observed whether this fluorescent ligand acted as an agonist in the calcium mobilisation assay. CHO SNAP M1-DREADD cells were loaded with Fluo-4 AM and fluorescence was read on the FlexStation 3. Concentration response curves indicated that **III** showed no intrinsic activity at the M1-DREADD receptor, with no concentration dependent calcium response seen up to 1µM (Fig 4.40).Next, it was examined whether **III** pre-treatment affected the action of clozapine derivatives in the assay. The presence of increasing concentrations of **III** although not significantly response ($P>0.05$ for all clozapine derivatives) did show a small rightward-shift in the calcium response ($P>0.05$ for all clozapine derivatives). There was a significant reduction in R_{max} ($P<0.001$ at **III** 10nM for all clozapine derivatives; Fig. 4.41 & Table 4.22). This may reflect non-competitive insurmountable antagonism under the conditions of the assay. This is supported by the knowledge that this compound does bind both the orthosteric and allosteric binding sites on this receptor. This provided confirmation that **III** interacted with the M1 DREADD receptors, and was likely to act as an antagonist (Fig. 4.41).

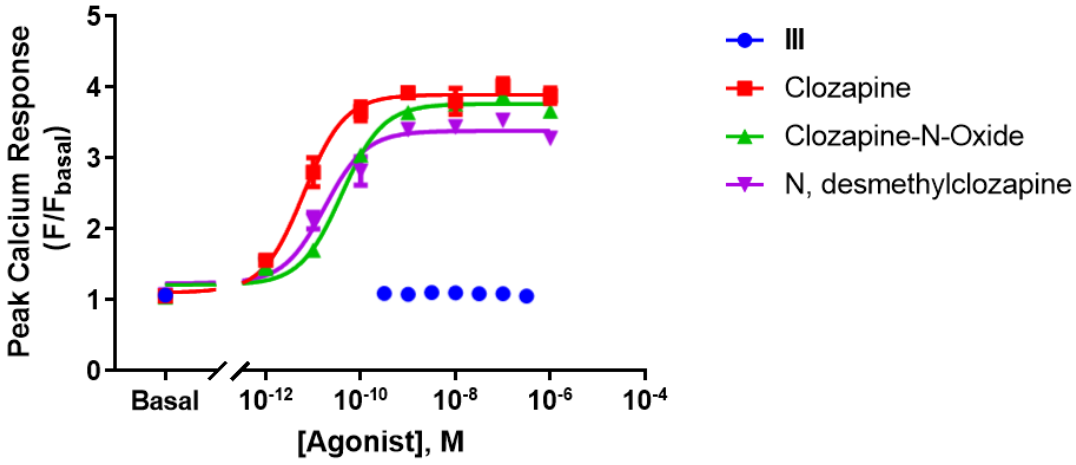


Figure 4.40: ***Calcium mobilisation assay to determine function of*** *III* ***at CHO SNAP hM1-DREADD cells****. Cells were loaded with Fluo-4 AM and* ***III*** *was added as an agonist at 15sec and the peak fluorescence was taken and compared against*

the clozapine derivatives. Values are mean ± SEM values of three independent experiments carried out in triplicate.

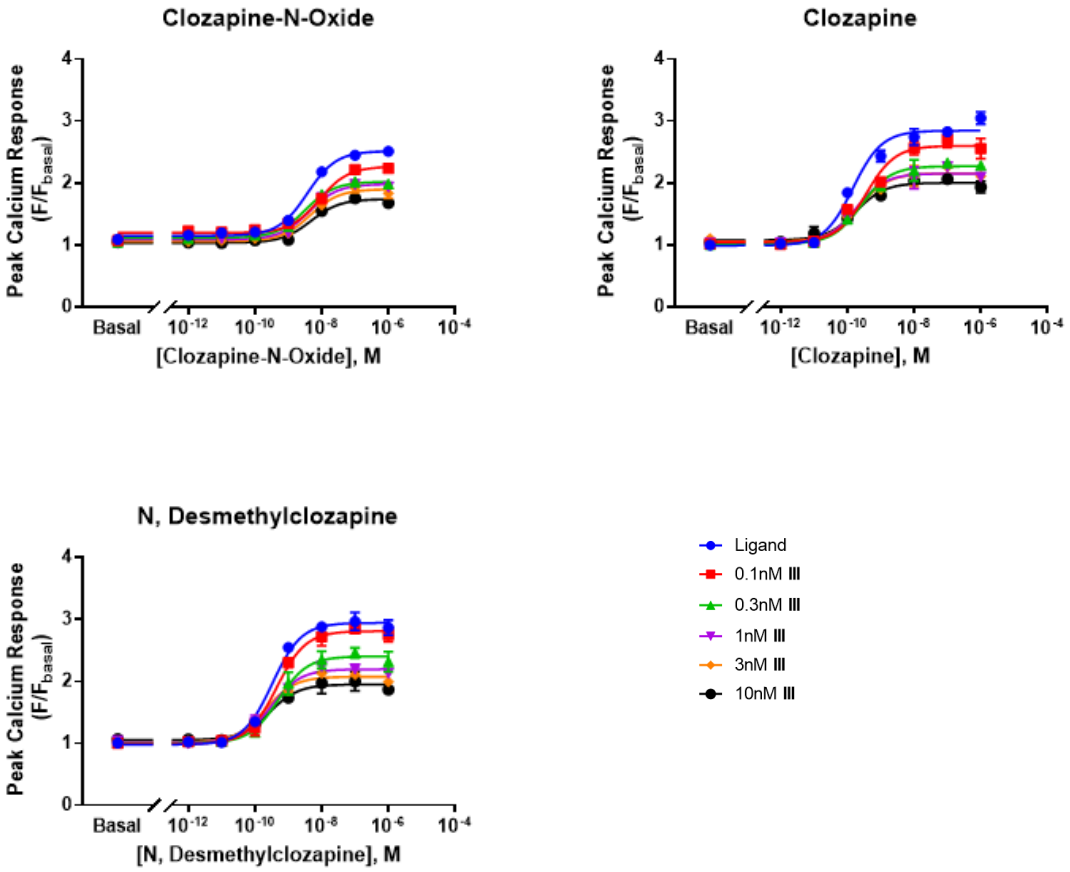


Figure 4.41: ***Verification the fluorescent ligand*** *III* ***acts as an antagonist against the clozapine derivatives at CHO SNAP hM1-DREADD receptors.*** *Cells were loaded with the calcium indicator Fluo-4 AM, pre-treated with* ***III*** *or vehicle for 30 mins and subsequent calcium mobilisation following clozapine derivative addition was measured on the FlexStation 3. Values are mean ± SEM values of five independent experiments*

Clozapine-N-Oxide	pEC_{50}	Fold change in potency (EC_{50} ratio)	R_{max} (change in F/F_{basal})
+Vehicle	9.82 ± 0.10	1.00	1.93 ± 0.08
+0.1nM **III**	9.37 ± 0.10 ^{NS}	2.82	1.62 ± 0.06 *
+0.3nM **III**	9.58 ± 0.10 ^{NS}	1.74	1.25 ± 0.05 ***
+1nM **III**	9.75 ± 0.12 ^{NS}	1.17	1.13 ± 0.05 ***
+3nM **III**	9.66 ± 0.12 ^{NS}	1.44	1.10 ± 0.05 ***
+10nM **III**	9.75 ± 0.12 ^{NS}	1.17	0.93 ± 0.05 ****
N, desmethylclozapine			
+Vehicle	9.48 ± 0.07	1.00	1.96 ± 0.06
+0.1nM **III**	9.35 ± 0.08 ^{NS}	1.35	1.82 ± 0.06 ^{NS}
+0.3nM **III**	9.30 ± 0.12 ^{NS}	1.51	1.40 ± 0.07 **
+1nM **III**	9.51 ± 0.10 ^{NS}	1.07	1.18 ± 0.04 ***
+3nM **III**	9.68 ± 0.08 ^{NS}	1.58	1.01 ± 0.03 ***
+10nM **III**	9.56 ± 0.17 ^{NS}	1.20	0.89 ± 0.06 ****
Clozapine			
+Vehicle	10.02 ± 0.10	1.00	1.99 ± 0.06
+0.1nM **III**	9.77 ± 0.09 ^{NS}	1.78	1.87 ± 0.05 ^{NS}
+0.3nM **III**	9.48 ± 0.10 ^{NS}	3.47	1.45 ± 0.05 **
+1nM **III**	9.61 ± 0.12 ^{NS}	2.57	1.24 ± 0.05 ***
+3nM **III**	9.67 ± 0.12 ^{NS}	2.23	1.07 ± 0.07 ***
+10nM **III**	9.72 ± 0.11 ^{NS}	2.00	0.92 ± 0.05 ****

*Table 4.22: **pEC_{50} and R_{max} values for clozapine derivatives in the absence or presence of different concentrations of** III **in CHO SNAP hM1-DREADD cells**. One-way ANOVA analysis, with Dunnett's post hoc comparison; NS – not significant; * P<0.05, ** P<0.01, *** P < 0.001, was carried to test for statistical significance as compared to the ligands in the absence of AP164.*

4.2.9Determination of III K_D Using Saturation Analysis

Fluorescent ligand images were acquired using the IX Ultra confocal plate reader and were analysed using an automated granularity algorithm (MetaXpress, Molecular Devices) to provide quantitative data reflecting the intensity of fluorescent ligand binding (Liu *et al.*, 2016). All images acquired were 16-bit greyscale without saturation, meaning the fluorescence intensity within pixel is represented as a number from 0 (black) to 65535 (white). Granules were identified between a diameter of 1-3µm and a threshold for grey level count was set according to the total (positive) and non-specific (atropine, negative) images on the day of the assay.

In order to determine the fluorescent ligand **III** binding affinity at M1-DREADD receptor saturation binding studies varying AP164 concentration were carried out, using the IX Ultra to image total and non-specific binding at 60 min, followed by granularity analysis to quantify the ligand fluorescence intensity within the images. Non-specific binding was calculated in the presence of 10µM atropine (Fig 4.42). B_{max} was calculated as 116.30 ± 5.98% and an equilibrium dissociation constant for AP164, K_D value, was derived as 90.4 ± 10.9nM (n=3).

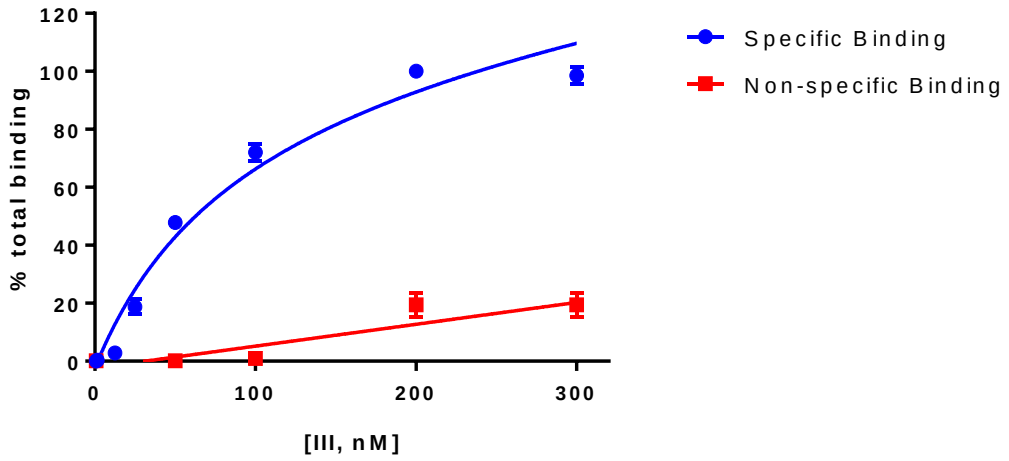


Figure 4.42: ***Saturation binding analysis of fluorescent ligand III at CHO SNAP hM1-DREADD cells.*** *Fluorescence read on the IX Ultra confocal microscope after incubation for 60 min at room temperature. Estimates of ligand binding were obtained via granularity analysis of the associated images, as described in Chapter 2. Responses were normalised to the intensity of total* ***III*** *bound at 300nM ligand concentration. Non-specific binding was defined in the presence of 10μM atropine. Pooled values are mean ± SEM of 3 experiments carried out triplicate.*

4.2.10 Establishing the Equilibrium Time Point for Whole Cell Competition Assays Using Fluorescent Ligand III

After establishing that **III** bound M1 DREADD receptors, its ability to be used as a tracer in competition binding studies against unlabelled ligands was determined, using 10nM of **III**, focusing on the three clozapine derivatives in the absence and presence of BQCA, and BQCA alone (Figure 4.43, 4.44). The homogenous assay format (without washing) allowed cells to be repeatedly imaged over a 60 min period to monitor the kinetic development of binding and determination of the appropriate time point at each equilibrium between the ligands has been reached. For each set of curves, total specific binding reached a plateau within 30 – 40 min of ligand addition, and this also corresponded to no further change in the IC_{50} (50% inhibition concentration for the unlabelled ligand(s)). True equilibrium is difficult to verify, especially in functional assays, therefore to improve accuracy it would be useful to determine the dissociation constant (K_{off}) of the ligands in the presence of **III** using membrane binding

preparations. The K_{off} values would also verify whether **III** is truly a competitive, non-competitive or perhaps a negative allosteric modulator.

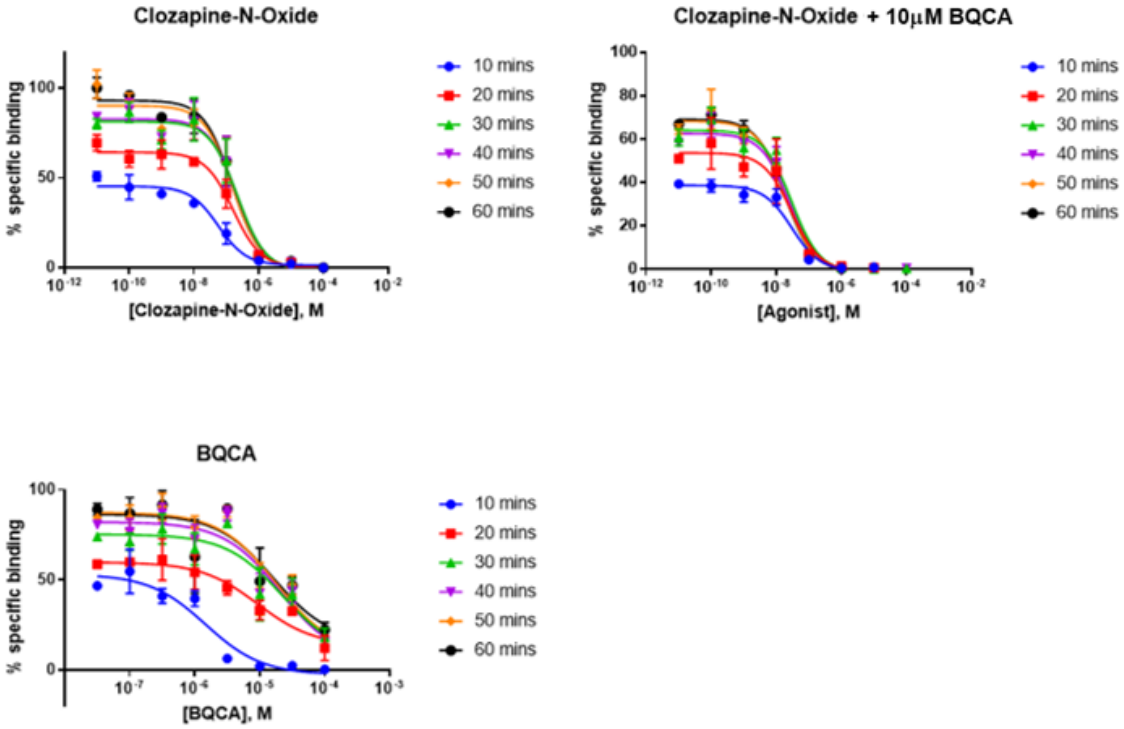


Figure 4.43: ***Changes in specific binding over a 60min incubation at the SNAP CHO hM1-DREADD cells.*** ***III*** *(10nM) was used as the competitive fluorescent ligand and images were acquired on the IX Ultra confocal microscope repeatedly at each time point. The calculated binding intensities from the images are shown as mean ± SEM of three experiments carried out in duplicate. Specific binding was normalised to the totals at 60 min (vehicle only, 100%) and non-specific binding (0%) defined in the presence of 10µM atropine.*

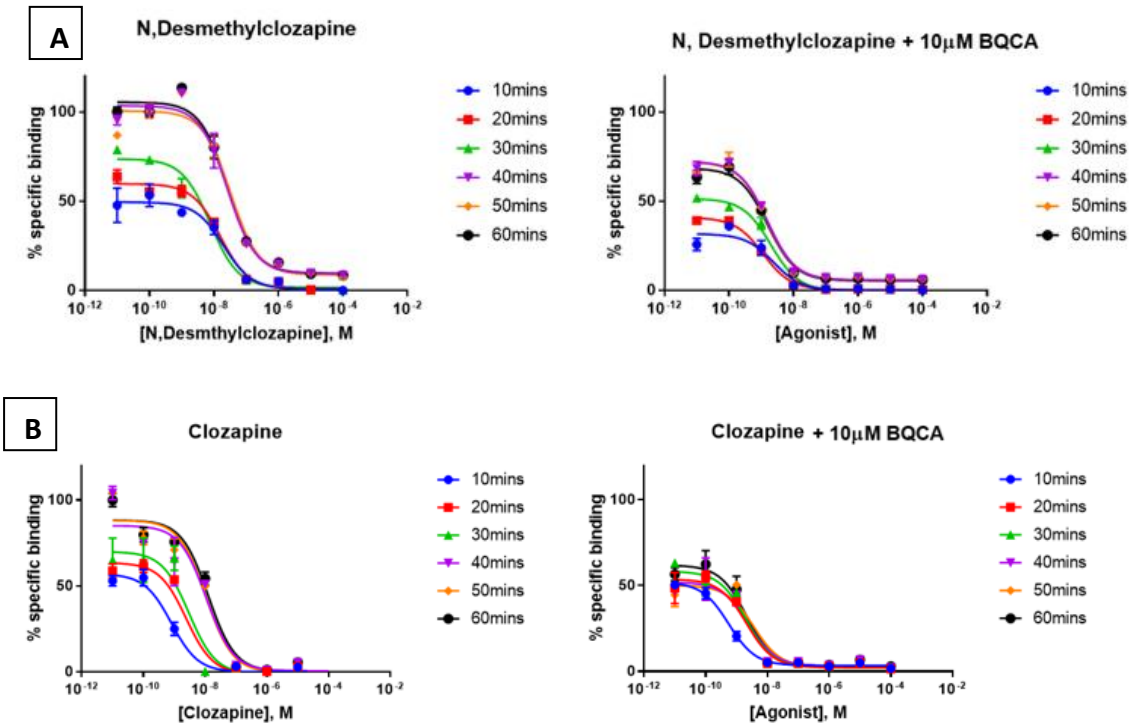


Figure 4.44: ***Changes in specific binding over a 60min incubation at the SNAP CHO hM1-DREADD cells.*** ***III*** *(10nM) was used as the competitive fluorescent ligand and images were acquired on the IX Ultra confocal microscope repeatedly at each timepoint. The calculated binding intensities from the images are shown as mean ± SEM of three experiments carried out in duplicate. Specific binding was normalised to the totals at 60 min (vehicle only, 100%) and non-specific binding (0%) defined in the presence of 10μM atropine.*

4.2.11 Determination of Clozapine Derivative and BQCA Affinities at the M1-DREADD Receptor, and the Effect of BQCA on Orthosteric Ligand Binding

At the 60min equilibrium time point, clozapine derivatives were all able to competitively inhibit **III** binding to the same extent as 10µM atropine (defining NSB at 0% specific binding). The order of affinity for these ligands was clozapine > N, desmethylclozapine > CNO (Figure 4.45; Table 4.23, A). However, ACh was unable to inhibit **III** binding at the M1-DREADD receptor and thus no IC_{50} value was determined (Fig 4.45). In fact, it appeared that with increasing concentrations of ACh there was a slight increase in **III** binding. ACh binds the WT receptor in a similar way as CNO bind the DREADD, although it has been reported that the Ala5.46Gly mutation increases the conformational flexibility of TM5 which may determine how **III** is able to displace ACh. Next, the effect of the allosteric modulator BQCA was investigated within a competition-binding assay. Interestingly, BQCA alone was also able to completely inhibit **III** binding with increasing concentrations (Fig. 4.46). The pIC_{50} value was determined to be 5.57 ± 0.14 (averaged across the three sets of experiments Table 4.15, giving a dissociation constant estimated by the gaddum equation of 5.69 ± 0.14). pKi values were then determined from the IC_{50} values using the Cheng-Prusoff correction for the clozapine derivatives were then studied in conjunction with 10µM BQCA, in comparison to vehicle (Table 4.23, B). Notably in each case the presence of 10µM BQCA reduced the total specific binding measured (by approximately 50%), which is consistent with its pKi value for displacement of the fluorescent ligand alone. However, the presence of BQCA was also correlated with an in increased apparent binding affinity for the clozapine derivatives, with a fold increase of IC_{50} values of 49.00 ($P<0.01$), 8.94 ($P<0.01$) and 2.09 ($P>0.05$) for CNO, clozapine and NDMC, respectively compared to curves in the absence of the modulator indicative of **III** being a competitive ligand towards BQCA and the allosteric binding site (Table 4.23, B).

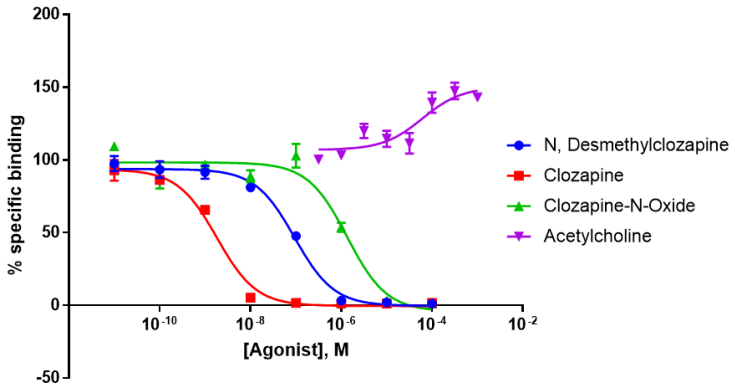


Figure 4.45: ***Competition binding assay was carried out with III (10nM) against the clozapine derivatives and ACh.*** *Live cells were incubated for 60min, at room temperature, shielded from light, with ligand and fluorescent ligand before being read on the IX Ultra confocal plate reader. There was no wash step in order to maintain binding equilibrium during the imaging process. Values are mean ± SEM of experiments carried out in duplicate (n=5).*

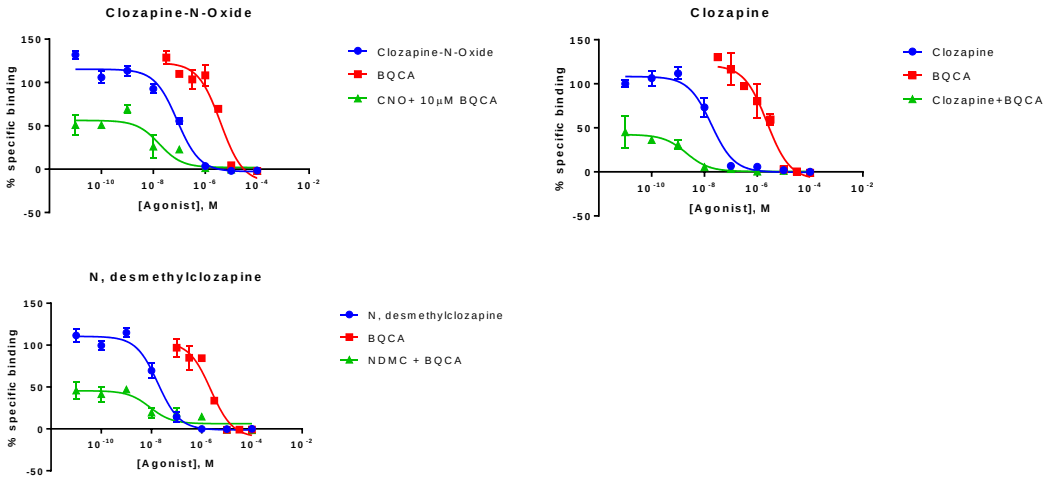


Figure 4.46: ***Competition binding assay using III (10nM), to determine the effect of BQCA alone, and its modulation of equilibrium binding of the clozapine derivatives at CHO SNAP hM1-DREADD cells.*** *Cells were visualised on the IX Ultra after a 60min incubation, at room temperature and in the dark. Values represent mean ± SEM of three experiments carried out in duplicate*

A

CHO SNAP-hM1-DREADD	pKi	Change in potency (IC_{50} ratio)	Total specific binding
Acetylcholine	NE	NE	NE
Clozapine N Oxide	5.93 ± 0.14	1.00	102.30 ± 6.73
N-Desmethylclozapine	7.07 ± 0.09 **	13.80	94.11 ± 2.26 NS
Clozapine	8.79 ± 0.08 ***	724.44	93.81 ± 3.28 NS
BQCA	5.69 ± 0.14 ***	0.58	114.30 ± 8.17 NS

B

CHO SNAP-hM1-DREADD	pKi	Fold Change in potency (IC_{50} ratio)	Total specific binding (as % TSB for CNO control
Clozapine-N-Oxide	7.07 ± 0.11	1.00	100.40 ± 5.27
CNO + 10µM BQCA	7.82 ± 0.28 *	49.00	54.72 ± 5.22 **
Clozapine	7.79 ± 0.10	1.00	108.70 ± 4.52
Clozapine + 10µM BQCA	8.74 ± 0.21 **	8.91	41.90 ± 3.71 ***
N, Desmethylclozapine	7.79 ± 0.09	1.00	111.7 ± 4.06
NMDC + 10µM BQCA	8.11 ± 0.30 NS	2.09	39.63 ± 5.00 ***

Table 4.23: ***pKi and total binding values from the III competition-binding assay to verify the binding affinity of clozapine derivatives, acetylcholine and BQCA.*** *(A), and the effects of the allosteric modulator BQCA (B), at CHO SNAP hM1-DREADD cells. The III concentration was 10nM, and where appropriate pKi values were estimated using the Cheng Prusoff correction (with the III Kd used from saturation binding of 90.4nM). Statistical significance between pIC50 values in the presence and absence of 10µM BQCA was determined by t-test analysis; NS, not significant; * P < 0.05, ** P < 0.01, *** P < 0.001, against the clozapine derivatives as a reference.*

4.3 Discussion

In this chapter, CHO cell lines stably expressing an N-terminal SNAP tagged M1-WT or M1-DREADD receptors were used to determine the allosteric modulation of BQCA in the presence of a number of orthosteric ligands. This was examined through Gq-coupled peak calcium mobilisation, as a standardised readout, compared against novel functional approaches that measured the direct coupling of mini Gq and β-arrestin2 at HEK LgBiT SNAP-tagged M1-WT or M1-DREADD stably expressing cells. Here we utilised a panel of muscarinic orthosteric ligands and clozapine derivatives in order to investigate their pharmacology in the presence or absence of allosteric ligands; BQCA and VU0357017. Novel fluorescent ligands were also utilised to investigate ligand binding, and allosteric modulation by BQCA, at the M1-DREADD receptor. The M1-DREADD preserves key pharmacology functions that allows Gq and β-ARR2 recruitment and function in cell systems, which would allow for future quantification of the allosteric effect of BQCA using the ternary complex model and gives confidence to using DREADD technologies *in vivo* to explore how the modulation of signalling pathways occur, particularly investigating G-protein interactions with the M1-DREADD.

4.3.1 Assessment of Novel Functional and Binding Assays to Explore M1-WT and M1- DREADD Pharmacology

This study utilised calcium mobilisation measurements as an indirect measurement of Gq-coupled intracellular signalling. This assay is advantageous in that it can measure native receptor responses, without significant modification of proteins required to produce a quantifiable fluorescent signal. We have shown that peak calcium response occurs rapidly after agonist addition; however, the response seen does not only depend upon receptor activation but also on the regulatory mechanism at the receptors and the downstream signalling molecules. There is significant signal amplification between receptor activation and the measured increase in intracellular calcium concentration (Hanson, Bootman and Roderick, 2004). This is evident in low

efficacy agonists that can appear as full agonists relative to reference ligands because of signal amplification (Kilpatrick and Holliday, 2012).

The NanoBiT complementation assay provides a method to investigate the direct interaction between the receptor and its effector protein; either mini Gq or β-ARR2. This allows assessment of pathway dependent pharmacology, which is a more direct measurement of the activation of the receptor, and the Rmax and EC_{50} values are more readily observed without the issues of signal of amplification. This novel complementation assay is reversible, an advantage over earlier complementation methods such as BiFC (Kilpatrick and Holliday, 2012). It is also a rapid system in which the luminescent signal enable the kinetic dynamics of the signalling response to be monitored. We utilised this advantage in this study by comparing the peak response (3-7min after ligand addition) to the response seen at a sustained time point, after equilibrium had been achieved.

Unlike the calcium mobilisation assay, NanoBiT complementation required both the receptor and effector proteins to be modified. The synthetic mini G protein is not a full length Gα subunit and lacks the GDP/GTP binding site, nor can it interact with the Gβγ subunit complex (Nehmé *et al.*, 2017). The mini G is recruited from the cytoplasm and does not undergo lipid modification, nor does it attach to the cell membrane, unlike the full-length Gα subunit (Wan, Okashah, Inoue, Nehmé, Carpenter, Tate, *et al.*, 2018). Therefore, it unlikely the signalling kinetics of the mini G recruitment accurately reflect that of the full-length G protein.

It is difficult to make direct comparisons between the two functional outcomes, calcium mobilisation and complementation of mini G or β-ARR2, because the cell type in which they were tested are different. NanoBiT studies were performed in HEK cells, which unlike CHO cells, used in calcium assays, express native Gq-coupled M3 mAChRs (Zagranichnaya, Wu and Villereal, 2005). The function of LgBiT-tagged receptors also depend on these receptors being correctly expressed by the cells. If the modification necessary to add the LgBiT-tag effect how the receptor is folded and trafficked to the cell membrane, expression levels of this receptor, therefore, have the potential to be reduced or their pharmacology modified.

In future experiments, it would be advantageous to express the LgBiT SNAP-tagged receptors within a stably expressing CHO cell line for more direct comparison between the two functional outcomes of calcium mobilisation and effector complementation. It would also be of interest to investigate additional effector proteins such as the full-length Gαq subunit to investigate the potential kinetic differences of recruitment to the M1-DREADD. Additionally, GRK would be an interesting future protein to investigate the role of β-ARR2 and M1 mAChR internalisation pathways.

The functional assays measured the potency and maximum response of the agonists and clozapine derivatives, in the presence or absence of the allosteric ligands. Such measurements depend on a combination of ligand affinity, efficacy and the functional outcome - that can be affected by signal amplification, as explained. It is therefore difficult to directly extract the affinity and efficacy of agonists at the M1 mAChR in these assays, when functional outcomes are taken from concentration curves in terms of EC_{50} and relative R_{max} values. Moreover, it can be difficult when evaluating subtle effects influenced by allosteric modulation. There are some mathematical models, such as the operational model, that aim to quantify allosteric cooperativity and the modulation of affinity and/or efficacy of the orthosteric agonist (Kenakin *et al.*, 2012). However, these models have their own limitations and are at times more theoretical, requiring parameters that are experimentally difficult to measure.

It was therefore advantageous to determine direct measurements of affinity for investigatory ligands using fluorescent ligand binding studies. In this study, the dissociation constants, K_D values, were obtained to explore the impact of the allosteric modulator BQCA in the presence of the clozapine derivatives at CHO SNAP M1-DREADD cells. Previous studies have relied on using radioligand binding techniques to determine binding affinity at the M1-DREADD, for example by using [^{3}H]NMS (Elham Khajehali *et al.*, 2018), however such assays require the separation of free ligand to quantify the bound radiolabel for every time point (Hulme and Trevethick, 2010).

In this study, a novel fluorescent ligand, **III** provided by the University of Regensburg, was identified to have high affinity for the M1-DREADD (K_D~90nM). From this, we were able to develop a high content imaging assay to measure ligand binding, and competition binding by unlabelled ligands, in a homogenous format, allowing ligand binding to be monitored at multiple time points, and equilibrium measurements, without the removal of the free ligand.

To optimise the fluorescent ligands used here, the pharmacophore currently based on pirenzepine, could be constructed around clozapine or CNO to improve our understanding of these ligands bind the M1-DREADD. Used in addition of NanoBRET or TR-FRET methodology (Stoddart *et al.*, 2018) would improve the throughput of these binding assays and allow for a more extensive kinetic evaluation of the clozapine derivatives at the M1-DREADD receptor (El Khamlichi *et al.*, 2019). Additionally, BRET can detect conformation changes within a bound-receptor complex, which could expand our understanding of how BQCA and other types of M1 allosteric modulators interacts with these ligands (Staus *et al.*, 2016).

4.3.2Agonist Pharmacology in the M1-WT NanoBiT Assay

The clozapine derivatives were inactive as agonists at the M1-WT receptor. However, when in the presence of the orthosteric ligands, our data was able to show the rapid binding of mini Gq and β-ARR2 at the M1-WT receptor, which had minimal changes in potency and/or the maximum responses when comparing the early time point to when equilibrium had been reached. This mini G recruitment is consistent with previously published data (Wan, Okashah, Inoue, Nehmé, Carpenter, Tate, *et al.*, 2018). The orthosteric ligands showed differences between the functional calcium responses they produced, when compared to the direct complementation assay. For example, xanomeline, a compound predicted to have therapeutic potential, was shown to have lower efficacy and was revealed as a partial agonist in the NanoBiT assay. This result is likely to reflect a more relevant representation of physiology due to low signal amplification and receptor reserve (Stott, Hall and Holliday, 2016).

4.3.3Agonist Pharmacolgoy at the M1-DREADD and the Effect of Clozapine Derivatives

Calcium and NanoBiT assays confirmed previous reports that DREADD mutations reduced the potency of many orthosteric M1 agonists (Abdul-Ridha, López, Keov, David M. Thal, *et al.*, 2014; Bradley, Tobin and Prihandoko, 2018). In the calcium mobilisation assay, iperoxo, xanomeline, oxotremorine-M and acetylcholine all presented as full agonists while pilocarpine and carbachol were partial agonists. This illuminates the role of signal amplification. When compared to the NanoBiT assay, all tested orthosteric agonists, except iperoxo, showed no response at the DREADD receptor.

The clozapine derivatives showed efficacious responses in the calcium and NanoBiT assays. Notably, clozapine and N, desmethylclozapine were more potent full agonists compare to CNO in all assays. This was most evident during the fluorescent ligand binding assays which showed CNO is have a significantly reduced affinity as compared to the two other clozapine derivatives, a result supported by the literature (Chen *et al.*, 2015). Clozapine is an antipsychotic drug with known activity at numerous endogenous receptors (Selent *et al.*, 2008). Therefore, during *in vivo* studies clozapine would likely be the cause of effects beyond those mediated only by the activated DREADDs. It is also possible clozapine-mediated responses could summate in DREADD-expressing animals and therefore produce greater side-effects than in WT animals (Mahler and Aston-Jones, 2018). New DREADD agonists that have reduced rates of metabolism have been developed including compound 21 and the FDA-approved sedative and antipsychotic perlapine, which have both been shown to produce functional responses at DREADDs *in vitro,* but continued *in vivo* screening is still necessary (Chen *et al.*, 2015). Perlapine is closely related to clozapine and has been highlighted as a potent ligand at the muscarinic DREADD receptors (Weston *et al.*, 2019).

The metabolite concentrations found in *in vivo* studies are sufficient to activate the DREADD receptors (Manvich *et al.*, 2018). In fact, our data shows clozapine is able

to bind with over 700-times that of the IC_{50} value of CNO at the M1 DREADD receptor, as shown by competition binding studies with **III** fluorescent ligand. To the best of the author's knowledge, no previous Ki values at the M1-DREADD have been published. A result supported by (D. E. Johnson *et al.*, 2005; Abdul-Ridha *et al.*, 2013b) who found ~1000-fold reduction in CNO EC_{50} value as compared to clozapine.

4.3.4VU0357017 May Act as a Bitopic Ligand with Affinity for the M1 mACh Receptor

VU0357017 was originally described as an M1 agonist that bound to an allosteric site, topographically distinct to the orthosteric site, however more recently it has been suggested that it can interact with the orthosteric binding pocket and therefore has the potential to be a bitopic ligand (Digby *et al.*, 2012; Davie, Christopoulos and Scammells, 2013).

In this chapter, it was shown that VU0357017 has the ability to produce a calcium response without an allosteric modulator present. Although, this by itself cannot determine whether VU0357017 is a bitopic ligand, in addition to the literature this adds to the relevance of exploring this further. It was shown that VU0357017 retains a low level of potency as an agonist at the M1-DREADD mutated orthosteric site. Dual stimulation of the M1-DREADD in the presence of ACh or CNO, measured by calcium mobilisation, suggested a level of competitive interaction consistent with VU0357017 occupying both the orthosteric site, as well as, the allosteric site.

It has been suggested that allosteric modulators that have intrinsic agonist activity may contribute to adverse effects, when used *in vivo* (Alt *et al.*, 2016). The bitopic ligands PF-06764427 and MK-7622 have been shown to have significant agonist activity inducing calcium mobilisation in M1-expressing cell lines and convulsions in mice, suggested to be a result of M1 mAChR activation (Moran, Cho, *et al.*, 2018). When compared to VU0453595, which has been described as a pure allosteric modulator, no adverse side effects were seen (Moran, Dickerson, *et al.*, 2018). Therefore, PAMs that lack intrinsic activity may be advantageous as they are

dependent on the orthosteric ligand being present for receptor activation, which may minimise adverse side effects.

4.3.5BQCA is an M1 Allosteric Modulator thatRetains its Effects in the DREADD Receptor System

At the M1-WT receptor, BQCA was shown to act as a PAM with approximately equivalent increases of ACh potency (EC_{50}) for both mini Gq and β-arrestin recruitment. This is similar to the concentration-dependent effects previously reported for BQCA at this receptor (Ma *et al.*, 2009; Shirey *et al.*, 2009a). There was no evidence of pathway selectivity influenced by BQCA between mini Gq compared to the arrestin pathway within the complementation assay. BQCA also had intrinsic agonist activity at the M1-WT receptor, as previously reported (Bradley *et al.*, 2017). This activity was observed in both complementation assays, which contrasts previous reports that the agonist effect of BQCA depends on the pathway measured (Wootten, Christopoulos and Sexton, 2013).

At the M1-DREADD receptor, BQCA also acted as a PAM with increased potency shown for all clozapine derivatives in the calcium mobilisation assay. In comparison, the NanoBiT assay showed BQCA modulation as an increased R_{max} effect. This difference is likely due to calcium amplification experienced during the calcium mobilisation, an effect not seen when there is less receptor reserve as that of the complementation assay. An increase in the relative maximal response is consistent with the suggested mode of action BQCA has to stabilise the ligand bound receptor in an active conformation. Similarly, to the M1-WT receptor, there were no differences observed between the level of mini Gq and β-ARR2 recruitment furthering the idea BQCA does not induce pathway dependence.

Within the calcium mobilisation assay, BQCA was able to increase both the potency and/or maximum response for the orthosteric ligands tested. Moreover, BQCA was able to rescue the reduced potency of ACh at the M1-DREADD receptor, in a comparable manner to published work (Sophie J Bradley *et al.*, 2018). BQCA had shown some evidence for intrinsic agonist activity at the M1-DREADD receptor within

the calcium mobilisation assay; however this indirect effect was less evident when evaluating the NanoBiT assays.

Fluorescent ligand binding was able to support the observation that BQCA acts as a PAM at the M1-DREADD receptor. This was observed by increases in affinity of the clozapine derivatives in the presence of BQCA. However, BQCA was shown to fully compete for the fluorescent ligand binding to the receptor. This suggests that the fluorescent ligand is capable of occupying both the orthosteric binding site and the allosteric site.

The data provided in this chapter is only a descriptive analysis of the allosteric interaction between BQCA and the orthosteric ligands. As described within Chapter 1 there are a number of mathematical models to quantify allosteric modulation, specifically the ternary complex model. This models aims to quantify the magnitude and direction of the allosteric effect between the orthosteric and allosteric binding sites within the receptor (Conn, Christopoulos and Lindsley, 2009). In order to fit these models, the equation requires the affinity of the both the allosteric ligand (K_B) and orthosteric agonist (K_A), as well as, the efficacy (τ) of the orthosteric ligand within the system. These measurements were not taken during the binding studies therefore; the equation is not possible to fit unambiguously without measuring the affinity of the orthosteric and allosteric ligands directly under the same conditions. This is a clear goal for future experiments as the binding affinity of the ligands, in whole cells, would allow the α- and β-factors to be determined for BQCA in the presence of each individual orthosteric ligand. The α factor describes the allosteric effect of the ligand on orthosteric affinity while the β factor describes the allosteric effect of the ligand on the orthosteric ligand efficacy (τ).

4.3.6Proposed Allosteric Mechanism for BQCA

It has been suggested that BQCA binds to a pocket defined by ECL2 (Tyr179, Phe182) and upper TM II (Tyr82) TMVII (Glu397, Trp400) residues above the orthosteric site (Abdul-Ridha *et al.*, 2014). The allosteric modulator binding stabilises the agonist-bound conformational state of the M1 receptor in accordance with the MWC model,

with the degree of cooperativity dependent on the efficacy of the orthosteric agonist (Canals *et al.*, 2012b). BQCA binding therefore also helps stabilise the high affinity, effector coupled GPCR state for the orthosteric agonist (ternary complex model), and can promote the active state alone (resulting in intrinsic agonist activity that can be detected in measurements with high signal amplification).

The BQCA interacting residues are all preserved in the M1-DREADD, and therefore a PAM effect in this receptor, based on a similar mechanism as that of M1-WT, is to be expected. As previously observed (Abdul-Ridha *et al.*, 2013b), the nature of the effect on concentration response curves was different in the M1-WT and M1-DREADD NanoBiT assays, likely due to the degree of cooperativity being influenced by the nature and efficacy of the orthosteric agonist. BQCA principally increases the relative maximal response in the presence of ACh, whereas with CNO the potency is increased, therefore indicating BQCA acts with a level of ligand dependency. This is supported within the literature, for example, it has been shown that BQCA was able to increase the potency of ACh to a greater extent than iperoxo or oxotremorine-M at the M1-mAChR (van der Westhuizen *et al.*, 2018). It may also be possible the DREADD mutations promote the active state conformation within the DREADD receptor (Wess, Nakajima and Jain, 2013; Thal *et al.*, 2018). (Abdul-Ridha *et al.*, 2014) were able to show BQCA rescued the functionality of carbachol, within a mutagenesis study, supporting the idea BQCA is able to promote the active conformation of M1 mAChRs.

Further experiments could explore whether the allosteric modulation of newer M1 PAMs are preserved in the DREADD receptor. There have been a number of allosteric modulators that would be interesting to investigate due to their differing modes of actions to that of BQCA. For example, VU0029767 an M1 allosteric modulator that has been shown to selectively increase calcium mobilisation but has no effect of phospholipase D (Marlo *et al.*, 2009). An effect predicted to be caused by selective Gαq recruitment to the allosteric-bound receptor, rather than G12/13 recruitment that would activate phospholipase D (De Jesús *et al.*, 2006). This predicts a novel method of allosteric modulation, in which allosteric modulators could promote an activated conformational that determines G protein binding as a mechanism of

action. Additionally, through computational mapping of available GPCR crystal structures, the possibility of extracellular, intracellular and TM allosteric sites has been highlighted (Wakefield *et al.*, 2019). A number of receptors have been identified (β2-AR (Liu *et al.*, 2017), CC chemokine receptor 2 (CCR2) (Zheng *et al.*, 2016) and CCR9 (Oswald *et al.*, 2016)) that can bind negative allosteric modulators at the intracellular sites of the receptor, where they act by sterically competing with G proteins within the cell.

4.4 Conclusions

In this Chapter, we have developed novel fluorescent ligand binding studies and functional complementation assays to investigate ligand affinity and function at the M1-DREADD receptor. In addition to the expected potencies for the M1 mAChR orthosteric agonist and CNO, our novel assays have revealed that clozapine has a much higher affinity at and potency for the M1-DREADD. This supports previous reports that clozapine and its derivatives are relevant stimulators of the M1-DREADD *in vivo*. Our functional and ligand-binding data support the mechanism of action BQCA has as a positive allosteric modulator of the M1-DREADD. We have shown BQCA to promote the active agonist-bound receptor conformation occupied by the clozapine derivatives, including CNO.

Findings within the chapter confirm that the pharmacology in the M1-DREADD is not disrupted when assessing BQCA and its allosteric modulation. Therefore, this is a tool that could be useful to investigate the subtle changes allosteric ligands have within complex *in vivo* systems. The high level of selectivity CNO offers to target DREADD receptors could help delineate how allosteric ligands could alter an astrocyte's role within the tripartite synapse. Directed expression of DREADD in astrocytes would allow intracellular pathways to be activated solely in astrocytes and not the surrounding neurones, which could not occur when applying ACh. It is therefore important to expand from this chapter into a primary cell type to determine the role of BQCA within this cell type.

Chapter 5

CHARACTERISATION OF CALCIUM AND cAMP SIGNALLING PATHWAYS IN ASTROCYTES FOR THE INVESTIGATION OF M1q- AND M3s-DREADD IN PRIMARY CELLS

5.1 Introduction

The pharmacological selectivity available by using chemogenetic DREADDs offers a unique mode of action to investigate the complexities of astrocyte intracellular signalling. The intricate tripartite synapse in a physiological structure with a number of different cells types, expressing a number of the same receptors in extremely close proximity. The selectivity the DREADD system offers to activate only one cell type at one receptor could expand our knowledge of how spatiotemporal aspects of cell signalling occurs. Using allosteric modulators in conjunction with the DREADD receptor would enable subtle changes in the signalling dynamics of an astrocyte to be tested without activating the surrounding neurones by using CNO rather than the endogenous ligand ACh. In this chapter, it is of interest to use the M1-Gq-DREADD in to investigate allosteric modulation of calcium signalling and the M3-Gs-DREADD to investigate BQCA's effect on stellation.

5.1.1 Utilising the M1q-DREADD to investigate calcium signalling in astrocytes

The primary form of astrocyte excitability is considered to be mediated through intracellular calcium spikes and oscillations produced by receptor activation from neurotransmitters originating from the synaptic network that astrocytes are intimately coupled to (Alfonso Araque *et al.*, 1999; Molnar *et al.*, 2016). Compared to what was described in Chapter 4, the fluorescent calcium dye Fluo-5F AM was used for single cell experiments in order to investigate intracellular calcium responses elicited by extracellular stimuli. Unlike Fluo-4 AM, Fluo-5F AM is a low affinity calcium dye (K_D = 2.3µM) which is advantageous when very little calcium buffering can be tolerated, or in cells where subcellular compartments have relatively high intracellular calcium responses (Paredes *et al.*, 2008). It has been shown that the use of high affinity calcium buffers attenuated calcium wave production in astrocytes, which was suggested to be caused by the buffering effect of the dye limiting the diffusion of calcium ions thus inhibiting the propagation of calcium waves (Wang *et al.*, 1997). Calcium responses seen within astrocytes can be transient (small and brief elevations due to calcium influx through membrane calcium channels), sustained (high or

sustained increase in calcium signal from calcium influx of both external and internal stores) or oscillatory signals (repeated brief increases in free calcium in the intercellular cytoplasm (Uhlén and Fritz, 2010). Therefore, Fluo-5F AM should enable these three temporal calcium patterns to occur without buffering the small transient responses or lowering the threshold needed for the large calcium responses. The acetoxymethyl ester enables the fluorescent dye to easily cross the astrocyte's cell membrane and bulk loading is very effective within this cell type.

Astrocytes are a highly heterogeneous cell type, which is evident in the myriad of intracellular calcium responses elicited by this cell. Some calcium responses are spontaneous, brief blips produced by single IP3 receptor activation (Parker, Choi and Yao, 1996). Calcium spikes, oscillations (Swillens *et al.*, 1999) and calcium propagation can also be seen after the addition of external stimuli (Bootman, Lipp and Berridge, 2001; Koizumi *et al.*, 2002). A calcium puff within a cell is an IP3-driven process led by the calcium release from a cluster of IP3 receptors on a small region of the ER (Golovina and Blaustein, 2000; Scemes, 2000; Sheppard et al., 1997). On the other hand, within the astrocytic processes the generation of strong calcium signals occurs by transmembrane calcium influx and can stimulate a calcium wave within neighbouring cells via IP3 diffusion through gap junctions (Politi *et al.*, 2006; Dityatev and Rusakov, 2011). Within a cell population, there are also likely to be cells that do not respond when their surrounding neighbours do, or they positively respond as an individual cell without triggering neighbouring cells to respond at all. The different calcium profiles, and their functional outcomes, are therefore diverse and nuanced.

In this chapter, astrocytes were investigated as an isolated, monoculture cell population and calcium signalling was investigated at a single cell level *in vitro*. As within Chapter 4, CNO was used alongside clozapine and N-desmethylclozapine in order to investigate whether these ligands are also relevant stimulators of the M1-DREADD, capable of initiating calcium responses in astrocytes. It is unknown how the kinetics of DREADD-activated intracellular signalling pathways compares to that of the endogenous ligand, acetylcholine, at the natively expressed receptors in astrocytes *in vivo*. It is therefore of value to evaluate the three clozapine derivatives as a comparison to the endogenous ligand at an *in vitro* level.

5.1.2 Limitations in Identifying Astrocytes

The astroglia family encompasses a number of cell subpopulations with radically distinct morphologies and functions, roughly, these include 10 distinct subpopulations (Verkhratsky and Nedergaard, 2018). Therefore, the matter of astrocytic classification and definition according to structure and function is continuously under debate (Kimelberg, 2004). The absence of a universal marker to label all cells of astroglial lineage exacerbates the problem. Current techniques depend upon immunocytochemistry, genetically controlled expression of fluorescent markers and incubation with fluorescent dyes to label astrocytes.

Glial fibrillary acidic protein (GFAP) has long been known to have specific expression in astrocytes (Eng *et al.*, 1971; Bignami *et al.*, 1972; Ludwin, Kosek and Eng, 1976) and is still widely used as a target for immunocytochemical studies (Hol and Pekny, 2015). GFAP is part of the family of intermediate filaments that form the astrocytic cytoskeleton (Pekny *et al.*, 2014; Hol and Pekny, 2015), thus GFAP+ staining only reveals major processes with finer structures, such as perisynaptic processes or endfeet connections to blood vessels, being lost (Connor and Berkowitz, 1985; Simard *et al.*, 2003; Reichenbach, Derouiche and Kirchhoff, 2010). More significantly, GFAP antibodies only label a percentage of *in situ* astrocytes with high levels of regional heterogeneity (Walz and Lang, 1998). In fact the striatum and tectum of mammals is almost completely devoid of GFAP immunoreactivity (Kálmán, 2002). On the other hand, *in vitro* astrocyte preparations are consistently GFAP+, which contrasts the lack of labelling seen *in situ* and *in vivo* (Walz, 2000). Other proteins used to label astrocytes are S100β (Souza *et al.*, 2013) and the glutamate transporters EAAT-1 (GLAST) and EAAT2 (GLT-1) (Schmitt *et al.*, 1997). S100β stains up to 3X more astrocytes than GFAP (Savchenko *et al.*, 2000), with one study showing only 80% of cells stained with S100β were also GFAP positive (Ogata and Kosaka, 2002). However, S100β lacks astrocyte-specificity and is also expressed in neurones found in the brain stem, cerebellum, forebrain and limbic system, (Rickmann and Wolff, 1995) as well as oligodendrocytes (Steiner *et al.*, 2007).

Once stained, astrocytes show remarkable morphological variations that are highly dynamic and can easily change under pathological conditions or after the addition of external stimuli. Rodent protoplasmic astrocytes are characterised by small round somata (~10µm) from which 5-10 (~50µm long) processes extend, distinctive of the spongiform morphology (Bushong *et al.*, 2002). There are many more morphological states that have been identified for astrocytes within different regions of the CNS (Ogata and Kosaka, 2002; Emsley and Macklis, 2006), and in fact differences in appearance of protoplasmic astrocytes differ within the same anatomical structures. For example, in the CA1 hippocampal region, fusiform, elongated, and spherical cells were identified (Nixdorf-Bergweiler, Albrecht and Heinemann, 1994; Bushong *et al.*, 2002). Moreover, human parenchymal astrocytes have been shown to be larger and far more complex than astrocytes from rodents. Human protoplasmic astrocytes have been shown to be 2.5X larger than that of rat astrocytes, and have 10X more processes extending from their somata (Oberheim *et al.*, 2009). This increase in size and complexity has been predicted to separate human astrocytes into a class of their own, which limits the transfer of information between functions found in non-primate models and what may occur in man (Heller and Rusakov, 2015; Hu *et al.*, 2016; Krencik, van Asperen and Ullian, 2017).

5.1.3 Utilising M3-DREADD Chimera to investigate Gαs activation of cAMP-dependent astrocyte stellation

Astrocytes *in vivo* have a stellate shape, with numerous fine processes extending from the main cell stoma, which is essential for their interaction with the pre- and postsynaptic terminals, as well as, neighbouring glial cells and surrounding circulatory vessels (Reichenbach, Derouiche and Kirchhoff, 2010). This proximity is important for the function of the astrocyte and maintains dynamic interactions. The astrocytic projections can respond to a change in its physiological environment and trigger changes in cell morphology. This is most evident when astrocytes become reactive in response to a pathogen or injury (Burda, Bernstein and Sofroniew, 2016). The astrocytes undergo substantial morphological changes, entering into astrogliosis

whereby the astrocytes act to coordinate inflammation and maintain the blood-brain barrier (Ben Haim *et al.*, 2015). In contrast, cultured astrocytes acquire a flat, epithelioid morphology. However, the *in situ* phenotype can be partially recovered in an actin-dependent, cAMP-led process known as stellation (Racchetti, D'Alessandro and Meldolesi, 2012; Vardjan, Kreft and Zorec, 2014). The cAMP pathway acts by activating the second messenger AC catalysing cAMP formation and later activation of the PKA pathway. It has been widely noted that increased intracellular cAMP levels, or activation of β-adrenergic receptors, altered the flat morphology to process-bearing, stellate astrocytes. This mode of cellular activation resulting in astrocyte stellation, gives a model that enables the investigation into the role of the cytoskeleton necessary to form typical morphology or the lesser understood gliosis-like astrocyte morphology (Schiweck, Britta J Eickholt and Murk, 2018). This model will also function as an assay to identifying the agents that activate cAMP, and how they affect the astrocytes' cytoskeleton.

The rM3s DREADD receptor is a chimera of the rat M3q-DREADD and turkey β1-adrenergic receptor, where the intracellular portions of the M3-muscarinic receptor were replaced with domains from the β1-adrenergic receptor that confer selectivity to Gαs relative to Gαq (Conklin *et al.*, 2008; Guettier, Gautam, Scarselli, de Azua, *et al.*, 2009; Urban and Roth, 2015). Thus, the M3-DREADD binds CNO extracellularly but can signal via the cAMP pathway intracellularly. Astrocytes express all three types of β-adrenergic receptors (β1-3), with these receptors being the dominant source of increased intracellular cAMP upon receptor activation in astrocytes (Shao and Sutin, 1992; Catus *et al.*, 2011; Horvat, Zorec and Vardjan, 2016). The β1-adrenergic receptors have been found to exclusively act via Gs pathways (Steinberg, 1999). Similarly to intracellular astrocytic calcium, the spatiotemporal dynamics of cAMP signalling is involved in astrocyte functions, including energy supply, maintenance of the extracellular environment and its immune response (Zhou, Ikegaya and Koyama, 2019). In fact, it is the complexity of cAMP signalling that allows for the selective activation of downstream targets, thus malfunctions in cAMP signalling are the underlying cause of many diseases (Pierre *et al.*, 2009).

Identification of stellate astrocytes remains as somewhat of a subjective procedure when evaluating each cell's morphology (Kimelberg, 2004). Identification has been obtained by measuring the decrease in cell cross-sectional area and increases in astrocyte cell perimeter (Vardjan, Kreft and Zorec, 2014). Others have used a stellation index dependent on the ratio of cell process area to cell body area (Beckerman *et al.*, 2015). However, when using an automated approach to identify cells there are issues with the software accurately designating cellular processes to the corresponding cell body, especially at higher cell densities where there can be an overlap of processes extending from a number of cell bodies in a relatively small area. To overcome this, an algorithm that evaluates the "fibrousness" of cells in a field of view, without segregating individual cells, was applied by one group (El *et al.*, 2018). This simply distinguishes between elongated shapes and spherical shapes, which is likely to limit the nuanced heterogeneity of astrocytic responses.

Another common method used by research teams is to use an immunocytochemical approach. Cells can be labelled then be traced and a number of software programmes can measure the size, number, and/or intensity of puncta present as a result of the label used (Beckerman *et al.*, 2015). One limitation to this method is the fact there is no one molecular marker identified for astrocytes (John Lin *et al.*, 2017). GFAP is used as the standard (Eng, 1985), however it is widely known that not all astrocytes express this marker, especially cells *in vivo* (Mishima and Hirase, 2010; Tatsumi *et al.*, 2018). Expression of GFAP can also change depending on the environment of the astrocyte (*in vitro* vs. *in vivo*), as explained in section 5.1.2 (Brahmachari and Pahan, 2006; Mishima and Hirase, 2010). This is not solely related to GFAP. For example, the expression of glial scar-associated CSPG (chondroitin sulfate proteoglycans) epitopes have numerous species expressed in the CNS, and the repertoire of CSPGs changes after CNS injury (McKeon, Jurynec and Buck, 1999; Andrews *et al.*, 2012; Yi *et al.*, 2012).

Within this chapter, the acetomethoxy-linked fluorescent dye calcein was used in combination with manual categorisation as a simple and straightforward method of identifying stellate astrocytes. This dye labels the cytoplasm of any viable cell and achieves a strong fluorescent signal at 488nm. The main advantage of this simpler

method is the fact that manual identification is likely more accurate than using an automated system in identifying the subtle differences between cells that are already heterogenous is their morphology.

5.1.4 DREADD transfection of astrocytes

The vast majority of studies that use DREADDs are within transgenic animal models. Of the transgenic animal models, the hM3q-DREADD, hM4i/o-DREADD and k-opioid receptor DREADD (KORD) are frequently used to study astrocyte function. Expression of the chemogenetic proteins have been achieved using viral and transgenic delivery in combination with astrocyte-specific promoters (Bang, Kim and Lee, 2016). The GFAP-promoter, in combination with tTA and tetO promoter-driven Mas-related G protein-couple receptoer A1 (MrgprA1), has been used to express the Gq-DREADD selectively in astrocytes (Dong *et al.*, 2001; Fiacco *et al.*, 2007; Cao *et al.*, 2013). Others have used Ro1-expressing transgenic mice, developed in GFAP-expressing astrocytes (Sweger *et al.*, 2007). Virally delivered DREADDs have also been successful in producing animals expressing DREADD receptors. The use of an AAV-expressing virus has been shown to deliver both the hM3Dq and hM4Di to produce a number of animal models (Spalding *et al.*, 2002; Bull *et al.*, 2014; Scofield *et al.*, 2015a; Yang, Qi and Yang, 2015a; Weston *et al.*, 2019).

Viral transduction offers a means to reach hard-to-transfect cell types for protein overexpression or knockdown (Hama *et al.*, 2007). High delivery rates have been achieved using viral vectors in primary cells but there are a number of limitations to this method including biosafety requirements, gene integration, limitations on insert size and its high cost (Karra and Dahm, 2010). As such, lipofection or physical transfection methods are more often used *in vitro*.

A more effective transfection method may be the physical method of electroporation. Nucleofection has been developed to act as a cell-specific form of electroporation, a clear improvement over standard electroporation systems (Zimmermann, 1982; Maurisse *et al.*, 2010). Nucleofection applies brief electric pulses to cells to increase the permeability of the membrane to DNA molecules (Sukharev *et al.*, 1992). Square pulses and exponential pulses can be used to improve transfection

efficiency in a cell dependent manner (Escoffre *et al.*, 2009). However, a large number of cells are required for this method as there is high level of cell mortality until optimal conditions can be reached.

A number of chemogenetic DREADD receptors have been expressed in astrocytes *in vivo*. The hM3Dq is one of the most frequently used chemogenetic tools. This is due to the compelling evidence that IP3-mediated calcium release is implicated in almost all aspects of neuronal synaptic transmission (Petravicz, Fiacco and McCarthy, 2008; Agulhon *et al.*, 2012; Haustein *et al.*, 2014; Kanemaru *et al.*, 2014). A number of groups have shown the hM3q-DREADD has a beneficial effect on astrocytes involved in cognitive flexibility and information processing (Agulhon *et al.*, 2013; Robinson *et al.*, 2014; Lopez *et al.*, 2015; Yau and McNally, 2015; Brockett *et al.*, 2018). This DREADD has been used to show the role of astrocytes in feeding behaviours (Krashes *et al.*, 2014; Yang, Qi and Yang, 2015b; Thompson *et al.*, 2018), and mood disorders (Zhou *et al.*, 2019).

Aims

This chapter aimed to transfect primary cortical astrocytes with two DREADD receptors; the SNAP hM1q-DREADD and SNAP rM3s-DREADD. The first aim was to investigate the calcium signalling produced by activation of hM1q-DREADD by clozapine derivatives, as compared to the muscarinic ligands, acetylcholine and carbachol. The second aim was to investigate cAMP-dependent cell stellation in astrocytes expressing rM3s-DREADD.

5.2 Results

5.2.1 Validation of Astrocytes for Pharmacological Investigation

Initial calcium mobilisation measurements were performed on non-transfected cortical astrocytes, loaded with Fluo-5F AM calcium dye. Representative traces of individual cell calcium spikes following ligand addition are shown in Fig 5.1 & 5.2. It can be seen that astrocytes activated by norepinephrine have heterogeneity in the

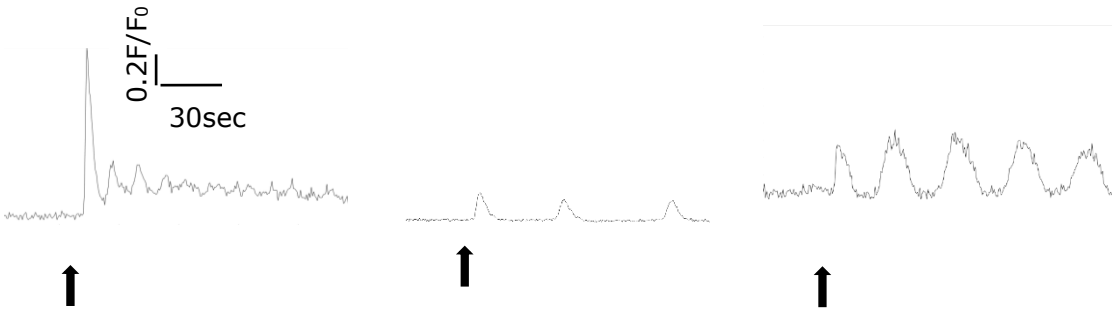
calcium spikes elicited. The magnitude and frequency of calcium spikes can be seen to vary between individual cells activated by the same ligand. Forskolin, on the other hand, produces an extremely flat calcium trace profile, with no cells showing activity after ligand addition. The muscarinic ligands, ACh and carbachol, were able to produce calcium responses within the astrocyte population. These mAChR agonist again highlight the heterogeneity in the calcium response they can produce in individual astrocytes. Carbachol elicits calcium spikes with greater magnitude than ACh, however it can be seen that ACh produces more calcium transients over time in a repetitive spiking pattern. The clozapine derivatives do not show calcium spikes (Fig 5.2), but can be seen to have slight deviations of baseline, which is in comparison to calcium kinetics elicited by forskolin.

As a ligand that produced the highest percentage of cells to respond, norepinephrine (10µM) was shown to have a pronounced effect as compared to the clozapine derivatives and forskolin that did not show calcium mobilisation. In fact, the clozapine derivatives (100µM) and forskolin (10µM) were comparable to the response seen when buffer alone was added to the astrocytes ($P>0.05$ one-way ANOVA with Dunnett's post hoc comparison). Carbachol (100µM) was able to elicit a similar percentage of cells that responded as norepinephrine, with 39.42% ± 9.96 as compared to 36.95% ± 6.98 of cells responding, respectively (Table 5.1, $P>0.05$, one-way ANOVA with Dunnet's post hoc as compared to norepinephrine). Acetylcholine (100µM) showed a lower percentage of cells exhibiting a calcium response; 18.54% ± 6.80 of cells responded, however was not statistically different to the response seen by addition of norepinephrine ($P>0.05$).

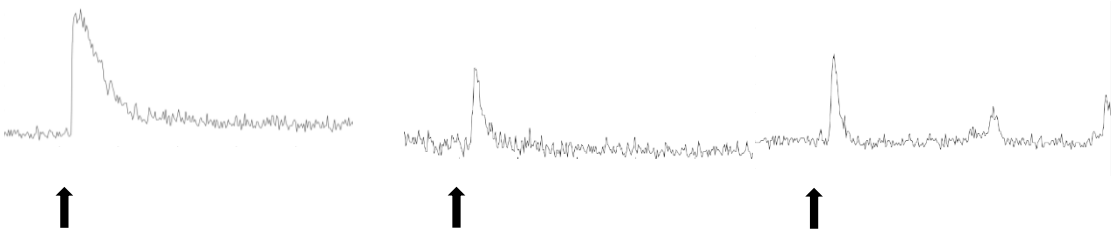
Next, the magnitude of calcium signalling in cells that responded to ligand addition was taken as a function of "area under the curve" (Fig 5.4, B). This is calculated using a "calcium GUI" written by Dr. Wayne Croft, University of Nottingham, in Matlab R2015b, that compares calcium intensity over baseline in individual cells against time to provide the magnitude of calcium responses. Each cell that responded was selected and the total magnitude of calcium spikes were measured through the GUI over the total timecourse in which the cells were measured. In future, it would be advantageous to verify that all cells were capable of producing a calcium response

before using the investigatory ligand on the astrocyte population. Again, norepinephrine showed the greatest calcium response, with carbachol and acetylcholine showing comparable responses; values shown in Table 5.1. The clozapine derivatives were shown not to be statistically similar to buffer-treated astrocytes, while forskolin was shown to have a slightly smaller AUC value (Fig. 5.1, B).

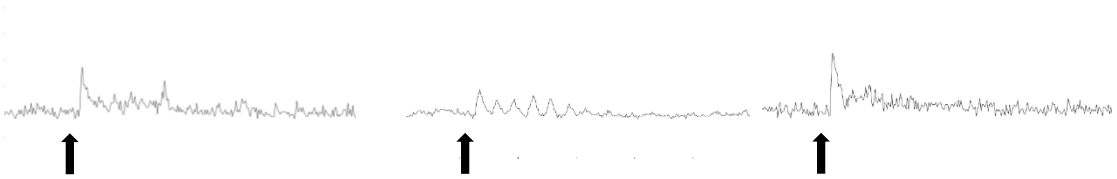
A) Norepinephrine



B) Carbachol



C) Acetylcholine



D) Forskolin

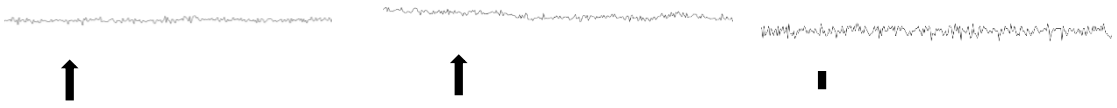
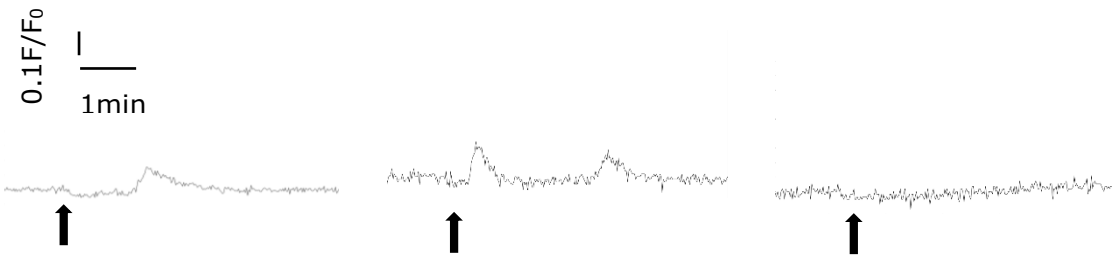
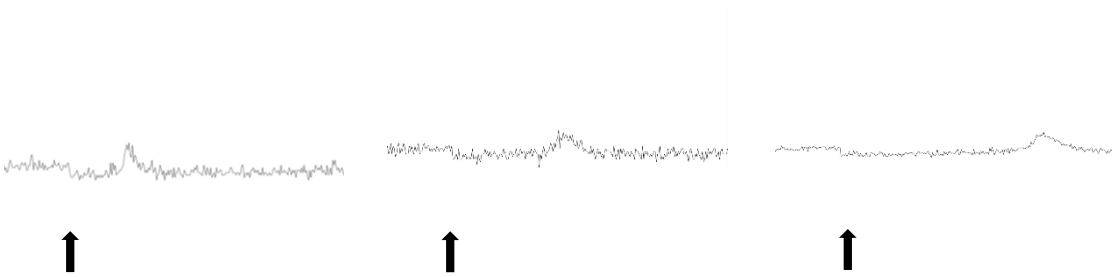


Fig 5.1: ***Representative calcium traces from individual cells after ligand addition, shown as fold change over basal across the time course taken.*** *The black arrow indicates when the ligand was added. Traces are able to show the initial calcium response to ligand addition and subsequent calcium spikes.*

A) Clozapine-N-Oxide



B) Clozapine



C) N, desmethylclozapine

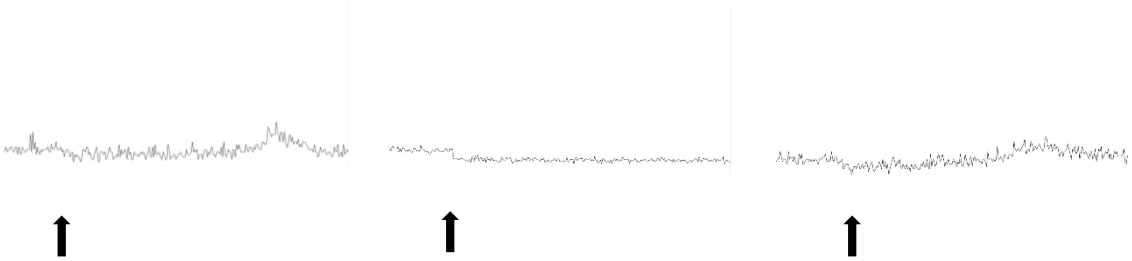


Figure 5.2: ***Representative calcium traces from individual cells after activation by clozapine and its dervatives, shown as fold change over basal across the time course taken.*** *The three clozapine derivatives did not elicit many calcium spikes, however showed the heterogeneity of calcium signalling in individual astrocytes even when receptor activation did not occur.*

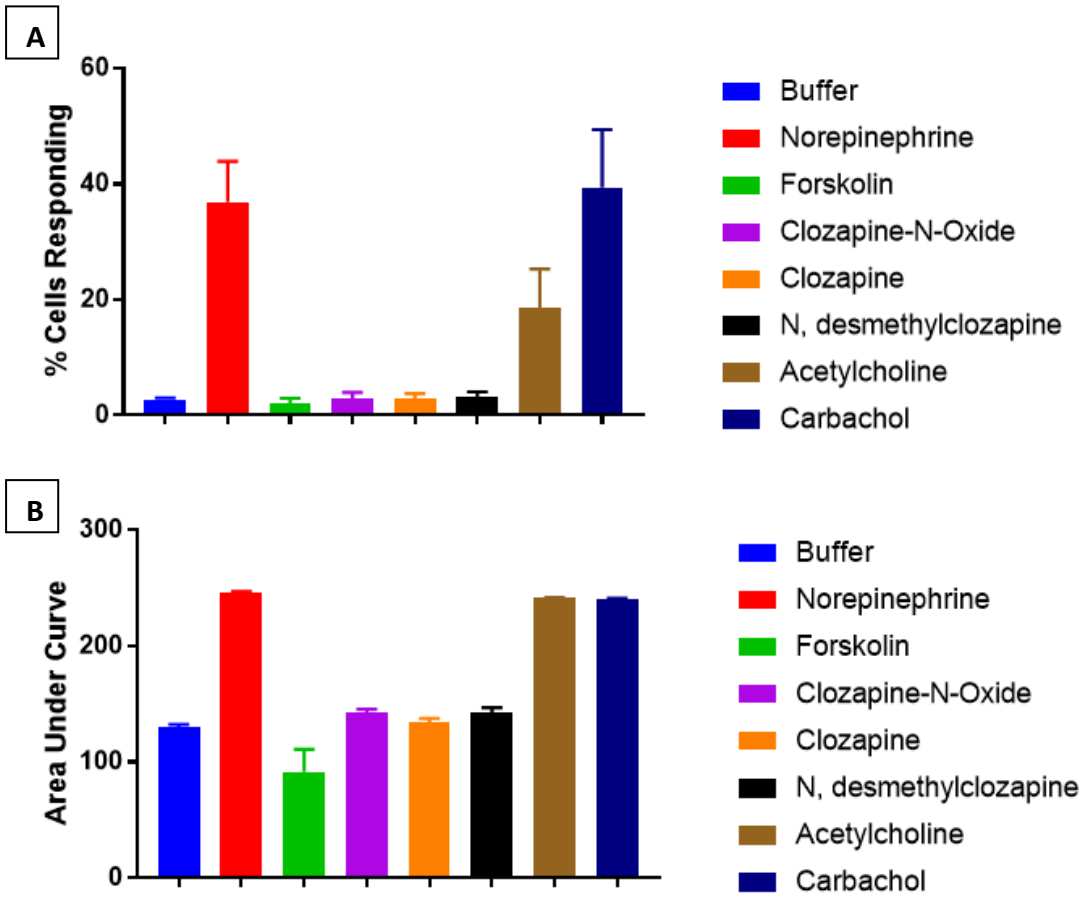


Figure 5.3: ***The calcium responses elicited by clozapine and its derivatives were investigated in non-transfected cortical astrocytes.*** *Cells were loaded with Fluo-5F AM and measured on the IX inverted microscope, and calcium response was measured as the percentage of cell that responded (A) and the area under the curve of calcium traces (B). Values are shown as mean ± SEM of duplicate experiments (n=5-6).*

Ligands	Cell response (% total cells)	Area Under Curve
Buffer	3.15 ± 1.78	129 ± 2.94
Norepinephrine	36.95 ± 6.98***	245 ± 1.61***
Forksolin	2.05 ± 0.93NS	91 ± 19.09*
Clozapine-N-Oxide	2.87 ± 1.12NS	142 ± 3.08 NS
Clozapine	2.88 ± 0.92NS	134 ± 3.27 NS
N, Desmethylclozapine	3.22 ± 0.85NS	142 ± 4.12NS
Acetylcholine	18.54 ± 6.80**	241 ± 0.58***
Carbachol	39.42 ± 9.96 ***	240 ± 1.08 ***

Table 5.1: ***The percentage of cells that responded to ligand addition and their magnitude as a function of the area under the curve.*** *Non-transfected cortical astrocytes, loaded with Fluo-5F AM, were exposed to a range of ligands to investigate calcium signalling. The percentage of cells which responded to ligand addition are shown, with the fold change in response as compared to norepinephrine. The area under the curve, indicative of intracellular calcium release, from calcium traces is also shown. Values are shown as mean ± SEM of calcium imaging experiments n=6. One-way ANOVA analysis was carried out with Dunnett's post hoc comparison to compare ligands against buffer. NS; non-significant, *P<0.05, **P<0.01 and ***P<0.001.*

5.2.2 Effect of Allosteric Modulation on Astrocyte Muscarinic Calcium Responses

To test the effect of the M1 allosteric modulator BQCA and the muscarinic antagonist atropine on calcium responses, these pharmacological tools were added in a dual addition protocol with acetylcholine (Fig 5.4, A) or carbachol (Fig 5.4, B). In this assay, non-transfected astrocytes were pre-incubated with either BQCA or atropine for 30mins prior to recording Fluo5F AM fluorescence. The mAChR agonists were added to the cells during the recording, 60sec after a base line reading.

The antagonist atropine significantly reduced the percentage of cells that were able to produce a calcium response. This correlated with a reduction in the AUC value seen in the presence of both acetylcholine and carbachol, indicative of a reduction in muscarinic receptor activation. This effect may be caused by either in calcium magnitude per spike or in the frequency of spikes, values shown in Table 5.6.

BQCA was unable to modulate the calcium signalling, in the percentage of cells that responded and area under the curve. In fact, BQCA activated astrocytes elicited comparable calcium responses as when the allosteric modulate was not present (Fig. 5.4, Table 5.2).

The α1-adrenergic antagonist prazosin was then used to investigate antagonism of the calcium responses elicited by norepinephrine in astrocytes. Prazosin was able to significantly inhibit calcium mobilisation initiated by norepinephrine-induced calcium signalling. The actions of this antagonist indicates that the calcium response induced by norepinephrine acts through α-adrenergic receptors, offering an alternative to muscarinic Gq-coupled GPCR pathway, in which astrocytes are able to signal (Fig 5.5, Table 5.3).

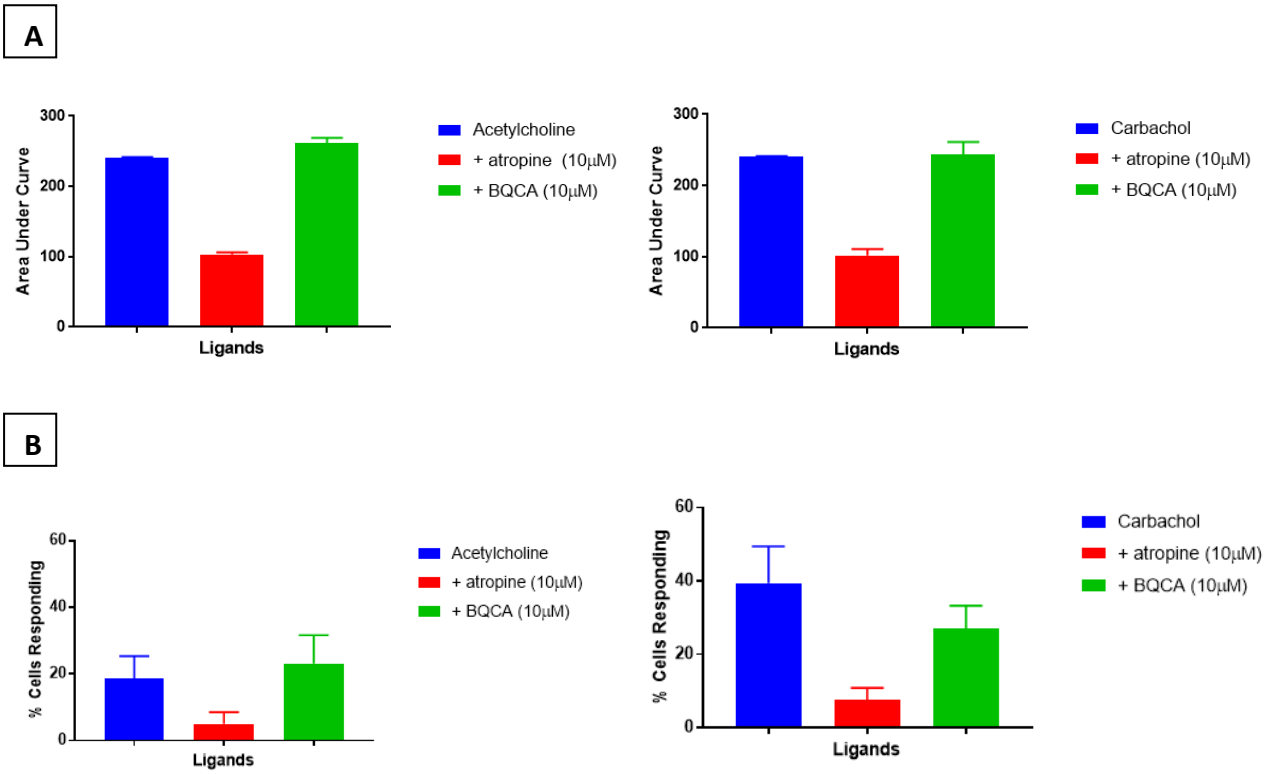


Figure 5.4: ***Percentage of cell responding to ligand addition and area under the curve of calcium responses****. Non-transfected cortical astrocytes, loaded with Fluo-5F AM, where measured on the IX inverted microscope, and calcium responses were measured as the percentage of cell that responded and the area under the curve of calcium traces. A) Shows calcium responses after carbachol addition, while B) shows the response after acetylcholine. Values are shown as mean ± SEM of duplicate experiments, with an average of 100 cells counted per experiment (n=6).*

	Acetylcholine	Acetylcholine + BQCA	Acetylcholine + atropine
% response	18.54 ± 6.80	23.11 ± 8.50^{NS}	1.82 ± 1.27**
AUC	241 ± 0.57	261± 7.66 ^{NS}	103 ± 2.85***
	Carbachol	**Carbachol + BQCA**	**Carbachol + atropine**
% response	39.42 ± 9.99	31.40 ± 3.38^{NS}	4.68 ± 1.54**
AUC	240 ± 1.30	101 ± 9.37 ^{NS}	101 ± 17.86 ***

Table 5.2: ***Non-transfected cortical astrocytes, loaded with Fluo-5F AM, were exposed to muscarinic ligands acetylcholine and carbachol in the presence of the M1 BQCA allosteric modulator and the mACh antagonist atropine****. The percentage of cells that responded to ligand addition and the area under the curve are shown. Values are shown as mean ± SEM of calcium imaging experiments n=6, with an average of 100 cells analysed per experiment. A paired t-test was carried out for statistical analysis to compare when the antagonist or allosteric modulator was present.*

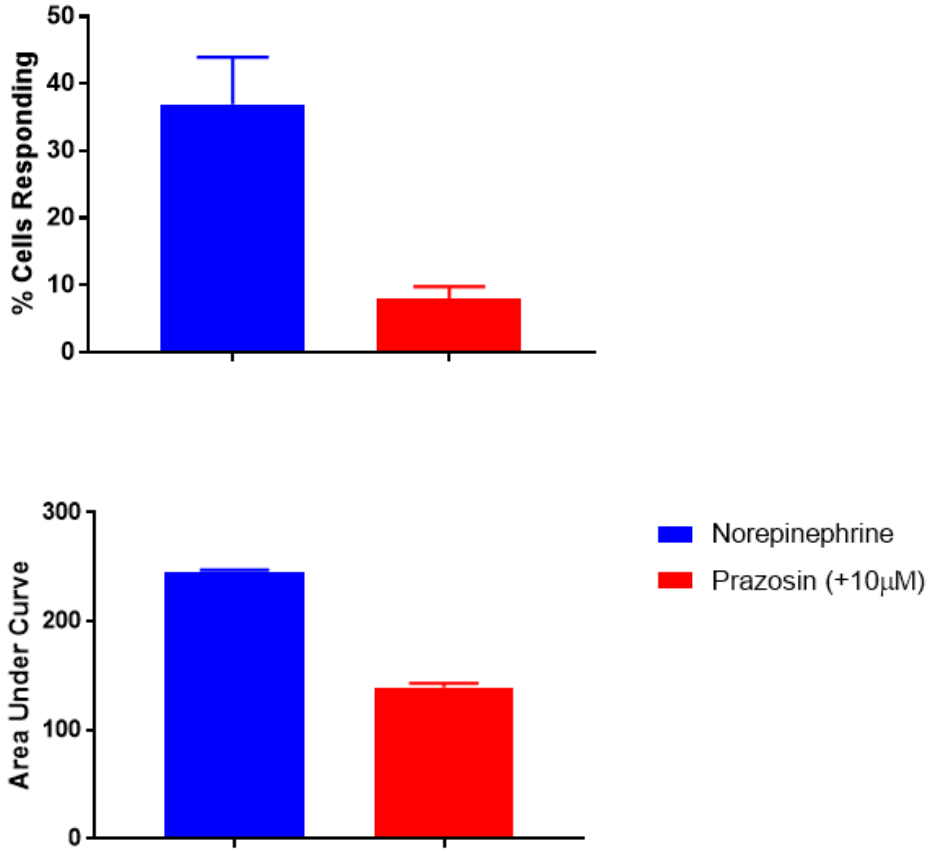


Figure 5.5: ***The effect of astrocytic calcium signalling with prazosin in the presence of norepinephrine was evaluated.*** *Non-transfected cortical astrocytes, loaded with Fluo-5F AM, where measured on the IX inverted microscope, and calcium response was measured as the percentage of cell that responded after prozosin inhibition of norepinephrine-induced calcium response. Values are shown as mean ± SEM of duplicate experiments, with an average of 100 cells counted per experiment (n=6).*

	Norepinephrine	**Norepinephrine + Prazosin**
Postive calcium response (% cells responding)	36.95 ± 6.98	8.02 ± 1.76**
Area Under the Curve	245 ± 1.61	139 ± 4.13***

Table 5.3: ***Non-transfected cortical astrocytes, loaded with Fluo-5F AM, were exposed norepinephrine in the presence and absence of prazosin.*** *The percentage of cells which responded to ligand addition and the area under the curve are shown. Values are shown as mean ± SEM of calcium imaging experiments n=6, with an average of 100 cells analysed per experiment. A paired t-test was carried out for statistical analysis to compared when the antagonist was present; **P<0.01 and ***P<0.001.*

5.2.3 Induction of Stellation in Astrocytes

The morphological changes seen during astrocyte stellation were manually assessed in a blinded study. Astrocytes were identified as stellate when it was clear that the soma was small relative to the total cellular area and the cell showed two or more extended cellular processes. Cells were also counted when these morphological structures could be identified at an intermediate stage, as indicated by the red arrows in Fig. 5.6. This ensured that cells identified as non-stellate were purely protoplasmic cells.

First, astrocytic stellation was investigated using the direct adenylate cyclase-activator forskolin (10μM) and the β-AR ligand norepinephrine (10μM), as compared to vehicle. Fig 5.8, panel A, clearly indicates that both forskolin and norepinephrine elicit the cells to become stellate with elongated with fine processes extending from the main cell body. In contrast, when astrocytes are treated with vehicle they are able to maintain a rounded, spongiform morphology, with little to no processes being identified (Fig. 5.7, Table 5.3).

When the three clozapine derivatives (100μM) clozapine-N-oxide, clozapine and N, desmethylclozapine, were investigated, the majority of cells were comparable to vehicle-treated cells. Few cells were identified with complex morphologies as those cells treated with forskolin (with multiple fibres clearly distinguishable from soma), however, there were cells which could be seen as "becoming" stellate (identified with red arrows; Fig 5.8, panel B). These were counted within the stellation assay to make a distinction from protoplasmic astrocyte (Fig. 5.7, Table 5.3).

Finally, the muscarinic ligands and the M1-mAChR allosteric modulator BQCA (100μM) were evaluated (Fig. 5.7, Table 5.3). Similarly, to clozapine derivatives, acetylcholine (100μM) and carbachol (100μM) generally showed non-stellate cells with a few that had cellular properties indicative of the start of the stellation process (indicated by red arrows). The allosteric modulator BQCA was unable to produce any cells which were identified as stellate (Fig 4.8, panel C).

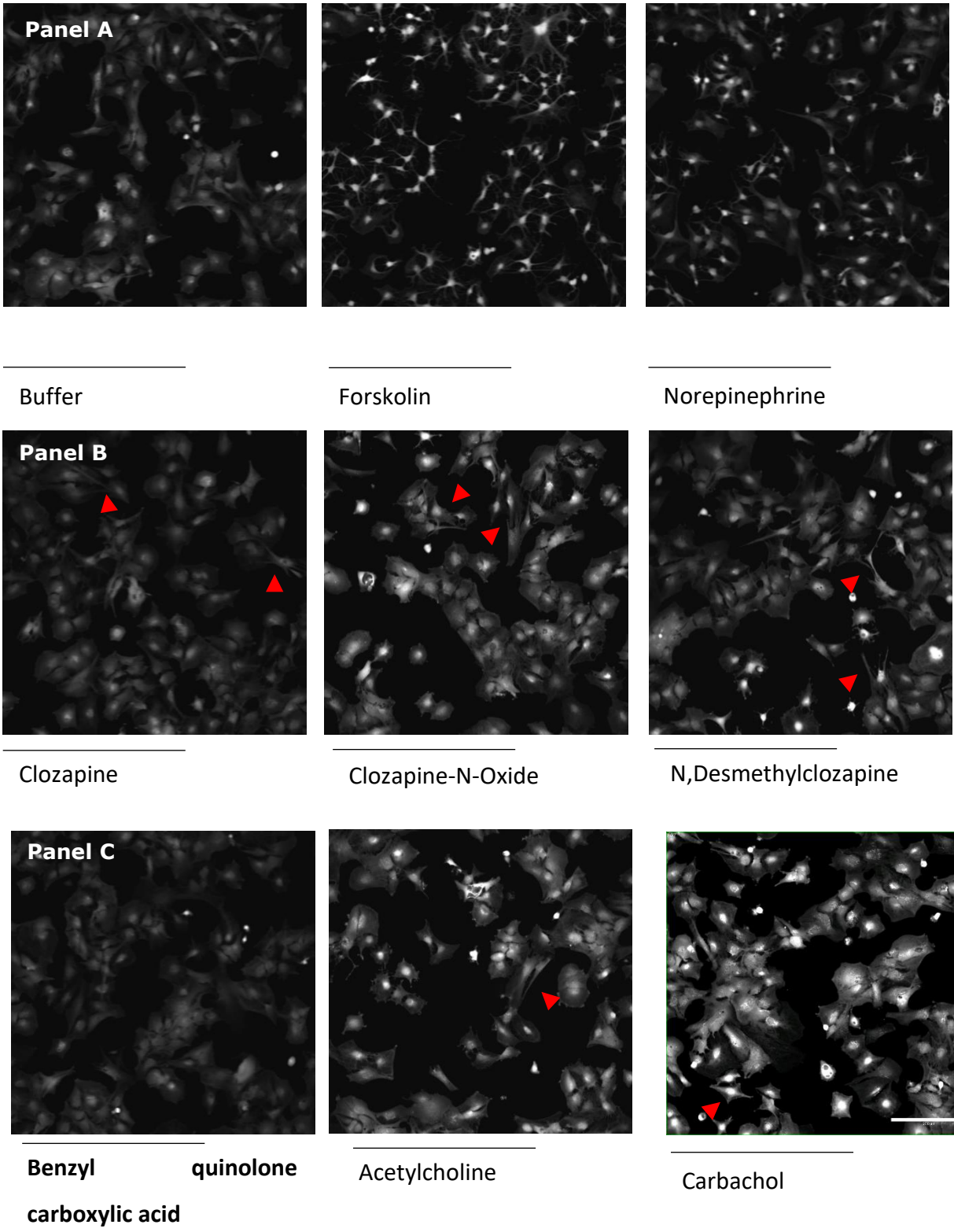


Figure 5.6: ***Morphological investigation of stellation in non-transfected cortical astrocytes****. Astrocytes were treated with ligands for 3hrs, before being loaded with Caclein AM, and imaged on the IX Ultra platereader. Panel A, shows forskolin (AC-activator), norepinephrine (β-ARR ligand) and vehicle treated astrocytes. Panel B, shows the clozapine derivatives and Panel C shows the muscarinic acting compounds. Each image is a representative experiment, and red arrows indicate cells which are deemed stellate. The scale bar indicates 200μm, and is the same for each image as that shown in carbachol.*

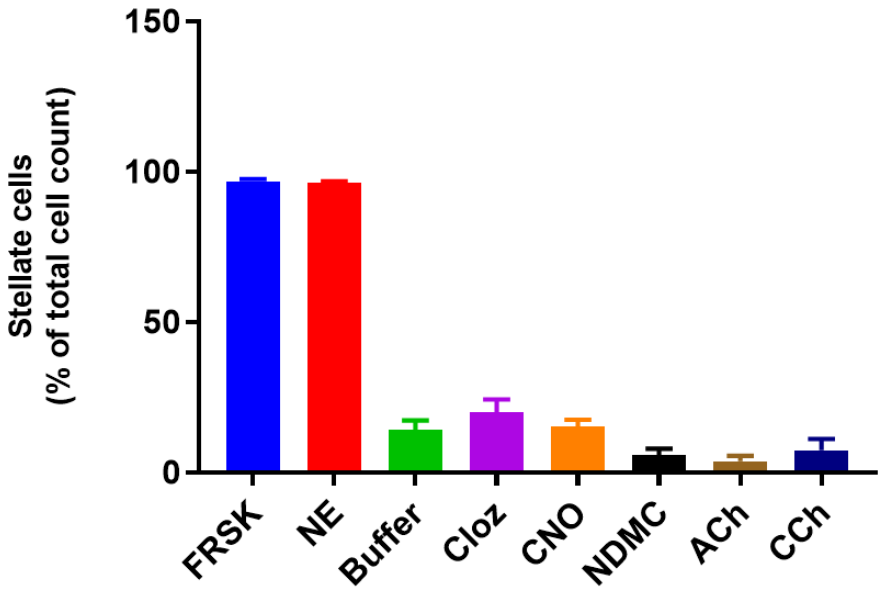


Figure 5.7: ***Percentage of cells identified as stellate after ligand addition****. Pharmacological investigation into the intracellular signalling pathways that elicited an astrocytic stellation response. Non-transfected cortical astrocytes were exposed to ligands for 3hrs before being morphologically evaluated for reduced cell body area with 3 or more long thin projections as indications of stellation using the fluorescent dye Calcein AM. Stellation is shown as a percentage of cells identified as stellate compared to total number of cells. Values are shown as mean ± SEM of experiment carried out in duplicate (n=8). On average, in each experiment 100 cells were counted in a blinded study.*

Pharmacological Ligand	Stellation cells (% total cell count)
Forskolin	96.27 ± 0.67
Norepinephrine	96.92 ± 0.82^{NS}
Buffer	12.64 ± 3.12***
Clozapine-N-Oxide	16.12 ± 2.33***
Clozapine	15.31 ± 2.38***
N, Desmethylclozapine	5.90 ± 2.22***
Acetylcholine	5.53 ± 2.41***
Carbachol	7.52 ± 3.78***

Table 5.3: ***Percentage of stellate cells after 3hrs of ligation addition.*** *One-way ANOVA with Dunnett's post hoc comparison shows the statistical significance between ligands as compared to forskolin. P = NS, non-signficant, P***;<0.001.*

Then, antagonist inhibition of stellation was used to identify the intracellular signalling pathways that control this process. The β-AR antagonist propranolol (10μM) was used against norepinephrine-induced astrocytes. After pre-treatment of this antagonist, it is clear they have a significant effect on reducing astrocytic stellation to a level comparable to that of vehicle-treated cells (Fig 5.8 & Table 5.4).

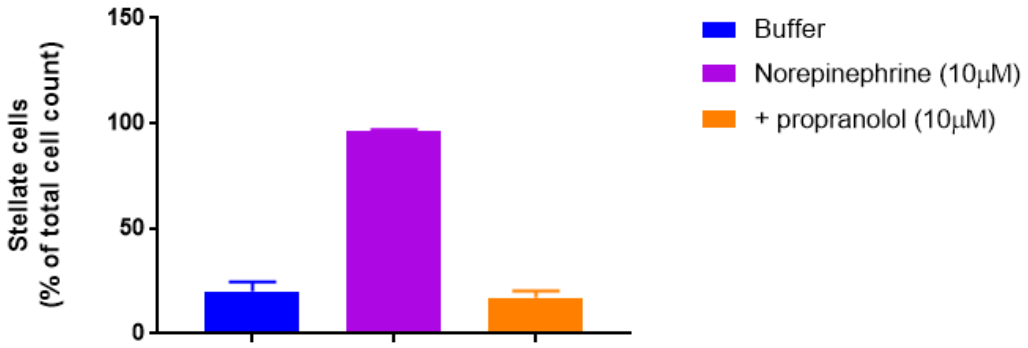


Figure 5.8: ***Antagonist effects of stellation in cortical astrocytes.*** *Pharmacological investigation into the intracellular signalling pathways which elicited an astrocytic stellation response. Non-transfected cortical astrocytes were exposed to propranolol for an hour before the agonists were incubated for 3hrs. Morphological evaluation for indications of stellation was carried out using the fluorescent dye Calcein. Stellation is shown as a percentage of the total cells and values are shown as mean ± SEM of experiment carried out in duplicate (n=8). On average, in each experiment 100 cells were counted.*

Pharmacological ligand	Stellate cells (% total cell count)
Norepinephrine	96.92 ± 0.82
Norepinephrine + propranolol	17.01 ± 3.34***
Buffer	12.64 ± 3.12***

Table 5.4: ***Percentage of stellate cells after 1hr pre-incubation with antagonist before 3hrs of ligation incubation.*** *An unpaired t-test shows the statistical significance between the number of stellate cells when norepinephrine was in the presence of the antagonist propranolol as compared to in the absence, ***P<0.001.*

5.2.4 Lipofectamine and Nucleofection Methods were able to Produce GFP-expressing Astrocytes, However were Unsuccessful in Producing Viable DREADD-Expressing Cells

In order to explore the two DREADD systems, the M1-DREADD Gq coupled calcium responses and the M3-DREADD chimera Gs-coupled responses in astrocytes, it was necessary to produce transient astrocytes expressing either of the DREADD receptors. Previously, in chapter 3, the method in which SNAP-tagged versions of these receptors were produced has been explained. SNAP-tagged rM3s-DREADD had been made previously by the Holliday Lab at the University of Nottingham.

Nucleofection was first used as a method of primary astrocyte transfection, due to its cell-specific protocol that should improve transfection efficiency. Transfections were carried out according to the manufacturer's recommended optimal conditions. It was recommended to use between 2-5µg of DNA. During optimisation, a median concentration of 3.5µg DNA appeared to be sufficient to produce some level of SNAP-labelling. When the DNA concentration was reduced no SNAP labelling was seen, while increasing the DNA concentration above 3.5µg did not appear to improve the efficiency of transfection when using the two DREADD constructs. Within the rat cortical preparation of astrocytes, for each brain ten T75 flasks were produced containing roughly 4 x10^6cells. Thus, the recommended number of cells (2x10^6cells) per transfection allowed for 2 transfections per flask. It was deemed that this would therefore be the maximum number of cells as an efficient use of animals. Therefore, after optimisation it was deemed 3.5µg of either SNAP hM1q-DREADD or SNAP rM3Ds-DREADD constructs was added to 2x10^6cells cells before nucleofection. However, it can clearly be seen that there is a high level of cell mortality for both DNA constructs even after optimisation (Fig. 5.x). The small percentage of SNAP-labelled cells present appear stellate and are generally low signal expressing cells.

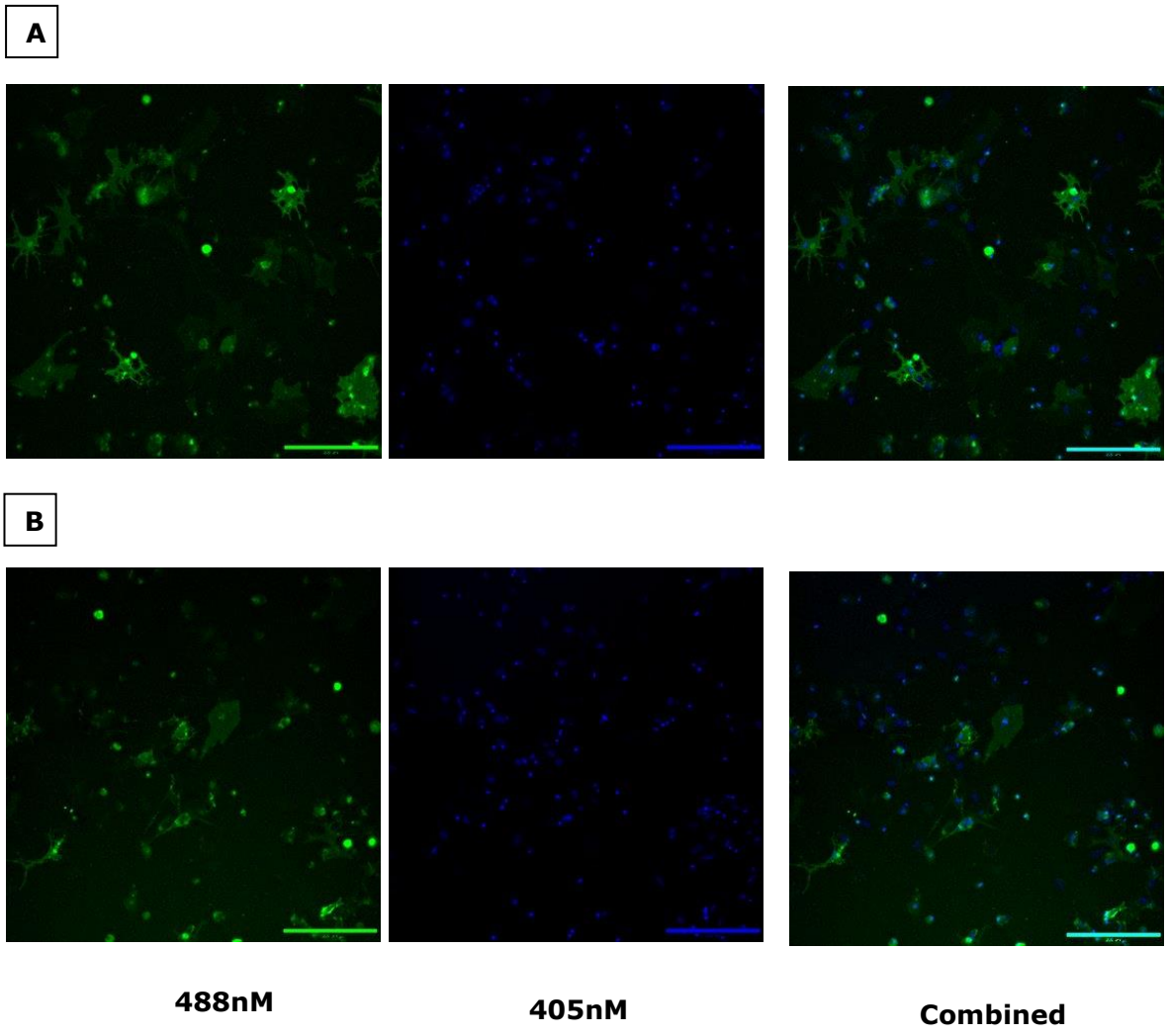


Figure 5.9: ***Astrocytes transfected using nucleofection, labelled with SNAP surface 488 and H33342.*** *Astrocytes were transfected with either hM1-DREADD (A) or rM3s-DREADD (B). Cells were imaged using the IX Ultra confocal plate reader, and visualised using SNAP staining at 488nm and H33342 nuclei stain at 405nm.*

In order to improve cell viability and reduce the damage caused by the nucleofection method, astrocytes were then transfected using Lipofectamine LTX. Again, the manufacture's recommended protocol was used for optimisation of astrocyte transfection. A 96-well plate format was chosen to transfect the cells, to reduce the need for high quantities of reagents. A cell density of 4×10^4 cells per well was found to produce a sufficient number of astrocytes per field of view. Astrocytes were plated in solution with 3.5µg of Lipofectamine-DNA complex. 24hr post lipofectamine transfection, cells were stained with SNAP surface 488, but no SNAP-labelling receptors could be seen indicating unsuccessful transfections. To further investigate, the lipofectamine-treated astrocytes were loaded with Calcein AM, which were then imaged, and were able to show the astrocytes were extremely stellate (Fig 5.10, A). Astrocytes were then left for another 24hrs to see if this time would be sufficient to reverse this morphology. At a total of 36hrs post transfection, it could be seen that the astrocytes were less stellate than before, however were still not suitable for use in the stellation assay (Fig. 5.10, B). This is an extremely critical limitation. The lack of DREADD expression may be overcome, however if the transfection method induces stellation within the astrocytes it would not be possible to investigate the role of Gαs-dependent morphological changes after ligand addition.

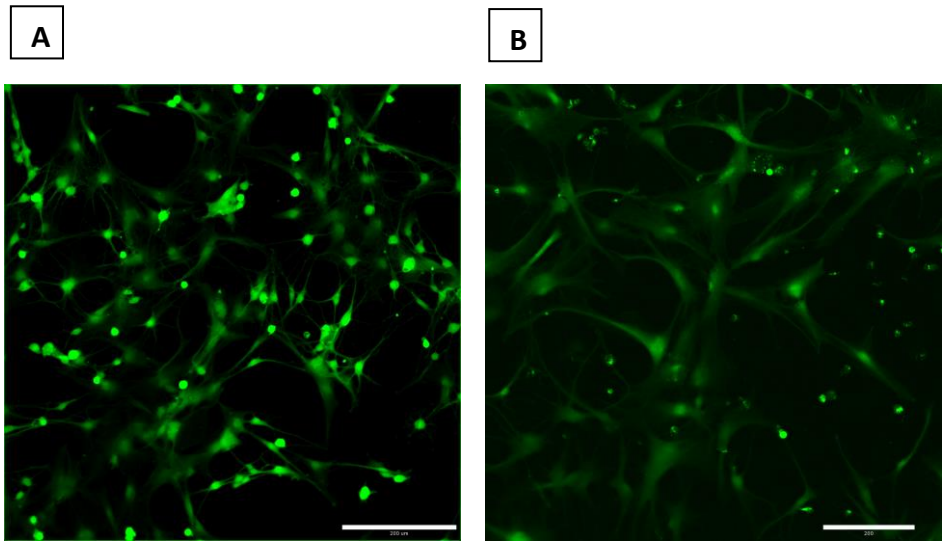


Figure 5.10: ***Astrocytes post lipofectamine transfection, imaged with Calcein AM, to investigate morpholigcal changes.*** *Astrocytes transfected with SNAP hM1q-DREADD using lipofectamin LTX were imaged to the IX Ultra platereader at 488nm. There was a lack of SNAP-tagged receptor expression, therefore viable cells were imaged with Calcein AM. A) 24hrs post transfection and B) 48hrs post transfection.*

To ensure optimal transfection conditions had been achieved a control GFP plasmid was used, and transfection was followed according the optimised protocols used for both nucleofection and lipofection. GFP was successfully expressed within the cells, following both lipofectamine (Fig 5.11, A) and nuecleofectamine (Fig 5.11, B). It appears the astrocyte morphology was not affected to the same extent as when DREADD receptors were used. This may be due to relatively small size of GFP, especially when compared to the DREADD receptors within the pc3.1neo vector. After nucleofection, there are small number of cells which appear to be slightly more fibrous, or to have extended processes, when compared to their rounded counterparts (Fig 5.3, B).

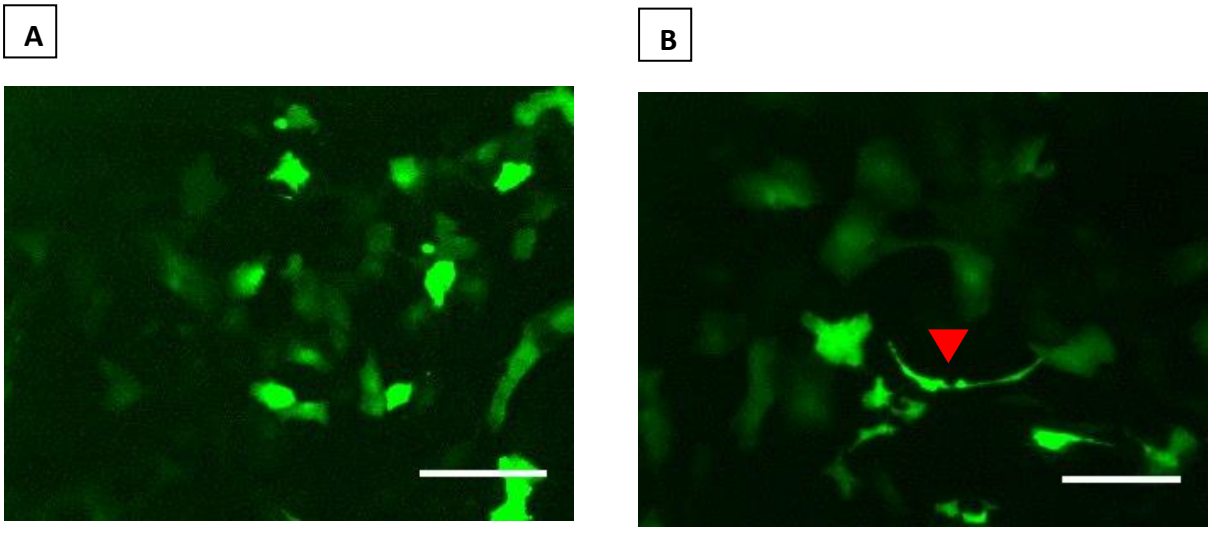


Figure 5.11: ***Control transfection protocols carried out using a GFP plasmid in order to verify methodology on non-transfected, imaged by the IX inverted microscope at 488nm****. A) Astrocytes transfected with lipofectamine LTX, with image taken 24hrs post transfection. B) Astrocytes transfected using the nucleofectamine method, image taken 18hrs post transfection.*

5.3 Discussion

In this chapter, non-transfected astrocytes were used to examine the muscarinic signalling pathways that produced calcium mobilisation in these cells, as well as, those ligands that could elicit astrocyte stellation. The muscarinic orthosteric ligands were used in order to investigate allosteric modulation induced by BQCA. Secondly, adrenergic antagonists were used to elucidate the receptors that norepinephrine could activate highlighting the differences between α- and β-adrenergic receptor signalling in astrocytes. This was to be compared against clozapine and its derivatives that selectively activate the M1-DREADD (Gq-coupled) and M3-DREADD (Gs-coupled). However, the *in vitro* methods of transfection tested here appear to be incompatible to produce DREADD-expressing astrocytes.

5.3.1 Assessment of Single Cell Calcium Mobilisation and Stellation to Investigate Muscarinic Pharmacology in Astrocytes

In order to expand our understanding from Chapter 4, calcium mobilisation measurements were investigated in astrocytes as an indirect measurement of Gq-coupled intracellular signalling. Using non-transfected cortical astrocytes gave the advantage of measuring native receptor responses, of receptors that are endogenously expressed within these cells. We have shown that calcium responses occur rapidly after agonist addition, but can be highly heterogeneous dependent on the ligand used to elicit such responses. We were also able to show that α-adrenergic receptors, which are also Gq coupled, when activated by NE, produce a marked calcium increase response supported throughout the literature (Pankratov and Lalo, 2015; El *et al.*, 2018). Area under the curve was investigated using the calcium traces obtained from astrocytes that responded after ligand addition. There was little difference between agonist responses, and a reduction in AUC values was only seen in the presence of forskolin, or when antagonists were present. This may show that overall changes in calcium response over time are relatively small, and perhaps

investigation into calcium spike frequency or maximal calcium spike would be a better measure in the future to distinguish between ligands.

The stellation assay provides a method to investigate agonists that can alter the astrocytic cytoskeleton forming stellate cells, which acts as an *in vitro* assessment of reactive gliosis. This assessment depends on morphological changes, that occur over hours but is a prominent alteration from protoplasmic morphology. This is particuarlly clear after the direct activation of AC after forskolin addition, and the activation of the β2-AR receptor upon norepinephrine binding.

These two functional assays can only measure indirect effects of receptor activation, or in the case of forskolin the direct activation of a downstream effector. It would therefore be of interest in future experiments to compare these data to a direct measure of receptor activation, such as the NanoBiT assay validated in Chapter 4. High resolution imaging has been shown to precisely decode the spatial aspects of astrocyte calcium events, for example, highlighting the role of microdomains in the fine processes of astrocytes (Di Castro *et al.*, 2011; Shigetomi, Patel and Khakh, 2016). Similarly, improvement in imaging techniques could reveal connections between the pharmacological activation and morphological changes produced in astrocytes (Katona *et al.*, 2012). However, these are expensive techniques that require highly specialised equipment, which were not feasible for the current study.

5.3.2 Agonist Functional Responses in Non-Transfected Astrocytes

We were able to confirm clozapine and its derivatives did not elicit calcium mobilisation or stellation in non-transfected astrocytes. This gives confidence to future studies that there will be minimal off-target effects of these ligands activating the endogenous mAChRs rather than the DREADDs. This is particularly interesting given that CNO is metabolised to clozapine, which is predicted to reduce the selectivity of this chemogenetic system by binding to a multitude of receptors (Mahler and Aston-Jones, 2018). Clozapine, an atypical antipsychotic, has been shown to reduce glutamate uptake in rat astrocytes, an effect shown to function primarily via GLT-1

(Vallejo-Illarramendi *et al.*, 2005). Clozapine has also been shown to induce L-glutamate release in astrocytes (Tanahashi *et al.*, 2012). Therefore, it is important to identify any off-target effects clozapine, and its derivatives, can have on non-transfect astrocytes before conclusions can be made on the use of these tools *in vivo*. Encouragingly, we have shown clozapine cannot produce a functional calcium response at these cortical astrocytes within our assay.

The muscarinic agonists, acetylcholine and carbachol, were able to produce calcium mobilisation in non-transfected astrocytes, a result supported by published data (Porter and McCarthy, 1997; Fiacco, Agulhon and McCarthy, 2009). This effect could be blocked by atropine, confirming calcium signalling occurs through muscarinic intracellular signalling. Contrary to literature, the M1 muscarinic allosteric modulator BQCA (100µM) did not significantly enhance calcium mobilisation in the presence of the mAChR agonists. When analysed in LgBiT SNAP M1-WT expressing HEK cells, in Chapter 4, BQCA was shown to induce mini Gq complementation at 1µM. Therefore, it could be expected that 100µM BQCA would elicit a response at the native mAChRs expressed in astrocytes, especially when considering the effects of calcium amplification in cells. Previously, the M1 selective antagonist pirenzepine has been shown to reduce astrocytic calcium signalling in response to carbachol (Shelton and McCarthy, 2000). It is therefore requires further elucidation as to why the M1 selective allosteric modulator BQCA did not elicit a modulatory effect.

Both the M1- and M3-mAChRs are expressed in astrocytes with M3 having a greater relative expression than M1 in the cortex, shown by RNA-Seq (Chai *et al.*, 2017). It would therefore be of interest to determine the differences in their Gαq-coupled responses in relation to calcium mobilisation. It could be possible that BQCA did not show significant efficacy as a PAM at the astrocyte because of the relatively higher expression of M3 mAChR which BQCA has reduced affinity for. In the future, the planned DREADD studies would be highly beneficial to elucidate M1-dependent calcium signals in astrocytes. However, it would be necessary to use a ligand that has high affinity for the DREADD receptor over endogenously expressed mAChRs, which CNO might not be able to provide *in vivo* (Mahler and Aston-Jones, 2018). Highly

selective allosteric modulators would also allow for the differences between M1 and M3-mAChR to be delineated.

Norepinephrine is one of the most abundant neurotransmitters in the brain which affects neuronal and glial cell activity through adrenergic receptors activation and IP3 mediated calcium oscillations (Smythies, 2005; O'Donnell *et al.*, 2012),. We confirmed norepinephrine, when activating endogenous adrenergic receptors, can elicit robust calcium mobilisation in our single cell analysis in a manner similar to published data (O'Donnell *et al.*, 2012; Ding *et al.*, 2013; Paukert, Agarwal, Cha, Van A Doze, *et al.*, 2014). Through inhibition of α-adrenergic receptors with prazosin (α1-adrenergic antagonist), it was shown that norepinephrine signals via this Gq-coupled receptor to produce a calcium response.

The muscarinic ligands, and clozapine derivatives, had no effect on the stellation observed in astrocytes confirming the lack of potency for Gαq signalling in this process. Norepinephrine was shown to play a dual role when activating adrenergic receptors expressed by the astrocytes. Through inhibition of α-adrenergic receptors by prazosin, it was shown that norepinephrine signals via this receptor to produce a calcium response. Conversely, propranolol (nonselective β-adrenergic receptor blocker) was used to propose that norepinephrine-induced astrocytic stellation was mediated by Gαs activation at the β-adrenergic receptors.

This pharmacological data validates the assays used here, calcium mobilisation and stellation, and that there is likely no off-target effects when using clozapine and its derivatives in DREADD-expressing astrocytes. Therefore, in future experiments astrocytes evaluated in these assays would be a suitable method to investigate DREADD functionality.

5.3.3 DREADD Receptors Could Allow the Investigation of the Cross-Talk between Calcium and cAMP Signalling

This study has shown that astrocytes in culture express both α- and β-adrenergic receptors, a result reported also in the brain (Ebersolt, Perez and Bockaert, 1981;

Hertz *et al.*, 1984; Atkinson and Minneman, 1991). Structural analysis revealed α- and β-adrenergic receptors in astrocytic processes (Aoki, 1992; Aoki, Venkatesan and Kurose, 1998), which are often closely associated with terminals of axons of noradrenergic neurons (Cohen, Molinatti and Hamel, 1997; Latsari *et al.*, 2002). The activation of β-adrenergic receptors is well documented as the mechanism underlying morphological changes in astrocytes. This activation causes adenylate cyclase to catalyse the conversion of ATP to cAMP. The cAMP-dependent protein kinase then goes on to phosphorylate cytoskeletal proteins altering the cell morphology (Shain *et al.*, 1987; Won and Oh, 2000; Sherpa *et al.*, 2016).

The simultaneous expression of α- and β-adrenergic receptors, triggers distinct cellular events for both calcium oscillations and cAMP intracellular release (Horvat, Zorec and Vardjan, 2016), however it has also been suggested there is cross-talk between these two signalling molecules (Cooper, Mons and Karpen, 1995). This early report found oscillations in cAMP were dependent upon the temporal patterns of calcium inhibition of adenylyl cyclase. More recently it was found the temporal patterns of calcium signalling was reliant on cAMP-dependent PKA activation, and these oscillations could be linked to early signs of stellation (Ujita *et al.*, 2016). It has been shown that injured astrocytes swell rapidly leading to oedema and studies suggest that this volumetric change is controlled in part by both calcium and cAMP (Song and Gunnarson, 2012). Pharmacological analysis of these astrocytes showed an increase in β-AR/cAMP signalling pathway which then mediated attenuation of intracellular calcium excitability (Horvat, Zorec and Vardjan, 2016). Significantly, these results show that intracellular calcium and cAMP interactions can have a clear causal direction, and may play a role in disease.

In future, it would be of interest to use the two DREADDs with their selective coupling to the two different G protein pathways to explore this intracellular cross-talk more thoroughly. In particular, allosteric modulation of Gq-mediated fast onset calcium responses could be assessed to determine if positive allosteric modulation increases the magnitude, or frequency, of calcium spike whether this alters the onset of stellation. Can we use calcium spiking patterns to predict whether a cell will become stellate? Conversely, it would be of interest to see whether calcium signalling

is disrupted within stellate astrocytes or if the spatiotemporal patterns of calcium signalling changes as stellation progresses and what this means for the cross talk between cells at the synapse in disease.

5.3.4 Reconciling the Difficulties of *In Vitro* Transfection Methodologies

Successful delivery of plasmid DNA is a crucial step for studying astrocytic cell biology at a molecular level, through over-expression of wild type or mutant versions of a receptor. Therefore, efficient transfection is important for the success of these experimental techniques especially in more challenging primary cells (Tinsley *et al.*, 2004). Astrocytes grown in primary cell culture retain many of the properties exhibited by these cells *in situ*. Thus, the use of techniques to selectively alter expression of specific proteins in these cells has considerable potential to assist in understanding the normal function of these cells and their responses to abnormal conditions associated with disease.

Transfection of astrocytes must be considered in some detail due to the particular need to preserve the cellular properties of this cell, which can easily take on a stellate morphology in response to a plethora of stimuli. Astrocytic activation is associated with changes in its molecular properties, as well as, dramatic morphological changes that would be major limitations when evaluating the effects of pharmacological agents on these cells. It is generally accepted viral transduction can achieve more than 80% transduction *in vivo*, including in astrocytes (Lundberg *et al.*, 1996). However, this technique has many disadvantages which can be mitigated by utilising more commonly used *in vitro* transfection techniques such as lipofection or nucleofection (Djurovic *et al.*, 2004).

Over time, there have been significant improvements in transfection efficiency using nucleofection. The majority of papers which discuss this method of transfection use neurones and are able to show impressive transfection efficiencies up to 95% (Fallini, Bassell and Rossoll, 2010; Marwick and Hardingham, 2017; Dai *et al.*, 2019; Sauter *et al.*, 2019); fewer papers evaluate astrocytes in particular. One paper

reported a maximum transfection efficiency of 10% in their astrocyte population (Mertz *et al.*, 2002). This appears comparable to other primary cell types, for example primary cardiomyocytes had 7.5% of cells transfected after nucleofection (Djurovic *et al.*, 2004). On the other hand, there have been substantially higher transfection efficiencies within the literature. A group achieved 76% of astrocytes having been transfected, however they also experienced an immediate 20% cell death after nucleofection (Muyderman *et al.*, 2010). Muyderman *et al*., state cell debris was instantly removed in subsequent handling of their astrocytes. This differs to the protocol followed in this chapter as astrocytes were directly plated after nucleofection, without a wash step, in the hope of retaining as many cells as possible. It may be that cytotoxicity from cell debris and the release of intracellular components could have increased the cell mortality rate over the initial 18hr incubation period. It appears that even with improved efficiencies cell death is still a critical limitation to this method, and probably will be a long term feature to this highly reactive cell type.

Lipofection was therefore evaluated in the hope it would overcome the high cell death, and reduce the number of cells that became reactive (Karra and Dahm, 2010; Kaestner, Scholz and Lipp, 2015). Again, the transfection rate in the literature was quite low with astrocytes being shown to have approximately 10-20% transfection efficiency (Wu *et al.*, 2000; Wolfes *et al.*, 2017), however a recent paper only achieved 6% of astrocytes having been transfected (Alabdullah *et al.*, 2019). In our data it appeared that there were strong inconsistencies in whether or not the astrocytes would be transfected. Then, when a positive transfection occurred, the astrocytes appeared to express low levels of the SNAP-tagged receptor and/or became stellate in morphology.

A transfection method that may be useful for future experiments is the use of polymeric gene carriers, which have been as an alternative to viral vectors but with comparable transfection levels (Kang, Lee and Bae, 2005). Poly-(β-amino ester)s (PBAEs) have been shown to condense plasmid DNA into nanoparticles with a high level of transfection shown in stem cells (Keeney *et al.*, 2013). PBAEs in primary human astrocytes have given encouraging results, with transfection efficiencies reported up to 56% and cell viability between 53-100% (Li *et al.*, 2016).

In opposition to the continuous improvement of transfection efficiencies, there are fundamental advantages to a low transfection rate. When cells are imaged, in one field of view, there are non-transfected cells alongside positively transfected, expressing cells. It is therefore possible to use the non-transfected cells as an internal control. Both cell types, expressing and non-expressing, will have been exposed to the same transfection procedure, ligand addition and imaging protocol. This is a method which can be truly beneficial in live-cell imaging experiments, for example in studying synaptic vesicle trafficking and endosomal dynamics (Lasiecka and Winckler, 2016). That being said, it is clear here that major improvements are needed to improve cell viability after transfection and to find an optimal protocol which does not alter cell morphology and produce reactive astrocytes. Once this is achieved, a lower transfection rate may be acceptable. However, currently it would be best to use transgenic animals which have been successfully expressing DREADDs for some time.

5.4 Conclusion

In this chapter, it was shown that clozapine and its derivatives to lack off-target effects when investigating calcium mobilisation and cAMP-dependent stellation in primary cortical astrocytes. This indicates these pharmacological ligands to be compatible for activation of selective DREADD- signalling pathways with minimal activation of the endogenously expressed GPCRs. Astrocytic calcium mobilisation did not support BQCA as a positive allosteric modulator at M1 mAChRs endogenously expressed in primary astrocytes, perhaps due to relative expression levels of this receptor compared to M3 mAChR. Interestingly, norepinephrine was shown to act via both α- and β-adrenergic receptors, to induce calcium mobilisation and stellation, respectively. This would be an interesting ligand to compare to selectively mimic using the two DREADDs to selectively target Gαq and Gαs signalling pathways.

Further studies should optimise astrocytic transfection, potentially by using polymeric gene carriers as an alternative *in vitro* method, and express the DREADDs as planned to investigate Gq-dependent calcium signalling and Gs-dependent stellation. This would be interesting to compare to the effects seen elicited by norepinephrine and explore the interplay between calcium and cAMP intracellular signalling.

Chapter 6

GENERAL DISCUSSION

The M1 mAChR has been implicated as an attractive therapeutic target for diseases where cognitive processes are impaired, such as AD and schizophrenia (Foster *et al.*, 2014). Identification of subtype-selective therapeutics has been a time-consuming challenge to achieve using pharmacological agents designed to bind the orthosteric site of a GPCR. The development of highly selective DREADDs and allosteric modulators, which bind to a topographically distinct site from the orthosteric binding site, have significantly improved how subtype selective pharmacology for the M1 receptor can now be investigated. Ultimately, greater understanding of allosteric modulation may also pave the way for more selective therapeutics acting at CNS muscarinic receptors, present within both neurones and glial cells. This thesis aimed to provide insight into the pharmacology of the M1-DREADD receptor and the extent to which it could be used as a tool to investigate allosteric modulation, in recombinant cells and astrocytes.

6.1 Improved Understanding of Orthosteric and Allosteric Ligands Acting at M1-DREADD Receptors

In this thesis, the pharmacology of the M1-DREADD has been demonstrated with a range of orthosteric muscarinic ligands, across a number of signalling readouts; calcium mobilisation, complementation assays and ligand binding studies. Within the same assays, we identified clozapine and N, desmethylclozapine as agonists with higher affinities for the M1-DREADD than CNO itself. Both results have implications for the way in which DREADDs can be used *in vivo*, particularly, when considering the assumption that CNO is 1) a biologically inert ligand and 2) provides selective stimulation of the DREADD receptor over other orthosteric ligands. In fact, it may be that clozapine is the main stimulus of DREADD function, but also leads to off-target effects having been shown to bind to endogenous ligands, such as dopamine D2/3 receptors (Olsen, Brennum and Kreilgaard, 2008). Novel selective DREADD ligands should therefore be designed, with particular interest given to finding a compound that has a slower rate of metabolism in the body to avoid further active metabolites that would reduce the systems selectivity. Compound 21 (11-(1-piperazinyl)-5H-

dibenzo[*b*,*e*][1,4]diazepine) has been suggested as such a ligand, with high permeability of the blood brain barrier and long-lasting effects, which is not metabolised to clozapine like CNO. A recent study found that this ligand did bind a number of endogenous receptors, including muscarinic, dopamine and adrenergic receptors (Jendryka *et al.*, 2019). This is a result supported by previous study also found compound 21 binds D1, D2 and M4 receptors (Thompson *et al.*, 2018). Both studies concluded that this unselective binding did not cause any major behavioural differences, of the parameters in the 5-choice serial-reaction-time task (5-CSRTT) test compound 21 showed a mild decrease in attentional accuracy (Jendryka *et al.*, 2019); however this is likely dependent on the animal model and assay being assessed.

BQCA was shown to act as a positive allosteric modulator for the M1-DREADD, across all signalling pathways investigated. Its mechanism and effects as a low potency agonist, previously reported, were all found in our study. We were able to show the M1-DREADD preserved the allosteric binding site in a comparable manner to the M1-WT receptors. This is encouraging data that shows the M1-DREADD system could be used to investigate allosteric modulation *in vivo*. Although, it would be necessary to consider the probe dependence of each allosteric modulator tested at the DREADD receptor. A drawback to the selectivity of the DREADD system is that the benefits of allosteric modulation; selectively amplifying the spatiotemporal effects of the endogenous ligand/neurotransmitter release, would be lost.

Future studies should extend the pharmacological profiles of a number of M1-allosteric modulators at the M1-DREADD receptor. Recently, a number of studies have been able to suggest different mechanisms of action for new allosteric modulators that do not function as BQCA does.

6.2 Novel Assay Systems for Exploring M1-DREADD Ligand Binding and Signalling Kinetics

This study successfully identified novel fluorescent ligands that could be used to determine ligand-binding affinity at the M1-DREADD. This is a clear advantage over

previous studies that have only used radioligands (Abdul-Ridha *et al.*, 2013b; Sophie J Bradley *et al.*, 2018). Beyond the advantages in safety considerations, these fluorescent ligands are able to image living whole cells, in a plate reader and allow for a homogeneous binding assay format, in which there is no need for the time-consuming separation of bound from the free ligand. BRET-based quantification of ligand binding has recently been developed using NanoLuc in conjunction with fluorescent ligands (Stoddart, Kilpatrick and Hill, 2018). Such proximity-based methods allow for real time measurements of the ligand binding kinetics at M1-DREADD receptors, with high levels of specificity that overcomes nonspecific binding commonly experienced when using fluorescent ligands. We were able to report on the effects of BQCA on orthosteric ligand affinity within this assay, however we also showed that the fluorescent likely binds to both the orthosteric and allosteric site complicating analysis. Developments in the structure used as the pharmacophore, for example using BQCA, could allow new allosteric compounds to be screened for their binding capabilities at the allosteric site in M1-WT or M1-DREADD receptors. Another way to expand on this data may be to use the fluorescent **III** within a Homogeneous Time Resolved Fluorescence (HTRF) assay. This is a technology which combines FRET with the time resolved measurement of fluorescence which would allow for greater sensitivity when exploring the protein-protein interaction between the SNAP-labelled receptors and the novel **III** compound.

The importance of signalling kinetics has been increasingly recognised as an important determining factor to the type of functional response that is seen within a cellular system. For example, the magnitude of cAMP signalling, in fibroblasts, was shown not to be as important as the temporal pattern (acute vs. chronic) in determining proliferation rates (Roberts *et al.*, 2018). It is therefore necessary that assay systems be designed to report the kinetic profiles of agonists' responses. We have developed the NanoBiT complementation assay to monitor the kinetics of receptor interactions with specific effector proteins (mini Gq or β-ARR2). This assay is in a single plate format and was shown to be successful in both M1-WT and M1-DREADD receptors. To improve the physiological relevance of this system in the future, receptor recruitment of the full-length Gαq subunit should be explored, rather

than just the mini Gq. It would also be advantageous to avoid, or reduce, receptor modification of the receptors with the aim of mitigating any deleterious alterations to normal cell function.

There is a degree of probe dependence influencing the nature of BQCA's allosteric effects dependent whether CNO or ACh is bound to the receptor. When evaluating the PAM effects it was shown that BQCA increases the potency of ACh's effect, whereas BQCA significantly increased the maximal effect produced by CNO. This probe dependence is supported within the literature (van der Westhuizen *et al.*, 2018), though in this instance it may reflect a similar mechanism underlying BQCA's action, in the presence of orthosteric agonists of differing efficacy at their respective receptors (i.e. CNO is a partial agonist in the system, with an increased stabilisation of active receptors in the presence of BQCA). The risk of probe dependence is a general consideration when using DREADDs. In future, to explore the action of other M1 allosteric modulators (even if the binding sites appear preserved), *in vitro* investigations should always confirm the allosteric modulator's action prior to any use in animal models.

The three different clozapine derivatives were seen to act with comparable potency in eliciting a calcium response after activating the M1-DREADD receptor. However, competition binding with the fluorescent ligand AP164 provided pKi values that indicated clozapine to have much greater affinity for the DREADD than N, desmethylclozapine or CNO. This adds another limitation when investigating these chemogenetic tools *in vivo*. CNO is known to be easily metabolised to clozapine and N, desmethylclozapine within the body. Animal studies have shown clozapine to occupy endogenous receptors after CNO administration (Bærentzen *et al.*, 2019), thereby limiting the *in vivo* selectivity of CNO ligand, and affecting valid interpretation of DREADD receptor "responses" *in vivo*. Therefore, the development of more selective DREADDs ligands would be a great advantage (Campbell and Marchant, 2018). Ligands that are selective for individual DREADD subtypes would also allow for a number of DREADDs to be activated and enable multiplex designs of receptor activation to be achieved. Recently, it was shown that activation of M3-DREADDs and

KORD could be selectively controlled using CNO and salvinorin B, respectively (Vardy *et al.*, 2015).

6.3 The Role of the Muscarinic Receptor System in Astrocyte Calcium Signalling and Stellation

It is also important to study the functional impact of different signalling kinetics in a primary cell system. Astrocytes are a key CNS cell type where this can be addressed. Astrocytes are a cell type in which the kinetics of calcium and cAMP signalling has been suggested to be critical for their normal physiological function of the CNS. The spatiotemporal dynamics of these intracellular signalling pathways are extremely complex and how the profiles of rapid second messenger increases (calcium and cAMP) might integrate into longer term morphological changes (stellation) is of great interest.

BQCA, which is selective for the M1 mAChR, did not act as a PAM within astrocytic calcium responses evoked by muscarinic ligands, potentially due to astrocytes endogenously expressing a high number of M3 mAChR compared to that of M1 mAChR. We were also able to show that external stimuli that cause astrocytes to become stellate act through the β-adrenergic receptor activation pathway, or through the direct activation of adenylate cyclase. Muscarinic ligands were unable to induce stellation, thus the use of M3s-DREADD, with the ICL 2 and 3 replaced by those of the β-adrenergic receptor (Farrell *et al.*, 2013), has the potential to be a highly selective tool to investigate cAMP-dependent changes in astrocyte morphology, *in vitro* and *in vivo*. As BQCA appears to act by increasing the overall abundance of receptors in an activated conformation it would be of interest to confirm this effect is still functional within this modified receptor in future experiments.

It would also be of interest to further develop our knowledge of the downstream effectors of the M1 and M3 Gαq muscarinic receptors. G protein-independent signalling is an area with increasing interest. Particularly, β-ARR2 independent signalling has been implicated in an increasing number of astrocytic functions, including in the inflammatory response (Fan, 2014) and alterations in the cytoskeleton

(Xie, Petravicz and McCarthy, 2015); pathways critical to astrocyte stellation. Therefore, it would be of interest to develop NanoBiT complementation assays that monitored β-ARR2 interaction with various effectors that it is reported to scaffold (for example, members of the ERK protein kinase cascade (Tohgo *et al.*, 2002; Gurevich and Gurevich, 2018). Given suitable transfection efficiency, these sensors could be expressed in primary astrocytes to investigate how native muscarinic and β-adrenoceptors trigger β-arrestin as a scaffold molecule to activate downstream effectors. Advances in subcellular luminescence imaging of NanoBiT complexes (Dixon et al 2016) might also provide evidence of whether these complexes are formed at the plasma membrane, in the cytosol, or are located in endosomes following receptor internalisation.

6.4 Future Perspective in Methodologies to Explore Spatiotemporal Signalling in Astrocytes

The importance of the spatiotemporal aspects of intracellular signalling molecules is at the forefront of scientific thought (Araque *et al.*, 2014; Cresswell-Clay *et al.*, 2018; Gordleeva *et al.*, 2019). This appears to be of particular importance when considering communication between neurones and astrocytes, where the temporal and spatial aspects of signalling have been suggested to be fundamental to their mechanism of action (Fields and Stevens-Graham, 2002; Araque and Navarrete, 2010). Information processing and neuronal plasticity has been shown to depend on neuronal firing frequency and cells have a threshold-dependent frequency that can induce activation (Kang and Othmer, 2009). Astrocyte calcium signalling includes local fast responses as well as, slow global responses resulting from the summation of such signals (Gordleeva *et al.*, 2019). Similarly, spatial organisation of the components that regulate cAMP signalling has been shown to regulate the specificity of signal transduction in many cell types (Lefkimmiatis and Zaccolo, 2014).

While chemogenetic approaches have unlocked the ability to selectively activate specific signalling pathways and mAChR subtypes *in vivo*, the main disadvantage is regulating temporal activation of these receptors (Bradley, Tobin and Prihandoko, 2018), which is governed by the binding kinetics of the ligand. Future

development of different DREADD agonists, with varying binding kinetics, (perhaps in part by using fluorescent ligand technologies to measure these kinetically (Herenbrink *et al.*, 2016; Sykes *et al.*, 2017; Sykes, Jain and Charlton, 2019)) might expand the toolbox in this regard.

A second approach is to develop the means to precisely regulate the delivery and the removal of the ligand of interest to the target cells. One option, microfluidics technology (Velve-Casquillas *et al.*, 2010)), was considered during the PhD. Microfluidic technology manipulates small amounts of fluids within a cellular chamber, and can be used as a tool for drug delivery (Damiati *et al.*, 2018). The majority of studies are carried out using a polydimethylsiloxane (PDMS)-based cell chamber, which allows the cells' microenvironment to interact with environmental oxygen and necessary component of the surrounding cell media. Astrocytes have been shown to have high viability within such chambers (Vukasinovic *et al.*, 2009). One model of microfluidic control is aimed at creating laminar flow between two streams of fluid forming a gradient at their interfaces. This allows for precise control of ligand concentration and the time cells are exposed to ligands, which can be varied in dynamic patterns (Whitesides, 2006). Cells can be loaded with a fluorescent dye, such as Fluo-5F AM, while the agonist solution is loaded with Alexa Fluor 594. Therefore, while intracellular signalling can be imaged, the temporal pattern of agonist addition can also be visualised and composite images allows cell signalling to be associated with the agonist being present (Fig 6.1).

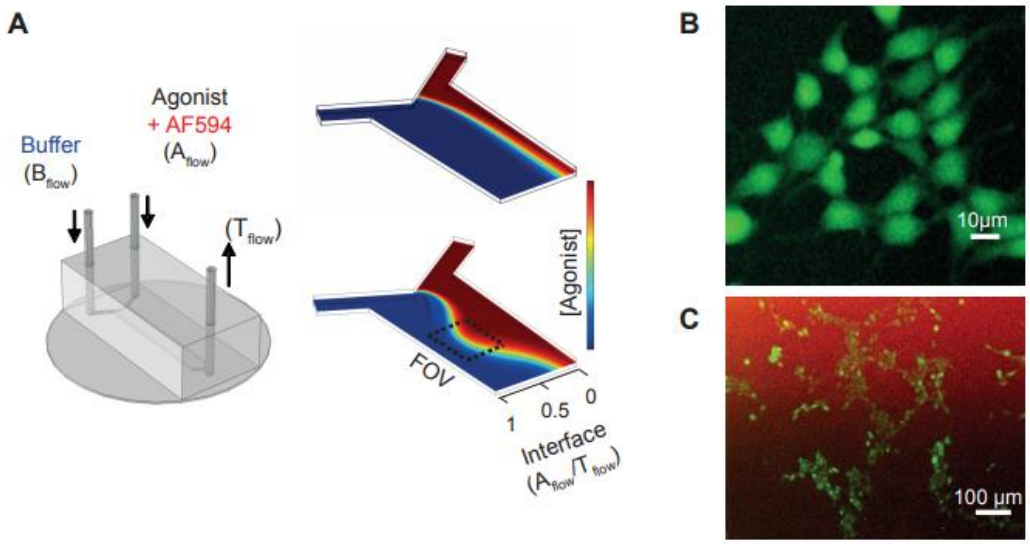


Figure 6.1: Microfluidic system in which laminar flow is used to control agonist addition to cells. A) Shows the PDMS cell chamber mounted on glass coverslip, where buffer (blue) forms laminar flow with agonist labelled with Alexa Fluor 594 (red). B) HEK293 cells seeded in the chamber and loaded with Fluo-5F AM. C) Composite of Alexa Fluor 594 and Fluo5F AM fluorescence in a typical field of view. Figure previously made by Dr. Wayne Croft (University of Nottingham).

Microfluidic ligand addition provides a novel assay that investigates intracellular signalling dynamics that would not have been observed under non-changing stimulus addition (Dhumpa and Roper, 2012). It has long been noted that there are clear differences between pulsatile stimulus delivery compared to continuous delivery at the whole cell level for calcium signalling (Schöfl *et al.*, 1991) and cAMP signalling (Schöfl *et al.*, 1993). We had initially aimed to investigate the spatiotemporal aspects of astrocytic signalling evoked by microfluidic stimulation of DREADD signalling, and how this was affected in the presence or absence of BQCA. Unfortunately, a variety of technical challenges prevented this ultimate aim from being realised, but it may still be addressed in future through new developments in chamber design, cellular support, and flow control.

6.5 Overall Conclusion

In conclusion, this thesis provided new insights into the orthosteric and allosteric ligand pharmacology at M1-DREADD receptor, which provide further context for the wide use of this system in chemogenetic investigations. We identified novel tools techniques to investigate ligand binding at the DREADD receptors using fluorescent imaging, and developed luciferase complementation assays to monitor the kinetics of

M1-WT and M1-DREADD signalling via different effectors. Although ultimately we were unable to use DREADDs in primary astrocytes, we were also able to characterise the role of muscarinic activation in regulating astrocytic calcium signalling and stellation pathways, relevant to normal physiology as well as in gliosis.

References

Abdul-Ridha, A. *et al.* (2013) 'Allosteric Modulation of a Chemogenetically Modified G Protein-Coupled Receptor', *Molecular Pharmacology*, 83(2), pp. 521–530. doi: 10.1124/mol.112.083006.

Abdul-Ridha, A., Lane, J. R., Mistry, S. N., López, Laura, *et al.* (2014) 'Mechanistic insights into allosteric structure-function relationships at the M1 muscarinic acetylcholine receptor.', *The Journal of biological chemistry*. American Society for Biochemistry and Molecular Biology, 289(48), pp. 33701–11. doi: 10.1074/jbc.M114.604967.

Abdul-Ridha, A., López, L., Keov, P., Thal, David M., *et al.* (2014) 'Molecular Determinants of Allosteric Modulation at the M $_1$ Muscarinic Acetylcholine Receptor', *Journal of Biological Chemistry*. American Society for Biochemistry and Molecular Biology, 289(9), pp. 6067–6079. doi: 10.1074/jbc.M113.539080.

Abdul-Ridha, A., López, L., Keov, P., Thal, David M, Mistry, S. N., Sexton, P. M., Robert Lane, J., *et al.* (2014) 'Structure-function analysis of M 1 receptor allostery 1 Molecular Determinants of Allosteric Modulation at the M 1 Muscarinic Acetylcholine Receptor'. doi: 10.1074/jbc.M113.539080.

Abrams, P. *et al.* (2006) 'Muscarinic receptors: their distribution and function in body systems, and the implications for treating overactive bladder.', *British journal of pharmacology*. Wiley-Blackwell, 148(5), pp. 565–78. doi: 10.1038/sj.bjp.0706780.

Aguado, F. *et al.* (2002) 'Neuronal activity regulates correlated network properties of spontaneous calcium transients in astrocytes in situ.', *The Journal of neuroscience : the official journal of the Society for Neuroscience*, 22(21), pp. 9430–44. Available at: http://www.ncbi.nlm.nih.gov/pubmed/12417668 (Accessed: 9 September 2019).

Agulhon, C. *et al.* (2012) 'Calcium Signaling and Gliotransmission in Normal vs. Reactive Astrocytes', *Frontiers in Pharmacology*, 3, p. 139. doi: 10.3389/fphar.2012.00139.

Agulhon, C. *et al.* (2013) 'Modulation of the autonomic nervous system and behaviour by acute glial cell Gq proteinâ•'coupled receptor activation in vivo', *J Physiol*, 59122(591), pp. 5599–560922. doi: 10.1113/jphysiol.2013.261289.

Alabdullah, A. A. *et al.* (2019) 'Estimating transfection efficiency in differentiated and undifferentiated neural cells', *BMC Research Notes*. BioMed Central, 12(1), p. 225. doi: 10.1186/s13104-019-4249-5.

Alexander, G. M. *et al.* (2009) 'Remote control of neuronal activity in transgenic mice expressing evolved G protein-coupled receptors.', *Neuron*. NIH Public Access, 63(1), pp. 27–39. doi: 10.1016/j.neuron.2009.06.014.

Allen, J. A. and Roth, B. L. (2011) 'Strategies to Discover Unexpected Targets for Drugs Active at G Protein–Coupled Receptors', *Annual Review of Pharmacology and Toxicology*, 51(1), pp. 117–144. doi: 10.1146/annurev-pharmtox-010510-100553.

Allman, K. *et al.* (2000) 'Scanning Mutagenesis Identifies Amino Acid Side Chains in Transmembrane Domain 5 of the M_1 Muscarinic Receptor that Participate in Binding the Acetyl Methyl Group of Acetylcholine', *Molecular Pharmacology*, 58(1), pp. 175–184. doi: 10.1124/mol.58.1.175.

Alt, A. *et al.* (2016) 'Evidence for Classical Cholinergic Toxicity Associated with Selective Activation of M1 Muscarinic Receptors', *Journal of Pharmacology and Experimental Therapeutics*, 356(2), pp. 293–304. doi: 10.1124/jpet.115.226910.

Alvaro, C. G. and Thorner, J. (2016) 'Heterotrimeric G Protein-coupled Receptor Signaling in Yeast Mating Pheromone Response', *Journal of Biological Chemistry*. American Society for Biochemistry and Molecular Biology, 291(15), pp. 7788–7795. doi: 10.1074/JBC.R116.714980.

André, C., Santos, G. Dos and Koulakoff, A. (1994) 'Muscarinic Receptor Profiles of Mouse Brain Astrocytes in Culture Vary With Their Tissue Of Origin but Differ From Those of Neurons', *European Journal of Neuroscience*. John Wiley & Sons, Ltd (10.1111), 6(11), pp. 1702–1709. doi: 10.1111/j.1460-9568.1994.tb00562.x.

Andrews, E. M. *et al.* (2012) 'Alterations in chondroitin sulfate proteoglycan expression occur both at and far from the site of spinal contusion injury', *Experimental*

Neurology, 235(1), pp. 174–187. doi: 10.1016/j.expneurol.2011.09.008.

Aoki, C. (1992) 'Beta-adrenergic receptors: astrocytic localization in the adult visual cortex and their relation to catecholamine axon terminals as revealed by electron microscopic immunocytochemistry.', *The Journal of neuroscience : the official journal of the Society for Neuroscience*. NIH Public Access, 12(3), pp. 781–92. doi: 10.1523/JNEUROSCI.12-03-00781.1992.

Aoki, C., Venkatesan, C. and Kurose, H. (1998) 'Noradrenergic modulation of the prefrontal cortex as revealed by electron microscopic immunocytochemistry.', *Advances in pharmacology (San Diego, Calif.)*, 42, pp. 777–80. Available at: http://www.ncbi.nlm.nih.gov/pubmed/9328013 (Accessed: 16 August 2019).

Aragay, A. M. *et al.* (1995) 'G12 Requirement for Thrombin-stimulated Gene Expression and DNA Synthesis in 1321N1 Astrocytoma Cells', *Journal of Biological Chemistry*, 270(34), pp. 20073–20077. doi: 10.1074/jbc.270.34.20073.

Araque, A *et al.* (1999a) 'Tripartite synapses: glia, the unacknowledged partner.', *Trends in neurosciences*, 22(5), pp. 208–15. Available at: http://www.ncbi.nlm.nih.gov/pubmed/10322493 (Accessed: 3 September 2019).

Araque, A *et al.* (1999b) 'Tripartite synapses: glia, the unacknowledged partner.', *Trends in neurosciences*, 22(5), pp. 208–15. Available at: http://www.ncbi.nlm.nih.gov/pubmed/10322493 (Accessed: 15 August 2019).

Araque, Alfonso *et al.* (1999) 'Tripartite synapses: glia, the unacknowledged partner', *Trends in Neurosciences*, 22(5), pp. 208–215. doi: 10.1016/S0166-2236(98)01349-6.

Araque, A. *et al.* (2014) 'Gliotransmitters Travel in Time and Space', *Neuron*, 81(4), pp. 728–739. doi: 10.1016/j.neuron.2014.02.007.

Araque, A. and Navarrete, M. (2010) 'Glial cells in neuronal network function.', *Philosophical transactions of the Royal Society of London. Series B, Biological sciences*. The Royal Society, 365(1551), pp. 2375–81. doi: 10.1098/rstb.2009.0313.

Armbruster *et al.* (2007) 'Evolving the lock to fit the key to create a family of G protein-coupled receptors potently activated by an inert ligand', *Proceedings of the National*

Academy of Sciences. National Academy of Sciences, 104(12), pp. 5163–5168. doi: 10.1073/pnas.0700293104.

Armbruster, B. N. *et al.* (2007) 'Evolving the lock to fit the key to create a family of G protein-coupled receptors potently activated by an inert ligand.', *Proceedings of the National Academy of Sciences of the United States of America*. National Academy of Sciences, 104(12), pp. 5163–8. doi: 10.1073/pnas.0700293104.

Asada, A. *et al.* (2015) 'Subtle modulation of ongoing calcium dynamics in astrocytic microdomains by sensory inputs', *Physiological Reports*, 3(10), p. e12454. doi: 10.14814/phy2.12454.

Asahina, M. *et al.* (1998) 'Brain muscarinic receptors in progressive supranuclear palsy and Parkinson's disease: a positron emission tomographic study.', *Journal of neurology, neurosurgery, and psychiatry*. BMJ Publishing Group, 65(2), pp. 155–63. doi: 10.1136/jnnp.65.2.155.

Atkinson, B. N. and Minneman, K. P. (1991) 'Multiple Adrenergic Receptor Subtypes Controlling Cyclic AMP Formation: Comparison of Brain Slices and Primary Neuronal and Glial Cultures', *Journal of Neurochemistry*, 56(2), pp. 587–595. doi: 10.1111/j.1471-4159.1991.tb08190.x.

Attwood, T. K. and Findlay, J. B. (1994) 'Fingerprinting G-protein-coupled receptors.', *Protein engineering*, 7(2), pp. 195–203. Available at: http://www.ncbi.nlm.nih.gov/pubmed/8170923 (Accessed: 25 August 2019).

Bærentzen, S. *et al.* (2019) 'The Chemogenetic Receptor Ligand Clozapine N-Oxide Induces in vivo Neuroreceptor Occupancy and Reduces Striatal Glutamate Levels', *Frontiers in Neuroscience*. Frontiers, 13, p. 187. doi: 10.3389/fnins.2019.00187.

Ballesteros, J. A. and Weinstein, H. (1995) 'Integrated methods for the construction of three-dimensional models and computational probing of structure-function relations in G protein-coupled receptors', *Methods in Neurosciences*. Academic Press, 25, pp. 366–428. doi: 10.1016/S1043-9471(05)80049-7.

Bang, J., Kim, H. Y. and Lee, H. (2016) 'Optogenetic and Chemogenetic Approaches for Studying Astrocytes and Gliotransmitters.', *Experimental neurobiology*. Korean

Society for Brain and Neural Science, 25(5), pp. 205–221. doi: 10.5607/en.2016.25.5.205.

Baorto, D. M., Mellado, W. and Shelanski, M. L. (1992) 'Astrocyte process growth induction by actin breakdown.', *The Journal of cell biology*. The Rockefeller University Press, 117(2), pp. 357–67. doi: 10.1083/jcb.117.2.357.

Bardehle, S. *et al.* (2013) 'Live imaging of astrocyte responses to acute injury reveals selective juxtavascular proliferation', *Nature Neuroscience*, 16(5), pp. 580–586. doi: 10.1038/nn.3371.

Basith, S. *et al.* (2018) 'Exploring G Protein-Coupled Receptors (GPCRs) Ligand Space via Cheminformatics Approaches: Impact on Rational Drug Design.', *Frontiers in pharmacology*. Frontiers Media SA, 9, p. 128. doi: 10.3389/fphar.2018.00128.

Batchelor, A. M. and Garthwaite, J. (1997) 'Frequency detection and temporally dispersed synaptic signal association through a metabotropic glutamate receptor pathway', *Nature*, 385(6611), pp. 74–77. doi: 10.1038/385074a0.

Bayburt, T. H. *et al.* (2011) 'Monomeric Rhodopsin Is Sufficient for Normal Rhodopsin Kinase (GRK1) Phosphorylation and Arrestin-1 Binding', *Journal of Biological Chemistry*, 286(2), pp. 1420–1428. doi: 10.1074/jbc.M110.151043.

Bazargani, N. and Attwell, D. (2016a) 'Astrocyte calcium signaling: the third wave.', *Nature neuroscience*, 19(2), pp. 182–9. doi: 10.1038/nn.4201.

Bazargani, N. and Attwell, D. (2016b) 'Astrocyte calcium signaling: The third wave', *Nature Neuroscience*. doi: 10.1038/nn.4201.

Beckerman, S. R. *et al.* (2015) 'Phenotypic Assays to Identify Agents That Induce Reactive Gliosis: A Counter-Screen to Prioritize Compounds for Preclinical Animal Studies', *ASSAY and Drug Development Technologies*. Mary Ann Liebert Inc, 13(7), pp. 377–388. doi: 10.1089/adt.2015.654.

Bender, D., Holschbach, M. and Stöcklin, G. (1994) 'Synthesis of n.c.a. carbon-11 labelled clozapine and its major metabolite clozapine-N-oxide and comparison of their biodistribution in mice.', *Nuclear medicine and biology*, 21(7), pp. 921–5. Available at:

http://www.ncbi.nlm.nih.gov/pubmed/9234345 (Accessed: 10 September 2019).

Berizzi, A. E. *et al.* (2016) 'Molecular Mechanisms of Action of M5 Muscarinic Acetylcholine Receptor Allosteric Modulators', *Molecular Pharmacology*, 90(4), pp. 427–436. doi: 10.1124/mol.116.104182.

Berridge, M. J., Bootman, M. D. and Roderick, H. L. (2003) 'Calcium signalling: dynamics, homeostasis and remodelling', *Nature Reviews Molecular Cell Biology*, 4(7), pp. 517–529. doi: 10.1038/nrm1155.

Beshore, D. C. *et al.* (2018) 'MK-7622: A First-in-Class M_1 Positive Allosteric Modulator Development Candidate', *ACS Medicinal Chemistry Letters*, 9(7), pp. 652–656. doi: 10.1021/acsmedchemlett.8b00095.

Bhattacharya, S., Hall, S. E. and Vaidehi, N. (2008) 'Agonist-Induced Conformational Changes in Bovine Rhodopsin: Insight into Activation of G-Protein-Coupled Receptors', *Journal of Molecular Biology*. Academic Press, 382(2), pp. 539–555. doi: 10.1016/J.JMB.2008.06.084.

Bhugra, D. (2005) 'The global prevalence of schizophrenia.', *PLoS medicine*. Public Library of Science, 2(5), p. e151; quiz e175. doi: 10.1371/journal.pmed.0020151.

Bicknell, R. J. *et al.* (1989) 'β-Adrenergic and opioid receptors on pituicytes cultured from adult rat neurohypophysis: Regulation of cell morphology', *Brain Research Bulletin*, 22(2), pp. 379–388. doi: 10.1016/0361-9230(89)90065-8.

Bignami, A. *et al.* (1972) 'Localization of the glial fibrillary acidic protein in astrocytes by immunofluorescence', *Brain Research*. Elsevier, 43(2), pp. 429–435. doi: 10.1016/0006-8993(72)90398-8.

Bindocci, E. *et al.* (2017) 'Three-dimensional Ca^{2+} imaging advances understanding of astrocyte biology', *Science*, 356(6339), p. eaai8185. doi: 10.1126/science.aai8185.

Bindslev, N. (2013) 'Allosteric transition: a comparison of two models.', *BMC pharmacology & toxicology*. BioMed Central, 14, p. 4. doi: 10.1186/2050-6511-14-4.

Birks, J. S. (2006) 'Cholinesterase inhibitors for Alzheimer's disease', in Birks, J. S. (ed.) *Cochrane Database of Systematic Reviews*. Chichester, UK: John Wiley & Sons, Ltd, p.

CD005593. doi: 10.1002/14651858.CD005593.

Bjarnadóttir, T. K. *et al.* (2006) 'Comprehensive repertoire and phylogenetic analysis of the G protein-coupled receptors in human and mouse', *Genomics*, 88(3), pp. 263–273. doi: 10.1016/j.ygeno.2006.04.001.

Bodick, N. C., Offen, W. W., Levey, A. I., *et al.* (1997) 'Effects of xanomeline, a selective muscarinic receptor agonist, on cognitive function and behavioral symptoms in Alzheimer disease.', *Archives of neurology*, 54(4), pp. 465–73. Available at: http://www.ncbi.nlm.nih.gov/pubmed/9109749 (Accessed: 31 August 2016).

Bodick, N. C., Offen, W. W., Shannon, H. E., *et al.* (1997) 'The selective muscarinic agonist xanomeline improves both the cognitive deficits and behavioral symptoms of Alzheimer disease.', *Alzheimer disease and associated disorders*, 11 Suppl 4, pp. S16-22. Available at: http://www.ncbi.nlm.nih.gov/pubmed/9339268 (Accessed: 31 August 2016).

Bonner, T. *et al.* (1987) 'Identification of a family of muscarinic acetylcholine receptor genes', *Science*, 237(4814), pp. 527–532. doi: 10.1126/science.3037705.

Bootman, M. D., Lipp, P. and Berridge, M. J. (2001) 'The organisation and functions of local Ca(2+) signals.', *Journal of cell science*. The Company of Biologists Ltd, 114(Pt 12), pp. 2213–22. doi: 10.1085/jgp.116.5.697.

Bosch, P. J. *et al.* (2014) 'Evaluation of fluorophores to label SNAP-tag fused proteins for multicolor single-molecule tracking microscopy in live cells.', *Biophysical journal*. The Biophysical Society, 107(4), pp. 803–14. doi: 10.1016/j.bpj.2014.06.040.

Bradley, S. J. *et al.* (2016) 'Mapping physiological G protein-coupled receptor signaling pathways reveals a role for receptor phosphorylation in airway contraction.', *Proceedings of the National Academy of Sciences of the United States of America*. National Academy of Sciences, 113(16), pp. 4524–9. doi: 10.1073/pnas.1521706113.

Bradley, S. J. *et al.* (2017) 'M1 muscarinic allosteric modulators slow prion neurodegeneration and restore memory loss', *Journal of Clinical Investigation*, 127(2). doi: 10.1172/JCI87526.

Bradley, Sophie J *et al.* (2018) 'Bitopic binding mode of an M 1 muscarinic acetylcholine receptor agonist associated with adverse clinical trial outcomes', *Molecular Pharmacology Fast Forward*. doi: 10.1124/mol.118.111872.

Bradley, Sophie J. *et al.* (2018) 'Bitopic Binding Mode of an M1 Muscarinic AcetylcholineReceptor Agonist Associated with Adverse Clinical Trial Outcomes', *Molecular Pharmacology*. American Society for Pharmacology and Experimental Therapeutics, 93(6), p. 645. doi: 10.1124/MOL.118.111872.

Bradley, S. J. and Tobin, A. B. (2016) 'Design of Next-Generation G Protein–Coupled Receptor Drugs: Linking Novel Pharmacology and In Vivo Animal Models', *Annual Review of Pharmacology and Toxicology*. Annual Reviews , 56(1), pp. 535–559. doi: 10.1146/annurev-pharmtox-011613-140012.

Bradley, S. J., Tobin, A. B. and Prihandoko, R. (2018) 'The use of chemogenetic approaches to study the physiological roles of muscarinic acetylcholine receptors in the central nervous system', *Neuropharmacology*, 136, pp. 421–426. doi: 10.1016/j.neuropharm.2017.11.043.

Brahmachari, S., Fung. Y. K., Pahan, K. (2006) 'Induction of Glial Fibrillary Acidic Protein Expression in Astrocytes by Nitric Oxide', *Journal of Neuroscience*, 26(18), pp. 4930–4939. doi: 10.1523/JNEUROSCI.5480-05.2006.

Briddon, S. J., Kellam, B. and Hill, S. J. (2011) 'Design and Use of Fluorescent Ligands to Study Ligand–Receptor Interactions in Single Living Cells', in, pp. 211–236. doi: 10.1007/978-1-61779-126-0_11.

Bridges, T. M. and Lindsley, C. W. (2008) 'G-Protein-Coupled Receptors: From Classical Modes of Modulation to Allosteric Mechanisms', *ACS Chemical Biology*. American Chemical Society, 3(9), pp. 530–541. doi: 10.1021/cb800116f.

Brockett, A. T. *et al.* (2018) 'Evidence supporting a role for astrocytes in the regulation of cognitive flexibility and neuronal oscillations through the Ca2+ binding protein S100β', *PLoS ONE*. Public Library of Science, 13(4). doi: 10.1371/journal.pone.0195726.

Bull, C. *et al.* (2014) 'Rat nucleus accumbens core astrocytes modulate reward and the

motivation to self-administer ethanol after abstinence', *Neuropsychopharmacology*. Nature Publishing Group, 39(12), pp. 2835–2845. doi: 10.1038/npp.2014.135.

Burda, J. E., Bernstein, A. M. and Sofroniew, M. V. (2016) 'Astrocyte roles in traumatic brain injury', *Experimental Neurology*. Academic Press Inc., pp. 305–315. doi: 10.1016/j.expneurol.2015.03.020.

Burger, W. A. C. *et al.* (2018) 'Toward an understanding of the structural basis of allostery in muscarinic acetylcholine receptors', *The Journal of General Physiology*. doi: 10.1085/jgp.201711979.

Bushong, E. A. *et al.* (2002) 'Protoplasmic astrocytes in CA1 stratum radiatum occupy separate anatomical domains.', *The Journal of neuroscience : the official journal of the Society for Neuroscience*, 22(1), pp. 183–92. Available at: http://www.ncbi.nlm.nih.gov/pubmed/11756501 (Accessed: 28 August 2019).

Caers, J. *et al.* (2014) 'Characterization of G Protein-coupled Receptors by a Fluorescence-based Calcium Mobilization Assay', *Journal of Visualized Experiments*, (89), p. e51516. doi: 10.3791/51516.

Cai, K., Itoh, Y. and Khorana, H. G. (2001) 'Mapping of contact sites in complex formation between transducin and light-activated rhodopsin by covalent crosslinking: Use of a photoactivatable reagent', *Proceedings of the National Academy of Sciences*, 98(9), pp. 4877–4882. doi: 10.1073/pnas.051632898.

Campbell, A. P. and Smrcka, A. V. (2018) 'Targeting G protein-coupled receptor signalling by blocking G proteins', *Nature Reviews Drug Discovery*, 17(11), pp. 789–803. doi: 10.1038/nrd.2018.135.

Campbell, E. J. and Marchant, N. J. (2018) 'The use of chemogenetics in behavioural neuroscience: receptor variants, targeting approaches and caveats', *British Journal of Pharmacology*, 175(7), pp. 994–1003. doi: 10.1111/bph.14146.

Canals, M. *et al.* (2012a) 'A Monod-Wyman-Changeux Mechanism Can Explain G Protein-coupled Receptor (GPCR) Allosteric Modulation', *Journal of Biological Chemistry*, 287(1), pp. 650–659. doi: 10.1074/jbc.M111.314278.

Canals, M. *et al.* (2012b) 'A Monod-Wyman-Changeux Mechanism Can Explain G Protein-coupled Receptor (GPCR) Allosteric Modulation', *Journal of Biological Chemistry*, 287(1), pp. 650–659. doi: 10.1074/jbc.M111.314278.

Canals, M., Sexton, P. M. and Christopoulos, A. (2011) 'Allostery in GPCRs: "MWC" revisited', *Trends in Biochemical Sciences*, 36(12), pp. 663–672. doi: 10.1016/j.tibs.2011.08.005.

Cannon, D. M. *et al.* (2011) 'Genetic variation in cholinergic muscarinic-2 receptor gene modulates M2 receptor binding in vivo and accounts for reduced binding in bipolar disorder', *Molecular Psychiatry*, 16(4), pp. 407–418. doi: 10.1038/mp.2010.24.

Cao, J. *et al.* (2009) 'Evolution of the class C GPCR Venus flytrap modules involved positive selected functional divergence', *BMC Evolutionary Biology*, 9(1), p. 67. doi: 10.1186/1471-2148-9-67.

Cao, X. *et al.* (2013) 'Astrocyte-derived ATP modulates depressive-like behaviors', *Nature Medicine*, 19(6), pp. 773–777. doi: 10.1038/nm.3162.

Carpenter, B. *et al.* (2016) 'Structure of the adenosine A2A receptor bound to an engineered G protein', *Nature*, 536(7614), pp. 104–107. doi: 10.1038/nature18966.

Carpenter, B. and Tate, C. G. (2016) 'Engineering a minimal G protein to facilitate crystallisation of G protein-coupled receptors in their active conformation', *Protein Engineering Design and Selection*, 29(12), pp. 583–594. doi: 10.1093/protein/gzw049.

Di Castro, M. A. *et al.* (2011) 'Local Ca2+ detection and modulation of synaptic release by astrocytes.', *Nature neuroscience*, 14(10), pp. 1276–84. doi: 10.1038/nn.2929.

Catus, S. L. *et al.* (2011) 'Role of β-adrenoceptors in glucose uptake in astrocytes using β-adrenoceptor knockout mice', *British Journal of Pharmacology*, 162(8), pp. 1700–1715. doi: 10.1111/j.1476-5381.2010.01153.x.

Caulfield, M. P. (1993) 'Receptors Muscarinic Characterization , Coupling and Function', 58, pp. 319–379.

Caulfield, M. P. and Birdsall, N. J. (1998) 'International Union of Pharmacology. XVII. Classification of muscarinic acetylcholine receptors.', *Pharmacological reviews*, 50(2),

pp. 279–90. Available at: http://www.ncbi.nlm.nih.gov/pubmed/9647869 (Accessed: 30 August 2019).

Chai, H. *et al.* (2017) 'Neural Circuit-Specialized Astrocytes: Transcriptomic, Proteomic, Morphological, and Functional Evidence', *Neuron*, 95(3), pp. 531-549.e9. doi: 10.1016/j.neuron.2017.06.029.

Chambon, C. *et al.* (2012) 'Using cholinergic M1 receptor positive allosteric modulators to improve memory via enhancement of brain cholinergic communication', *European Journal of Pharmacology*, 697(1–3), pp. 73–80. doi: 10.1016/j.ejphar.2012.10.011.

Chang, S. D. and Bruchas, M. R. (2014) 'Functional Selectivity at GPCRs: New Opportunities in Psychiatric Drug Discovery', *Neuropsychopharmacology*. Nature Publishing Group, 39(1), pp. 248–249. doi: 10.1038/npp.2013.205.

Chang, W.-H. *et al.* (1998) 'Reversible metabolism of clozapine and clozapine N-oxide in schizophrenic patients', *Progress in Neuro-Psychopharmacology and Biological Psychiatry*. Elsevier, 22(5), pp. 723–739. doi: 10.1016/S0278-5846(98)00035-9.

Changeux, J.-P. (2010) 'Allosteric Receptors: From Electric Organ to Cognition', *Annual Review of Pharmacology and Toxicology*, 50(1), pp. 1–38. doi: 10.1146/annurev.pharmtox.010909.105741.

Changeux, J.-P. and Christopoulos, A. (2016) 'Allosteric Modulation as a Unifying Mechanism for Receptor Function and Regulation', *Cell*, 166(5), pp. 1084–1102. doi: 10.1016/j.cell.2016.08.015.

Charles, A. C. *et al.* (1991) 'Intercellular signaling in glial cells: calcium waves and oscillations in response to mechanical stimulation and glutamate.', *Neuron*. Academic Press, New York, 6(6), pp. 983–92. doi: 10.1016/0896-6273(91)90238-U.

Chen, X. *et al.* (2015) 'The First Structure–Activity Relationship Studies for Designer Receptors Exclusively Activated by Designer Drugs', *ACS Chemical Neuroscience*, 6(3), pp. 476–484. doi: 10.1021/cn500325v.

Cherfils, J. and Zeghouf, M. (2013) 'Regulation of Small GTPases by GEFs, GAPs, and

GDIs', *Physiological Reviews*, 93(1), pp. 269–309. doi: 10.1152/physrev.00003.2012.

Chiba, Y., Sakai, H. and Misawa, M. (2001) 'Augmented acetylcholine-induced translocation of RhoA in bronchial smooth muscle from antigen-induced airway hyperresponsive rats.', *British journal of pharmacology*. Wiley-Blackwell, 133(6), pp. 886–90. doi: 10.1038/sj.bjp.0704137.

Chini, B. and Parenti, M. (2009) 'G-protein-coupled receptors, cholesterol and palmitoylation: facts about fats', *Journal of Molecular Endocrinology*, 42(5), pp. 371–379. doi: 10.1677/JME-08-0114.

Choe, H.-W. *et al.* (2011) 'Crystal structure of metarhodopsin II', *Nature*. Nature Publishing Group, 471(7340), pp. 651–655. doi: 10.1038/nature09789.

Christopoulos, A. (2014) 'Advances in G Protein-Coupled Receptor Allostery: From Function to Structure', *Molecular Pharmacology*, 86(5), pp. 463–478. doi: 10.1124/mol.114.094342.

Christopoulos, A. *et al.* (2016) 'M1 muscarinic allosteric modulators slow prion neurodegeneration and restore memory loss', *Journal of Clinical Investigation*, 127(2), pp. 487–499. doi: 10.1172/jci87526.

Christopoulos, A. and Kenakin, T. (2002) 'G protein-coupled receptor allosterism and complexing.', *Pharmacological reviews*, 54(2), pp. 323–374. doi: 10.1124/pr.54.2.323.

Christopoulos, A. and Mitchelson, F. (1997) 'Application of an Allosteric Ternary Complex Model to the Technique of Pharmacological Resultant Analysis', *Journal of Pharmacy and Pharmacology*, 49(8), pp. 781–786. doi: 10.1111/j.2042-7158.1997.tb06112.x.

Chun, L., Zhang, W. and Liu, J. (2012) 'Structure and ligand recognition of class C GPCRs', *Acta Pharmacologica Sinica*. Nature Publishing Group, 33(3), pp. 312–323. doi: 10.1038/aps.2011.186.

Cieślik, P. *et al.* (2019) 'Simultaneous activation of muscarinic and GABAB receptors as a bidirectional target for novel antipsychotics', *Behavioural Brain Research*, 359, pp. 671–685. doi: 10.1016/j.bbr.2018.09.019.

Codazzi, F., Teruel, M. N. and Meyer, T. (2001) 'Control of astrocyte Ca(2+) oscillations and waves by oscillating translocation and activation of protein kinase C.', *Current biology : CB*, 11(14), pp. 1089–97. doi: 10.1016/s0960-9822(01)00326-8.

Cohen, Z., Molinatti, G. and Hamel, E. (1997) 'Astroglial and Vascular Interactions of Noradrenaline Terminals in the Rat Cerebral Cortex', *Journal of Cerebral Blood Flow & Metabolism*, 17(8), pp. 894–904. doi: 10.1097/00004647-199708000-00008.

Congreve, M., Oswald, C. and Marshall, F. H. (2017) 'Applying Structure-Based Drug Design Approaches to Allosteric Modulators of GPCRs', *Trends in Pharmacological Sciences*, 38(9), pp. 837–847. doi: 10.1016/j.tips.2017.05.010.

Conklin, B. R. *et al.* (1993) 'Substitution of three amino acids switches receptor specificity of Gqα to that of Giα', *Nature*, 363(6426), pp. 274–276. doi: 10.1038/363274a0.

Conklin, B. R. *et al.* (2008) 'Engineering GPCR signaling pathways with RASSLs.', *Nature methods*. NIH Public Access, 5(8), pp. 673–8. doi: 10.1038/nmeth.1232.

Conn, P. J., Christopoulos, A. and Lindsley, C. W. (2009) 'Allosteric modulators of GPCRs: a novel approach for the treatment of CNS disorders.', *Nature reviews. Drug discovery*, 8(1), pp. 41–54. doi: 10.1038/nrd2760.

Connor, J. R. and Berkowitz, E. M. (1985) 'A demonstration of glial filament distribution in astrocytes isolated from rat cerebral cortex', *Neuroscience*. Pergamon, 16(1), pp. 33–44. doi: 10.1016/0306-4522(85)90044-2.

Cooper, D. M. F., Mons, N. and Karpen, J. W. (1995) 'Adenylyl cyclases and the interaction between calcium and cAMP signalling', *Nature*, 374(6521), pp. 421–424. doi: 10.1038/374421a0.

Cooper, S. L. *et al.* (2019) 'Probe dependence of allosteric enhancers on the binding affinity of adenosine A1 -receptor agonists at rat and human A1-receptors measured using N ano BRET', *British Journal of Pharmacology*. Wiley-Blackwell, 176(7), pp. 864–878. doi: 10.1111/bph.14575.

Cormack, B. (1998) 'Green fluorescent protein as a reporter of transcription and

protein localization in fungi', *Current Opinion in Microbiology*. Elsevier Current Trends, 1(4), pp. 406–410. doi: 10.1016/S1369-5274(98)80057-X.

Cornell-Bell, A. *et al.* (1990) 'Glutamate induces calcium waves in cultured astrocytes: long-range glial signaling', *Science*, 247(4941), pp. 470–473. doi: 10.1126/science.1967852.

Corriden, R. *et al.* (2014) 'Kinetic analysis of antagonist-occupied adenosine-A $_3$ receptors within membrane microdomains of individual cells provides evidence of receptor dimerization and allosterism', *The FASEB Journal*, 28(10), pp. 4211–4222. doi: 10.1096/fj.13-247270.

Cottet, M. *et al.* (2011) 'Original Fluorescent Ligand-Based Assays Open New Perspectives in G-Protein Coupled Receptor Drug Screening', *Pharmaceuticals*. Multidisciplinary Digital Publishing Institute (MDPI), 4(1), pp. 202–214. doi: 10.3390/ph4010202.

Cregg, J. M. *et al.* (2014) 'Functional regeneration beyond the glial scar', *Experimental Neurology*, 253, pp. 197–207. doi: 10.1016/j.expneurol.2013.12.024.

Cresswell-Clay, E. *et al.* (2018) 'A Compartmental Model to Investigate Local and Global Ca2+ Dynamics in Astrocytes', *Frontiers in Computational Neuroscience*. Frontiers Media SA, 12. doi: 10.3389/fncom.2018.00094.

Croft, W. *et al.* (2016) 'Probabilistic encoding of stimulus strength in astrocyte global calcium signals.', *Glia*, 64(4), pp. 537–52. doi: 10.1002/glia.22947.

Crook, J. M. *et al.* (2000) 'Decreased muscarinic receptor binding in subjects with schizophrenia: a study of the human hippocampal formation.', *Biological psychiatry*, 48(5), pp. 381–8. doi: 10.1016/s0006-3223(00)00918-5.

Dai, S. B. *et al.* (2019) 'Plasmid-based generation of neural cells from human fibroblasts using non-integrating episomal vectors', *Neural Regeneration Research*. Wolters Kluwer Medknow Publications, 14(3), pp. 501–505. doi: 10.4103/1673-5374.245476.

Dale, N. C. *et al.* (2019) 'NanoBRET: The Bright Future of Proximity-Based Assays',

Frontiers in Bioengineering and Biotechnology. Frontiers, 7, p. 56. doi: 10.3389/fbioe.2019.00056.

Damiati, S. *et al.* (2018) 'Microfluidic Devices for Drug Delivery Systems and Drug Screening.', *Genes*. Multidisciplinary Digital Publishing Institute (MDPI), 9(2). doi: 10.3390/genes9020103.

Dani, J. W., Chernjavsky, A. and Smith, S. J. (1992) 'Neuronal activity triggers calcium waves in hippocampal astrocyte networks.', *Neuron*, 8(3), pp. 429–40. doi: 10.1016/0896-6273(92)90271-e.

Davie, B. J., Christopoulos, A. and Scammells, P. J. (2013) 'Development of M1 mAChR allosteric and bitopic ligands: prospective therapeutics for the treatment of cognitive deficits.', *ACS chemical neuroscience*, 4(7), pp. 1026–48. doi: 10.1021/cn400086m.

Davis, A. A. *et al.* (2010) 'Deletion of M1 muscarinic acetylcholine receptors increases amyloid pathology in vitro and in vivo.', *The Journal of neuroscience : the official journal of the Society for Neuroscience*. Society for Neuroscience, 30(12), pp. 4190–6. doi: 10.1523/JNEUROSCI.6393-09.2010.

Davoren, J. E. *et al.* (2016) 'Discovery of the Potent and Selective M1 PAM-Agonist *N* -[(3 *R* ,4 *S*)-3-Hydroxytetrahydro-2 *H* -pyran-4-yl]-5-methyl-4-[4-(1,3-thiazol-4-yl)benzyl]pyridine-2-carboxamide (PF-06767832): Evaluation of Efficacy and Cholinergic Side Effects', *Journal of Medicinal Chemistry*, 59(13), pp. 6313–6328. doi: 10.1021/acs.jmedchem.6b00544.

Day, R. N. and Davidson, M. W. (2009) 'The fluorescent protein palette: tools for cellular imaging.', *Chemical Society reviews*. NIH Public Access, 38(10), pp. 2887–921. doi: 10.1039/b901966a.

Dean, B. *et al.* (2002) 'Decreased muscarinic1 receptors in the dorsolateral prefrontal cortex of subjects with schizophrenia', *Molecular Psychiatry*, 7(10), pp. 1083–1091. doi: 10.1038/sj.mp.4001199.

Dean, B., Copolov, D. and Scarr, E. (2016) 'Understanding the pathophysiology of schizophrenia: Contributions from the Melbourne Psychiatric Brain Bank', *Schizophrenia Research*, 177(1–3), pp. 108–114. doi: 10.1016/j.schres.2016.04.037.

Decker, M. and Holzgrabe, U. (2012) 'M1 muscarinic cetylcholine receptor allosteric modulators as potential therapeutic opportunities for treating Alzheimer's disease', *MedChemComm*. The Royal Society of Chemistry, 3(7), p. 752. doi: 10.1039/c2md20025b.

Deng, C. and Huang, X.-F. (2005) 'Decreased density of muscarinic receptors in the superior temporal gyrusin schizophrenia', *Journal of Neuroscience Research*, 81(6), pp. 883–890. doi: 10.1002/jnr.20600.

Denker, B. M., Neer, E. J. and Schmidt, C. J. (1992) 'Mutagenesis of the amino terminus of the alpha subunit of the G protein Go. In vitro characterization of alpha o beta gamma interactions.', *The Journal of biological chemistry*, 267(9), pp. 6272–7. Available at: http://www.ncbi.nlm.nih.gov/pubmed/1556134 (Accessed: 27 August 2019).

Desai, A. K. and Grossberg, G. T. (2005) 'Diagnosis and treatment of Alzheimer's disease.', *Neurology*, 64(12 Suppl 3), pp. S34-9. doi: 10.1212/wnl.64.12_suppl_3.s34.

DeVree, B. T. *et al.* (2016) 'Allosteric coupling from G protein to the agonist-binding pocket in GPCRs', *Nature*, 535(7610), pp. 182–186. doi: 10.1038/nature18324.

Dhumpa, R. and Roper, M. G. (2012) 'Temporal gradients in microfluidic systems to probe cellular dynamics: a review.', *Analytica chimica acta*. NIH Public Access, 743, pp. 9–18. doi: 10.1016/j.aca.2012.07.006.

Digby, G. J. *et al.* (2012) 'Chemical modification of the M(1) agonist VU0364572 reveals molecular switches in pharmacology and a bitopic binding mode.', *ACS chemical neuroscience*. American Chemical Society, 3(12), pp. 1025–36. doi: 10.1021/cn300103e.

Dijkman, P. M. *et al.* (2018) 'Dynamic tuneable G protein-coupled receptor monomer-dimer populations', *Nature Communications*. Nature Publishing Group, 9(1), p. 1710. doi: 10.1038/s41467-018-03727-6.

Ding, F. *et al.* (2013) 'α1-Adrenergic receptors mediate coordinated Ca2+ signaling of cortical astrocytes in awake, behaving mice.', *Cell calcium*. NIH Public Access, 54(6), pp. 387–94. doi: 10.1016/j.ceca.2013.09.001.

Ding, J. *et al.* (2006) 'RGS4-dependent attenuation of M4 autoreceptor function in striatal cholinergic interneurons following dopamine depletion', *Nature Neuroscience*, 9(6), pp. 832–842. doi: 10.1038/nn1700.

Dityatev, A. and Rusakov, D. A. (2011) 'Molecular signals of plasticity at the tetrapartite synapse', *Current Opinion in Neurobiology*. Elsevier Current Trends, 21(2), pp. 353–359. doi: 10.1016/J.CONB.2010.12.006.

Dixon, A. S. *et al.* (2016) 'NanoLuc Complementation Reporter Optimized for Accurate Measurement of Protein Interactions in Cells', *ACS Chemical Biology*, 11(2), pp. 400–408. doi: 10.1021/acschembio.5b00753.

Djurovic, S. *et al.* (2004) 'Comparison of nonviral transfection and adeno-associated viral transduction on cardiomyocytes.', *Molecular biotechnology*, 28(1), pp. 21–32. doi: 10.1385/MB:28:1:21.

Dong, X. *et al.* (2001) 'A diverse family of GPCRs expressed in specific subsets of nociceptive sensory neurons', *Cell*. Cell Press, 106(5), pp. 619–632. doi: 10.1016/S0092-8674(01)00483-4.

Doré, A. S. *et al.* (2014) 'Structure of class C GPCR metabotropic glutamate receptor 5 transmembrane domain', *Nature*, 511(7511), pp. 557–562. doi: 10.1038/nature13396.

Draper-Joyce, C. J. *et al.* (2018) 'The structural determinants of the bitopic binding mode of a negative allosteric modulator of the dopamine D 2 receptor', *Biochemical Pharmacology*, 148, pp. 315–328. doi: 10.1016/j.bcp.2018.01.002.

Dror, R. O. *et al.* (2011) 'Pathway and mechanism of drug binding to G-protein-coupled receptors.', *Proceedings of the National Academy of Sciences of the United States of America*. National Academy of Sciences, 108(32), pp. 13118–23. doi: 10.1073/pnas.1104614108.

Dror, R. O. *et al.* (2013) 'Structural basis for modulation of a G-protein-coupled receptor by allosteric drugs', *Nature*. Nature Publishing Group, 503(7475), pp. 295–299. doi: 10.1038/nature12595.

Du, Y. *et al.* (2019) 'Assembly of a GPCR-G Protein Complex', *Cell*, 177(5), pp. 1232-1242.e11. doi: 10.1016/j.cell.2019.04.022.

Dupré, D. J. *et al.* (2009) 'The role of Gbetagamma subunits in the organization, assembly, and function of GPCR signaling complexes.', *Annual review of pharmacology and toxicology*. NIH Public Access, 49, pp. 31–56. doi: 10.1146/annurev-pharmtox-061008-103038.

Durkee, C. A. *et al.* (2019) '$G_{i/o}$ protein-coupled receptors inhibit neurons but activate astrocytes and stimulate gliotransmission', *Glia*, 67(6), pp. 1076–1093. doi: 10.1002/glia.23589.

Ebersolt, C., Perez, M. and Bockaert, J. (1981) ?'1 and ?2 Adrenergic receptors in mouse brain astrocytes from primary cultures', *Journal of Neuroscience Research*, 6(5), pp. 643–652. doi: 10.1002/jnr.490060509.

Eglen, R. M. (2012) 'Overview of Muscarinic Receptor Subtypes', in *Handbook of experimental pharmacology*, pp. 3–28. doi: 10.1007/978-3-642-23274-9_1.

Eglen, R. M., Choppin, A. and Watson, N. (2001) 'Therapeutic opportunities from muscarinic receptor research.', *Trends in pharmacological sciences*, 22(8), pp. 409–14. Available at: http://www.ncbi.nlm.nih.gov/pubmed/11479003 (Accessed: 5 July 2019).

El, Y. B. *et al.* (2018) 'Activity changes in neuron-Astrocyte networks in culture under the effect of norepinephrine', *PLoS ONE*. Public Library of Science, 13(10). doi: 10.1371/journal.pone.0203761.

Emsley, J. G. and Macklis, J. D. (2006) 'Astroglial heterogeneity closely reflects the neuronal-defined anatomy of the adult murine CNS', *Neuron Glia Biology*, 2(3), pp. 175–186. doi: 10.1017/S1740925X06000202.

Emtage, A. L. *et al.* (2017) 'GPCRs through the keyhole: the role of protein flexibility in ligand binding to β-adrenoceptors', *Journal of Biomolecular Structure and Dynamics*, 35(12), pp. 2604–2619. doi: 10.1080/07391102.2016.1226197.

Eng, L. F. *et al.* (1971) 'An acidic protein isolated from fibrous astrocytes', *Brain*

Research, 28(2), pp. 351–354. doi: 10.1016/0006-8993(71)90668-8.

Eng, L. F. (1985) 'Glial fibrillary acidic protein (GFAP): the major protein of glial intermediate filaments in differentiated astrocytes', *Journal of Neuroimmunology*, 8(C), pp. 203–214. doi: 10.1016/S0165-5728(85)80063-1.

Erdmann, R. S. *et al.* (2019) 'Labeling Strategies Matter for Super-Resolution Microscopy: A Comparison between HaloTags and SNAP-tags', *Cell Chemical Biology*, 26(4), pp. 584-592.e6. doi: 10.1016/j.chembiol.2019.01.003.

Eroglu, C. and Barres, B. A. (2010) 'Regulation of synaptic connectivity by glia', *Nature*, 468(7321), pp. 223–231. doi: 10.1038/nature09612.

Escoffre, J.-M. *et al.* (2009) 'What is (still not) known of the mechanism by which electroporation mediates gene transfer and expression in cells and tissues.', *Molecular biotechnology*, 41(3), pp. 286–95. doi: 10.1007/s12033-008-9121-0.

Escribá, P. V. *et al.* (2007) 'Lipid–protein interactions in GPCR-associated signaling', *Biochimica et Biophysica Acta (BBA) - Biomembranes*. Elsevier, 1768(4), pp. 836–852. doi: 10.1016/J.BBAMEM.2006.09.001.

Fallini, C., Bassell, G. J. and Rossoll, W. (2010) 'High-efficiency transfection of cultured primary motor neurons to study protein localization, trafficking, and function', *Molecular Neurodegeneration*, 5(1). doi: 10.1186/1750-1326-5-17.

Fan, H. (2014) 'β-Arrestins 1 and 2 are critical regulators of inflammation', *Innate Immunity*. SAGE PublicationsSage UK: London, England, 20(5), pp. 451–460. doi: 10.1177/1753425913501098.

Farrants, H. *et al.* (2018) 'SNAP-Tagged Nanobodies Enable Reversible Optical Control of a G Protein-Coupled Receptor *via* a Remotely Tethered Photoswitchable Ligand', *ACS Chemical Biology*, 13(9), pp. 2682–2688. doi: 10.1021/acschembio.8b00628.

Farrell, M. S. *et al.* (2013) 'A Gαs DREADD Mouse for Selective Modulation of cAMP Production in Striatopallidal Neurons', *Neuropsychopharmacology*, 38(5), pp. 854–862. doi: 10.1038/npp.2012.251.

Felder *et al.* (2000) 'Therapeutic Opportunities for Muscarinic Receptors in the Central

Nervous System'. American Chemical Society. doi: 10.1021/JM990607U.

Felder, C. C. *et al.* (2018) 'Current status of muscarinic M1 and M4 receptors as drug targets for neurodegenerative diseases', *Neuropharmacology*, 136(Pt C), pp. 449–458. doi: 10.1016/j.neuropharm.2018.01.028.

Feldman, H. H. *et al.* (2007) 'Effect of rivastigmine on delay to diagnosis of Alzheimer's disease from mild cognitive impairment: the InDDEx study', *The Lancet Neurology*, 6(6), pp. 501–512. doi: 10.1016/S1474-4422(07)70109-6.

Ferré, S. *et al.* (2014) 'G Protein–Coupled Receptor Oligomerization Revisited: Functional and Pharmacological Perspectives', *Pharmacological Reviews*. American Society for Pharmacology and Experimental Therapeutics, 66(2), pp. 413–434. doi: 10.1124/PR.113.008052.

Fiacco, T. A. *et al.* (2007) 'Selective Stimulation of Astrocyte Calcium In Situ Does Not Affect Neuronal Excitatory Synaptic Activity', *Neuron*, 54(4), pp. 611–626. doi: 10.1016/j.neuron.2007.04.032.

Fiacco, T. A., Agulhon, C. and McCarthy, K. D. (2009) 'Sorting Out Astrocyte Physiology from Pharmacology', *Annual Review of Pharmacology and Toxicology*. doi: 10.1146/annurev.pharmtox.011008.145602.

Fields, R. D. and Stevens-Graham, B. (2002) 'New Insights into Neuron-Glia Communication', *Science*, 298(5593), pp. 556–562. doi: 10.1126/science.298.5593.556.

Fisher, A. (2000) 'Therapeutic strategies in Alzheimer's disease: M1 muscarinic agonists.', *Japanese journal of pharmacology*, 84(2), pp. 101–12. Available at: http://www.ncbi.nlm.nih.gov/pubmed/11128032 (Accessed: 5 July 2019).

Flock, T. *et al.* (2017) 'Selectivity determinants of GPCR–G-protein binding', *Nature*, 545(7654), pp. 317–322. doi: 10.1038/nature22070.

Foo, L. C. *et al.* (2011) 'Development of a Method for the Purification and Culture of Rodent Astrocytes', *Neuron*, 71(5), pp. 799–811. doi: 10.1016/j.neuron.2011.07.022.

Foster, D. J. *et al.* (2014) 'Activation of M1 and M4 muscarinic receptors as potential

treatments for Alzheimer's disease and schizophrenia.', *Neuropsychiatric disease and treatment*. Dove Press, 10, pp. 183–91. doi: 10.2147/NDT.S55104.

Foster, D. J., Jones, C. K. and Conn, P. J. (2012) 'Emerging approaches for treatment of schizophrenia: modulation of cholinergic signaling.', *Discovery medicine*. NIH Public Access, 14(79), pp. 413–20. Available at: http://www.ncbi.nlm.nih.gov/pubmed/23272693 (Accessed: 25 August 2019).

Foster, S. R. and Bräuner-Osborne, H. (2017) 'Investigating Internalization and Intracellular Trafficking of GPCRs: New Techniques and Real-Time Experimental Approaches', in, pp. 41–61. doi: 10.1007/164_2017_57.

Fredriksson, R. *et al.* (2003) 'The G-Protein-Coupled Receptors in the Human Genome Form Five Main Families. Phylogenetic Analysis, Paralogon Groups, and Fingerprints', *Molecular Pharmacology*, 63(6), pp. 1256–1272. doi: 10.1124/mol.63.6.1256.

Fujii, Y., Maekawa, S. and Morita, M. (2017) 'Astrocyte calcium waves propagate proximally by gap junction and distally by extracellular diffusion of ATP released from volume-regulated anion channels', *Scientific Reports*. Nature Publishing Group, 7(1), p. 13115. doi: 10.1038/s41598-017-13243-0.

Galés, C. *et al.* (2005) 'Real-time monitoring of receptor and G-protein interactions in living cells', *Nature Methods*, 2(3), pp. 177–184. doi: 10.1038/nmeth743.

Galés, C. *et al.* (2006) 'Probing the activation-promoted structural rearrangements in preassembled receptor–G protein complexes', *Nature Structural & Molecular Biology*, 13(9), pp. 778–786. doi: 10.1038/nsmb1134.

Galvin, V. C., Arnsten, A. F. T. and Wang, M. (2018) 'Evolution in Neuromodulation-The Differential Roles of Acetylcholine in Higher Order Association vs. Primary Visual Cortices.', *Frontiers in neural circuits*. Frontiers Media SA, 12, p. 67. doi: 10.3389/fncir.2018.00067.

Gannon, R. L. and Millan, M. J. (2012) 'LY2033298, a positive allosteric modulator at muscarinic M4 receptors, enhances inhibition by oxotremorine of light-induced phase shifts in hamster circadian activity rhythms', *Psychopharmacology*, 224(2), pp. 231–240. doi: 10.1007/s00213-012-2743-8.

Gao, Z.-G. and Jacobson, K. A. (2013) 'Allosteric modulation and functional selectivity of G protein-coupled receptors.', *Drug discovery today. Technologies*. NIH Public Access, 10(2), pp. e237-43. doi: 10.1016/j.ddtec.2012.08.004.

Garcia-Higuera, I. *et al.* (1998) 'Folding a WD repeat propeller. Role of highly conserved aspartic acid residues in the G protein beta subunit and Sec13.', *The Journal of biological chemistry*. American Society for Biochemistry and Molecular Biology, 273(15), pp. 9041–9. doi: 10.1074/jbc.273.15.9041.

García-Nafría, J. and Tate, C. G. (2019) 'Cryo-EM structures of GPCRs coupled to Gs, Gi and Go', *Molecular and Cellular Endocrinology*, 488, pp. 1–13. doi: 10.1016/j.mce.2019.02.006.

Garner, A. R. *et al.* (2012) 'Generation of a synthetic memory trace.', *Science (New York, N.Y.)*. NIH Public Access, 335(6075), pp. 1513–6. doi: 10.1126/science.1214985.

Gautam, D. *et al.* (2008) 'Metabolic Roles of the M3 Muscarinic Acetylcholine Receptor Studied with M3 Receptor Mutant Mice: A Review', *Journal of Receptors and Signal Transduction*, 28(1–2), pp. 93–108. doi: 10.1080/10799890801942002.

Gee, K. R. *et al.* (2000) 'Chemical and physiological characterization of fluo-4 Ca2+-indicator dyes', *Cell Calcium*, 27(2), pp. 97–106. doi: 10.1054/ceca.1999.0095.

Geula, C. (1998) 'Abnormalities of neural circuitry in Alzheimer's disease: hippocampus and cortical cholinergic innervation.', *Neurology*, 51(1 Suppl 1), pp. S18-29; discussion S65-7. Available at: http://www.ncbi.nlm.nih.gov/pubmed/9674759 (Accessed: 23 February 2016).

Ghoshal, A. *et al.* (2016) 'Potentiation of M1 Muscarinic Receptor Reverses Plasticity Deficits and Negative and Cognitive Symptoms in a Schizophrenia Mouse Model', *Neuropsychopharmacology*, 41(2), pp. 598–610. doi: 10.1038/npp.2015.189.

Gibb, W. R. and Lees, A. J. (1991) 'Anatomy, pigmentation, ventral and dorsal subpopulations of the substantia nigra, and differential cell death in Parkinson's disease.', *Journal of neurology, neurosurgery, and psychiatry*. BMJ Publishing Group, 54(5), pp. 388–96. doi: 10.1136/jnnp.54.5.388.

Golovina, V. A. and Blaustein, M. P. (2000) 'Unloading and refilling of two classes of spatially resolved endoplasmic reticulum Ca(2+) stores in astrocytes.', *Glia*, 31(1), pp. 15–28. Available at: http://www.ncbi.nlm.nih.gov/pubmed/10816603 (Accessed: 9 September 2019).

Gomeza, J. *et al.* (1999) 'Enhancement of D1 dopamine receptor-mediated locomotor stimulation in M(4) muscarinic acetylcholine receptor knockout mice.', *Proceedings of the National Academy of Sciences of the United States of America*. National Academy of Sciences, 96(18), pp. 10483–8. doi: 10.1073/pnas.96.18.10483.

Goodman, O. B. *et al.* (1996) 'β-Arrestin acts as a clathrin adaptor in endocytosis of the β2-adrenergic receptor', *Nature*, 383(6599), pp. 447–450. doi: 10.1038/383447a0.

Gordleeva, S. Y. *et al.* (2019) 'Astrocyte as spatiotemporal integrating detector of neuronal activity', *Frontiers in Physiology*. Frontiers Media S.A., 10(MAR). doi: 10.3389/fphys.2019.00294.

Gould, R. W. *et al.* (2015) 'Role for the M_1 Muscarinic Acetylcholine Receptor in Top-Down Cognitive Processing Using a Touchscreen Visual Discrimination Task in Mice', *ACS Chemical Neuroscience*, 6(10), pp. 1683–1695. doi: 10.1021/acschemneuro.5b00123.

Granados, M. E., Soriano, E. and Saavedra-Molina, A. (1997) 'Use of pluronic acid F-127 with Fluo-3/AM probe to determine intracellular calcium changes elicited in bean protoplasts', *Phytochemical Analysis*. John Wiley & Sons, Ltd, 8(4), pp. 204–208. doi: 10.1002/(SICI)1099-1565(199707)8:4<204::AID-PCA354>3.0.CO;2-L.

Grannan, M. D. *et al.* (2016) 'Prefrontal Cortex-Mediated Impairments in a Genetic Model of NMDA Receptor Hypofunction Are Reversed by the Novel M1 PAM VU6004256.', *ACS chemical neuroscience*, 7(12), pp. 1706–1716. doi: 10.1021/acschemneuro.6b00230.

Gregory, K., Sexton, P. and Christopoulos, A. (2007) 'Allosteric Modulation of Muscarinic Acetylcholine Receptors', *Current Neuropharmacology*, 5(3), pp. 157–167. doi: 10.2174/157015907781695946.

Guerra-Gomes, S. *et al.* (2018) 'Functional Roles of Astrocyte Calcium Elevations: From

Synapses to Behavior', *Frontiers in Cellular Neuroscience*. Frontiers, 11, p. 427. doi: 10.3389/fncel.2017.00427.

Guettier, J.-M., Gautam, D., Scarselli, M., Ruiz de Azua, I., *et al.* (2009a) 'A chemical-genetic approach to study G protein regulation of beta cell function in vivo.', *Proceedings of the National Academy of Sciences of the United States of America*. National Academy of Sciences, 106(45), pp. 19197–202. doi: 10.1073/pnas.0906593106.

Guettier, J.-M., Gautam, D., Scarselli, M., Ruiz de Azua, I., *et al.* (2009b) 'A chemical-genetic approach to study G protein regulation of beta cell function in vivo.', *Proceedings of the National Academy of Sciences of the United States of America*, 106(45), pp. 19197–202. doi: 10.1073/pnas.0906593106.

Guettier, J.-M., Gautam, D., Scarselli, M., de Azua, I. R., *et al.* (2009) 'A chemical-genetic approach to study G protein regulation of β cell function in vivo', *Proceedings of the National Academy of Sciences*, 106(45), pp. 19197–19202. doi: 10.1073/pnas.0906593106.

Gupta, S. *et al.* (2009) 'Ratiometric Ca $^{+2}$ measurement in human recombinant muscarinic receptor subtypes using the Flexstation scanning fluorometer', *Journal of Receptors and Signal Transduction*, 29(2), pp. 100–106. doi: 10.1080/10799890902802634.

Gurevich, V. V. and Gurevich, E. V. (2018) 'Arrestins and G proteins in cellular signaling: The coin has two sides', *Science Signaling*, 11(549), p. eaav1646. doi: 10.1126/scisignal.aav1646.

Gurevich, V. V and Gurevich, E. V (2006) 'The structural basis of arrestin-mediated regulation of G-protein-coupled receptors.', *Pharmacology & therapeutics*. NIH Public Access, 110(3), pp. 465–502. doi: 10.1016/j.pharmthera.2005.09.008.

Haga, K. *et al.* (1996) 'Phosphorylation of Human m1 Muscarinic Acetylcholine Receptors by G Protein-coupled Receptor Kinase 2 and Protein Kinase C', *Journal of Biological Chemistry*, 271(5), pp. 2776–2782. doi: 10.1074/jbc.271.5.2776.

Haga, K. *et al.* (2012) 'Structure of the human M2 muscarinic acetylcholine receptor

bound to an antagonist', *Nature*, 482(7386), pp. 547–551. doi: 10.1038/nature10753.

Ben Haim, L. *et al.* (2015) 'Elusive roles for reactive astrocytes in neurodegenerative diseases', *Frontiers in Cellular Neuroscience*. Frontiers Media SA, 9. doi: 10.3389/fncel.2015.00278.

Halassa, M. M. *et al.* (2007) 'Synaptic islands defined by the territory of a single astrocyte.', *The Journal of neuroscience : the official journal of the Society for Neuroscience*. Society for Neuroscience, 27(24), pp. 6473–7. doi: 10.1523/JNEUROSCI.1419-07.2007.

Hall (2000) 'Second messengers, ion channels and pharmacology of airway smooth muscle.', *The European respiratory journal*. European Respiratory Society, 15(6), pp. 1120–7. doi: 10.1034/j.1399-3003.2000.01523.x.

Hall, D. A. (2000) 'Modeling the Functional Effects of Allosteric Modulators at Pharmacological Receptors: An Extension of the Two-State Model of Receptor Activation', *Molecular Pharmacology*, 58(6), pp. 1412–1423. doi: 10.1124/mol.58.6.1412.

Hall, M. P. *et al.* (2012) 'Engineered Luciferase Reporter from a Deep Sea Shrimp Utilizing a Novel Imidazopyrazinone Substrate', *ACS Chemical Biology*, 7(11), pp. 1848–1857. doi: 10.1021/cb3002478.

Hama, S. *et al.* (2007) 'Quantitative and mechanism-based investigation of post-nuclear delivery events between adenovirus and lipoplex', *Nucleic Acids Research*, 35(5), pp. 1533–1543. doi: 10.1093/nar/gkl1165.

Hamm, H. *et al.* (1988) 'Site of G protein binding to rhodopsin mapped with synthetic peptides from the alpha subunit', *Science*, 241(4867), pp. 832–835. doi: 10.1126/science.3136547.

Hammer, R. *et al.* (1980) 'Pirenzepine distinguishes between different subclasses of muscarinic receptors', *Nature*, 283(5742), pp. 90–92. doi: 10.1038/283090a0.

Han, M. *et al.* (2001) 'Crystal structure of beta-arrestin at 1.9 A: possible mechanism of receptor binding and membrane Translocation.', *Structure (London, England :*

1993), 9(9), pp. 869–80. Available at: http://www.ncbi.nlm.nih.gov/pubmed/11566136 (Accessed: 30 August 2019).

Hanazono, Y. *et al.* (1997) 'Green Fluorescent Protein Retroviral Vectors: Low Titer and High Recombination Frequency Suggest a Selective Disadvantage', *Human Gene Therapy*, 8(11), pp. 1313–1319. doi: 10.1089/hum.1997.8.11-1313.

Hanson, C. J., Bootman, M. D. and Roderick, H. L. (2004) 'Cell Signalling: IP3 Receptors Channel Calcium into Cell Death', *Current Biology*. Cell Press, 14(21), pp. R933–R935. doi: 10.1016/J.CUB.2004.10.019.

Hardy, J. and Higgins, G. (1992) 'Alzheimer's disease: the amyloid cascade hypothesis', *Science*, 256(5054), pp. 184–185. doi: 10.1126/science.1566067.

Harikumar, K. G. *et al.* (2012) 'Glucagon-like peptide-1 receptor dimerization differentially regulates agonist signaling but does not affect small molecule allostery', *Proceedings of the National Academy of Sciences*, 109(45), pp. 18607–18612. doi: 10.1073/pnas.1205227109.

Harrison, S. and Bers, D. (1987) 'The effect of temperature and ionic strength on the apparent Ca-affinity of EGTA and the analogous Ca-chelators BAPTA and dibromo-BAPTA', *Biochimica et Biophysica Acta (BBA) - General Subjects*, 925(2), pp. 133–143. doi: 10.1016/0304-4165(87)90102-4.

Haruki, H., Gonzalez, M. R. and Johnsson, K. (2012) 'Exploiting Ligand-Protein Conjugates to Monitor Ligand-Receptor Interactions', *PLoS ONE*. Edited by B. G. Vertessy. Public Library of Science, 7(5), p. e37598. doi: 10.1371/journal.pone.0037598.

Haseloff, J. *et al.* (1997) 'Removal of a cryptic intron and subcellular localization of green fluorescent protein are required to mark transgenic Arabidopsis plants brightly.', *Proceedings of the National Academy of Sciences of the United States of America*. National Academy of Sciences, 94(6), pp. 2122–7. doi: 10.1073/pnas.94.6.2122.

Hasselmo, M. E. (2006) 'The role of acetylcholine in learning and memory.', *Current opinion in neurobiology*, 16(6), pp. 710–5. doi: 10.1016/j.conb.2006.09.002.

Hauser, A. S. *et al.* (2017) 'Trends in GPCR drug discovery: new agents, targets and indications', *Nature Reviews Drug Discovery*, 16(12), pp. 829–842. doi: 10.1038/nrd.2017.178.

Haustein, M. D. *et al.* (2014) 'Conditions and Constraints for Astrocyte Calcium Signaling in the Hippocampal Mossy Fiber Pathway', *Neuron*, 82(2), pp. 413–429. doi: 10.1016/j.neuron.2014.02.041.

Hein, P. *et al.* (2005) 'Dynamics of receptor/G protein coupling in living cells', *The EMBO Journal*, 24(23), pp. 4106–4114. doi: 10.1038/sj.emboj.7600870.

Heller, J. P. and Rusakov, D. A. (2015) 'Morphological plasticity of astroglia: Understanding synaptic microenvironment', *Glia*, 63(12), pp. 2133–2151. doi: 10.1002/glia.22821.

Hepnarova, V. *et al.* (2018) 'The concept of hybrid molecules of tacrine and benzyl quinolone carboxylic acid (BQCA) as multifunctional agents for Alzheimer's disease', *European Journal of Medicinal Chemistry*, 150, pp. 292–306. doi: 10.1016/j.ejmech.2018.02.083.

Hermans, E. (2003) 'Biochemical and pharmacological control of the multiplicity of coupling at G-protein-coupled receptors.', *Pharmacology & therapeutics*, 99(1), pp. 25–44. Available at: http://www.ncbi.nlm.nih.gov/pubmed/12804697 (Accessed: 3 September 2019).

Hertz, L. *et al.* (1984) 'Receptor expression in primary cultures of neurons or astrocytes.', *Progress in neuro-psychopharmacology & biological psychiatry*, 8(4–6), pp. 521–7. Available at: http://www.ncbi.nlm.nih.gov/pubmed/6099585 (Accessed: 15 August 2019).

Hertz, L. *et al.* (2004) 'Astrocytic adrenoceptors: a major drug target in neurological and psychiatric disorders?', *Current drug targets. CNS and neurological disorders*, 3(3), pp. 239–67. Available at: http://www.ncbi.nlm.nih.gov/pubmed/15180484 (Accessed: 9 September 2019).

Hertz, L. *et al.* (2010) 'Adrenoceptors in brain: Cellular gene expression and effects on astrocytic metabolism and [Ca2+]i', *Neurochemistry International*, 57(4), pp. 411–420.

doi: 10.1016/j.neuint.2010.03.019.

Hill, A. V. (1910) 'The possible effects of the aggregation of the molecules of haemoglobin on its oxygen dissociation curve', *J. Physiol.* Available at: https://www.scienceopen.com/document?vid=7a9a2f9a-b092-4ef0-834b-13edd3beae47 (Accessed: 5 September 2019).

Hill, A. V (1909) 'The mode of action of nicotine and curari, determined by the form of the contraction curve and the method of temperature coefficients.', *The Journal of physiology*. Wiley-Blackwell, 39(5), pp. 361–73. doi: 10.1113/jphysiol.1909.sp001344.

Hirshman, C. A. and Emala, C. W. (1999) 'Actin reorganization in airway smooth muscle cells involves Gq and Gi2 activation of Rho', *American Journal of Physiology-Lung Cellular and Molecular Physiology*, 277(3), pp. L653–L661. doi: 10.1152/ajplung.1999.277.3.L653.

Hlavackova, V. *et al.* (2012) 'Sequential Inter- and Intrasubunit Rearrangements During Activation of Dimeric Metabotropic Glutamate Receptor 1', *Science Signaling*, 5(237), pp. ra59–ra59. doi: 10.1126/scisignal.2002720.

Hoare, S. (2005) 'Mechanisms of peptide and nonpeptide ligand binding to Class B G-protein-coupled receptors', *Drug Discovery Today*, 10(6), pp. 417–427. doi: 10.1016/S1359-6446(05)03370-2.

Hoffmann, C. *et al.* (2005) 'A FlAsH-based FRET approach to determine G protein–coupled receptor activation in living cells', *Nature Methods*, 2(3), pp. 171–176. doi: 10.1038/nmeth742.

Hol, E. M. and Pekny, M. (2015) 'Glial fibrillary acidic protein (GFAP) and the astrocyte intermediate filament system in diseases of the central nervous system', *Current Opinion in Cell Biology*, 32, pp. 121–130. doi: 10.1016/j.ceb.2015.02.004.

Hollingsworth, S. A. *et al.* (2019) 'Cryptic pocket formation underlies allosteric modulator selectivity at muscarinic GPCRs', *Nature Communications*, 10(1), p. 3289. doi: 10.1038/s41467-019-11062-7.

Van Horn, M. R. *et al.* (2017) 'The Gliotransmitter d-Serine Promotes Synapse

Maturation and Axonal Stabilization *In Vivo*', *The Journal of Neuroscience*, 37(26), pp. 6277–6288. doi: 10.1523/JNEUROSCI.3158-16.2017.

Horvat, A. and Vardjan, N. (2019) 'Astroglial cAMP signalling in space and time', *Neuroscience Letters*. doi: 10.1016/j.neulet.2018.06.025.

Horvat, A., Zorec, R. and Vardjan, N. (2016) 'Adrenergic stimulation of single rat astrocytes results in distinct temporal changes in intracellular Ca2+ and cAMP-dependent PKA responses', *Cell Calcium*, 59(4), pp. 156–163. doi: 10.1016/j.ceca.2016.01.002.

Hu, J. *et al.* (2010) 'Structural basis of G protein–coupled receptor–G protein interactions', *Nature Chemical Biology*, 6(7), pp. 541–548. doi: 10.1038/nchembio.385.

Hu, X. *et al.* (2016) 'Heterogeneous astrocytes: Active players in CNS', *Brain Research Bulletin*. Elsevier Inc., 125, pp. 1–18. doi: 10.1016/j.brainresbull.2016.03.017.

Huang, X.-P. *et al.* (2005) 'Critical Amino Acid Residues of the Common Allosteric Site on the M_2 Muscarinic Acetylcholine Receptor: More Similarities than Differences between the Structurally Divergent Agents Gallamine and Bis(ammonio)alkane-Type Hexamethylene- *bis* -[dimethyl-(3-phthalimidopropyl)ammonium]dibromide', *Molecular Pharmacology*, 68(3), pp. 769–778. doi: 10.1124/mol.105.014043.

Huang, X. P. *et al.* (1999) 'Roles of threonine 192 and asparagine 382 in agonist and antagonist interactions with M1 muscarinic receptors.', *British journal of pharmacology*. Wiley-Blackwell, 126(3), pp. 735–45. doi: 10.1038/sj.bjp.0702301.

Hüfner, K., Frajo-Apor, B. and Hofer, A. (2015) 'Neurology Issues in Schizophrenia', *Current Psychiatry Reports*, 17(5), p. 32. doi: 10.1007/s11920-015-0570-4.

Hughes, P. *et al.* (2007) 'The costs of using unauthenticated, over-passaged cell lines: how much more data do we need?', *BioTechniques*, 43(5), pp. 575–586. doi: 10.2144/000112598.

Hulme, E. C. and Trevethick, M. A. (2010) 'Ligand binding assays at equilibrium: validation and interpretation.', *British journal of pharmacology*. Wiley-Blackwell,

161(6), pp. 1219–37. doi: 10.1111/j.1476-5381.2009.00604.x.

Isberg, V. *et al.* (2015) 'Generic GPCR residue numbers - aligning topology maps while minding the gaps.', *Trends in pharmacological sciences*. NIH Public Access, 36(1), pp. 22–31. doi: 10.1016/j.tips.2014.11.001.

Jacob, F. and Monod, J. (1961) 'Genetic regulatory mechanisms in the synthesis of proteins', *Journal of Molecular Biology*. Academic Press, 3(3), pp. 318–356. doi: 10.1016/S0022-2836(61)80072-7.

Jakubík, J. *et al.* (1997) 'Positive Cooperativity of Acetylcholine and Other Agonists with Allosteric Ligands on Muscarinic Acetylcholine Receptors', *Molecular Pharmacology*, 52(1), pp. 172–179. doi: 10.1124/mol.52.1.172.

Jann, M. W., Lam, Y. W. and Chang, W. H. (1994) 'Rapid formation of clozapine in guinea-pigs and man following clozapine-N-oxide administration.', *Archives internationales de pharmacodynamie et de therapie*, 328(2), pp. 243–50. Available at: http://www.ncbi.nlm.nih.gov/pubmed/7710309 (Accessed: 21 June 2019).

Jendryka, M. *et al.* (2019) 'Pharmacokinetic and pharmacodynamic actions of clozapine-N-oxide, clozapine, and compound 21 in DREADD-based chemogenetics in mice', *Scientific Reports*, 9(1), p. 4522. doi: 10.1038/s41598-019-41088-2.

Jensen, D. D. *et al.* (2017) 'Neurokinin 1 receptor signaling in endosomes mediates sustained nociception and is a viable therapeutic target for prolonged pain relief', *Science Translational Medicine*, 9(392), p. eaal3447. doi: 10.1126/scitranslmed.aal3447.

Jeon, W. J. *et al.* (2015) 'The Role of Muscarinic Receptors in the Pathophysiology of Mood Disorders: A Potential Novel Treatment?', *Current neuropharmacology*. Bentham Science Publishers, 13(6), pp. 739–49. doi: 10.2174/1570159X13666150612230045.

De Jesús, M. L. *et al.* (2006) 'Cyclic AMP-dependent and Epac-mediated Activation of R-Ras by G Protein-coupled Receptors Leads to Phospholipase D Stimulation', *Journal of Biological Chemistry*, 281(31), pp. 21837–21847. doi: 10.1074/jbc.M604156200.

Jiang, S. *et al.* (2014a) 'M1 muscarinic acetylcholine receptor in Alzheimer's disease', *Neuroscience Bulletin*, 30(2), pp. 295–307. doi: 10.1007/s12264-013-1406-z.

Jiang, S. *et al.* (2014b) 'M1 muscarinic acetylcholine receptor in Alzheimer's disease', *Neuroscience Bulletin*, 30(2), pp. 295–307. doi: 10.1007/s12264-013-1406-z.

John, G. R. *et al.* (2004) 'Interleukin-1beta induces a reactive astroglial phenotype via deactivation of the Rho GTPase-Rock axis.', *The Journal of neuroscience : the official journal of the Society for Neuroscience*, 24(11), pp. 2837–45. doi: 10.1523/JNEUROSCI.4789-03.2004.

John Lin, C. C. *et al.* (2017) 'Identification of diverse astrocyte populations and their malignant analogs', *Nature Neuroscience*. Nature Publishing Group, 20(3), pp. 396–405. doi: 10.1038/nn.4493.

Johnson, A. A. T. *et al.* (2005) 'Spatial control of transgene expression in rice (Oryza sativa L.) using the GAL4 enhancer trapping system', *The Plant Journal*, 41(5), pp. 779–789. doi: 10.1111/j.1365-313X.2005.02339.x.

Johnson, D. E. *et al.* (2005) 'Inhibitory Effects of Antipsychotics on Carbachol-Enhanced Insulin Secretion From Perifused Rat Islets: Role of Muscarinic Antagonism in Antipsychotic-Induced Diabetes and Hyperglycemia', *Diabetes*, 54(5), pp. 1552–1558. doi: 10.2337/diabetes.54.5.1552.

Jones, C. K. *et al.* (2008) 'Novel selective allosteric activator of the M1 muscarinic acetylcholine receptor regulates amyloid processing and produces antipsychotic-like activity in rats.', *The Journal of neuroscience : the official journal of the Society for Neuroscience*, 28(41), pp. 10422–33. doi: 10.1523/JNEUROSCI.1850-08.2008.

Juillerat, A. *et al.* (2003) 'Directed evolution of O6-alkylguanine-DNA alkyltransferase for efficient labeling of fusion proteins with small molecules in vivo.', *Chemistry & biology*, 10(4), pp. 313–7. Available at: http://www.ncbi.nlm.nih.gov/pubmed/12725859 (Accessed: 15 September 2019).

Jung, S.-R. *et al.* (2017) 'Muscarinic receptor regulates extracellular signal regulated kinase by two modes of arrestin binding', *Proceedings of the National Academy of Sciences*, 114(28), pp. E5579–E5588. doi: 10.1073/pnas.1700331114.

Kaestner, L., Scholz, A. and Lipp, P. (2015) 'Conceptual and technical aspects of transfection and gene delivery.', *Bioorganic & medicinal chemistry letters*, 25(6), pp. 1171–6. doi: 10.1016/j.bmcl.2015.01.018.

Kálmán, M. (2002) 'GFAP expression withdraws--a trend of glial evolution?', *Brain research bulletin*. Elsevier Inc., 57(3–4), pp. 509–11. doi: 10.1016/s0361-9230(01)00713-4.

Kamal, F. A. *et al.* (2014) 'Simultaneous adrenal and cardiac g-protein-coupled receptor-gβγ inhibition halts heart failure progression.', *Journal of the American College of Cardiology*. NIH Public Access, 63(23), pp. 2549–2557. doi: 10.1016/j.jacc.2014.02.587.

Kan, W. *et al.* (2014) 'M3 muscarinic receptor interaction with phospholipase C β3 determines its signaling efficiency.', *The Journal of biological chemistry*. American Society for Biochemistry and Molecular Biology, 289(16), pp. 11206–18. doi: 10.1074/jbc.M113.538546.

Kanemaru, K. *et al.* (2013) 'Calcium-dependent N-cadherin up-regulation mediates reactive astrogliosis and neuroprotection after brain injury', *Proceedings of the National Academy of Sciences*, 110(28), pp. 11612–11617. doi: 10.1073/pnas.1300378110.

Kanemaru, K. *et al.* (2014) 'In Vivo Visualization of Subtle, Transient, and Local Activity of Astrocytes Using an Ultrasensitive Ca2+ Indicator', *Cell Reports*, 8(1), pp. 311–318. doi: 10.1016/j.celrep.2014.05.056.

Kang, D. S., Tian, X. and Benovic, J. L. (2014) 'Role of β-arrestins and arrestin domain-containing proteins in G protein-coupled receptor trafficking.', *Current opinion in cell biology*. NIH Public Access, 27, pp. 63–71. doi: 10.1016/j.ceb.2013.11.005.

Kang, H. C., Lee, M. and Bae, Y. H. (2005) 'Polymeric gene carriers.', *Critical reviews in eukaryotic gene expression*, 15(4), pp. 317–42. Available at: http://www.ncbi.nlm.nih.gov/pubmed/16472063 (Accessed: 23 September 2019).

Kang, M. and Othmer, H. G. (2009) 'Spatiotemporal characteristics of calcium dynamics in astrocytes.', *Chaos (Woodbury, N.Y.)*. American Institute of Physics, 19(3),

p. 037116. doi: 10.1063/1.3206698.

Kang, Y. *et al.* (2015) 'Crystal structure of rhodopsin bound to arrestin by femtosecond X-ray laser', *Nature*, 523(7562), pp. 561–567. doi: 10.1038/nature14656.

Karra, D. and Dahm, R. (2010) 'Transfection techniques for neuronal cells.', *The Journal of neuroscience : the official journal of the Society for Neuroscience*. Society for Neuroscience, 30(18), pp. 6171–7. doi: 10.1523/JNEUROSCI.0183-10.2010.

Katerina, Z. *et al.* (2004) 'Investigation of M1/M4 Muscarinic Receptors in the Anterior Cingulate Cortex in Schizophrenia, Bipolar Disorder, and Major Depression Disorder', *Neuropsychopharmacology*, 29(3), pp. 619–625. doi: 10.1038/sj.npp.1300367.

Katona, G. *et al.* (2012) 'Fast two-photon in vivo imaging with three-dimensional random-access scanning in large tissue volumes', *Nature Methods*, 9(2), pp. 201–208. doi: 10.1038/nmeth.1851.

Katzenschlager, R. *et al.* (2002) 'Anticholinergics for symptomatic management of Parkinson´s disease', *Cochrane Database of Systematic Reviews*, (2), p. CD003735. doi: 10.1002/14651858.CD003735.

Kawai, H., Lazar, R. and Metherate, R. (2007) 'Nicotinic control of axon excitability regulates thalamocortical transmission', *Nature Neuroscience*, 10(9), pp. 1168–1175. doi: 10.1038/nn1956.

Keeney, M. *et al.* (2013) 'Development of poly(β-amino ester)-based biodegradable nanoparticles for nonviral delivery of minicircle DNA.', *ACS nano*. NIH Public Access, 7(8), pp. 7241–50. doi: 10.1021/nn402657d.

Kenakin, T. (2005) 'New Concepts in Drug Discovery: Collateral Efficacy and Permissive Antagonism', *Nature Reviews Drug Discovery*, 4(11), pp. 919–927. doi: 10.1038/nrd1875.

Kenakin, T. (2007) 'Allosteric Agonist Modulators', *Journal of Receptors and Signal Transduction*, 27(4), pp. 247–259. doi: 10.1080/10799890701509000.

Kenakin, T. *et al.* (2012) 'A simple method for quantifying functional selectivity and agonist bias.', *ACS chemical neuroscience*. American Chemical Society, 3(3), pp. 193–

203. doi: 10.1021/cn200111m.

Kenakin, T. (2016) 'The mass action equation in pharmacology.', *British journal of clinical pharmacology*. Wiley-Blackwell, 81(1), pp. 41–51. doi: 10.1111/bcp.12810.

Kenakin, T. and Miller, L. J. (2010) 'Seven Transmembrane Receptors as Shapeshifting Proteins: The Impact of Allosteric Modulation and Functional Selectivity on New Drug Discovery', *Pharmacological Reviews*, 62(2), pp. 265–304. doi: 10.1124/pr.108.000992.

Kenakin, T. P. (2012a) 'Biased signalling and allosteric machines: new vistas and challenges for drug discovery.', *British journal of pharmacology*. Wiley-Blackwell, 165(6), pp. 1659–1669. doi: 10.1111/j.1476-5381.2011.01749.x.

Kenakin, T. P. (2012b) 'Biased signalling and allosteric machines: new vistas and challenges for drug discovery.', *British journal of pharmacology*. Wiley-Blackwell, 165(6), pp. 1659–69. doi: 10.1111/j.1476-5381.2011.01749.x.

Kendall, R. T. and Luttrell, L. M. (2009) 'Diversity in arrestin function', *Cellular and Molecular Life Sciences*, 66(18), pp. 2953–2973. doi: 10.1007/s00018-009-0088-1.

Keov, P. *et al.* (2014) 'Molecular Mechanisms of Bitopic Ligand Engagement with the M1 Muscarinic Acetylcholine Receptor', *Journal of Biological Chemistry*, 289(34), pp. 23817–23837. doi: 10.1074/jbc.M114.582874.

Keov, P., Sexton, P. M. and Christopoulos, A. (2011) 'Allosteric modulation of G protein-coupled receptors: a pharmacological perspective.', *Neuropharmacology*, 60(1), pp. 24–35. doi: 10.1016/j.neuropharm.2010.07.010.

Keppler, A., Kindermann, M., *et al.* (2004) 'Labeling of fusion proteins of O6-alkylguanine-DNA alkyltransferase with small molecules in vivo and in vitro', *Methods*, 32(4), pp. 437–444. doi: 10.1016/j.ymeth.2003.10.007.

Keppler, A., Pick, H., *et al.* (2004) 'Labeling of fusion proteins with synthetic fluorophores in live cells.', *Proceedings of the National Academy of Sciences of the United States of America*. National Academy of Sciences, 101(27), pp. 9955–9. doi: 10.1073/pnas.0401923101.

Khajehali, Elham *et al.* (2018) 'Probing the binding site of novel selective positive allosteric modulators at the M 1 muscarinic acetylcholine receptor', *Biochemical Pharmacology*, 154, pp. 243–254. doi: 10.1016/j.bcp.2018.05.009.

Khajehali, E *et al.* (2018) 'Probing the binding site of novel selective positive allosteric modulators at the M1 muscarinic acetylcholine receptor', *Biochemical Pharmacology*. Elsevier, 154, pp. 243–254. doi: 10.1016/J.BCP.2018.05.009.

El Khamlichi, C. *et al.* (2019) 'Bioluminescence Resonance Energy Transfer as a Method to Study Protein-Protein Interactions: Application to G Protein Coupled Receptor Biology.', *Molecules (Basel, Switzerland)*. Multidisciplinary Digital Publishing Institute (MDPI), 24(3). doi: 10.3390/molecules24030537.

Kilpatrick, L. E. and Holliday, N. D. (2012) 'Dissecting the Pharmacology of G Protein-Coupled Receptor Signaling Complexes Using Bimolecular Fluorescence Complementation', in *Methods in molecular biology (Clifton, N.J.)*, pp. 109–138. doi: 10.1007/978-1-61779-909-9_6.

Kilpatrick, L. E., Humphrys, L. J. and Holliday, N. D. (2015) 'A G Protein–Coupled Receptor Dimer Imaging Assay Reveals Selectively Modified Pharmacology of Neuropeptide Y Y1/Y5 Receptor Heterodimers', *Molecular Pharmacology*, 87(4), pp. 718–732. doi: 10.1124/mol.114.095356.

Kimelberg, H. K. (2004) 'The problem of astrocyte identity', *Neurochemistry International*. Elsevier Ltd, 45(2–3), pp. 191–202. doi: 10.1016/j.neuint.2003.08.015.

Kirchberg, K. *et al.* (2011) 'Conformational dynamics of helix 8 in the GPCR rhodopsin controls arrestin activation in the desensitization process.', *Proceedings of the National Academy of Sciences of the United States of America*. National Academy of Sciences, 108(46), pp. 18690–5. doi: 10.1073/pnas.1015461108.

Klein Herenbrink, C. *et al.* (2016) 'The role of kinetic context in apparent biased agonism at GPCRs', *Nature Communications*. Nature Publishing Group, 7(1), p. 10842. doi: 10.1038/ncomms10842.

Kniazeff, J. *et al.* (2011) 'Dimers and beyond: The functional puzzles of class C GPCRs', *Pharmacology & Therapeutics*, 130(1), pp. 9–25. doi:

10.1016/j.pharmthera.2011.01.006.

Koehl, A. *et al.* (2018) 'Structure of the μ-opioid receptor–Gi protein complex', *Nature*. Nature Publishing Group, 558(7711), pp. 547–552. doi: 10.1038/s41586-018-0219-7.

Koizumi, S. *et al.* (2002) 'Spatial and temporal aspects of Ca2+ signaling mediated by P2Y receptors in cultured rat hippocampal astrocytes.', *Life sciences*, 72(4–5), pp. 431–42. doi: 10.1016/s0024-3205(02)02273-7.

Kolakowski, L. F. (1994) 'GCRDb: a G-protein-coupled receptor database.', *Receptors & channels*, 2(1), pp. 1–7. Available at: http://www.ncbi.nlm.nih.gov/pubmed/8081729 (Accessed: 25 August 2019).

Koyama, Y. (2015) 'Functional alterations of astrocytes in mental disorders: pharmacological significance as a drug target', *Frontiers in Cellular Neuroscience*. Frontiers, 9, p. 261. doi: 10.3389/fncel.2015.00261.

Krencik, R., van Asperen, J. V and Ullian, E. M. (2017) 'Human astrocytes are distinct contributors to the complexity of synaptic function.', *Brain research bulletin*. NIH Public Access, 129, pp. 66–73. doi: 10.1016/j.brainresbull.2016.08.012.

Krupnick, J. G. *et al.* (1997) 'Arrestin/Clathrin Interaction', *Journal of Biological Chemistry*, 272(23), pp. 15011–15016. doi: 10.1074/jbc.272.23.15011.

Kruse, A. C. *et al.* (2012) 'Structure and dynamics of the M3 muscarinic acetylcholine receptor', *Nature*, 482(7386), pp. 552–556. doi: 10.1038/nature10867.

Kruse, A. C. *et al.* (2013) 'Activation and allosteric modulation of a muscarinic acetylcholine receptor', *Nature*, 504(7478), pp. 101–106. doi: 10.1038/nature12735.

Kruse, Andrew C *et al.* (2014) 'Muscarinic acetylcholine receptors: novel opportunities for drug development.', *Nature reviews. Drug discovery*. Nature Publishing Group, a division of Macmillan Publishers Limited. All Rights Reserved., 13(7), pp. 549–60. doi: 10.1038/nrd4295.

Kruse, Andrew C. *et al.* (2014) 'Novel insights into M3 muscarinic acetylcholine receptor physiology and structure', *Journal of Molecular Neuroscience*, 53(3), pp. 316–323. doi: 10.1007/s12031-013-0127-0.

Kurimoto, E. *et al.* (2018) 'An Approach to Discovering Novel Muscarinic M $_1$ Receptor Positive Allosteric Modulators with Potent Cognitive Improvement and Minimized Gastrointestinal Dysfunction', *Journal of Pharmacology and Experimental Therapeutics*, 364(1), pp. 28–37. doi: 10.1124/jpet.117.243774.

Lagerström, M. C. and Schiöth, H. B. (2008) 'Structural diversity of G protein-coupled receptors and significance for drug discovery', *Nature Reviews Drug Discovery*, 7(4), pp. 339–357. doi: 10.1038/nrd2518.

Lambright, D. G. *et al.* (1994) 'Structural determinants for activation of the α-subunit of a heterotrimeric G protein', *Nature*, 369(6482), pp. 621–628. doi: 10.1038/369621a0.

Lambright, D. G. *et al.* (1996) 'The 2.0 Å crystal structure of a heterotrimeric G protein', *Nature*, 379(6563), pp. 311–319. doi: 10.1038/379311a0.

Lander, E. S. *et al.* (2001) 'Initial sequencing and analysis of the human genome', *Nature*, 409(6822), pp. 860–921. doi: 10.1038/35057062.

Lane, J. R., Abdul-ridha, A. and Canals, M. (2013) 'Regulation of G Protein-Coupled Receptors by Allosteric Ligands.pdf', *ACS chemical neuroscience*, 4, pp. 527–534.

Langmead, C. J. *et al.* (2006) 'Probing the molecular mechanism of interaction between 4-n-butyl-1-[4-(2-methylphenyl)-4-oxo-1-butyl]-piperidine (AC-42) and the muscarinic M(1) receptor: direct pharmacological evidence that AC-42 is an allosteric agonist.', *Molecular pharmacology*, 69(1), pp. 236–46. doi: 10.1124/mol.105.017814.

Lasiecka, Z. M. and Winckler, B. (2016) 'Studying endosomes in cultured neurons by live-cell imaging.', *Methods in cell biology*, 131, pp. 389–408. doi: 10.1016/bs.mcb.2015.07.002.

Latorraca, N. R., Venkatakrishnan, A. J. and Dror, R. O. (2017) 'GPCR Dynamics: Structures in Motion', *Chemical Reviews*, 117(1), pp. 139–155. doi: 10.1021/acs.chemrev.6b00177.

Latsari, M. *et al.* (2002) 'Noradrenergic innervation of the developing and mature visual and motor cortex of the rat brain: A light and electron microscopic

immunocytochemical analysis', *The Journal of Comparative Neurology*. John Wiley & Sons, Ltd, 445(2), pp. 145–158. doi: 10.1002/cne.10156.

Leach, K. *et al.* (2010) 'Molecular mechanisms of action and in vivo validation of an M4 muscarinic acetylcholine receptor allosteric modulator with potential antipsychotic properties.', *Neuropsychopharmacology : official publication of the American College of Neuropsychopharmacology*. Nature Publishing Group, 35(4), pp. 855–69. doi: 10.1038/npp.2009.194.

Lebois, E. P. *et al.* (2010) 'Discovery and characterization of novel subtype-selective allosteric agonists for the investigation of M(1) receptor function in the central nervous system.', *ACS chemical neuroscience*. American Chemical Society, 1(2), pp. 104–121. doi: 10.1021/cn900003h.

Lebois, E. P. *et al.* (2011) 'Development of a highly selective, orally bioavailable and CNS penetrant M1 agonist derived from the MLPCN probe ML071.', *Bioorganic & medicinal chemistry letters*. NIH Public Access, 21(21), pp. 6451–5. doi: 10.1016/j.bmcl.2011.08.084.

Lee, S.-M., Booe, J. M. and Pioszak, A. A. (2015) 'Structural insights into ligand recognition and selectivity for classes A, B, and C GPCRs.', *European journal of pharmacology*. NIH Public Access, 763(Pt B), pp. 196–205. doi: 10.1016/j.ejphar.2015.05.013.

Lefkimmiatis, K. and Zaccolo, M. (2014) 'CAMP signaling in subcellular compartments', *Pharmacology and Therapeutics*. Elsevier Inc., pp. 295–304. doi: 10.1016/j.pharmthera.2014.03.008.

Letzkus, J. J. *et al.* (2011) 'A disinhibitory microcircuit for associative fear learning in the auditory cortex', *Nature*, 480(7377), pp. 331–335. doi: 10.1038/nature10674.

Levey, A. I. (1993) 'Immunological localization of m1-m5 muscarinic acetylcholine receptors in peripheral tissues and brain.', *Life sciences*, 52(5–6), pp. 441–8. Available at: http://www.ncbi.nlm.nih.gov/pubmed/8441326 (Accessed: 23 February 2016).

Levey, A. I. *et al.* (1994) 'Localization of muscarinic M3 receptor protein and M3 receptor binding in rat brain', *Neuroscience*, 63(1), pp. 207–221. doi: 10.1016/0306-

4522(94)90017-5.

Levey, A. I. (1996) 'Muscarinic acetylcholine receptor expression in memory circuits: Implications for treatment of Alzheimer disease', *Proceedings of the National Academy of Sciences of the United States of America*. National Academy of Sciences, 93(24), p. 13541. doi: 10.1073/PNAS.93.24.13541.

Levoye, A. *et al.* (2015) 'A Broad G Protein-Coupled Receptor Internalization Assay that Combines SNAP-Tag Labeling, Diffusion-Enhanced Resonance Energy Transfer, and a Highly Emissive Terbium Cryptate', *Frontiers in Endocrinology*, 6, p. 167. doi: 10.3389/fendo.2015.00167.

Li, X. *et al.* (2016) 'Nanoparticle-mediated conversion of primary human astrocytes into neurons and oligodendrocytes.', *Biomaterials science*. NIH Public Access, 4(7), pp. 1100–12. doi: 10.1039/c6bm00140h.

Liang, Y.-L. *et al.* (2017) 'Phase-plate cryo-EM structure of a class B GPCR–G-protein complex', *Nature*, 546(7656), pp. 118–123. doi: 10.1038/nature22327.

Liang, Y.-L. *et al.* (2018) 'Phase-plate cryo-EM structure of a biased agonist-bound human GLP-1 receptor–Gs complex', *Nature*, 555(7694), pp. 121–125. doi: 10.1038/nature25773.

Lipp, P., Lüscher, C. and Niggli, E. (1996) 'Photolysis of caged compounds characterized by ratiometric confocal microscopy: a new approach to homogeneously control and measure the calcium concentration in cardiac myocytes.', *Cell calcium*, 19(3), pp. 255–66. Available at: http://www.ncbi.nlm.nih.gov/pubmed/8732265 (Accessed: 16 September 2019).

Liu, H.-S. *et al.* (1999) 'Is Green Fluorescent Protein Toxic to the Living Cells?', *Biochemical and Biophysical Research Communications*, 260(3), pp. 712–717. doi: 10.1006/bbrc.1999.0954.

Liu, M. *et al.* (2016) 'Optically Pure, Structural, and Fluorescent Analogues of a Dimeric Y_4 Receptor Agonist Derived by an Olefin Metathesis Approach', *Journal of Medicinal Chemistry*, 59(13), pp. 6059–6069. doi: 10.1021/acs.jmedchem.6b00310.

Liu, X. *et al.* (2017) 'Mechanism of intracellular allosteric β2AR antagonist revealed by X-ray crystal structure', *Nature*, 548(7668), pp. 480–484. doi: 10.1038/nature23652.

Liu, Y. *et al.* (1992) 'Morphology and distribution of neurons and glial cells expressing ß-adrenergic receptors in developing kitten visual cortex', *Developmental Brain Research*. Elsevier, 65(2), pp. 269–273. doi: 10.1016/0165-3806(92)90188-3.

Logothetis, D. E. *et al.* (1987) 'The βγ subunits of GTP-binding proteins activate the muscarinic K+ channel in heart', *Nature*, 325(6102), pp. 321–326. doi: 10.1038/325321a0.

Lohse, M. J., Maiellaro, I. and Calebiro, D. (2014) 'Kinetics and mechanism of G protein-coupled receptor activation', *Current Opinion in Cell Biology*. Elsevier Current Trends, 27, pp. 87–93. doi: 10.1016/J.CEB.2013.11.009.

Lopez, A. J. *et al.* (2015) 'Promoter specific effects of DREADD modulation on synaptic plasticity and hippocampal learning', *Journal of Neuroscience*, 36(12), pp. 3588–3599. doi: 10.1523/JNEUROSCI.3682-15.2016.

Lu, S. *et al.* (2014) 'The Structural Basis of ATP as an Allosteric Modulator', *PLoS Computational Biology*. Edited by G. Wei, 10(9), p. e1003831. doi: 10.1371/journal.pcbi.1003831.

Ludwin, S. K., Kosek, J. C. and Eng, L. F. (1976) 'The topographical distribution of S-100 and GFA proteins in the adult rat brain: An immunohistochemical study using horseradish peroxidase-labelled antibodies', *The Journal of Comparative Neurology*. John Wiley & Sons, Ltd, 165(2), pp. 197–207. doi: 10.1002/cne.901650206.

Lundberg, C. *et al.* (1996) 'Generation of DOPA-producing astrocytes by retroviral transduction of the human tyrosine hydroxylase gene: In vitro characterization and in vivo effects in the rat Parkinson model', *Experimental Neurology*. Academic Press Inc., 139(1), pp. 39–53. doi: 10.1006/exnr.1996.0079.

Luttrell, L. M. *et al.* (1999) 'β-Arrestin-Dependent Formation of β_2 Adrenergic Receptor-Src Protein Kinase Complexes', *Science*, 283(5402), pp. 655–661. doi: 10.1126/science.283.5402.655.

Luttrell, L. M. *et al.* (2001) 'Activation and targeting of extracellular signal-regulated kinases by -arrestin scaffolds', *Proceedings of the National Academy of Sciences*, 98(5), pp. 2449–2454. doi: 10.1073/pnas.041604898.

Luttrell, L. M. and Lefkowitz, R. J. (2002) 'The role of beta-arrestins in the termination and transduction of G-protein-coupled receptor signals.', *Journal of cell science*. The Company of Biologists Ltd, 115(Pt 3), pp. 455–65. doi: 10.1074/jbc.274.3.1185.

Ma, L. *et al.* (2009) 'Selective activation of the M1 muscarinic acetylcholine receptor achieved by allosteric potentiation.', *Proceedings of the National Academy of Sciences of the United States of America*. National Academy of Sciences, 106(37), pp. 15950–5. doi: 10.1073/pnas.0900903106.

Ma, Z. *et al.* (2016) 'Neuromodulators signal through astrocytes to alter neural circuit activity and behaviour', *Nature*, 539(7629), pp. 428–432. doi: 10.1038/nature20145.

Macias-Contreras, M., He, H. and Zhu, L. (2018) 'Beyond O ^{6} -Benzylguanine: O ^{6} -(5-Pyridylmethyl)guanine as a Substrate for the Self-Labeling Enzyme SNAP-Tag', *Bioconjugate Chemistry*, 29(12), pp. 4104–4109. doi: 10.1021/acs.bioconjchem.8b00703.

MacLaren, D. A. A. *et al.* (2016) 'Clozapine N-Oxide Administration Produces Behavioral Effects in Long–Evans Rats: Implications for Designing DREADD Experiments', *eNeuro*. Society for Neuroscience, 3(5). doi: 10.1523/ENEURO.0219-16.2016.

Maeda, S. *et al.* (2019) 'Structures of the M1 and M2 muscarinic acetylcholine receptor/G-protein complexes', *Science*, 364(6440), pp. 552–557. doi: 10.1126/science.aaw5188.

Mahler, S. V and Aston-Jones, G. (2018) 'CNO Evil? Considerations for the Use of DREADDs in Behavioral Neuroscience', *Neuropsychopharmacology*. Nature Publishing Group, 43(5), pp. 934–936. doi: 10.1038/npp.2017.299.

Mahoney, J. P. and Sunahara, R. K. (2016) 'Mechanistic insights into GPCR-G protein interactions.', *Current opinion in structural biology*. NIH Public Access, 41, pp. 247–254. doi: 10.1016/j.sbi.2016.11.005.

Maier-Peuschel, M. *et al.* (2010) 'A fluorescence resonance energy transfer-based M2 muscarinic receptor sensor reveals rapid kinetics of allosteric modulation.', *The Journal of biological chemistry*, 285(12), pp. 8793–800. doi: 10.1074/jbc.M109.098517.

Manglik, A. *et al.* (2015) 'Structural Insights into the Dynamic Process of β 2 -Adrenergic Receptor Signaling', *Cell*, 161(5), pp. 1101–1111. doi: 10.1016/j.cell.2015.04.043.

Mantyh, P. W. *et al.* (1995) 'Beta 2-adrenergic receptors are expressed by glia in vivo in the normal and injured central nervous system in the rat, rabbit, and human.', *The Journal of neuroscience : the official journal of the Society for Neuroscience*, 15(1 Pt 1), pp. 152–64. Available at: http://www.ncbi.nlm.nih.gov/pubmed/7823126 (Accessed: 9 September 2019).

Manuscript, A. *et al.* (2014) 'An excitatory paraventricular nucleus to AgRP neuron circuit that drives hunger.', *Nature*, 507(7491), pp. 238–242. doi: 10.1038/nature12956.A.

Manvich *et al.* (2018) 'The DREADD agonist clozapine N-oxide (CNO) is reverse-metabolized to clozapine and produces clozapine-like interoceptive stimulus effects in rats and mice', *Scientific Reports*. Nature Publishing Group, 8(1), p. 3840. doi: 10.1038/s41598-018-22116-z.

Marlo, J. E. *et al.* (2009) 'Discovery and characterization of novel allosteric potentiators of M1 muscarinic receptors reveals multiple modes of activity.', *Molecular pharmacology*, 75(3), pp. 577–88. doi: 10.1124/mol.108.052886.

Marquer, C. *et al.* (2011) 'Structural Model of Ligand-G Protein-coupled Receptor (GPCR) Complex Based on Experimental Double Mutant Cycle Data', *Journal of Biological Chemistry*, 286(36), pp. 31661–31675. doi: 10.1074/jbc.M111.261404.

Martin-Fernandez, M. *et al.* (2017) 'Synapse-specific astrocyte gating of amygdala-related behavior', *Nature Neuroscience*, 20(11), pp. 1540–1548. doi: 10.1038/nn.4649.

Marwick, K. F. M. and Hardingham, G. E. (2017) 'Transfection in primary cultured

neuronal cells', in *Methods in Molecular Biology*. Humana Press Inc., pp. 137–144. doi: 10.1007/978-1-4939-7321-7_6.

Maurisse, R. *et al.* (2010) 'Comparative transfection of DNA into primary and transformed mammalian cells from different lineages', *BMC Biotechnology*, 10. doi: 10.1186/1472-6750-10-9.

May, L. T. *et al.* (2007) 'Allosteric Modulation of G Protein–Coupled Receptors', *Annual Review of Pharmacology and Toxicology*, 47(1), pp. 1–51. doi: 10.1146/annurev.pharmtox.47.120505.105159.

McKeon, R. J., Jurynec, M. J. and Buck, C. R. (1999) 'The chondroitin sulfate proteoglycans neurocan and phosphacan are expressed by reactive astrocytes in the chronic CNS glial scar.', *The Journal of neuroscience : the official journal of the Society for Neuroscience*, 19(24), pp. 10778–88. Available at: http://www.ncbi.nlm.nih.gov/pubmed/10594061 (Accessed: 12 August 2019).

McKinley, J. W. *et al.* (2019) 'Dopamine Deficiency Reduces Striatal Cholinergic Interneuron Function in Models of Parkinson's Disease', *Neuron*. Cell Press. doi: 10.1016/J.NEURON.2019.06.013.

Melancon, B. J. *et al.* (2012) 'Allosteric Modulation of Seven Transmembrane Spanning Receptors: Theory, Practice, and Opportunities for Central Nervous System Drug Discovery', *Journal of Medicinal Chemistry*, 55(4), pp. 1445–1464. doi: 10.1021/jm201139r.

Melancon, B. J. *et al.* (2013) 'Allosteric modulation of the M1 muscarinic acetylcholine receptor: improving cognition and a potential treatment for schizophrenia and Alzheimer's disease.', *Drug discovery today*. NIH Public Access, 18(23–24), pp. 1185–99. doi: 10.1016/j.drudis.2013.09.005.

Meltzer, H. Y. (1994) 'An overview of the mechanism of action of clozapine.', *The Journal of clinical psychiatry*, 55 Suppl B, pp. 47–52. Available at: http://www.ncbi.nlm.nih.gov/pubmed/7961573 (Accessed: 21 June 2019).

Mertz, K. D. *et al.* (2002) 'Electroporation of primary neural cultures: a simple method for directed gene transfer in vitro.', *Histochemistry and cell biology*, 118(6), pp. 501–

6. doi: 10.1007/s00418-002-0473-4.

Michnick, S. W. *et al.* (2011) 'Protein-Fragment Complementation Assays for Large-Scale Analysis, Functional Dissection and Dynamic Studies of Protein–Protein Interactions in Living Cells', in, pp. 395–425. doi: 10.1007/978-1-61779-160-4_25.

Mie, M. *et al.* (2012) 'Development of a split SNAP-tag protein complementation assay for visualization of protein–protein interactions in living cells', *The Analyst*, 137(20), p. 4760. doi: 10.1039/c2an35762c.

Milligan, G. and Kostenis, E. (2009) 'Heterotrimeric G-proteins: a short history', *British Journal of Pharmacology*, 147(S1), pp. S46–S55. doi: 10.1038/sj.bjp.0706405.

Milligan, G., Ward, R. J. and Marsango, S. (2019) 'GPCR homo-oligomerization', *Current Opinion in Cell Biology*, 57, pp. 40–47. doi: 10.1016/j.ceb.2018.10.007.

Mishima, T. and Hirase, H. (2010) 'In Vivo Intracellular Recording Suggests That Gray Matter Astrocytes in Mature Cerebral Cortex and Hippocampus Are Electrophysiologically Homogeneous', *Journal of Neuroscience*. Society for Neuroscience, 30(8), pp. 3093–3100. doi: 10.1523/jneurosci.5065-09.2010.

Mistry, S. N. *et al.* (2013) 'Synthesis and pharmacological profiling of analogues of benzyl quinolone carboxylic acid (BQCA) as allosteric modulators of the M1 muscarinic receptor.', *Journal of medicinal chemistry*, 56(12), pp. 5151–72. doi: 10.1021/jm400540b.

Mistry, S. N. *et al.* (2016) '4-Phenylpyridin-2-one Derivatives: A Novel Class of Positive Allosteric Modulator of the M_1 Muscarinic Acetylcholine Receptor', *Journal of Medicinal Chemistry*. American Chemical Society, 59(1), pp. 388–409. doi: 10.1021/acs.jmedchem.5b01562.

Miyakawa, T. *et al.* (2001) 'Hyperactivity and Intact Hippocampus-Dependent Learning in Mice Lacking the M1 Muscarinic Acetylcholine Receptor', *Journal of Neuroscience*. Society for Neuroscience, 21(14), pp. 5239–5250. doi: 10.1523/JNEUROSCI.21-14-05239.2001.

Molnar, T. *et al.* (2016) 'Store-Operated Calcium Entry in Muller Glia Is Controlled by

Synergistic Activation of TRPC and Orai Channels', *Journal of Neuroscience*. doi: 10.1523/jneurosci.4069-15.2016.

Mondal, S. *et al.* (2013) 'Membrane Driven Spatial Organization of GPCRs', *Scientific Reports*. Nature Publishing Group, 3(1), p. 2909. doi: 10.1038/srep02909.

Monod, J., Changeux, J. P. and Jacob, F. (1963) 'Allosteric proteins and cellular control systems.', *Journal of molecular biology*, 6, pp. 306–29. doi: 10.1016/s0022-2836(63)80091-1.

Monod, J., Wyman, J. and Changeux, J. P. (1965) 'ON THE NATURE OF ALLOSTERIC TRANSITIONS: A PLAUSIBLE MODEL.', *Journal of molecular biology*, 12, pp. 88–118. Available at: http://www.ncbi.nlm.nih.gov/pubmed/14343300 (Accessed: 17 August 2016).

Moran, S. P., Dickerson, J. W., *et al.* (2018) 'M1-positive allosteric modulators lacking agonist activity provide the optimal profile for enhancing cognition', *Neuropsychopharmacology*, 43(8), pp. 1763–1771. doi: 10.1038/s41386-018-0033-9.

Moran, S. P., Cho, H. P., *et al.* (2018) 'PF-06827443 Displays Robust Allosteric Agonist and Positive Allosteric Modulator Activity in High Receptor Reserve and Native Systems', *ACS Chemical Neuroscience*, 9(9), pp. 2218–2224. doi: 10.1021/acschemneuro.8b00106.

Muñoz-Torrero, D. (2008) 'Acetylcholinesterase inhibitors as disease-modifying therapies for Alzheimer's disease.', *Current medicinal chemistry*, 15(24), pp. 2433–55. doi: 10.2174/092986708785909067.

Murk, K. *et al.* (2013) 'The antagonistic modulation of Arp2/3 activity by N-WASP, WAVE2 and PICK1 defines dynamic changes in astrocyte morphology', *Journal of Cell Science*, 126(17), pp. 3873–3883. doi: 10.1242/jcs.125146.

Murphy, S., Pearce, B. and Morrow, C. (1986) 'Astrocytes have both M1 and M2 muscarinic receptor subtypes.', *Brain research*, 364(1), pp. 177–80. Available at: http://www.ncbi.nlm.nih.gov/pubmed/3004648 (Accessed: 4 June 2017).

Muyderman, H. *et al.* (2010) 'Astrocytic responses to DNA delivery using

nucleofection.', *Neurochemical research*, 35(11), pp. 1771–9. doi: 10.1007/s11064-010-0243-y.

Myer, D. J. (2006) 'Essential protective roles of reactive astrocytes in traumatic brain injury', *Brain*, 129(10), pp. 2761–2772. doi: 10.1093/brain/awl165.

Nathan, P. J. *et al.* (2013) 'The potent M1 receptor allosteric agonist GSK1034702 improves episodic memory in humans in the nicotine abstinence model of cognitive dysfunction', *The International Journal of Neuropsychopharmacology*, 16(04), pp. 721–731. doi: 10.1017/S1461145712000752.

Naumenko, V. S. and Ponimaskin, E. (2018) 'Palmitoylation as a Functional Regulator of Neurotransmitter Receptors.', *Neural plasticity*. Hindawi Limited, 2018, p. 5701348. doi: 10.1155/2018/5701348.

Nawaratne, V. *et al.* (2010) 'Structural Determinants of Allosteric Agonism and Modulation at the M $_4$ Muscarinic Acetylcholine Receptor', *Journal of Biological Chemistry*, 285(25), pp. 19012–19021. doi: 10.1074/jbc.M110.125096.

Neer, E. J. *et al.* (1994) 'The ancient regulatory-protein family of WD-repeat proteins', *Nature*, 371(6495), pp. 297–300. doi: 10.1038/371297a0.

Neer, E. J., Pulsifer, L. and Wolf, L. G. (1988) 'The amino terminus of G protein alpha subunits is required for interaction with beta gamma.', *The Journal of biological chemistry*, 263(18), pp. 8996–70. Available at: http://www.ncbi.nlm.nih.gov/pubmed/3132454 (Accessed: 27 August 2019).

Nehmé, R. *et al.* (2017) 'Mini-G proteins: Novel tools for studying GPCRs in their active conformation', *PLOS ONE*. Edited by A. Shukla. Public Library of Science, 12(4), p. e0175642. doi: 10.1371/journal.pone.0175642.

Nett, W. J., Oloff, S. H. and McCarthy, K. D. (2002) 'Hippocampal Astrocytes In Situ Exhibit Calcium Oscillations That Occur Independent of Neuronal Activity', *Journal of Neurophysiology*, 87(1), pp. 528–537. doi: 10.1152/jn.00268.2001.

Nickols, H. H. and Conn, P. J. (2014) 'Development of allosteric modulators of GPCRs for treatment of CNS disorders.', *Neurobiology of disease*. NIH Public Access, 61, pp.

55–71. doi: 10.1016/j.nbd.2013.09.013.

Nixdorf-Bergweiler, B. E., Albrecht, D. and Heinemann, U. (1994) 'Developmental changes in the number, size, and orientation of GFAP-positive cells in the CA1 region of rat hippocampus', *Glia*, 12(3), pp. 180–195. doi: 10.1002/glia.440120304.

Noyce, A. and Bandopadhyay, R. (2017) 'Parkinson's Disease: Basic Pathomechanisms and a Clinical Overview', in *Advances in neurobiology*, pp. 55–92. doi: 10.1007/978-3-319-57193-5_3.

O'Donnell, J. *et al.* (2012) 'Norepinephrine: a neuromodulator that boosts the function of multiple cell types to optimize CNS performance.', *Neurochemical research*. NIH Public Access, 37(11), pp. 2496–512. doi: 10.1007/s11064-012-0818-x.

Oberheim, N. A. *et al.* (2009) 'Uniquely Hominid Features of Adult Human Astrocytes', *Journal of Neuroscience*, 29(10), pp. 3276–3287. doi: 10.1523/JNEUROSCI.4707-08.2009.

Ogata, K. and Kosaka, T. (2002) 'Structural and quantitative analysis of astrocytes in the mouse hippocampus.', *Neuroscience*, 113(1), pp. 221–33. doi: 10.1016/s0306-4522(02)00041-6.

Oki, T. *et al.* (2005) 'Quantitative analysis of binding parameters of [3H]N-methylscopolamine in central nervous system of muscarinic acetylcholine receptor knockout mice', *Molecular Brain Research*, 133(1), pp. 6–11. doi: 10.1016/j.molbrainres.2004.09.012.

Oldham, W. M. and Hamm, H. E. (2008) 'Heterotrimeric G protein activation by G-protein-coupled receptors', *Nature Reviews Molecular Cell Biology*, 9(1), pp. 60–71. doi: 10.1038/nrm2299.

Olsen, C. K., Brennum, L. T. and Kreilgaard, M. (2008) 'Using pharmacokinetic-pharmacodynamic modelling as a tool for prediction of therapeutic effective plasma levels of antipsychotics.', *European journal of pharmacology*, 584(2–3), pp. 318–27. doi: 10.1016/j.ejphar.2008.02.005.

Osterholm, R. K. and Camoriano, J. K. (1982) 'Transdermal scopolamine psychosis.',

JAMA, 247(22), p. 3081. Available at: http://www.ncbi.nlm.nih.gov/pubmed/7077797 (Accessed: 25 August 2019).

Oswald, C. *et al.* (2016) 'Intracellular allosteric antagonism of the CCR9 receptor', *Nature*, 540(7633), pp. 462–465. doi: 10.1038/nature20606.

Owen, D. J., Collins, B. M. and Evans, P. R. (2004) 'Adaptros for clathrin coats: Structure and Function', *Annual Review of Cell and Developmental Biology*, 20(1), pp. 153–191. doi: 10.1146/annurev.cellbio.20.010403.104543.

Pakaski, M. and Kalman, J. (2008) 'Interactions between the amyloid and cholinergic mechanisms in Alzheimer's disease', *Neurochemistry International*, 53(5), pp. 103–111. doi: 10.1016/j.neuint.2008.06.005.

Palczewski, K. *et al.* (1991) 'Role of the carboxyl-terminal region of arrestin in binding to phosphorylated rhodopsin.', *The Journal of biological chemistry*, 266(23), pp. 15334–9. Available at: http://www.ncbi.nlm.nih.gov/pubmed/1651326 (Accessed: 30 August 2019).

Palczewski, K. *et al.* (2000) 'Crystal Structure of Rhodopsin: A G Protein-Coupled Receptor', *Science*, 289(5480), pp. 739–745. doi: 10.1126/science.289.5480.739.

Palmer, E. and Freeman, T. (2004) 'Investigation into the use of C- and N-terminal GFP fusion proteins for subcellular localization studies using reverse transfection microarrays.', *Comparative and functional genomics*. Hindawi Limited, 5(4), pp. 342–53. doi: 10.1002/cfg.405.

Pankratov, Y. and Lalo, U. (2015) 'Role for astroglial α1-adrenoreceptors in gliotransmission and control of synaptic plasticity in the neocortex', *Frontiers in Cellular Neuroscience*, 9, p. 230. doi: 10.3389/fncel.2015.00230.

Paredes, R. M. *et al.* (2008) 'Chemical calcium indicators', *Methods*. doi: 10.1016/j.ymeth.2008.09.025.

Park, P. S.-H., Lodowski, D. T. and Palczewski, K. (2008) 'Activation of G protein-coupled receptors: beyond two-state models and tertiary conformational changes.', *Annual review of pharmacology and toxicology*. NIH Public Access, 48, pp. 107–41. doi:

10.1146/annurev.pharmtox.48.113006.094630.

Parker, I., Choi, J. and Yao, Y. (1996) 'Elementary events of InsP3-induced Ca2+ liberation in Xenopus oocytes: hot spots, puffs and blips.', *Cell calcium*, 20(2), pp. 105–21. Available at: http://www.ncbi.nlm.nih.gov/pubmed/8889202 (Accessed: 16 August 2019).

Parpura, V. *et al.* (1994) 'Glutamate-mediated astrocyte–neuron signalling', *Nature*, 369(6483), pp. 744–747. doi: 10.1038/369744a0.

Parpura, V. and Zorec, R. (2010) 'Gliotransmission: Exocytotic release from astrocytes', *Brain Research Reviews*, 63(1–2), pp. 83–92. doi: 10.1016/j.brainresrev.2009.11.008.

Parri, H. . and Crunelli, V. (2003) 'The role of Ca2+ in the generation of spontaneous astrocytic Ca2+ oscillations', *Neuroscience*. Pergamon, 120(4), pp. 979–992. doi: 10.1016/S0306-4522(03)00379-8.

Parri, H. R., Gould, T. M. and Crunelli, V. (2001) 'Spontaneous astrocytic Ca2+ oscillations in situ drive NMDAR-mediated neuronal excitation', *Nature Neuroscience*, 4(8), pp. 803–812. doi: 10.1038/90507.

Paukert, M., Agarwal, A., Cha, J., Doze, Van A, *et al.* (2014) 'Norepinephrine controls astroglial responsiveness to local circuit activity.', *Neuron*. NIH Public Access, 82(6), pp. 1263–70. doi: 10.1016/j.neuron.2014.04.038.

Paukert, M., Agarwal, A., Cha, J., Doze, Van A., *et al.* (2014) 'Norepinephrine Controls Astroglial Responsiveness to Local Circuit Activity', *Neuron*, 82(6), pp. 1263–1270. doi: 10.1016/j.neuron.2014.04.038.

Paulus, W. and Jellinger, K. (1991) 'The Neuropathologic Basis of Different Clinical Subgroups of Parkinson's Disease', *Journal of Neuropathology & Experimental Neurology*, 50(6), pp. 743–755. doi: 10.1097/00005072-199111000-00006.

Pavlos, N. J. and Friedman, P. A. (2017) 'GPCR Signaling and Trafficking: The Long and Short of It.', *Trends in endocrinology and metabolism: TEM*. NIH Public Access, 28(3), pp. 213–226. doi: 10.1016/j.tem.2016.10.007.

Pekny, M. and Pekna, M. (2016) 'Reactive gliosis in the pathogenesis of CNS diseases',

Biochimica et Biophysica Acta (BBA) - Molecular Basis of Disease, 1862(3), pp. 483–491. doi: 10.1016/j.bbadis.2015.11.014.

Pekny, T. *et al.* (2014) 'Synemin is expressed in reactive astrocytes and Rosenthal fibers in Alexander disease', *APMIS*, 122(1), pp. 76–80. doi: 10.1111/apm.12088.

Perea, G. and Araque, A. (2005a) 'Properties of Synaptically Evoked Astrocyte Calcium Signal Reveal Synaptic Information Processing by Astrocytes', *Journal of Neuroscience*, 25(9), pp. 2192–2203. doi: 10.1523/JNEUROSCI.3965-04.2005.

Perea, G. and Araque, A. (2005b) 'Properties of Synaptically Evoked Astrocyte Calcium Signal Reveal Synaptic Information Processing by Astrocytes', *Journal of Neuroscience*, 25(9), pp. 2192–2203. doi: 10.1523/JNEUROSCI.3965-04.2005.

Perea, G., Sur, M. and Araque, A. (2014) 'Neuron-glia networks: integral gear of brain function', *Frontiers in Cellular Neuroscience*, 8. doi: 10.3389/fncel.2014.00378.

Petravicz, J., Fiacco, T. A. and McCarthy, K. D. (2008) 'Loss of IP3 Receptor-Dependent Ca2+ Increases in Hippocampal Astrocytes Does Not Affect Baseline CA1 Pyramidal Neuron Synaptic Activity', *Journal of Neuroscience*, 28(19), pp. 4967–4973. doi: 10.1523/JNEUROSCI.5572-07.2008.

Picciotto, M. R., Higley, M. J. and Mineur, Y. S. (2012) 'Acetylcholine as a neuromodulator: cholinergic signaling shapes nervous system function and behavior.', *Neuron*. NIH Public Access, 76(1), pp. 116–29. doi: 10.1016/j.neuron.2012.08.036.

Pierre, S. *et al.* (2009) 'Capturing adenylyl cyclases as potential drug targets', *Nature Reviews Drug Discovery*, pp. 321–335. doi: 10.1038/nrd2827.

Piggott, M. A. *et al.* (2003) 'Muscarinic receptors in basal ganglia in dementia with Lewy bodies, Parkinson's disease and Alzheimer's disease.', *Journal of chemical neuroanatomy*, 25(3), pp. 161–73. Available at: http://www.ncbi.nlm.nih.gov/pubmed/12706204 (Accessed: 3 September 2019).

Ploier, B. *et al.* (2016) 'Dimerization deficiency of enigmatic retinitis pigmentosa-linked rhodopsin mutants', *Nature Communications*. Nature Publishing Group, 7(1), p. 12832. doi: 10.1038/ncomms12832.

Politi, A. *et al.* (2006) 'Models of IP3 and Ca2+ oscillations: frequency encoding and identification of underlying feedbacks.', *Biophysical journal*. The Biophysical Society, 90(9), pp. 3120–33. doi: 10.1529/biophysj.105.072249.

Porter, J. T. and McCarthy, K. D. (1997) 'Astrocytic neurotransmitter receptors in situ and in vivo.', *Progress in neurobiology*, 51(4), pp. 439–55. Available at: http://www.ncbi.nlm.nih.gov/pubmed/9106901 (Accessed: 22 July 2019).

Presland, J. (2005) 'Identifying novel modulators of G protein-coupled receptors via interaction at allosteric sites.', *Current opinion in drug discovery & development*, 8(5), pp. 567–76. Available at: http://www.ncbi.nlm.nih.gov/pubmed/16159018 (Accessed: 5 July 2019).

Putney, J. W. and Tomita, T. (2012) 'Phospholipase C signaling and calcium influx.', *Advances in biological regulation*. NIH Public Access, 52(1), pp. 152–64. doi: 10.1016/j.advenzreg.2011.09.005.

Racchetti, G., D'Alessandro, R. and Meldolesi, J. (2012) 'Astrocyte stellation, a process dependent on Rac1 is sustained by the regulated exocytosis of enlargeosomes', *Glia*, 60(3), pp. 465–475. doi: 10.1002/glia.22280.

Rang, H. P. (2006) 'The receptor concept: pharmacology's big idea.', *British journal of pharmacology*. Wiley-Blackwell, 147 Suppl 1(Suppl 1), pp. S9-16. doi: 10.1038/sj.bjp.0706457.

Raper, J. *et al.* (2017) 'Metabolism and Distribution of Clozapine-N-oxide: Implications for Nonhuman Primate Chemogenetics', *ACS Chemical Neuroscience*. American Chemical Society, 8(7), pp. 1570–1576. doi: 10.1021/acschemneuro.7b00079.

Rasmussen *et al.* (2011) 'Crystal structure of the β2 adrenergic receptor-Gs protein complex.', *Nature*. NIH Public Access, 477(7366), pp. 549–55. doi: 10.1038/nature10361.

Rasmussen, S. G. F., DeVree, B. T., *et al.* (2011) 'Crystal structure of the β2 adrenergic receptor–Gs protein complex', *Nature*, 477(7366), pp. 549–555. doi: 10.1038/nature10361.

Rasmussen, S. G. F., Choi, H.-J., *et al.* (2011) 'Structure of a nanobody-stabilized active state of the β2 adrenoceptor', *Nature*, 469(7329), pp. 175–180. doi: 10.1038/nature09648.

Rasmussen, T. *et al.* (2001) 'The muscarinic receptor agonist BuTAC, a novel potential antipsychotic, does not impair learning and memory in mouse passive avoidance.', *Schizophrenia research*, 49(1–2), pp. 193–201. Available at: http://www.ncbi.nlm.nih.gov/pubmed/11343877 (Accessed: 30 August 2019).

Reichenbach, A., Derouiche, A. and Kirchhoff, F. (2010) 'Morphology and dynamics of perisynaptic glia', *Brain Research Reviews*, 63(1–2), pp. 11–25. doi: 10.1016/j.brainresrev.2010.02.003.

Reichman, W. E. (2003) 'Current pharmacologic options for patients with Alzheimer's disease', *Annals of General Hospital Psychiatry*. BioMed Central, 2(1), p. 1. doi: 10.1186/1475-2832-2-1.

Ren, Z. *et al.* (2016) 'Transmembrane Helices Tilt, Bend, Slide, Torque, and Unwind between Functional States of Rhodopsin', *Scientific Reports*. Nature Publishing Group, 6(1), p. 34129. doi: 10.1038/srep34129.

Renault-Mihara, F. *et al.* (2017) 'Regulation of RhoA by STAT3 coordinates glial scar formation', *The Journal of Cell Biology*, 216(8), pp. 2533–2550. doi: 10.1083/jcb.201610102.

Reuschlein, A. K. *et al.* (2019) 'Aspects of astrocytic cAMP signaling with an emphasis on the putative power of compartmentalized signals in health and disease', *GLIA*. doi: 10.1002/glia.23622.

Reyes-Alcaraz, A. *et al.* (2018) 'Conformational signatures in β-arrestin2 reveal natural biased agonism at a G-protein-coupled receptor', *Communications Biology*. Nature Publishing Group, 1(1), p. 128. doi: 10.1038/s42003-018-0134-3.

Rhee, S. G. (2001) 'Regulation of Phosphoinositide-Specific Phospholipase C', *Annual Review of Biochemistry*, 70(1), pp. 281–312. doi: 10.1146/annurev.biochem.70.1.281.

Rice, M. E. and Cragg, S. J. (2004) 'Nicotine amplifies reward-related dopamine signals

in striatum', *Nature Neuroscience*, 7(6), pp. 583–584. doi: 10.1038/nn1244.

Rickmann, M. and Wolff, J. R. (1995) 'S100 protein expression in subpopulations of neurons of rat brain', *Neuroscience*. Pergamon, 67(4), pp. 977–991. doi: 10.1016/0306-4522(94)00615-C.

Riobo, N. A. and Manning, D. R. (2005) 'Receptors coupled to heterotrimeric G proteins of the G12 family', *Trends in Pharmacological Sciences*, 26(3), pp. 146–154. doi: 10.1016/j.tips.2005.01.007.

Robel, S. *et al.* (2015) 'Reactive astrogliosis causes the development of spontaneous seizures.', *The Journal of neuroscience : the official journal of the Society for Neuroscience*. Society for Neuroscience, 35(8), pp. 3330–45. doi: 10.1523/JNEUROSCI.1574-14.2015.

Roberts, M. J. *et al.* (2018) 'The inhibition of human lung fibroblast proliferation and differentiation by Gs-coupled receptors is not predicted by the magnitude of cAMP response', *Respiratory Research*, 19(1), p. 56. doi: 10.1186/s12931-018-0759-2.

Robinson, S. *et al.* (2014) 'Chemogenetic silencing of neurons in retrosplenial cortex disrupts sensory preconditioning.', *The Journal of neuroscience : the official journal of the Society for Neuroscience*, 34(33), pp. 10982–8. doi: 10.1523/JNEUROSCI.1349-14.2014.

Rochais, F. *et al.* (2007) 'Real-time optical recording of beta1-adrenergic receptor activation reveals supersensitivity of the Arg389 variant to carvedilol.', *The Journal of clinical investigation*, 117(1), pp. 229–35. doi: 10.1172/JCI30012.

Rook, J. M. *et al.* (2018) 'A Novel M $_1$ PAM VU0486846 Exerts Efficacy in Cognition Models without Displaying Agonist Activity or Cholinergic Toxicity', *ACS Chemical Neuroscience*, 9(9), pp. 2274–2285. doi: 10.1021/acschemneuro.8b00131.

Rose, R. H., Briddon, S. J. and Holliday, N. D. (2010) 'Bimolecular fluorescence complementation: lighting up seven transmembrane domain receptor signalling networks', *British Journal of Pharmacology*. John Wiley & Sons, Ltd (10.1111), 159(4), pp. 738–750. doi: 10.1111/j.1476-5381.2009.00480.x.

Roth, B. L. (2016) 'DREADDs for Neuroscientists.', *Neuron*, 89(4). doi: 10.1016/j.neuron.2016.01.040.

Roth, B. L. (2019) 'How structure informs and transforms chemogenetics', *Current Opinion in Structural Biology*. Elsevier Current Trends, 57, pp. 9–16. doi: 10.1016/J.SBI.2019.01.016.

Roth, T. C. and Krochmal, A. R. (2018) 'Of molecules, memories and migration: M1 acetylcholine receptors facilitate spatial memory formation and recall during migratory navigation', *Proceedings of the Royal Society B: Biological Sciences*, 285(1891), p. 20181904. doi: 10.1098/rspb.2018.1904.

Ruberg, M. *et al.* (1982) 'Muscarinic binding and choline acetyltransferase activity in Parkinsonian subjects with reference to dementia', *Brain Research*, 232(1), pp. 129–139. doi: 10.1016/0006-8993(82)90615-1.

Rusakov, D. A. (2015) 'Disentangling calcium-driven astrocyte physiology', *Nature Reviews Neuroscience*. doi: 10.1038/nrn3878.

Sako, Y. *et al.* (2019) 'TAK-071, a novel M1 positive allosteric modulator with low cooperativity, improves cognitive function in rodents with few cholinergic side effects', *Neuropsychopharmacology*, 44(5), pp. 950–960. doi: 10.1038/s41386-018-0168-8.

Salah-Uddin, H. *et al.* (2009) 'Altered M1 Muscarinic Acetylcholine Receptor (CHRM1)-Gαq/11 Coupling in a Schizophrenia Endophenotype', *Neuropsychopharmacology*, 34(9), pp. 2156–2166. doi: 10.1038/npp.2009.41.

Sample, V., Newman, R. H. and Zhang, J. (2009) 'The structure and function of fluorescent proteins', *Chemical Society Reviews*, 38(10), p. 2852. doi: 10.1039/b913033k.

Santos, R. *et al.* (2017) 'A comprehensive map of molecular drug targets', *Nature Reviews Drug Discovery*. Nature Publishing Group, 16(1), pp. 19–34. doi: 10.1038/nrd.2016.230.

Sarvazyan, N. A., Remmers, A. E. and Neubig, R. R. (1998) 'Determinants of Gi1 α and

βγ Binding', *Journal of Biological Chemistry*, 273(14), pp. 7934–7940. doi: 10.1074/jbc.273.14.7934.

Sauter, E. J. *et al.* (2019) 'Induced neurons for the study of neurodegenerative and neurodevelopmental disorders', in *Methods in Molecular Biology*. Humana Press Inc., pp. 101–121. doi: 10.1007/978-1-4939-9080-1_9.

Savchenko, V. L. *et al.* (2000) 'Microglia and astrocytes in the adult rat brain: comparative immunocytochemical analysis demonstrates the efficacy of lipocortin 1 immunoreactivity', *Neuroscience*. Pergamon, 96(1), pp. 195–203. doi: 10.1016/S0306-4522(99)00538-2.

Scarr, E. *et al.* (2013) 'Decreased cortical muscarinic M1 receptors in schizophrenia are associated with changes in gene promoter methylation, mRNA and gene targeting microRNA.', *Translational psychiatry*. Nature Publishing Group, 3(2), p. e230. doi: 10.1038/tp.2013.3.

Scheerer, P. *et al.* (2008) 'Crystal structure of opsin in its G-protein-interacting conformation', *Nature*. Nature Publishing Group, 455(7212), pp. 497–502. doi: 10.1038/nature07330.

Schelshorn, D. *et al.* (2012) 'Lateral Allosterism in the Glucagon Receptor Family: Glucagon-Like Peptide 1 Induces G-Protein-Coupled Receptor Heteromer Formation', *Molecular Pharmacology*, 81(3), pp. 309–318. doi: 10.1124/mol.111.074757.

Schiweck, J., Eickholt, Britta J and Murk, K. (2018) 'Important Shapeshifter: Mechanisms Allowing Astrocytes to Respond to the Changing Nervous System During Development, Injury and Disease.', *Frontiers in cellular neuroscience*. Frontiers Media SA, 12, p. 261. doi: 10.3389/fncel.2018.00261.

Schiweck, J., Eickholt, Britta J. and Murk, K. (2018) 'Important Shapeshifter: Mechanisms Allowing Astrocytes to Respond to the Changing Nervous System During Development, Injury and Disease', *Frontiers in Cellular Neuroscience*. Frontiers Media SA, 12. doi: 10.3389/fncel.2018.00261.

Schmitt, A. *et al.* (1997) 'Cellular and regional distribution of the glutamate transporter GLAST in the CNS of rats: nonradioactive in situ hybridization and comparative

immunocytochemistry.', *The Journal of neuroscience : the official journal of the Society for Neuroscience*, 17(1), pp. 1–10. Available at: http://www.ncbi.nlm.nih.gov/pubmed/8987731 (Accessed: 28 August 2019).

Schöfl, C. *et al.* (1991) 'Frequency and amplitude enhancement of calcium transients by cyclic AMP in hepatocytes.', *The Biochemical journal*. Portland Press Limited, 273 (Pt 3)(3), pp. 799–802. doi: 10.1042/bj2730799.

Schöfl, C. *et al.* (1993) 'Temporal patterns of alpha 1-receptor stimulation regulate amplitude and frequency of calcium transients.', *The American journal of physiology*. American Physiological Society Bethesda, MD , 265(4 Pt 1), pp. C1030-6. doi: 10.1152/ajpcell.1993.265.4.C1030.

Schweinhuber, S. K. *et al.* (2015) 'Profilin Isoforms Modulate Astrocytic Morphology and the Motility of Astrocytic Processes', *PLOS ONE*. Edited by A. Dunaevsky, 10(1), p. e0117244. doi: 10.1371/journal.pone.0117244.

Scofield, M. D. *et al.* (2015a) 'Gq-DREADD selectively initiates glial glutamate release and inhibits cue-induced cocaine seeking', *Biological Psychiatry*, 78(7), pp. 441–451. doi: 10.1016/j.biopsych.2015.02.016.

Scofield, M. D. *et al.* (2015b) 'Gq-DREADD Selectively Initiates Glial Glutamate Release and Inhibits Cue-induced Cocaine Seeking', *Biological Psychiatry*, 78(7), pp. 441–451. doi: 10.1016/j.biopsych.2015.02.016.

Selent, J. *et al.* (2008) 'Multi-Receptor Binding Profile of Clozapine and Olanzapine: A Structural Study Based on the New β_2 Adrenergic Receptor Template', *ChemMedChem*, 3(8), pp. 1194–1198. doi: 10.1002/cmdc.200800074.

Semack, A. *et al.* (2016) 'Structural Elements in the Gαs and Gαq C Termini That Mediate Selective G Protein-coupled Receptor (GPCR) Signaling.', *The Journal of biological chemistry*. American Society for Biochemistry and Molecular Biology, 291(34), pp. 17929–40. doi: 10.1074/jbc.M116.735720.

Shain, W. *et al.* (1987) 'Morphology of astroglial cells is controlled by beta-adrenergic receptors', *The Journal of Cell Biology*, 105(5), pp. 2307–2314. doi: 10.1083/jcb.105.5.2307.

Shao, Y. and Sutin, J. (1992) 'Expression of adrenergic receptors in individual astrocytes and motor neurons isolated from the adult rat brain', *Glia*, 6(2), pp. 108–117. doi: 10.1002/glia.440060205.

Shekhar, A. *et al.* (2008) 'Selective Muscarinic Receptor Agonist Xanomeline as a Novel Treatment Approach for Schizophrenia', *American Journal of Psychiatry*, 165(8), pp. 1033–1039. doi: 10.1176/appi.ajp.2008.06091591.

Shelton, M. K. and McCarthy, K. D. (2000) 'Hippocampal astrocytes exhibit Ca2+-elevating muscarinic cholinergic and histaminergic receptors in situ.', *Journal of neurochemistry*, 74(2), pp. 555–63. Available at: http://www.ncbi.nlm.nih.gov/pubmed/10646506 (Accessed: 4 June 2017).

Sherpa, A. D. *et al.* (2016) 'Activation of β-adrenergic receptors in rat visual cortex expands astrocytic processes and reduces extracellular space volume', *Synapse*, 70(8), pp. 307–316. doi: 10.1002/syn.21908.

Shigetomi, E., Patel, S. and Khakh, B. S. (2016) 'Probing the Complexities of Astrocyte Calcium Signaling', *Trends in Cell Biology*, 26(4), pp. 300–312. doi: 10.1016/j.tcb.2016.01.003.

Shinoe, T. *et al.* (2005) 'Modulation of Synaptic Plasticity by Physiological Activation of M1 Muscarinic Acetylcholine Receptors in the Mouse Hippocampus', *Journal of Neuroscience*, 25(48), pp. 11194–11200. doi: 10.1523/JNEUROSCI.2338-05.2005.

Shirey, J. K. *et al.* (2009a) 'A selective allosteric potentiator of the M1 muscarinic acetylcholine receptor increases activity of medial prefrontal cortical neurons and restores impairments in reversal learning.', *The Journal of neuroscience : the official journal of the Society for Neuroscience*, 29(45), pp. 14271–86. doi: 10.1523/JNEUROSCI.3930-09.2009.

Shirey, J. K. *et al.* (2009b) 'A selective allosteric potentiator of the M1 muscarinic acetylcholine receptor increases activity of medial prefrontal cortical neurons and restores impairments in reversal learning.', *The Journal of neuroscience : the official journal of the Society for Neuroscience*, 29(45), pp. 14271–86. doi: 10.1523/JNEUROSCI.3930-09.2009.

Shoichet, B. K. and Kobilka, B. K. (2012) 'Structure-based drug screening for G-protein-coupled receptors', *Trends in Pharmacological Sciences*, 33(5), pp. 268–272. doi: 10.1016/j.tips.2012.03.007.

Shukla, A. K. *et al.* (2013) 'Structure of active β-arrestin-1 bound to a G-protein-coupled receptor phosphopeptide', *Nature*, 497(7447), pp. 137–141. doi: 10.1038/nature12120.

Siddiquee, K. *et al.* (2013) 'The apelin receptor inhibits the angiotensin II type 1 receptor via allosteric trans-inhibition.', *British journal of pharmacology*. Wiley-Blackwell, 168(5), pp. 1104–17. doi: 10.1111/j.1476-5381.2012.02192.x.

Silverman, W., Locovei, S. and Dahl, G. (2008) 'Probenecid, a gout remedy, inhibits pannexin 1 channels.', *American journal of physiology. Cell physiology*. American Physiological Society, 295(3), pp. C761-7. doi: 10.1152/ajpcell.00227.2008.

Simard, M. *et al.* (2003) 'Signaling at the gliovascular interface.', *The Journal of neuroscience : the official journal of the Society for Neuroscience*, 23(27), pp. 9254–62. Available at: http://www.ncbi.nlm.nih.gov/pubmed/14534260 (Accessed: 28 August 2019).

Siso-Nadal, F. *et al.* (2009) 'Cross-Talk between Signaling Pathways Can Generate Robust Oscillations in Calcium and cAMP', *PLoS ONE*. Edited by D. Di Bernardo, 4(10), p. e7189. doi: 10.1371/journal.pone.0007189.

Sloan, S. A. and Barres, B. A. (2014) 'Mechanisms of astrocyte development and their contributions to neurodevelopmental disorders', *Current Opinion in Neurobiology*, 27, pp. 75–81. doi: 10.1016/j.conb.2014.03.005.

Smith, J. S. and Rajagopal, S. (2016) 'The β-Arrestins: Multifunctional Regulators of G Protein-coupled Receptors.', *The Journal of biological chemistry*. American Society for Biochemistry and Molecular Biology, 291(17), pp. 8969–77. doi: 10.1074/jbc.R115.713313.

Smrcka, A. V. and Fisher, I. (2019a) 'G-protein βγ subunits as multi-functional scaffolds and transducers in G-protein-coupled receptor signaling', *Cellular and Molecular Life Sciences*. Springer International Publishing, pp. 1–13. doi: 10.1007/s00018-019-

03275-2.

Smrcka, A. V. and Fisher, I. (2019b) ‘G-protein βγ subunits as multi-functional scaffolds and transducers in G-protein-coupled receptor signaling’, *Cellular and Molecular Life Sciences*. doi: 10.1007/s00018-019-03275-2.

Smrcka, A. V (2008) ‘G protein βγ subunits: central mediators of G protein-coupled receptor signaling.’, *Cellular and molecular life sciences : CMLS*, 65(14), pp. 2191–214. doi: 10.1007/s00018-008-8006-5.

Smythies, J. (2005) ‘Section III. The Norepinephrine System’, in *International review of neurobiology*, pp. 173–211. doi: 10.1016/S0074-7742(05)64003-2.

Sondek, J. *et al.* (1996) ‘Crystal structure of a GA protein βγdimer at 2.1 Å resolution’, *Nature*, 379(6563), pp. 369–374. doi: 10.1038/379369a0.

Song, Y. and Gunnarson, E. (2012) ‘Potassium Dependent Regulation of Astrocyte Water Permeability Is Mediated by cAMP Signaling’, *PLoS ONE*. Edited by S. Barnes. Public Library of Science, 7(4), p. e34936. doi: 10.1371/journal.pone.0034936.

Souza, D. G. *et al.* (2013) ‘Characterization of adult rat astrocyte cultures.’, *PloS one*. Public Library of Science, 8(3), p. e60282. doi: 10.1371/journal.pone.0060282.

Spalding, T. A. *et al.* (2002) ‘Discovery of an ectopic activation site on the M(1) muscarinic receptor.’, *Molecular pharmacology*, 61(6), pp. 1297–302. Available at: http://www.ncbi.nlm.nih.gov/pubmed/12021390 (Accessed: 31 August 2016).

Spalding, T. A. *et al.* (2006) ‘Structural requirements of transmembrane domain 3 for activation by the M1 muscarinic receptor agonists AC-42, AC-260584, clozapine, and N-desmethylclozapine: evidence for three distinct modes of receptor activation.’, *Molecular pharmacology*, 70(6), pp. 1974–83. doi: 10.1124/mol.106.024901.

Sprang, S. R. (1997) ‘G protein mechanisms:Insights from Structural Analysis’, *Annual Review of Biochemistry*, 66(1), pp. 639–678. doi: 10.1146/annurev.biochem.66.1.639.

Sprang, S. R. (2016) ‘Invited review: Activation of G proteins by GTP and the mechanism of Gα-catalyzed GTP hydrolysis.’, *Biopolymers*. NIH Public Access, 105(8), pp. 449–62. doi: 10.1002/bip.22836.

Sridharan, R. *et al.* (2014) 'Fluorescent approaches for understanding interactions of ligands with G protein coupled receptors', *Biochimica et Biophysica Acta (BBA) - Biomembranes*. Elsevier, 1838(1), pp. 15–33. doi: 10.1016/J.BBAMEM.2013.09.005.

Srinivasan, R. *et al.* (2015) 'Ca2+ signaling in astrocytes from Ip3r2−/− mice in brain slices and during startle responses in vivo', *Nature Neuroscience*, 18(5), pp. 708–717. doi: 10.1038/nn.4001.

Staus, D. P. *et al.* (2016) 'Allosteric nanobodies reveal the dynamic range and diverse mechanisms of G-protein-coupled receptor activation', *Nature*, 535(7612), pp. 448–452. doi: 10.1038/nature18636.

Steinberg, S. F. (1999) 'The molecular basis for distinct β-adrenergic receptor subtype actions in cardiomyocytes', *Circulation Research*. Lippincott Williams and Wilkins, pp. 1101–1111. doi: 10.1161/01.RES.85.11.1101.

Steiner, J. *et al.* (2007) 'Evidence for a wide extra-astrocytic distribution of S100B in human brain.', *BMC neuroscience*. BioMed Central, 8, p. 2. doi: 10.1186/1471-2202-8-2.

Stępnicki, P., Kondej, M. and Kaczor, A. A. (2018) 'Current Concepts and Treatments of Schizophrenia', *Molecules*, 23(8), p. 2087. doi: 10.3390/molecules23082087.

Sternson, S. M. and Roth, B. L. (2014) 'Chemogenetic Tools to Interrogate Brain Functions', *Annual Review of Neuroscience*, 37(1), pp. 387–407. doi: 10.1146/annurev-neuro-071013-014048.

Stobart, J. L. *et al.* (2018) 'Cortical Circuit Activity Evokes Rapid Astrocyte Calcium Signals on a Similar Timescale to Neurons', *Neuron*, 98(4), pp. 726-735.e4. doi: 10.1016/j.neuron.2018.03.050.

Stoddart, L. A. *et al.* (2016) 'Fluorescence- and bioluminescence-based approaches to study GPCR ligand binding.', *British journal of pharmacology*, 173(20), pp. 3028–37. doi: 10.1111/bph.13316.

Stoddart, L. A. *et al.* (2018) 'Development of novel fluorescent histamine H1-receptor antagonists to study ligand-binding kinetics in living cells', *Scientific Reports*, 8(1), p.

1572. doi: 10.1038/s41598-018-19714-2.

Stoddart, L. A., Kilpatrick, L. E. and Hill, S. J. (2018) 'NanoBRET Approaches to Study Ligand Binding to GPCRs and RTKs.', *Trends in pharmacological sciences*. Elsevier, 39(2), pp. 136–147. doi: 10.1016/j.tips.2017.10.006.

Stoll, K. *et al.* (2018) 'Effects of muscarinic M1 and M4 acetylcholine receptor stimulation on extinction and reinstatement of cocaine seeking in male mice, independent of extinction learning', *Psychopharmacology*, 235(3), pp. 815–827. doi: 10.1007/s00213-017-4797-0.

Stott, Lisa A, Hall, D. A. and Holliday, N. D. (2016) 'Unravelling intrinsic efficacy and ligand bias at G protein coupled receptors: A practical guide to assessing functional data.', *Biochemical pharmacology*, 101, pp. 1–12. doi: 10.1016/j.bcp.2015.10.011.

Stott, Lisa A., Hall, D. A. and Holliday, N. D. (2016) 'Unravelling intrinsic efficacy and ligand bias at G protein coupled receptors: A practical guide to assessing functional data', *Biochemical Pharmacology*. Elsevier Inc., 101, pp. 1–12. doi: 10.1016/j.bcp.2015.10.011.

Strange, P. G. (2009) 'Agonist binding, agonist affinity and agonist efficacy at G protein-coupled receptors', *British Journal of Pharmacology*, 153(7), pp. 1353–1363. doi: 10.1038/sj.bjp.0707672.

Sugimoto, Naotoshi *et al.* (2003) 'Inhibitory and stimulatory regulation of Rac and cell motility by the G12/13-Rho and Gi pathways integrated downstream of a single G protein-coupled sphingosine-1-phosphate receptor isoform.', *Molecular and cellular biology*, 23(5), pp. 1534–45. doi: 10.1128/mcb.23.5.1534-1545.2003.

Sugimoto, N. *et al.* (2003) 'Inhibitory and Stimulatory Regulation of Rac and Cell Motility by the G12/13-Rho and Gi Pathways Integrated Downstream of a Single G Protein-Coupled Sphingosine-1-Phosphate Receptor Isoform', *Molecular and Cellular Biology*, 23(5), pp. 1534–1545. doi: 10.1128/MCB.23.5.1534-1545.2003.

Sukharev, S. I. *et al.* (1992) 'Electroporation and electrophoretic DNA transfer into cells. The effect of DNA interaction with electropores.', *Biophysical journal*, 63(5), pp. 1320–7. doi: 10.1016/S0006-3495(92)81709-5.

Sweger, E. J. *et al.* (2007) 'Development of Hydrocephalus in Mice Expressing the Gi-Coupled GPCR Ro1 RASSL Receptor in Astrocytes', *Journal of Neuroscience*. Society for Neuroscience, 27(9), pp. 2309–2317. doi: 10.1523/jneurosci.4565-06.2007.

Swillens, S. *et al.* (1999) 'From calcium blips to calcium puffs: Theoretical analysis of the requirements for interchannel communication', *Proceedings of the National Academy of Sciences*, 96(24), pp. 13750–13755. doi: 10.1073/pnas.96.24.13750.

Sykes, D. A. *et al.* (2017) 'Extrapyramidal side effects of antipsychotics are linked to their association kinetics at dopamine D2 receptors', *Nature Communications*. Nature Publishing Group, 8(1), p. 763. doi: 10.1038/s41467-017-00716-z.

Sykes, D. A., Jain, P. and Charlton, S. J. (2019) 'Investigating the Influence of Tracer Kinetics on Competition-Kinetic Association Binding Assays: Identifying the Optimal Conditions for Assessing the Kinetics of Low-Affinity Compounds', *Molecular Pharmacology*, 96(3), pp. 378–392. doi: 10.1124/mol.119.116764.

Tabor, A. *et al.* (2016) 'Visualization and ligand-induced modulation of dopamine receptor dimerization at the single molecule level', *Scientific Reports*, 6(1), p. 33233. doi: 10.1038/srep33233.

Tan, Z. *et al.* (2017) 'Glia-derived ATP inversely regulates excitability of pyramidal and CCK-positive neurons', *Nature Communications*, 8(1), p. 13772. doi: 10.1038/ncomms13772.

Tanahashi, S. *et al.* (2012) 'Clozapine, but not haloperidol, enhances glial D-serine and L-glutamate release in rat frontal cortex and primary cultured astrocytes.', *British journal of pharmacology*. Wiley-Blackwell, 165(5), pp. 1543–55. doi: 10.1111/j.1476-5381.2011.01638.x.

Tandon, R. *et al.* (1991) 'Muscarinic cholinergic hyperactivity in schizophrenia. Relationship to positive and negative symptoms.', *Schizophrenia research*, 4(1), pp. 23–30. Available at: http://www.ncbi.nlm.nih.gov/pubmed/2009253 (Accessed: 25 August 2019).

Tang, W. *et al.* (2015) 'Stimulation-Evoked Ca2+ Signals in Astrocytic Processes at Hippocampal CA3-CA1 Synapses of Adult Mice Are Modulated by Glutamate and ATP',

Journal of Neuroscience, 35(7), pp. 3016–3021. doi: 10.1523/JNEUROSCI.3319-14.2015.

Tanzi, R. E. and Bertram, L. (2005) 'Twenty Years of the Alzheimer's Disease Amyloid Hypothesis: A Genetic Perspective', *Cell*, 120(4), pp. 545–555. doi: 10.1016/j.cell.2005.02.008.

Tarasova, N. I. *et al.* (1997) 'Visualization of G Protein-coupled Receptor Trafficking with the Aid of the Green Fluorescent Protein', *Journal of Biological Chemistry*, 272(23), pp. 14817–14824. doi: 10.1074/jbc.272.23.14817.

Tatsumi, K. *et al.* (2018) 'Olig2-Lineage Astrocytes: A Distinct Subtype of Astrocytes That Differs from GFAP Astrocytes', *Frontiers in Neuroanatomy*. Frontiers Media SA, 12. doi: 10.3389/fnana.2018.00008.

Taussig, R. and Zimmermann, G. (1998) 'Type-specific regulation of mammalian adenylyl cyclases by G protein pathways.', *Advances in second messenger and phosphoprotein research*, 32, pp. 81–98. Available at: http://www.ncbi.nlm.nih.gov/pubmed/9421586 (Accessed: 3 September 2019).

Thal, D. M. *et al.* (2016) 'Crystal structures of the M1 and M4 muscarinic acetylcholine receptors.', *Nature*. Nature Publishing Group, a division of Macmillan Publishers Limited. All Rights Reserved., 531(7594), pp. 335–340. doi: 10.1038/nature17188.

Thal, D. M. *et al.* (2018) 'Structural insights into G-protein-coupled receptor allostery', *Nature*. Nature Publishing Group, pp. 45–53. doi: 10.1038/s41586-018-0259-z.

Thinakaran, G. and Koo, E. H. (2008) 'Amyloid Precursor Protein Trafficking, Processing, and Function', *Journal of Biological Chemistry*, 283(44), pp. 29615–29619. doi: 10.1074/jbc.R800019200.

Thomas, D. *et al.* (2000) 'A comparison of fluorescent Ca2+indicator properties and their use in measuring elementary and global Ca2+signals', *Cell Calcium*, 28(4), pp. 213–223. doi: 10.1054/ceca.2000.0152.

Thomas, J. M. and Hoffman, B. B. (1996) 'Isoform-specific sensitization of adenylyl cyclase activity by prior activation of inhibitory receptors: role of beta gamma subunits

in transducing enhanced activity of the type VI isoform.', *Molecular pharmacology*, 49(5), pp. 907–14. Available at: http://www.ncbi.nlm.nih.gov/pubmed/8622641 (Accessed: 3 September 2019).

Thompson, K. J. *et al.* (2018) 'DREADD Agonist 21 Is an Effective Agonist for Muscarinic-Based DREADDs in Vitro and in Vivo'. doi: 10.1021/acsptsci.8b00012.

Thore, S. *et al.* (2005) 'Feedback activation of phospholipase C via intracellular mobilization and store-operated influx of Ca2+ in insulin-secreting beta-cells.', *Journal of cell science*. The Company of Biologists Ltd, 118(Pt 19), pp. 4463–71. doi: 10.1242/jcs.02577.

Thurley, K. *et al.* (2014) 'Reliable Encoding of Stimulus Intensities Within Random Sequences of Intracellular Ca2+ Spikes', *Science Signaling*, 7(331), pp. ra59–ra59. doi: 10.1126/scisignal.2005237.

Tian, H., Fürstenberg, A. and Huber, T. (2017) 'Labeling and Single-Molecule Methods To Monitor G Protein-Coupled Receptor Dynamics', *Chemical Reviews*. American Chemical Society, 117(1), pp. 186–245. doi: 10.1021/acs.chemrev.6b00084.

Tian, X., Kang, D. S. and Benovic, J. L. (2014) 'β-arrestins and G protein-coupled receptor trafficking.', *Handbook of experimental pharmacology*. NIH Public Access, 219, pp. 173–86. doi: 10.1007/978-3-642-41199-1_9.

Tinsley, R. B. *et al.* (2004) 'Improved non-viral transfection of glial and adult neural stem cell lines and of primary astrocytes by combining agents with complementary modes of action', *Journal of Gene Medicine*, 6(9), pp. 1023–1032. doi: 10.1002/jgm.584.

Tiwari, P. *et al.* (2013) 'Basic and modern concepts on cholinergic receptor: A review', *Asian Pacific Journal of Tropical Disease*. China Humanity Technology Publishing House, 3(5), pp. 413–420. doi: 10.1016/S2222-1808(13)60094-8.

Tohgo, A. *et al.* (2002) 'β-Arrestin Scaffolding of the ERK Cascade Enhances Cytosolic ERK Activity but Inhibits ERK-mediated Transcription following Angiotensin AT1a Receptor Stimulation', *Journal of Biological Chemistry*, 277(11), pp. 9429–9436. doi: 10.1074/jbc.M106457200.

Tsai, C.-J. *et al.* (2018) 'Crystal structure of rhodopsin in complex with a mini-Go sheds light on the principles of G protein selectivity', *Science Advances*, 4(9), p. eaat7052. doi: 10.1126/sciadv.aat7052.

Tsai, C.-J. *et al.* (2019) 'Cryo-EM structure of the rhodopsin-Gαi-βγ complex reveals binding of the rhodopsin C-terminal tail to the gβ subunit.', *eLife*. eLife Sciences Publications, Ltd, 8. doi: 10.7554/eLife.46041.

Tsien, R. Y. (1980) 'New calcium indicators and buffers with high selectivity against magnesium and protons: design, synthesis, and properties of prototype structures', *Biochemistry*. American Chemical Society, 19(11), pp. 2396–2404. doi: 10.1021/bi00552a018.

Tsien, R. Y. (1981) 'A non-disruptive technique for loading calcium buffers and indicators into cells', *Nature*, 290(5806), pp. 527–528. doi: 10.1038/290527a0.

Uchiyama, H. *et al.* (1990) 'Location in Muscarinic Acetylcholine Receptors of Sites for [3H]Propylbenzilcholine Mustard Binding and for Phosphorylation with Protein Kinase C', *Journal of Neurochemistry*. John Wiley & Sons, Ltd (10.1111), 54(6), pp. 1870–1881. doi: 10.1111/j.1471-4159.1990.tb04885.x.

Uhlén, P. and Fritz, N. (2010) 'Biochemistry of calcium oscillations.', *Biochemical and biophysical research communications*, 396(1), pp. 28–32. doi: 10.1016/j.bbrc.2010.02.117.

Ujita, S. *et al.* (2016) 'cAMP-Dependent Calcium Oscillations of Astrocytes: An Implication for Pathology', *Cerebral Cortex*, 27(2), p. bhv310. doi: 10.1093/cercor/bhv310.

Unger, V. M. and Schertler, G. F. (1995) 'Low resolution structure of bovine rhodopsin determined by electron cryo-microscopy', *Biophysical Journal*, 68(5), pp. 1776–1786. doi: 10.1016/S0006-3495(95)80354-1.

Uno, S. *et al.* (2015) 'A guide to use photocontrollable fluorescent proteins and synthetic smart fluorophores for nanoscopy', *Microscopy*, 64(4), pp. 263–277. doi: 10.1093/jmicro/dfv037.

Urban, D. J. and Roth, B. L. (2015) 'DREADDs (Designer Receptors Exclusively Activated by Designer Drugs): Chemogenetic Tools with Therapeutic Utility', *Annual Review of Pharmacology and Toxicology*, 55(1), pp. 399–417. doi: 10.1146/annurev-pharmtox-010814-124803.

Urban, J. D. *et al.* (2007) 'Functional Selectivity and Classical Concepts of Quantitative Pharmacology', *Journal of Pharmacology and Experimental Therapeutics*, 320(1), pp. 1–13. doi: 10.1124/jpet.106.104463.

Uslaner, J. M. *et al.* (2013) 'The muscarinic M1 receptor positive allosteric modulator PQCA improves cognitive measures in rat, cynomolgus macaque, and rhesus macaque.', *Psychopharmacology*, 225(1), pp. 21–30. doi: 10.1007/s00213-012-2788-8.

Uttamapinant, C. *et al.* (2010) 'A fluorophore ligase for site-specific protein labeling inside living cells', *Proceedings of the National Academy of Sciences*, 107(24), pp. 10914–10919. doi: 10.1073/pnas.0914067107.

Valant, C. *et al.* (2012) 'Probe Dependence in the Allosteric Modulation of a G Protein-Coupled Receptor: Implications for Detection and Validation of Allosteric Ligand Effects', *Molecular Pharmacology*, 81(1), pp. 41–52. doi: 10.1124/mol.111.074872.

Vallejo-Illarramendi, A. *et al.* (2005) 'Clozapine reduces GLT-1 expression and glutamate uptake in astrocyte cultures', *Glia*, 50(3), pp. 276–279. doi: 10.1002/glia.20172.

VanDeMark, K. L. *et al.* (2009) 'The Activation of M1 Muscarinic Receptor Signaling Induces Neuronal Differentiation in Pyramidal Hippocampal Neurons', *Journal of Pharmacology and Experimental Therapeutics*, 329(2), pp. 532–542. doi: 10.1124/jpet.108.150128.

Vardjan, N., Kreft, M. and Zorec, R. (2014) 'Dynamics of β-adrenergic/cAMP signaling and morphological changes in cultured astrocytes.', *Glia*, 62(4), pp. 566–79. doi: 10.1002/glia.22626.

Vardy, E. *et al.* (2015) 'A New DREADD Facilitates the Multiplexed Chemogenetic Interrogation of Behavior', *Neuron*, 86(4), pp. 936–946. doi:

10.1016/j.neuron.2015.03.065.

Velve-Casquillas, G. *et al.* (2010) 'Microfluidic tools for cell biological research.', *Nano today*. NIH Public Access, 5(1), pp. 28–47. doi: 10.1016/j.nantod.2009.12.001.

Venkatakrishnan, A. J. *et al.* (2013) 'Molecular signatures of G-protein-coupled receptors', *Nature*, 494(7436), pp. 185–194. doi: 10.1038/nature11896.

Verkhratsky, A. and Nedergaard, M. (2018) 'Physiology of Astroglia', *Physiological Reviews*, 98(1), pp. 239–389. doi: 10.1152/physrev.00042.2016.

Vilardaga, J.-P. (2011) 'Recording kinetics of adrenergic receptor activation in live cells.', *Current topics in membranes*. NIH Public Access, 67, pp. 101–11. doi: 10.1016/B978-0-12-384921-2.00005-7.

Vishnivetskiy, S. A. *et al.* (2000) 'An Additional Phosphate-binding Element in Arrestin Molecule', *Journal of Biological Chemistry*, 275(52), pp. 41049–41057. doi: 10.1074/jbc.M007159200.

Vishnivetskiy, S. A. *et al.* (2011) 'Few Residues within an Extensive Binding Interface Drive Receptor Interaction and Determine the Specificity of Arrestin Proteins', *Journal of Biological Chemistry*, 286(27), pp. 24288–24299. doi: 10.1074/jbc.M110.213835.

Voigtländer, U. *et al.* (2003) 'Allosteric Site on Muscarinic Acetylcholine Receptors: Identification of Two Amino Acids in the Muscarinic M_2 Receptor That Account Entirely for the M_2/M_5 Subtype Selectivities of Some Structurally Diverse Allosteric Ligands in *N* -Methylscopolamine-Occupied Receptors', *Molecular Pharmacology*, 64(1), pp. 21–31. doi: 10.1124/mol.64.1.21.

Volpicelli, L. A. and Levey, A. I. (2004) 'Muscarinic acetylcholine receptor subtypes in cerebral cortex and hippocampus', in, pp. 59–66. doi: 10.1016/S0079-6123(03)45003-6.

Volterra, A. and Meldolesi, J. (2005) 'Astrocytes, from brain glue to communication elements: the revolution continues', *Nature Reviews Neuroscience*, 6(8), pp. 626–640. doi: 10.1038/nrn1722.

Vukasinovic, J. *et al.* (2009) 'A microperfused incubator for tissue mimetic 3D cultures',

Biomedical Microdevices, 11(6), pp. 1155–1165. doi: 10.1007/s10544-009-9332-6.

Wakefield, A. E. *et al.* (2019) 'Analysis of tractable allosteric sites in G protein-coupled receptors.', *Scientific reports*. Nature Publishing Group, 9(1), p. 6180. doi: 10.1038/s41598-019-42618-8.

Wall, M. A. *et al.* (1995a) 'The structure of the G protein heterotrimer Giα1β1γ2', *Cell*. Cell Press, 83(6), pp. 1047–1058. doi: 10.1016/0092-8674(95)90220-1.

Wall, M. A. *et al.* (1995b) 'The structure of the G protein heterotrimer Giα1β1γ2', *Cell*, 83(6), pp. 1047–1058. doi: 10.1016/0092-8674(95)90220-1.

Walz, W. (2000) 'Controversy surrounding the existence of discrete functional classes of astrocytes in adult gray matter', *Glia*, 31(2), pp. 95–103. doi: 10.1002/1098-1136(200008)31:2<95::AID-GLIA10>3.0.CO;2-6.

Walz, W. and Lang, M. K. (1998) 'Immunocytochemical evidence for a distinct GFAP-negative subpopulation of astrocytes in the adult rat hippocampus.', *Neuroscience letters*, 257(3), pp. 127–30. doi: 10.1016/s0304-3940(98)00813-1.

Wan, Q., Okashah, N., Inoue, A., Nehmé, R., Carpenter, B., Tate, *et al.* (2018) 'Mini G protein probes for active G protein-coupled receptors (GPCRs) in live cells.', *The Journal of biological chemistry*. American Society for Biochemistry and Molecular Biology, 293(19), pp. 7466–7473. doi: 10.1074/jbc.RA118.001975.

Wan, Q., Okashah, N., Inoue, A., Nehmé, R., Carpenter, B., Tate, C. G., *et al.* (2018) 'Mini G protein probes for active G protein–coupled receptors (GPCRs) in live cells', *Journal of Biological Chemistry*, 293(19), pp. 7466–7473. doi: 10.1074/jbc.RA118.001975.

Wang, Z. *et al.* (1997) 'Impact of cytoplasmic calcium buffering on the spatial and temporal characteristics of intercellular calcium signals in astrocytes.', *The Journal of neuroscience : the official journal of the Society for Neuroscience*, 17(19), pp. 7359–71. Available at: http://www.ncbi.nlm.nih.gov/pubmed/9295382 (Accessed: 23 September 2019).

Watson, S.-J., Brown, A. J. H. and Holliday, N. D. (2012a) 'Differential signaling by splice

variants of the human free fatty acid receptor GPR120.', *Molecular pharmacology*. American Society for Pharmacology and Experimental Therapeutics, 81(5), pp. 631–42. doi: 10.1124/mol.111.077388.

Watson, S.-J., Brown, A. J. H. and Holliday, N. D. (2012b) 'Differential signaling by splice variants of the human free fatty acid receptor GPR120.', *Molecular pharmacology*, 81(5), pp. 631–42. doi: 10.1124/mol.111.077388.

Weis and Kobilka (2018a) 'The Molecular Basis of G Protein-Coupled Receptor Activation.', *Annual review of biochemistry*. NIH Public Access, 87, pp. 897–919. doi: 10.1146/annurev-biochem-060614-033910.

Weis and Kobilka (2018b) 'The Molecular Basis of G Protein–Coupled Receptor Activation', *Annual Review of Biochemistry*, 87(1), pp. 897–919. doi: 10.1146/annurev-biochem-060614-033910.

Wenthur, C. J. *et al.* (2014) 'Drugs for Allosteric Sites on Receptors', *Annual Review of Pharmacology and Toxicology*, 54(1), pp. 165–184. doi: 10.1146/annurev-pharmtox-010611-134525.

Wess, J. (2003) 'Novel insights into muscarinic acetylcholine receptor function using gene targeting technology.', *Trends in pharmacological sciences*, 24(8), pp. 414–20. doi: 10.1016/S0165-6147(03)00195-0.

Wess, J. (2004) 'MUSCARINIC ACETYLCHOLINE RECEPTOR KNOCKOUT MICE : Novel Phenotypes and Clinical Implications', *Annual Review of Pharmacology and Toxicology*, 44(1), pp. 423–450. doi: 10.1146/annurev.pharmtox.44.101802.121622.

Wess, J. *et al.* (2008) 'Conformational changes involved in G-protein-coupled-receptor activation.', *Trends in pharmacological sciences*. NIH Public Access, 29(12), pp. 616–25. doi: 10.1016/j.tips.2008.08.006.

Wess, J., Eglen, R. M. and Gautam, D. (2007) 'Muscarinic acetylcholine receptors: mutant mice provide new insights for drug development', *Nature Reviews Drug Discovery*, 6(9), pp. 721–733. doi: 10.1038/nrd2379.

Wess, J., Nakajima, K. and Jain, S. (2013) 'Novel designer receptors to probe GPCR

signaling and physiology.', *Trends in pharmacological sciences*, 34(7), pp. 385–92. doi: 10.1016/j.tips.2013.04.006.

van der Westhuizen, E. T. *et al.* (2018) 'Assessment of the Molecular Mechanisms of Action of Novel 4-Phenylpyridine-2-One and 6-Phenylpyrimidin-4-One Allosteric Modulators at the M $_1$ Muscarinic Acetylcholine Receptors', *Molecular Pharmacology*, 94(1), pp. 770–783. doi: 10.1124/mol.118.111633.

Weston, M. *et al.* (2019) 'Olanzapine: A potent agonist at the hM4D(Gi) DREADD amenable to clinical translation of chemogenetics', *Science Advances*. American Association for the Advancement of Science, 5(4). doi: 10.1126/sciadv.aaw1567.

Wettschureck, N. *et al.* (2005) 'Loss of Gq/11 Family G Proteins in the Nervous System Causes Pituitary Somatotroph Hypoplasia and Dwarfism in Mice', *Molecular and Cellular Biology*, 25(5), pp. 1942–1948. doi: 10.1128/MCB.25.5.1942-1948.2005.

Wettschureck, N. and Offermanns, S. (2005) 'Mammalian G Proteins and Their Cell Type Specific Functions', *Physiological Reviews*. American Physiological Society, 85(4), pp. 1159–1204. doi: 10.1152/physrev.00003.2005.

Wheatley, M. *et al.* (2012) 'Lifting the lid on GPCRs: the role of extracellular loops.', *British journal of pharmacology*. Wiley-Blackwell, 165(6), pp. 1688–1703. doi: 10.1111/j.1476-5381.2011.01629.x.

Whitesides, G. M. (2006) 'The origins and the future of microfluidics.', *Nature*, 442(7101), pp. 368–73. doi: 10.1038/nature05058.

Willets, J. M. *et al.* (2004) 'Imaging of Muscarinic Acetylcholine Receptor Signaling in Hippocampal Neurons: Evidence for Phosphorylation-Dependent and -Independent Regulation by G-Protein-Coupled Receptor Kinases', *Journal of Neuroscience*, 24(17), pp. 4157–4162. doi: 10.1523/JNEUROSCI.5506-03.2004.

Willets, J. M., Nahorski, S. R. and Challiss, R. A. J. (2005) 'Roles of Phosphorylation-dependent and -independent Mechanisms in the Regulation of M1 Muscarinic Acetylcholine Receptors by G Protein-coupled Receptor Kinase 2 in Hippocampal Neurons', *Journal of Biological Chemistry*, 280(19), pp. 18950–18958. doi: 10.1074/jbc.M412682200.

Wolfes, A. C. *et al.* (2017) 'A novel method for culturing stellate astrocytes reveals spatially distinct Ca2+ signaling and vesicle recycling in astrocytic processes.', *The Journal of general physiology*. Rockefeller University Press, 149(1), pp. 149–170. doi: 10.1085/jgp.201611607.

Won, C.-K. and Oh, Y. S. (2000) 'cAMP-induced stellation in primary astrocyte cultures with regional heterogeneity', *Brain Research*, 887(2), pp. 250–258. doi: 10.1016/S0006-8993(00)02922-X.

Wonnacott, S. (1997) 'Presynaptic nicotinic ACh receptors.', *Trends in neurosciences*, 20(2), pp. 92–8. Available at: http://www.ncbi.nlm.nih.gov/pubmed/9023878 (Accessed: 3 September 2019).

Wootten, D., Christopoulos, A. and Sexton, P. M. (2013) 'Emerging paradigms in GPCR allostery: implications for drug discovery', *Nature Reviews Drug Discovery*, 12(8), pp. 630–644. doi: 10.1038/nrd4052.

Wu, B. Y. *et al.* (2000) 'Multi-lipofection efficiently transfected genes into astrocytes in primary culture.', *Journal of neuroscience methods*, 102(2), pp. 133–41. Available at: http://www.ncbi.nlm.nih.gov/pubmed/11040410 (Accessed: 14 August 2019).

Wu, H. *et al.* (2014) 'Structure of a Class C GPCR Metabotropic Glutamate Receptor 1 Bound to an Allosteric Modulator', *Science*, 344(6179), pp. 58–64. doi: 10.1126/science.1249489.

Xiang, Z. *et al.* (2012) 'Roles of the M1 Muscarinic Acetylcholine Receptor Subtype in the Regulation of Basal Ganglia Function and Implications for the Treatment of Parkinson's Disease', *The Journal of Pharmacology and Experimental Therapeutics*. American Society for Pharmacology and Experimental Therapeutics, 340(3), p. 595. doi: 10.1124/JPET.111.187856.

Xie, A. X., Petravicz, J. and McCarthy, K. D. (2015) 'Molecular approaches for manipulating astrocytic signaling in vivo.', *Frontiers in cellular neuroscience*. Frontiers Media SA, 9, p. 144. doi: 10.3389/fncel.2015.00144.

Yamada, M. *et al.* (2001) 'Mice lacking the M3 muscarinic acetylcholine receptor are hypophagic and lean', *Nature*, 410(6825), pp. 207–212. doi: 10.1038/35065604.

Yamaguchi, Y., Katoh, H. and Negishi, M. (2003) 'N-terminal short sequences of alpha subunits of the G12 family determine selective coupling to receptors.', *The Journal of biological chemistry*. American Society for Biochemistry and Molecular Biology, 278(17), pp. 14936–9. doi: 10.1074/jbc.M301409200.

Yang, F. V *et al.* (2010) 'Parallel synthesis of N-biaryl quinolone carboxylic acids as selective M(1) positive allosteric modulators.', *Bioorganic & medicinal chemistry letters*, 20(2), pp. 531–6. doi: 10.1016/j.bmcl.2009.11.100.

Yang, J.-S. *et al.* (2012) 'Rational Engineering of Enzyme Allosteric Regulation through Sequence Evolution Analysis', *PLoS Computational Biology*. Edited by S. A. Teichmann. Public Library of Science, 8(7), p. e1002612. doi: 10.1371/journal.pcbi.1002612.

Yang, L., Qi, Y. and Yang, Y. (2015a) 'Astrocytes Control Food Intake by Inhibiting AGRP Neuron Activity via Adenosine A<inf>1</inf> Receptors', *Cell Reports*. Elsevier, 11(5), pp. 798–807. doi: 10.1016/j.celrep.2015.04.002.

Yang, L., Qi, Y. and Yang, Y. (2015b) 'Astrocytes control food intake by inhibiting AGRP neuron activity via adenosine A1 receptors.', *Cell reports*, 11(5), pp. 798–807. doi: 10.1016/j.celrep.2015.04.002.

Yau, J. O.-Y. and McNally, G. P. (2015) 'Pharmacogenetic excitation of dorsomedial prefrontal cortex restores fear prediction error.', *The Journal of neuroscience : the official journal of the Society for Neuroscience*, 35(1), pp. 74–83. doi: 10.1523/JNEUROSCI.3777-14.2015.

Yeatman, H. R. *et al.* (2014) 'Allosteric modulation of M1 muscarinic acetylcholine receptor internalization and subcellular trafficking.', *The Journal of biological chemistry*. American Society for Biochemistry and Molecular Biology, 289(22), pp. 15856–66. doi: 10.1074/jbc.M113.536672.

Yi, J. H. *et al.* (2012) 'Alterations in sulfated chondroitin glycosaminoglycans following controlled cortical impact injury in mice', *Journal of Comparative Neurology*, 520(15), pp. 3295–3313. doi: 10.1002/cne.23156.

Yu, A. J. and Dayan, P. (2005) 'Uncertainty, Neuromodulation, and Attention', *Neuron*, 46(4), pp. 681–692. doi: 10.1016/j.neuron.2005.04.026.

Yung-Chi, C. and Prusoff, W. H. (1973) 'Relationship between the inhibition constant (KI) and the concentration of inhibitor which causes 50 per cent inhibition (I50) of an enzymatic reaction', *Biochemical Pharmacology*, 22(23), pp. 3099–3108. doi: 10.1016/0006-2952(73)90196-2.

Zagranichnaya, T. K., Wu, X. and Villereal, M. L. (2005) 'Endogenous TRPC1, TRPC3, and TRPC7 Proteins Combine to Form Native Store-operated Channels in HEK-293 Cells', *Journal of Biological Chemistry*, 280(33), pp. 29559–29569. doi: 10.1074/jbc.M505842200.

van der Zee, E. A. *et al.* (1993) 'Muscarinic acetylcholine receptor-expression in astrocytes in the cortex of young and aged rats', *Glia*, 8(1), pp. 42–50. doi: 10.1002/glia.440080106.

Zeng, Shuai *et al.* (2009) 'Simulation of Spontaneous Ca2+ Oscillations in Astrocytes Mediated by Voltage-Gated Calcium Channels', *Biophysical Journal*. Cell Press, 97(9), pp. 2429–2437. doi: 10.1016/J.BPJ.2009.08.030.

Zhang, H. and Sulzer, D. (2004) 'Frequency-dependent modulation of dopamine release by nicotine', *Nature Neuroscience*, 7(6), pp. 581–582. doi: 10.1038/nn1243.

Zhang, J. *et al.* (2010) 'Targeting Bcr–Abl by combining allosteric with ATP-binding-site inhibitors', *Nature*, 463(7280), pp. 501–506. doi: 10.1038/nature08675.

Zhang, L. *et al.* (2006) 'The G 12 Family of G Proteins as a Reporter of Thromboxane A2 Receptor Activity', *Molecular Pharmacology*, 69(4), pp. 1433–1440. doi: 10.1124/mol.105.019703.

Zhang, W. *et al.* (2002) 'Multiple muscarinic acetylcholine receptor subtypes modulate striatal dopamine release, as studied with M1-M5 muscarinic receptor knock-out mice.', *The Journal of neuroscience : the official journal of the Society for Neuroscience*, 22(15), pp. 6347–52. doi: 20026644.

Zhang, X. C., Zhou, Y. and Cao, C. (2015) 'Thermodynamics of GPCR activation.', *Biophysics reports*. Springer, 1, pp. 115–119. doi: 10.1007/s41048-016-0017-4.

Zhang, Y. *et al.* (2017) 'Cryo-EM structure of the activated GLP-1 receptor in complex

with a G protein', *Nature*, 546(7657), pp. 248–253. doi: 10.1038/nature22394.

Zhao, L.-H. *et al.* (2019) 'Structure and dynamics of the active human parathyroid hormone receptor-1', *Science*, 364(6436), pp. 148–153. doi: 10.1126/science.aav7942.

Zheng, Y. *et al.* (2016) 'Structure of CC chemokine receptor 2 with orthosteric and allosteric antagonists', *Nature*, 540(7633), pp. 458–461. doi: 10.1038/nature20605.

Zhou, B., Zuo, Y. and Jiang, R. (2019) 'Astrocyte morphology: Diversity, plasticity, and role in neurological diseases', *CNS Neuroscience & Therapeutics*, 25(6), pp. 665–673. doi: 10.1111/cns.13123.

Zhou, X. *et al.* (2019) 'Astrocyte, a Promising Target for Mood Disorder Interventions', *Frontiers in Molecular Neuroscience*. Frontiers, 12, p. 136. doi: 10.3389/fnmol.2019.00136.

Zhou, Z., Ikegaya, Y. and Koyama, R. (2019) 'The Astrocytic cAMP Pathway in Health and Disease', *International Journal of Molecular Sciences*, 20(3), p. 779. doi: 10.3390/ijms20030779.

Zimmermann, U. (1982) 'Electric field-mediated fusion and related electrical phenomena', *BBA - Reviews on Biomembranes*, pp. 227–277. doi: 10.1016/0304-4157(82)90007-7.